Design Improvement of a Pump Wear Ring
Labyrinth Seal

FINAL REPORT
February 1987
Contract NAS8-36161

By David L. Rhode, G.L Morrison, S.H. Ko
and S.P. Waughtal

Prepared for
George C. Marshall Space Flight Center
Marshall Space Flight Center, AL 35812

TL-SEAL-2-87

Turbomachinery Laboratories
Mechanical Engineering Department
Texas A&M University
College Station, Texas 77843-3123

(NASA-CR-179161) DESIGN IMPROVEMENT OF A PUMP WEAR RING LABYRINTH SEAL Final Report (Texas A&M Univ.) 201 p CSCL 13I
N88-19555
Unclas
G3/37 0192940

or in part. Date for general release 02-89.

Turbomachinery Laboratories

Texas A&M University

Mechanical Engineering Department

College Station, Texas 77843

"Design Improvement of a Pump Wear Ring Labyrinth Seal"

Final Report

February 1987

Contract NAS8-36161

David L. Rhode

Gerald L. Morrison

Sung-Ho Ko

Scott P. Waughtal

Prepared for

George C. Marshall Space Flight Center

Marshall Space Flight Center, Alabama 35812

ABSTRACT

The investigation was successful in obtaining two improved designs for the impeller wear ring seal of the liquid hydrogen turbopump of interest. A finite difference computer code was extensively used in a parametric computational study in determining a cavity configuration with high flow resistance due to turbulence dissipation. These two new designs, along with that currently used, were fabricated and tested. The improved designs were denoted as Type O (seal #2 in the test sequence) and Type S (seal #3 in the test sequence). The measurements showed that Type O and Type S given 67 and 30 percent reduction in leakage over the current design, respectively.

It was found that the number of cavities, the step height and the presence of a small stator groove are quite important design features. Also, the tooth thickness is of some significance. Finally, the tooth height and an additional large cavity cut out from the stator (upstream of the step) are of negligible importance.

TABLE OF CONTENTS

ABSTRACT ---------- i

TABLE OF CONTENTS ---------- ii

NOMENCLATURE ---------- iii

I. INTRODUCTION ---------- 1

II. PREVIOUS WORK ---------- 5

III. NUMERICAL PROCEDURE ---------- 9

IV. EXPERIMENTAL VERIFICATION ---------- 21

V. SEAL DESIGN IMPROVEMENT ---------- 29

VI. EMPIRICAL LEAKAGE PREDICTION PROGRAM ---------- 69

VII. EXPERIMENTAL FACILITY ---------- 113

VIII. EXPERIMENTAL RESULTS ---------- 120

IX. EMPIRICAL PREDICTION COMPARISON WITH CURRENT DATA - 159

X. CLOSURE ---------- 162

REFERENCES ---------- 164

APPENDIX A Curve fit experimental data 168

APPENDIX B Empirical leakage estimation program 174

APPENDIX C Equipment specifications 192

NOMENCLATURE

A_t	Seal leakage area
A	Control volume face area
AQ	Solution using QUICK for all equations
AQEWF	Solution using QUICK for all equations with extended wall function
B	Coefficients including the convective and diffusive effects
c	Seal clearance
	Turbulence Model
C_1, C_2, C_μ, C_D	Constants
D	Seal diameter
f	Friction factor
G	Kinetic energy generation term
k	Turbulence kinetic energy
m	Seal pitch
$\dot{m}$	Mass flow rate
MQ	Solution using QUICK only for momentum equations
N	Number of throttles in seal
P	Static pressure,Production of turbulence energy
P_o	Seal inlet pressure
P_n	Outlet pressure of the seal
P_0	Reference pressure at the cavity inlet
P_r	Po/Pn
Re_x	Axial Reynolds number
Re_θ	Azimuthal Reynolds number

$S\phi$	Source/sink of variable ϕ
$S\phi, S\phi$	Linerarized source/sink term
x, r, Θ	Axial, radial, and azimuthal coordinates
u, v, w	Fluctuating velocities in x, r, Θ directions, respectively
U, V, W	Mean velocities in x, r, Θ directions, respectively
X	Wall shear stress direction
α_x, β_x	Coefficients
δ_{ij}	Kronecker delta
μ	Absolute viscosity
ϕ	Generalized dependent variable
Γ	Turbulent diffusion coefficient
ν	Kinematic viscosity
ρ	Fluid density
ρ_o	Fluid density at seal inlet
ε	Turbulent energy dissipation rate
ε_c	Carry over coefficient
K	von Karman constant
τ_t	Total tangential wall shear stress
τ_k	Approximation for τ_t very near wall
ψ	Stream function
σ_k, σ_ε	Turbulence constants

Subscripts

n, s, e, w	North, south, east, west faces of a control volume
N, S, E, W	North, South, East, West neighboring grid points
o	Cavity inlet bulk value

P	Value corresponding to the center of a control volume
ϕ	general flow variable
l	Laminar
t	Turbulent
eff	Effective
	Free stream value
CTOP	Clearance-to-Pitch Ratio
PR	Pressure Ratio = P_n/Po
WTOP	Tooth Width-to-Pitch Ratio
TNUM	Number of Teeth
AXLO	Axial Location of tooth with respect to step

I. INTRODUCTION

Labyrinth seals are primarily used to reduce the internal leakage of fluid from systems such as gas and steam turbines, compressors, and pumps. The seal designer accomplishes this objective by providing a highly dissipative flow path between high and low pressure regions. Tests indicate a diminishing advantage beyond a certain number of cavities, particularly where the shaft doesn't stay centered. In such cases, the simpler labyrinths are as good as the more serpentine types and are also much less expensive. The flow passage through a labyrinth is illustrated in Fig.1 for a simple straight-through seal configuration. Each tooth converts a portion of the available pressure head into mean flow kinetic energy, some of which is dissipated within the cavity immediately downstream.

Many investigators have studied several flow characteristics of labyrinth seals in attempting to obtain simple empirically based relations for estimating the leakage rate. Leakage has been analyzed as a function of overall pressure drop, friction factor, seal clearance, tooth thickness, cavity width, shaft speed, and number of teeth. The resulting relations are very successful when applied to seals which are very similar to those tested; however, any significant difference in seal design often leads to error. Therefore, a universally valid method is needed which is applicable for arbitrary seal geometry, shaft speed, pressure drop, etc.

Objective

The primary objective was to re-design the impeller inlet labyrinth seal of the HP hydrogen turbopump. The motivation behind this was to reduce the seal leakage for a given pressure drop. This was accomplished through an extensive parametric study of the leakage characteristic using a finite difference computer code. The best two seal designs resulting from this procedure, along with the currently used design, were experimentally tested. The results of these tests were used to evaluate the two new design candidates. The tests also

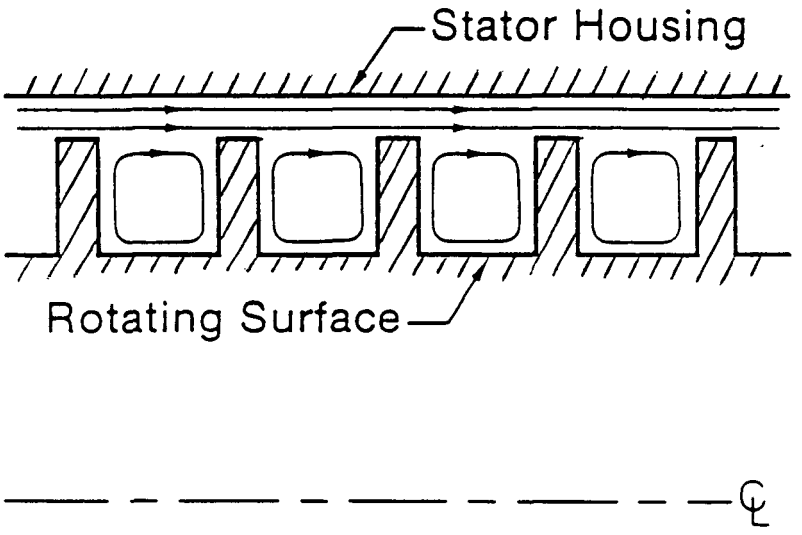

Fig. 1 Configuration and expected streamline pattern for a generic straight-through labyrinth seal

determined the effects of pressure ratio, shaft speed, tooth-to-step location, and number of teeth upon the leakage rate. In addition to leakage rate, pressure distributions throughout the three seals were measured to obtain additional insight.

An additional objective was to modify the empirical seal leakage model developed under contract NAS8-34536 to include the effects of step height. This refinement was needed since the initial model was based upon tests obtained from only one stepped labyrinth seal.

Approach

The finite difference computer code for labyrinth seals (employed under contract NAS8-34536) has proven to be very successful in computing highly detailed flow measurements in several related flow fields. This advanced computer code accurately simulates all mean flowfield phenomena. Hence it is generally applicable without the uncertainty found in simple algebraic models regarding which design-dependent empirical "friction factor" value is valid for a given seal configuration.

The first step was to extend the capability of the finite difference computer code in order to allow more variation in the stator wall configuration. This code development involved several things, including finding a new way of treating the inflow boundary condition values. Once the computer code was properly extended, it was extensively employed to predict the leakage characteristic of numerous candidates for the optimum seal design. Both current as well as various new labyrinth seal design concepts were considered.

The two seals designed using this computer code were locally manufactured. Included in the manufactured seals was a series of static wall pressure taps along the length of the seals. Each seal was tested with the leakage rate and pressure distributions measured for several pressure ratios (outlet pressure/inlet pressure) ranging from 0.1 to 0.9. At each pressure ratio the shaft speed was varied from 0 to 5000 rpm and the location of the teeth with

respect to the steps in the stator was varied (at least three locations). This matrix of measurements provided the data necessary for refinement of the empirical leakage prediction model.

False Diffusion

In the realm of computational fluid mechanics, false diffusion can be an obstacle in obtaining accurate and economical solutions to the governing equations. Therefore, it is desirable to use discretization schemes having little false diffusion. The previously used hybrid upwind/central differencing scheme introduces false diffusion numerical error which can obscure the turbulence modeling effects on physical processes [1,2]. This error source is found in flow regions exhibiting streamline-to-grid skewness and diffusive transport normal to the flow direction where convection dominates diffusion. The QUICK scheme developed by Leonard [3] generally reduces false diffusion by introducing a quadratic upwind-shifted interpolation formula for evaluating dependent variables at each control volume face. Thus, this scheme was employed in the present work and pertinent details are discussed in Chapter III. The numerical convergence difficulties which arise from implementation of the QUICK scheme were alleviated as discussed by Rhode et al. [4].

II. PREVIOUS WORK

Most of the previous work focused on determining simple empirical relationships between the leakage flow rate and the overall pressure drop,seal geometry, shaft speed, and Reynolds number. Surprisingly, the earliest analytical method [5] remains, to this day, one of the most popular. However, many of these studies and tests only present overall pressure drop and leakage flow rather than detailed flow characteristics within a labyrinth seal. Recently, some experimental studies have been attempted to measure details such as velocity profiles and kinetic energy within the clearance gap and within a cavity. In addition, a few investigators have presented detailed flowfields within cavities using numerical analyses.

Becker [6] appears to be the first one who attempted to describe the flow through a labyrinth. He treated the leakage as a simple annular flow by using a coefficient of friction. Shortly after Becker published his paper, Martin [5] proposed an analytical method which has become a landmark. He considered the labyrinth to be a series of discrete throttling processes and derived two equations based on the following assumptions: (a) the flow through the labyrinth is isothermal, (b) there are a large number of identical teeth and cavities of equal flow coefficient, (c) the conversion of kinetic energy to thermal energy is complete in the cavity between the teeth, and (d) the pressure ratio across each tooth is less than 0.8. Many authors have adopted the Martin model and extended it in various ways.

Stodola [7] applied Bernoulli's equation to each restrictor to get a formula for the leakage flow rate for subcritical leakage flow. Like Martin, he treated the process as isothermal and neglected the effects of rotation and kinetic energy carry-over between restrictors. A graphical method for analyzing seals with varying areas was also developed.

By assuming an adiabatic, isothermal flow Gercke [8] extended Martin's formulation to allow for varying flow area and kinetic energy carry-over for

subcritical flow. He included an experimentally determined flow coefficient to account for the contraction of the flow area at the vena contract and for friction as the fluid passed through the throttling constrictions.

One of the most often quoted authors on the subject of labyrinth seals is Egli [9]. The analysis began by examining the isentropic expansion of a compressible fluid through a single ideal orifice. He then extended the analysis to include more than one orifice. Values of kinetic energy carry-over coefficient were shown as a function of the number of throttles and the clearance- to- pitch ratio. The results showed that the kinetic energy carry-over increased with an increase in clearance- to- pitch ratio ,number of throttles, seal clearance, tooth thickness, and overall pressure ratio. His experimental results indicate that the flow coefficient is independent of the seal clearance- to- tooth width ratios for values of this ratio over 3.5. For values less than 3.5, the flow coefficient increases as the clearance decreases.He recommended that Martin's formula should be used only when there were four or more throttlings in series. Test results in graphical form were also offered for staggered labyrinths which show that the flow coefficient depends on the clearance and thickness of the restrictor.

Hodkinson [10] made the first attempt to analytically predict the kinetic energy carry-over effect from a fluid mechanics viewpoint rather than a thermodynamic viewpoint. He modeled the leakage in a labyrinth seal as flow passing through a series of perfect nozzles. The final equation depends on a flow coefficient which accounts for the non-ideal nature of the flow through the throttling constrictions. The resulting predictions agreed with the corresponding measurements within about five percent.

Jerie [11] performed an analysis and testing program of leakage for straight-through labyrinth seals. It was concluded

that when the restrictor thickness-to- clearance ratio was greater than two, the restrictor behaves more like a rounded nozzle than a sharp-edged orifice. The equation he derived to predict leakage, which includes an empirically determined flow coefficient and a velocity carry-over coefficient, is valid only for the following assumptions: small pressure gradient, constant density, constant clearances, constant flow coefficients, and constant diffusion angles through the throttle constrictions. The experiments showed that the carry-over coefficient decreases with a decrease in the number of throttles and the pitch. Futher,the flow coefficient decreases as the clearance decreases and as the tooth thickness increases. He recommended an optimum tooth depth- to- spacing ratio of slightly less than unity. The paper also included flow visualization photographs which illustrate the complex nature of labyrinth flowfields.

Kearton and Keh [12] presented extensive experimental data concerning the variation of the flow coefficient with pressure ratio for single annular constrictions under subcritical and supercritical flow conditions. They derived a theoretical leakage formula for a staggered labyrinth in which the kinetic energy carry-over is extremely small.

Zabriskie and Sternlicht [13] determined a friction factor as a function of Reynolds number and seal geometry and then related the mass flow rate to this friction factor and the pressure ratio across the seal. Data gathered from previous studies were utilized. Unfortunately, the scarcity of friction factor data limits the usefulness of this alternative approach.

Vermes [14] included all the best theoretical and experimental results of references [5,8,9,13] in his paper. His basic model is Martin's formula adjusted for non-isothermal effects. He applied boundary layer theory to the flow through the throttling constrictions and used the flow coefficients which were developed by Bell and Bergelin [15]. This analysis was applied for straight-through seals. For stepped seals, he used

Gercke's method. The experimental data gathered by Vermes indicate that the mass flow rate decreases as the pressure drop decreases and seal clearance decreases. The equations derived by Vermes predicted the leakage in his experiments within five percent for both straight-through and stepped seals.

Han [16] studied incompressible fluid leakage in straight-through labyrinth seals for turbulent flow conditions. The flow was analyzed as it passed over a seal tooth and through a cavity, summing up all the friction coefficients along the flow path. The equations he developed predict leakage as a function of the pressure difference across the seal, the length of the seal, the width of a cavity, the seal clearance, and some empirical constants. The comparison of predictions to experimental data showed 80 to 120 percent discrepancies.

Stoff [17] used a finite difference computer program based on the TEACH program [18] to solve the Navier-Stokes equations. The k-ε turbulence model was used to analyze the effect of turbulence on the mean flowfield. Experimental measurements were obtained by using a Laser-Doppler anemometer. He compared numerical predictions to measurements for a large scale straight-through seal facility. His predictions and measurements of mean swirl velocity differed by about seven percent.

Rhode et al. [4] developed a new numerical approach for alleviating the substantial convergence difficulty which results from implementation of the QUICK differencing scheme into a TEACH-type computer code. The resulting CPU time and number of numerical iterations required to obtain a solution were shown to compare favorably with a previously recommended approach. Good agreement with measurements was demonstrated for both straight-through and stepped labyrinths.

III. NUMERICAL PROCEDURE

General Methodology

The numerical procedure was developed from a previous finite difference procedure based on the TEACH computer program of Gosman and Pun [18]. The governing turbulent Reynolds equations for conservation of momentum (with x,r, and θ time-mean velocity components U,V,W), turbulence energy k and turbulence dissipation rate ε are to be solved simultaneously. The equations for the two-dimensional, axisymmetric, swirling, steady flow may be expressed in the general form

$$\frac{1}{r}\left[\frac{\partial}{\partial x}(\rho U r\phi) + \frac{\partial}{\partial r}(\rho V r\phi) - \frac{\partial}{\partial x}(r\Gamma_\phi \frac{\partial \phi}{\partial x}) - \frac{\partial}{\partial r}(r\Gamma_\phi \frac{\partial \phi}{\partial r})\right] = S^\phi \qquad (1)$$

where ϕ represents any of the dependent variables, Γ_ϕ is the turbulent diffusion exchange coefficient, and the source S^ϕ contains any remaining terms. The contents of the source terms are given in Table 1.

The standard k-ε model formulation developed by Jones and Launder[19] is based on the modified Boussinesq relationship, in which the Reynolds stresses assume the form

$$\rho\overline{u_i u_j} = \frac{2}{3}\delta_{ij}(\rho k) - \mu_t(\frac{\partial U_i}{\partial x_j} + \frac{\partial U_j}{\partial x_i}) \qquad (2)$$

An isotropic effective viscosity is defined as

$$\mu_{eff} \equiv \mu_t + \mu_l$$

The isotropic turbulent viscosity μ_t appearing above, is defined in terms of a characteristic length and velocity. If this length is taken as the turbulence length scale $k^{3/2}/\varepsilon$, and the velocity as the turbulent velocity scale $k^{1/2}$, μ_t can be expressed as

$$\mu_t \equiv C_\mu \rho k^2/\epsilon$$

where C_μ is an empirical constant. The distribution of k and ε is determined

Table 1 The form of the source term in the general equation for ϕ

ϕ	S^{ϕ}
U	$-\frac{\partial P}{\partial x}+S^{u}$
V	$-\frac{\partial P}{\partial r}+\frac{\rho W^{2}}{r}-\frac{2\mu V}{r^{2}}+S^{v}$
W	$-\frac{\rho V W}{r}-\frac{W}{r^{2}}\frac{\partial}{\partial r}(r\mu)$
k	$G-C_{D}\rho\epsilon$
ϵ	$(C_{1}\epsilon G-C_{2}\rho\epsilon^{2})/k$

where

$$S^{u}=\frac{\partial}{\partial x}(\mu\frac{\partial U}{\partial x})+\frac{1}{r}\frac{\partial}{\partial r}(r\mu\frac{\partial V}{\partial x})$$

$$S^{v}=\frac{\partial}{\partial x}(\mu\frac{\partial U}{\partial r})+\frac{1}{r}\frac{\partial}{\partial r}(r\mu\frac{\partial V}{\partial r})$$

$$G=\mu[2\{(\frac{\partial U}{\partial x})^{2}+(\frac{\partial V}{\partial r})^{2}+(\frac{V}{r})^{2}\}+(\frac{\partial U}{\partial r}+\frac{\partial V}{\partial x})^{2}+\{r\frac{\partial}{\partial r}(\frac{W}{r})\}^{2}+(\frac{\partial W}{\partial x})^{2}]$$

and μ is the effective viscosity

from the solution of semi-empirical transport equations

$$U_j \frac{\partial k}{\partial x_j} = P - \epsilon + \frac{\partial}{\partial x_j}((\nu_l + \frac{\nu_t}{\sigma_k})\frac{\partial k}{\partial x_j}) \tag{3}$$

$$U_j \frac{\partial \epsilon}{\partial x_j} = C_1 \frac{\epsilon}{k} P - C_2 \frac{\epsilon^2}{k} + \frac{\partial}{\partial x_j}((\nu_l + \frac{\nu_t}{\sigma_\epsilon})\frac{\partial \epsilon}{\partial x_j}) \tag{4}$$

where the production of turbulence kinetic energy P is given by

$$P = -\overline{u_i u_j}(\frac{\partial U_i}{\partial x_j}) \tag{5}$$

and C_1 and C_2 are two constants evaluated,respectively,by reference to near-wall turbulence and decay of grid turbulence. Comparison of the modeled k-ε equations with their exact analogs shows that the turbulent kinetic energy expressions retain much of their original physical meaning whereas this is not true for the dissipation equation. Probably the weakest point in the closure of the problem by the model is the determination of the turbulent kinetic energy dissipation rate ε.

The computational domain with an extremely coarse uniform grid is shown in Fig.2. Observe that the domain includes only a single cavity of a seal. Naturally it would be preferable to include all cavities, however computational resource limitations preclude this possibility. Figure 3 shows a magnified view of a small portion of the grid, showing a typical grid point at an arbitrary intersection of the grid lines. All variables except U and V are calculated at these grid points. The U and V variables are calculated at the arrows which lie on the faces of the control volume centered at point P.

Discretization is based in all cases on the control volume approach which ensures that the conservation principle embodied in the continuum equations is preserved in the numerical analog. Following this approach, the differential equation is formally integrated over the appropriate control volume shown in

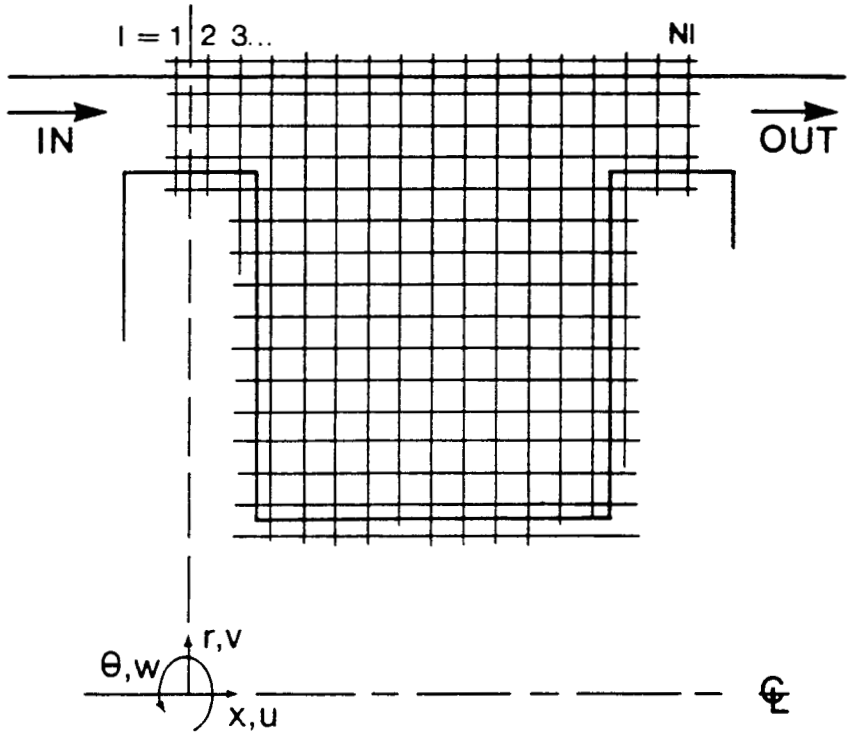

Fig. 2 Computational domain with a coarse uniform grid

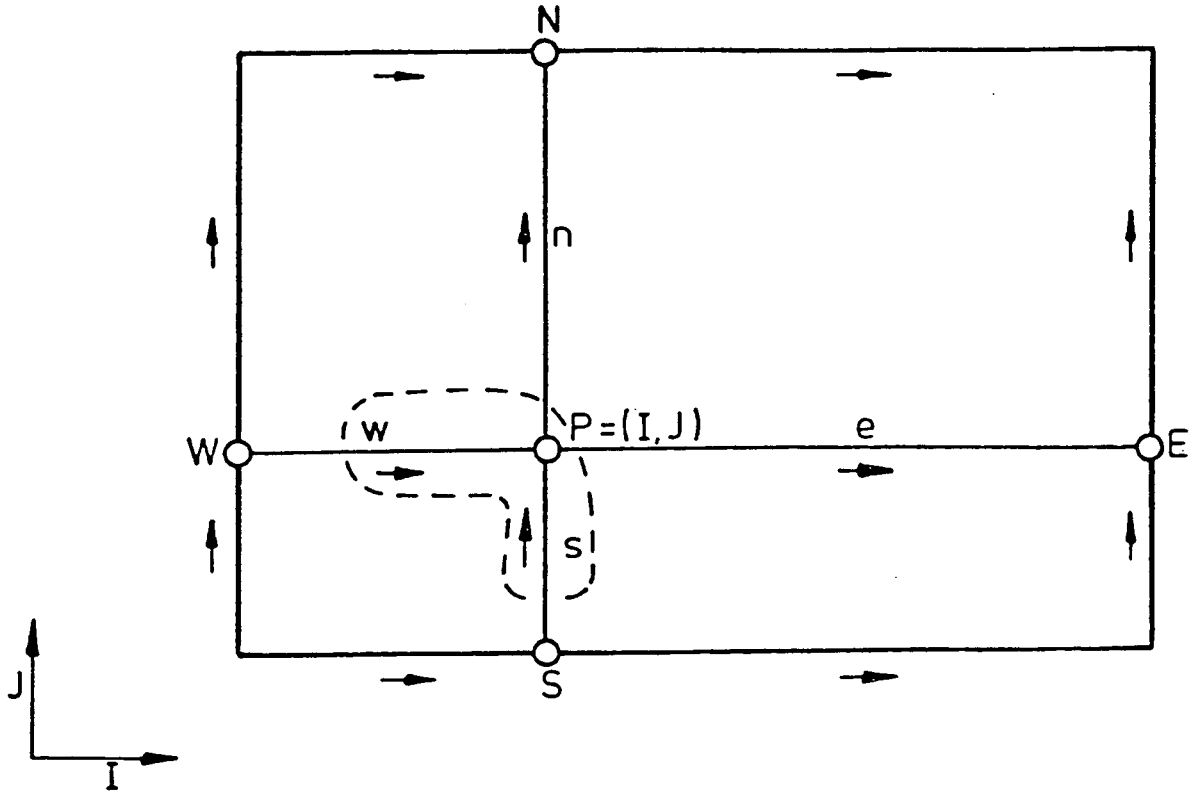

THREE GRIDS: FOR P,W ETC. — AT POSITION MARKED (O)
FOR U VELOCITY - AT POSITION MARKED (→)
FOR V VELOCITY - AT POSITION MARKED (↑)

Fig. 3 Magnified view of the staggered grid and notation

Fig.4 by applying the Gauss theorem. The result is

$$\{\rho U\phi - \Gamma_\phi \frac{\partial \phi}{\partial x}\}_e A_e^\phi - \{\rho U\phi - \Gamma_\phi \frac{\partial \phi}{\partial x}\}_w A_w^\phi$$

$$+\{\rho V\phi - \Gamma_\phi \frac{\partial \phi}{\partial r}\}_n A_n^\phi - \{\rho V\phi - \Gamma_\phi \frac{\partial \phi}{\partial r}\}_s A_s^\phi = S^\phi \cdot Vol \qquad (6)$$

where the A's represent the areas of the cell faces in four compass-point directions (n,e,s,w) located mid-way between the grid points. Each convected quantity ϕ in the convection terms of the difference equations is evaluated using the appropriate interpolation formula. Upon collecting terms the finite difference form of the generic differential equation can be obtained

$$B_P^\phi \phi_P = \sum_j B_j^\phi \phi_j + S_u^\phi \qquad (7)$$

$$B_P^\phi = \sum_j B_j^\phi - S_P^\phi$$

$$j = E, W, N, S, EE, WW, NN, SS$$

The B's are coefficients consisting of contributions from diffusion and convection and the S's are the linearized source terms. Obviously, the B's and S's are uniquely formulated for each differencing scheme.

According to the SIMPLER (Semi-Implicit Method for Pressure Linked Equations Revised) algorithm of Patankar [20], the pressure field is obtained from the pressure equation which is derived from the continuity and momentum equations. Next, the axial and radial momentum equations are solved for U and V velocity components, respectively. Then, in order to conserve mass locally, the correction of velocity is accomplished with the pressure- correction equation, which is also derived from the continuity and momentum equations. Finally the swirl momentum as well as the k and ε equations are solved. Further details can be found in reference [20].

The discretization equations are linear and are solved line-by-line using the tridiagonal matrix algorithm (TDMA) applied in an ADI (Alternating

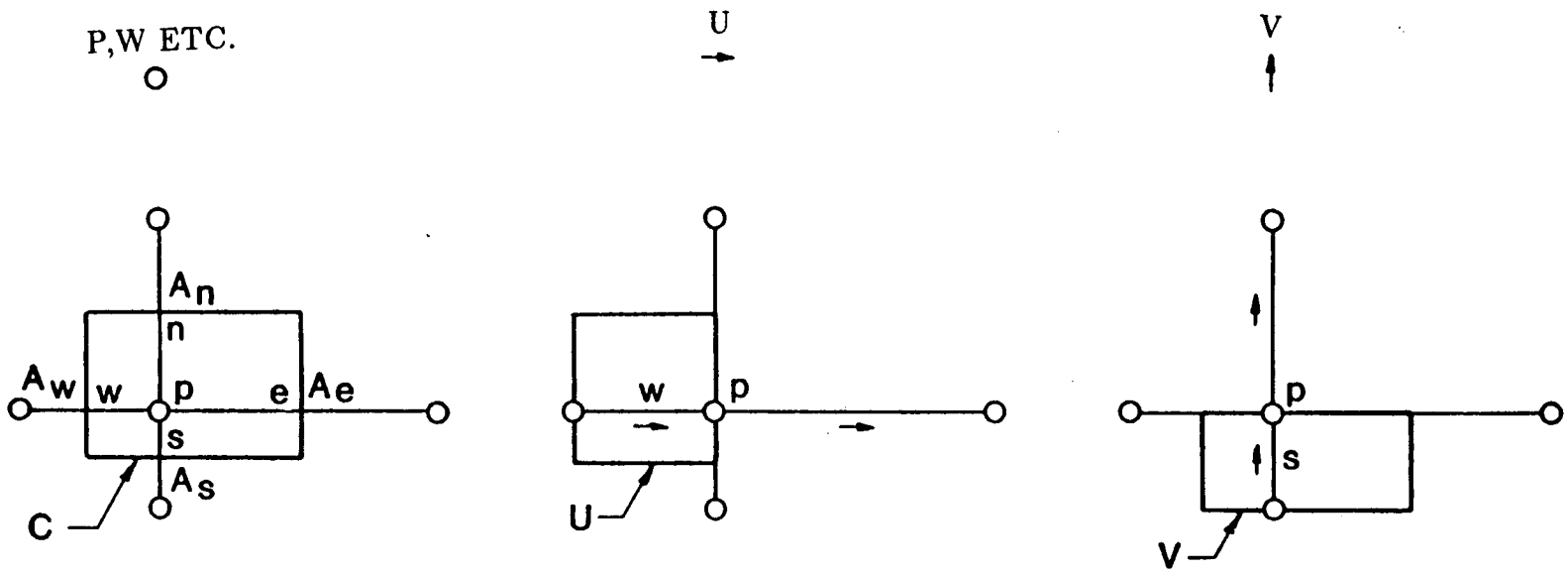

CONTROL VOLUMES C,U,V. FACE
AREAS A_n, A_s, A_e AND A_w FOR C, SIMILAR FOR U AND V

Fig. 4 The three control volumes associated with points of the three grids.

Direction Implicit) manner. Boundary conditions are incorporated into the finite difference equations for the computational cells having a face which lies on a boundary. During each iteration, the inlet boundary values for each dependent variable except pressure are taken as the corresponding outlet values after accounting for the difference in flow area between the inlet and the outlet. Since convection dominates over diffusion at the exit, no outlet boundary values are needed due to the upwind nature of the flow. However, the exit axial velocity values are adjusted so as to conserve mass over the entire domain. For velocity components normal to a wall, zero values are specified whereas for velocities tangential to a wall, the quantity $\mu_{eff} \frac{\partial \phi}{\partial n} A$ on the boundary is specified via the popular Law of the Wall as a wall function.

Implementation of the QUICK Scheme

False diffusion is a second-order truncation numerical error. Under certain conditions it can become a significant source of inaccuracy. The upwind differencing component of the Hybrid upwind/central differencing scheme introduces this error. It is generally found in flow regions exhibiting streamline-to-grid skewness and diffusive transport normal to the flow direction where convection dominates diffusion.

The QUICK scheme developed by Leonard [3] reduces false diffusion by introducing a quadratic upwind-shifted interpolation formula for evaluating dependent variables at each face of a control volume. With reference to Fig.5, the QUICK three-point formula for a west face, for example, using a uniform grid for simplicity is

$$\phi_w = \begin{cases} \frac{1}{2}(\phi_W + \phi_P) - \frac{1}{8}(\phi_{WW} + \phi_P - 2\phi_W), & \text{if } U_w > 0 \\ \frac{1}{2}(\phi_W + \phi_P) - \frac{1}{8}(\phi_E + \phi_W - 2\phi_P), & \text{if } U_w < 0 \end{cases}$$

The first term in these expressions represents the centered difference formula and the second is the upstream-weighted

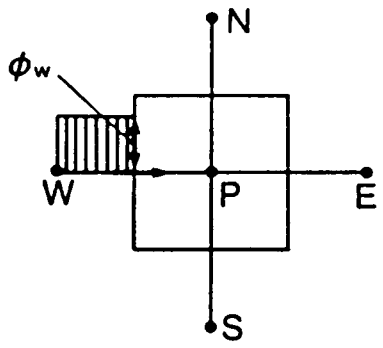

(a) Upwind differencing concept

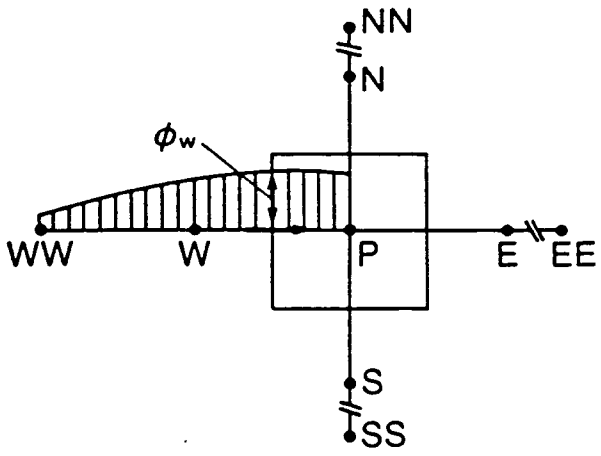

(b) QUICK differencing concept

Fig. 5 Illustration of (a) Upwind and (b) QUICK differencing concepts for evaluating ϕ at the west face of a control volume with flow from left to right.

curvature contribution. The interpolation expressions actually implemented were formulated for an arbitrary non-uniform grid spacing.

Previously, only the momentum difference equations were formulated using the QUICK scheme [3], while the k and ε equations employed the Hybrid scheme.This was justified by, for example, Leschziner and Rodi [21] who found that the solution values for k and ε using the QUICK and Hybrid schemes were the same. Further, these two equations are source-term dominated. The present work scrutinizes this contention. This required the development of a new version of the code which includes the QUICK scheme for the k and ε equations. The modification involved expressing each convective quantity ϕ in the convection terms of the k and ε difference equations using the QUICK interpolation expression. Upon implementing QUICK into these equations, numerical convergence became so unstable that a converged solution could not be achieved [22], even with very low under-relaxation factors. Since then the more stable SIMPLER (Semi—Implicit Method for Pressure-Linked Equations Revised) solution strategy of Patankar [20] has replaced the SIMPLE approach. Thus converged solutions using QUICK for all equations have become possible.

Extended Wall Function

In turbulent flows the direct influence of molecular viscosity is important only in a very thin layer adjacent to a wall. In the region where the direct effect of molecular viscosity is negligible, the simple law of the wall predicts a logarithmic velocity distribution. For a two-dimensional wall flow, an assumption in the derivation of the simple law of the wall is that the shear stress in the thin layer near the wall is constant and equal to the wall value. However, in three-dimensional boundary layers, it has been found that significant changes occur close to the wall. When the velocity increases rapidly with distance from the wall in such turbulent flows, the effect of the inertial forces on shear stress variation appears to be far from negligible. Several attempts have previously been made to derive formulae for the velocity

distribution near the wall which are more accurate than that given by the simple law of the wall. To obtain useful extended laws of the wall, inertial effects as well as pressure gradient effects should be accounted for.

Van Den Berg [23] derived such an extended law of the wall which includes both effects. It is valid only when the deviation from the simple law of the wall is not large, that is when the variation in shear stress with distance from the wall is small. This results from the fact that Van Den Berg utilized the simple law in approximating the inertia terms. Van Den Berg assumed that the velocity is determined completely by the wall distance and the local wall shear stress vector. Consequently, the contribution of the inertial terms could be deduced from the local wall shear stress gradients. The final formula for the dimensionless velocity in log-law coordinates is

$$U_X^+ = \frac{1}{\kappa}[\ln y^+ + A + \frac{1}{2}\alpha_x y^+ + \frac{1}{2}\beta_x \frac{(\ln y^+)^2 y^+}{\kappa^2}] \tag{8}$$

where

$$U_X^+ = U_X/U_\tau \qquad \alpha_x = \frac{\nu}{\rho U_\tau^3}\frac{\partial P}{\partial X}$$

$$U_\tau = (\tau_t/\rho)^{1/2} \qquad \beta_x = \frac{\nu}{U_\tau^2}\frac{\partial U_\tau}{\partial X}$$

$$y^+ = \frac{yU_\tau}{\nu}$$

and the X-axis is taken in the local wall shear stress direction.
The velocity increment in the viscous sublayer and the change in the direction are accounted for by the constant A which is taken equal to 2. In this study the above equation is applied to a two- dimensional axisymmetric flow.

As mentioned earlier, wall functions are used to implement boundary values for diffusive terms. For the case of a wall boundary located along a line of constant radius for example, the total tangential wall shear stress $\tau_t = (\tau^2_{rx} + \tau^2_{r\theta})^{1/2}$ is obtained from

$$U_X(\tau_k\rho)^{1/2}/\tau_t = \frac{1}{\kappa}[\ln y^+ + A + \frac{1}{2}\alpha_x y^+ + \frac{1}{2}\beta_x \frac{(\ln y^+)^2 y^+}{\kappa^2}] \tag{9}$$

where τ_k is an approximation for τ_t very near the wall. The quantity τ_k is approximated from the kinetic energy equation upon neglecting convection and diffusion terms in the near wall region. The result is

$$\tau_k = (C_D C_\mu)^{1/2}\rho k \tag{10}$$

Thus one obtains τ_t from eq.(9)

$$\tau_t = \kappa \frac{U_X C_\mu^{1/4} C_D^{1/4} \rho k^{1/2}}{[\ln y^+ + A + \frac{1}{2}\alpha_x y^+ + \frac{1}{2}\beta_x \frac{(\ln y^+)^2 y^+}{\kappa^2}]} \tag{11}$$

The τ_{rx} component of τ_t is given by

$$\tau_{rx} = \mu_{eff}(\frac{\partial U}{\partial r} + \frac{\partial V}{\partial x}) \tag{12}$$

However in the near-wall region $\frac{\partial V}{\partial x}$ approaches zero. Hence the desired wall function expression for the diffusion flux for the x-momentum equation is

$$\mu_{eff}\frac{\partial U}{\partial r} = \kappa \frac{U C_\mu^{1/4} C_D^{1/4} \rho k^{1/2}}{[\ln y^+ + A + \frac{1}{2}\alpha_x y^+ + \frac{1}{2}\beta_x \frac{(\ln y^+)^2 y^+}{\kappa^2}]} \tag{13}$$

IV. EXPERIMENTAL VERIFICATION

In order to assess the potential refinements resulting from the previously discussed developments, comparison with detailed distributions of measured quantities of a related flowfield was undertaken. The measurements of the flow across a rectangular wall cavity by Sinha [24] were chosen as the test case.

The Flowfield Considered

The flow geometry is shown in Fig.6. The experiment [24] was conducted in a low speed wind tunnel. A constant-temperature hot-wire anemometer was used. The breadth of the cavity along the span of the test section was uniform. The computational domain was overlaid with a 42 X 60 nonuniform grid in the x- and r-directions, respectively. The free stream velocity was 10.02 m/sec and the experiment was performed at a Reynolds number based on cavity inlet velocity and cavity width of 1.9×10^4. The boundary conditions at the domain inlet as well as the free stream included the measured values for U. Inlet values for k were estimated from measurements of $\overline{u^2}$ assuming isotropic turbulence.

Effect of QUICK on the k and ε Equations

There are three solutions to be compared. The solution MQ (Momentum equations using QUICK) is obtained when QUICK is applied to solve the U,V and W momentum equations, whereas Hybrid upwind/central differencing is used for the k and ε equations. The solution AQ (All equations using QUICK) is obtained when QUICK is employed for not only the momentum equations but also for the k and ε equations. The solution AQEWF (All equations using QUICK with Extended Wall Function) was obtained upon adding the new extended wall function.

As shown in Figs. 7 and 8, the solutions AQ and MQ are compared with experimental measurements [24] to show the effect of QUICK on the k and ε equations. The axial velocity distributions are shown in Fig.7, which reveals no significant difference between the two solutions. Also, the predicted

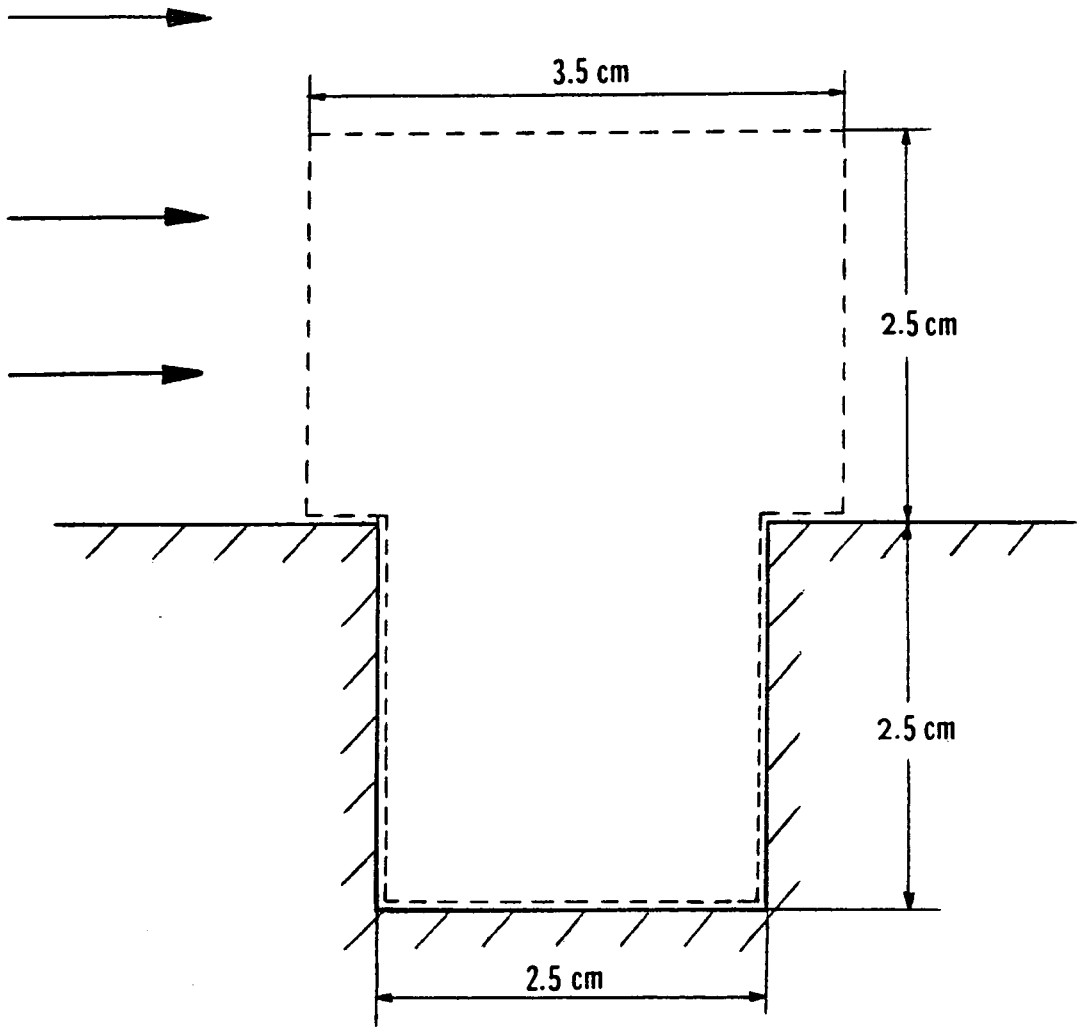

Fig. 6 Computational domain (- - -) for the wall cavity flowfield measured by Sinha [24]

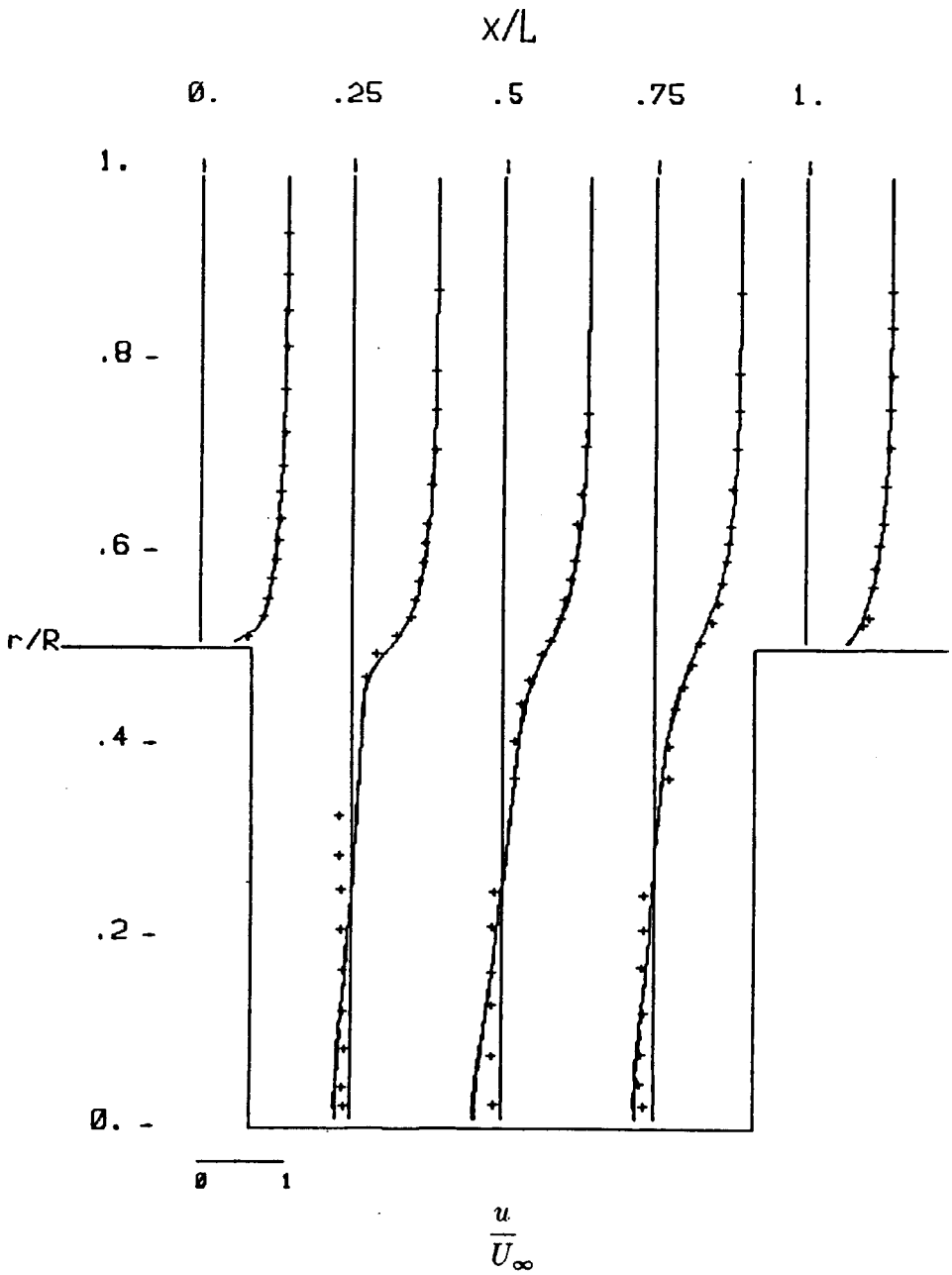

Fig. 7 Mean axial velocity distribution showing predictions using : (a) QUICK for all equations (—) and (b) QUICK only for the momentum equations (- - -) along with previous measurements [24] (+ + +)

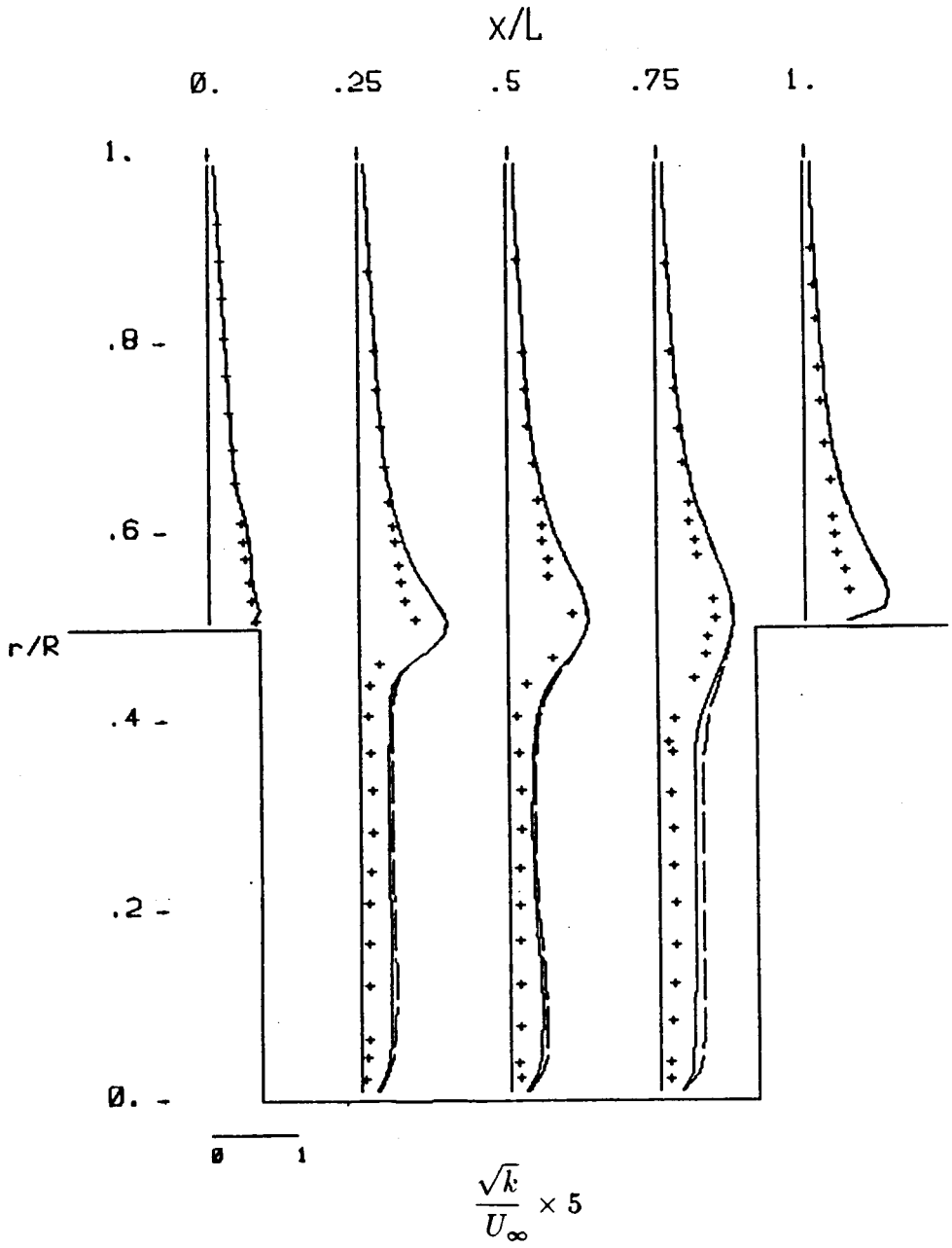

Fig. 8 Turbulence kinetic energy distribution showing predictions using : (a) QUICK for all equations (—) and (b) QUICK only for the momentum equations (- - -) along with previous measurements [24] (+ + +)

solutions indicate generally good agreement with measurements. Fig.8 exhibits turbulence kinetic energy distributions. Note that there are deviations here between the AQ and MQ solutions inside the cavity region where significant streamline-to-grid skewness was expected. Compared with measurements, the solution AQ shows a small improvement. There are, however, more substantial differences between measurements and predictions. It is not clear if this is due to the lack of a stationary flow experimentally, or to some modeling inadequancy such as that inherent in the ε equation source terms.

Effect of the Extended Wall Function

In Figs.9 and 10, the solutions AQ and AQEWF are compared with measurements to examine the effect of the extended wall function. Observe that, at least for this case, the solution AQEWF is almost identical to the solution AQ. Apparently the Reynolds number of the flow considered here is too low to illuminate the effect of the extended wall function which includes pressure gradient and inertial effects.

The Stepped Labyrinth Seal Test Case

The measurements of Morrison et al. [25] for the tooth-to-tooth pressure distribution of stepped labyrinth seals flowing water were employed in a series of further prediction tests. In the experimental facility, a single static pressure tap was located at each tooth on the stator wall. The dimensionless flow parameters were $Re_x = 4.95X10^3$ and $Ta = 6.7X10^3$. The result for one case with six cavities is given in Fig. 11. The predicted value of bulk pressure drop per cavity for the streamwise periodic cavities was 105 kPa. This was translated into the predicted streamwise periodic pressure distribution, which was plotted by graphical construction using this slope while matching the pressure measured at the third tooth. Note that streamwise periodicity commences at approximately the third tooth. The measured pressure drop per cavity averaged 123 kPa in this region, yielding a discrepancy of under 15.0 percent.

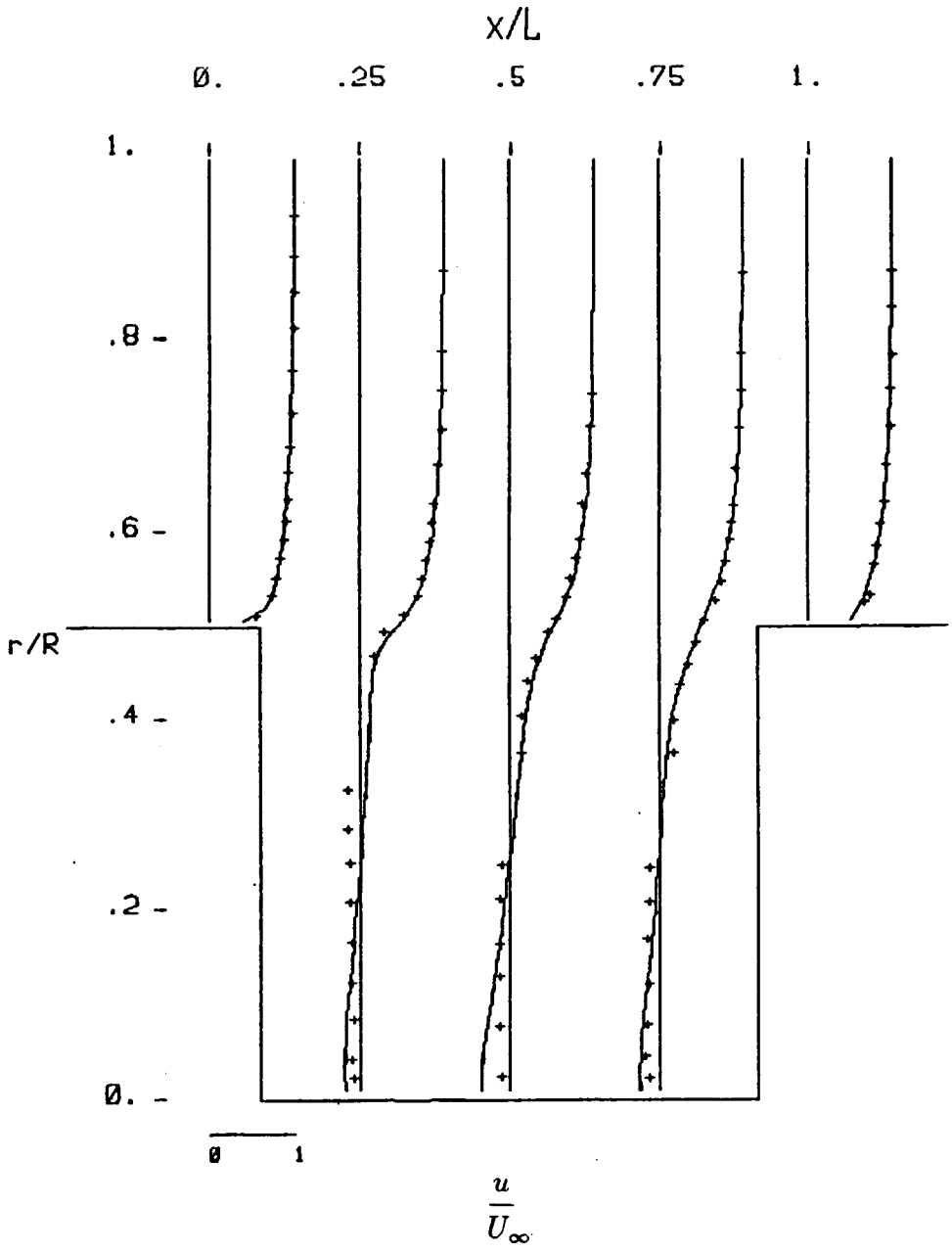

Fig. 9 Mean axial velocity distribution showing predictions using : (a) QUICK for all equations (—) and (b) QUICK for all equations with the extended wall function (- - -) along with previous measurements [24] (+ + +)

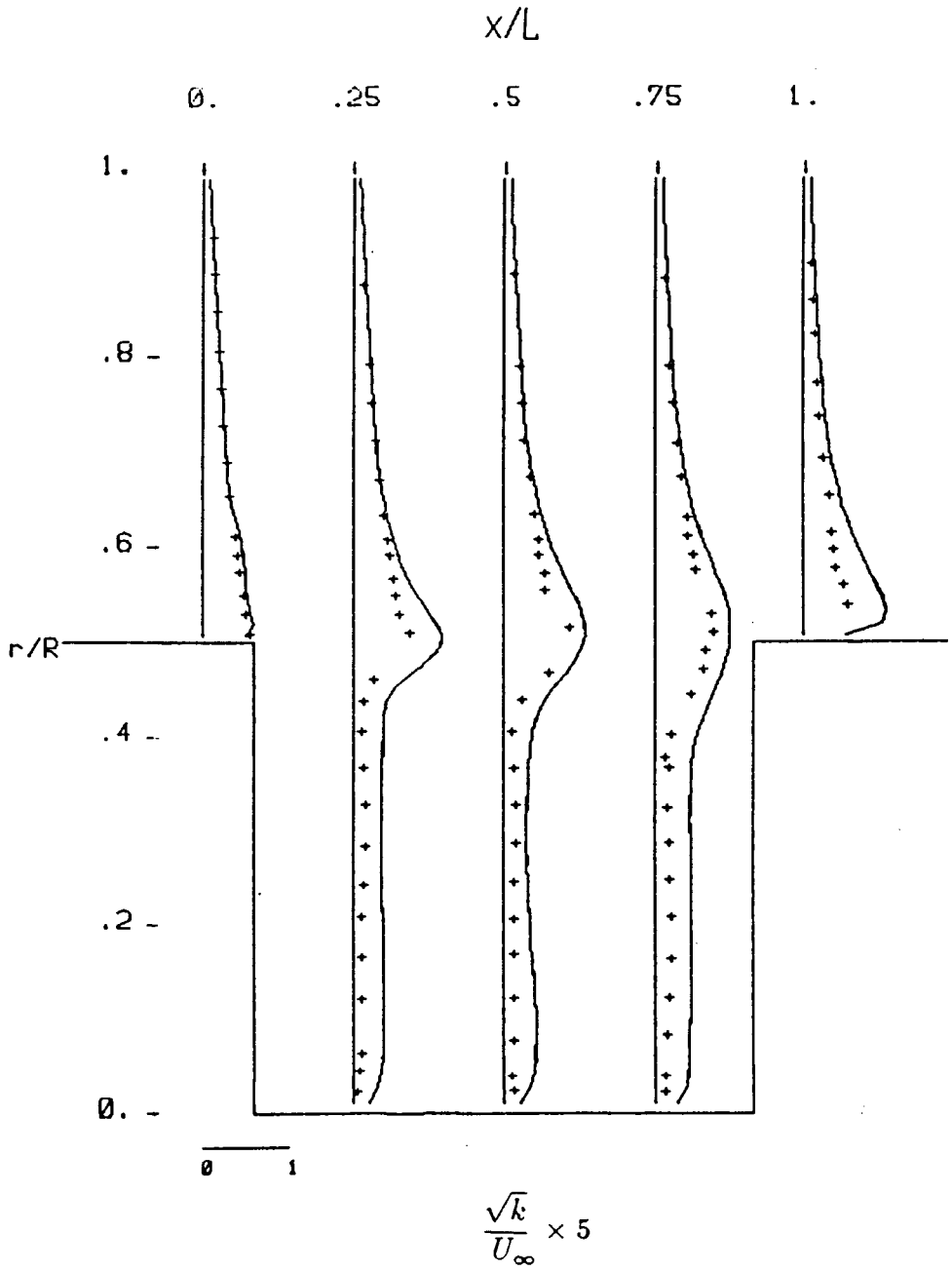

Fig. 10 Turbulence kinetic energy distribution showing predictions using : (a) QUICK for all equations (—) and (b) QUICK for all equations with the extended wall function (- - -) along with previous measurements [24] (+ + +)

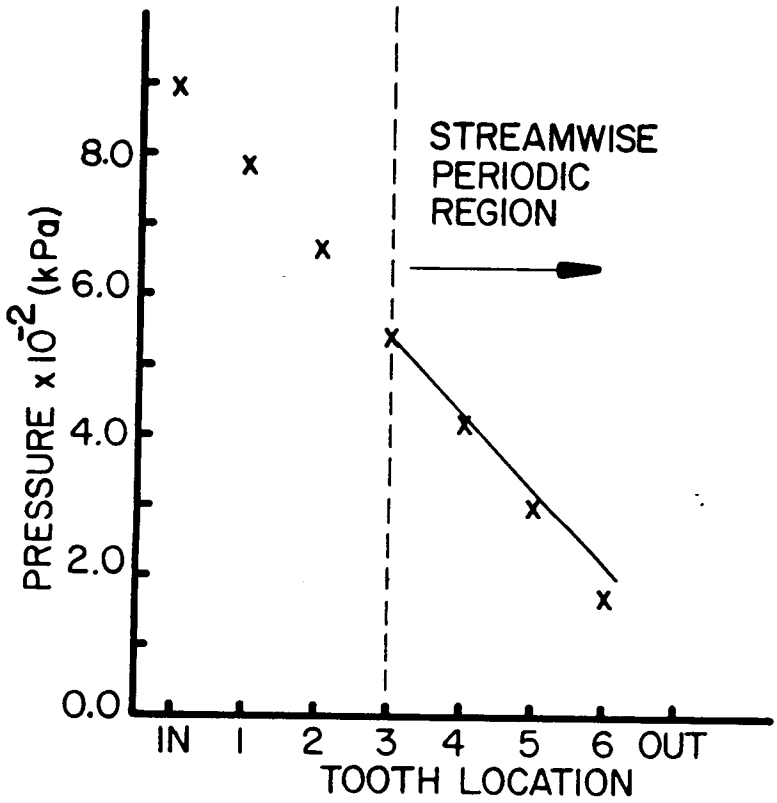

Fig. 11 Measured tooth-to-tooth pressure distribution (xxxx) illustrating the streamwise periodic prediction (———) constructed to match the measured pressure at the third tooth

V. SEAL DESIGN IMPROVEMENT

As mentioned earlier, the objective of this portion of the research program was to decrease the leakage through the wear ring seal on each impeller of the high pressure liquid hydrogen turbopump of the Space Shuttle. This seal is shown in Fig. 12. This objective was accomplished by utilizing the previously discussed finite difference computer code to predict the frictional characteristic for each of numerous relatively simple geometries for a single cavity of a stepped seal. Naturally one would prefer to include all of the seal cavities in a single computation, however present day computer CPU and storage constraints preclude this possibility. Thus a single cavity was numerically simulated for each seal design considered.

The numerical solution of such elliptic flow fields is quite expensive in terms of both CPU and storage requirements. As many cases as possible were run in attempting to optimize the design dimensions of a stepped seal. The computations were conducted in two phases. In Phase I a significant design constraint was relaxed. This constraint is the allowance for the present level of axial movement of the stator housing relative to the rotor as the pump starts from rest. By relaxing this constraint so that more cavities of smaller pitch could be used, the stator housing of the pump would have to be stiffened so as to give less movement. The Phase II computations allowed the current level of axial movement.

On several occasions the need arose to incorporate various extensions into the software. These refinements allowed much greater flexibility in generating grids which are amenable to a wider range of cavity geometries. The grid generation step was accomplished in a separate, user friendly pre-processor code.

Grid dependence tests were run for certain basic cavity configurations. One significant outcome is that the important flow throttling region of the downstream tooth can be resolved with seven grid lines of constant r. This is

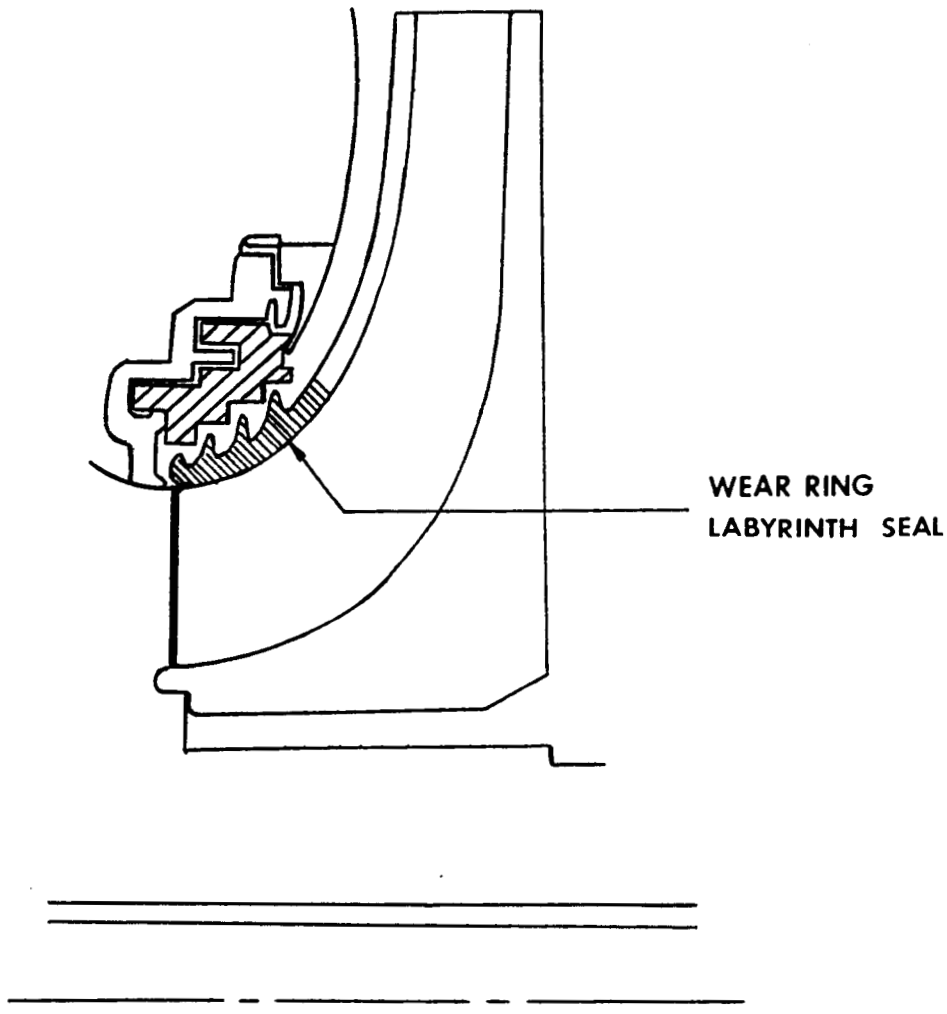

Fig. 12 Wear ring labyrinth seal being investigated

due to the fact that one solution using twelve grid lines and another using seven grid lines of constant r proved to be grid independent. Hence, seven grid lines of constant r were used in the clearance region above both the inlet and the outlet tooth.

Grid dependency is a function of grid point clustering as well as the total number of grid points; several rates of grid spacing expansion or contraction in each of several zones of the domain were tested for grid dependency. Depending on the particular dimensions of a given cavity, a grid size from 50 x 40 up to 50 x 90 in the x- and r- directions, respectively, was used. Also, approximately a seven percent rate of expansion or contraction in both coordinate directions within each of several grid regions was specified.

Preliminary computations revealed that the expected asymptotic invariance of the dimensionless solution for a typical cavity occurred near $Re_x \equiv 2\rho U_o c/\nu = 5.0 \times 10^4$ and $Re_\theta \equiv 2\rho W c/\nu = 2.03 \times 10^4$. Inasmuch as the seal leakage flow conditions in the actual pump application vary over a wide range of high Reynolds numbers, values of $Re_x = 7.0 \times 10^4$ and $Re_\theta = 2.03 \times 10^4$ were maintained throughout Phase I and Phase II computations.

Phase I Computations

As previously mentioned, the design objective here assumed that the pump housing can be modied to restrict the axial motion of the stator housing upon pump shut-down to essentially any value desired by the seal designer. Observe in the figure accompanying Table 2 that this distance moved upon shut-down must be less than $b - t_1/2$ in order to avoid the stator wall step of height s from impacting on the left-hand tooth.

Implementation of the QUICK differencing scheme into the k and ε transport equations was completed near the end of the Phase I computations. Thus this series of the computations was obtained using QUICK only in the momentum equations. The use of QUICK only for the momentum equations was supported by, for example, Leschziner and Rodi [21] who found that the solution values for k

TABLE 2. CAVITY DESIGN DIMENSIONS *

CAVITY TYPE

	A	B	C	D	E	F	G	H	I	J	K	L	M	N	O	P	Q	R	S	T
m	4.83	3.19	1.59	0.97	1.59	1.59	1.59	1.59	1.59	1.59	1.59	1.59	1.59	1.59	1.59	1.59	4.83	4.83	4.83	4.83
b	2.90	1.91	0.96	0.58	0.96	0.96	0.96	0.96	0.96	0.96	0.96	0.96	0.96	0.96	0.96	0.96	3.84	3.84	3.84	3.84
s	3.61	3.61	3.61	3.61	2.38	1.19	0.58	0.43	0.58	0.43	0.22	0.58	0.58	0.58	0.58	0.58	0.58	0.58	1.08	1.40
c	0.216	0.216	0.216	0.216	0.216	0.216	0.216	0.216	0.108	0.108	0.108	0.216	0.216	0.216	0.216	0.216	0.216	0.216	0.216	0.216
h	0.86	0.86	0.86	0.86	0.86	0.86	0.86	0.86	0.86	0.86	0.86	5.2	2.6	0.36	0.86	0.86	0.86	0.86	0.86	0.86
t_1	0.76	0.50	0.25	0.15	0.25	0.25	0.25	0.25	0.25	0.25	0.25	0.25	0.25	0.25	0.38	0.13	0.38	0.38	0.38	0.38
t_2	0.76	0.50	0.25	0.15	0.25	0.25	0.25	0.25	0.25	0.25	0.25	0.25	0.25	0.25	0.38	0.13	1.05	1.05	1.05	1.05
r_s	87.9	87.9	87.9	87.9	89.1	90.3	90.9	91.1	91.0	91.2	91.4	86.6	89.2	91.4	90.9	90.9	90.9	90.9	90.9	90.9
r	92.6	92.6	92.6	92.6	92.6	92.6	92.6	92.6	92.6	92.6	92.6	92.6	92.6	92.6	92.6	92.6	92.6	92.6	93.1	93.4
Stator Groove	NO	NO	NO	NO	NO	NO	NO	NO	NO	NO	NO	NO	NO	NO	NO	NO	NO	YES	YES	YES
t_3	-	-	-	-	-	-	-	-	-	-	-	-	-	-	-	-	-	0.21	0.21	0.21
l_s	-	-	-	-	-	-	-	-	-	-	-	-	-	-	-	-	-	0.59	0.59	0.59

* All dimensions are in mm.

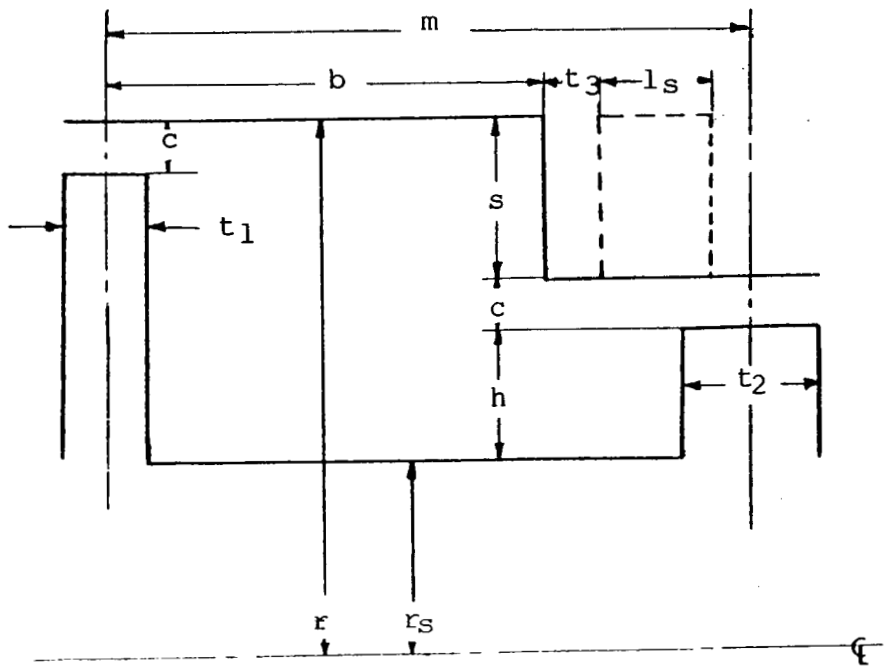

ORIGINAL PAGE IS
OF POOR QUALITY

and ε using the QUICK and Hybrid schemes were the same.

It is reasonably clear from the open literature that the best value of tooth clearance c is the smallest value which is practical from rubbing considerations. It was decided to focus on the non-abradable type seals. At actual hydrogen operating conditions, the worst case or largest tooth clearance of the currently employed design was estimated by the manufacturer to be approximately 0.08 mm(0.0031 in). This is very small compared to the radial extent of most of the cavity designs considered. Thus appropriate finite difference grids gave either an excessive number of points or grid spacing expansion/contraction factors that were too large for practical use. In either case the numerical convergence rate, i.e. CPU time requirement, was impractical. It was found that a clearance value of 0.216 mm (0.0085 in) was computationally practical while also being a lower limit for the experimental testing due to machining tolerances. Therefore it was decided that most of the computations would use this larger value, and that important design effects would be computed again using the much smaller value of 0.108 mm (0.0043 in).

Stepped seals are considered here because it is widely known that they are generally more effective than straight-through seals, albeit their manufacturing cost is somewhat higher. The literature reviewed in ref. [25] shows that there was no information available concerning the effect of seal pitch, step height, tooth thickness and tooth height for stepped seals. Thus optimization of these rather basic design dimensions was undertaken in Phase I.

Detailed distributions of numerous flowfield quantities for each cavity configuration are very similar, and a sample will be presented later for the best configuration of Phase I. Before examining the effect of individually varying the basic design dimensions listed above, the overall character of a typical cavity flowfield is indicated by the streamline pattern shown in Fig. 13. This particular solution, obtained at the end of Phase I, used the QUICK scheme in all the equations. It exhibits the flow pattern for the Type 0 cavity

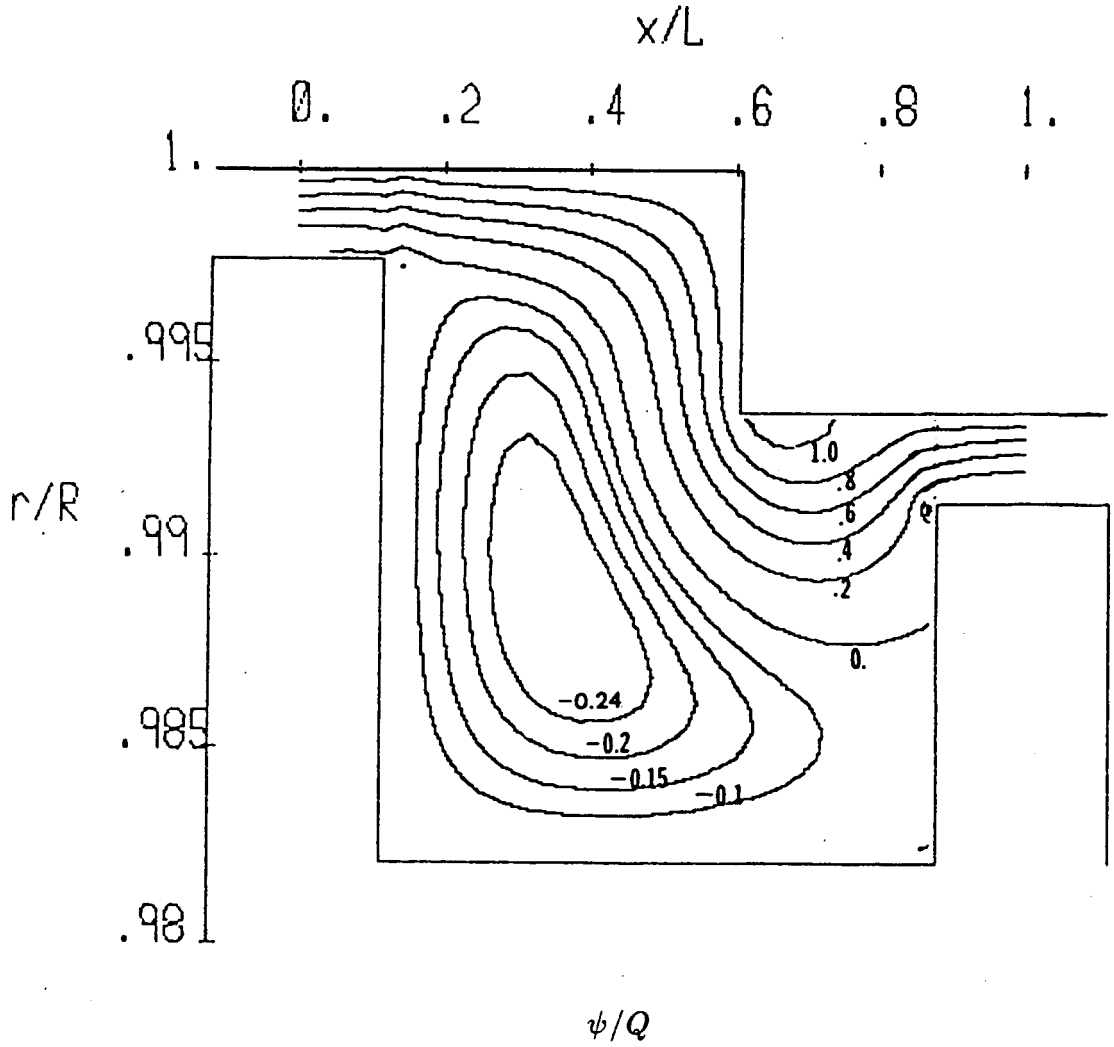

Fig. 13 Streamline pattern for the Type 0 cavity using QUICK for all equations

which is considered the best from Phase I. The flow here is from left to right, as this view is a mirror image of that in Fig. 12. Note that the dividing streamline has a reattachment stagnation point on the downstream tooth. Also, observe that the streamlines have a slope of nearly 45 degrees in the regions near x/L=0.5 and 0.65. In these regions one can expect significant levels of false diffusion when using upwind differencing for convection terms.

The first design variable investigated is the cavity pitch which is shown in the figure of Table 2. Egli's [9] equation for the case of compressible fluid leakage shows that the leakage mass flow is proportional to $1/\sqrt{n}$ where n is the number of throttlings. Thus a larger number of cavities of smaller pitch m would occupy the same space, and this was expected to give a reduced leakage characteristic. Figure 14 shows the dimensionless cavity inlet-to-outlet bulk pressure drop predicted using a fixed leakage rate for various values of m. The fixed leakage flow rate was specified and the corresponding ΔP was calculated rather than the reverse because this is more practical using the current computational methodology. The greater values of ΔP for the fixed leakage rate are the more desirable since they result from greater flow resistance. The more common statement regarding flow resistance is that lower leakage rates for a fixed pressure drop result from greater flow resistance. Thus an inverse design approach was employed wherein the desired performance was specified and the corresponding flow condition for each design was computed.

In Fig. 14, not only m, but all axial design dimensions of the cavity were altered by a constant scale factor. The remaining design variables were held constant for the four predictions shown. The Type A cavity with m/c = 22.35 corresponds to a seal of the original pitch with three cavities while that of Type D for m/c = 4.47 corresponds to a seal of fifteen cavities with a pitch one-fifth that of Type A. The complete design dimensions are found in Table 2. Comparing the relative changes of ΔP in the figure with the relative changes of $1/\sqrt{n}$, it was estimated that approximately nine cavities is near the optimum

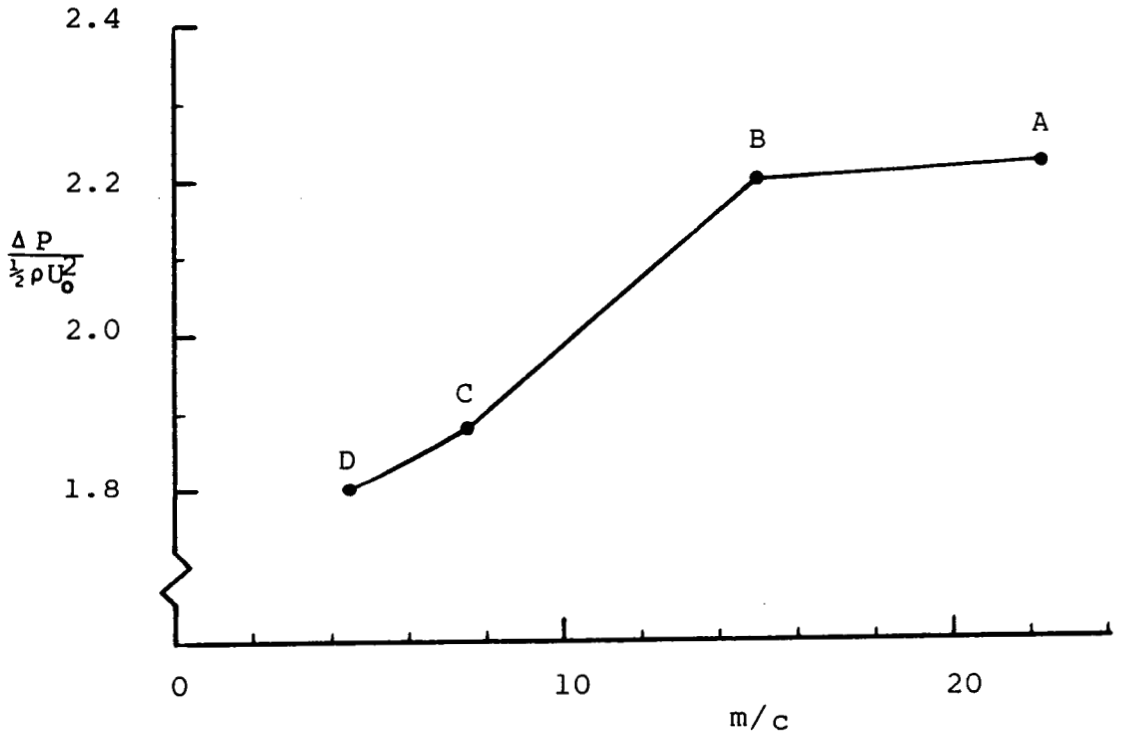

Fig. 14 Predicted effect of cavity pitch on bulk cavity inlet-to-outlet pressure drop for cavity Types A through D

choice. Thus the pitch m = 1.59 mm of Type C, one-third that of the currently used design, was used throughout the remainder of Phase I computations.

The second design dimension investigated is the step height s which is illustrated in the figure of Table 2. Figure 15 shows the substantial effect of step height on pressure drop. The seal design currently employed in the shuttle uses s = 3.61 mm as in Type C. Upon learning that step height is an important design variable, it was found that practical computations could be obtained using grids for a tooth clearance of 0.108 mm (0.0043 in), but only for the smaller step height cases. The results shown for a clearance of 0.216 mm (0.0085 in) indicate a rather large peak with a fairly sharp decrease for Type H. It was found that this peak shifts to the left as shown for the 0.108 mm (0.0043 in) value for clearance.

For each clearance the maximum value of pressure drop results from maximum turbulence generation, and in turn, maximum viscous dissipation of turbulence energy into heat. The detailed field predictions indicate that there are two opposing mechanisms involving step height. For step heights above the optimum, the radial velocity along the step exiting downward from the step corner at r/R = 0.993 (see Fig. 13) has a relatively low velocity. This is attributed to significant turbulent diffusion of radial momentum normal to the streamlines. This diminishes turbulence generation in the important region from x/L = 0.6 to x/L = 0.9. The opposing effect is that for short steps such as Type H, the leakage flow passes through the cavity without the sharply curved streamlines shown in Fig. 13 near the exit. This also reduces turbulence generation in this region. Type J with s = 0.43 mm (0.0169 in) is the recommended choice for the actual turbopump application. This is because it has the smaller clearance which is close to that of the turbopump at actual operating conditions. As mentioned earlier, the great majority of the design effects to be considered could not be computed or tested at the very tight clearance at actual running conditions. Hence the design optimization continued with Type G as the best

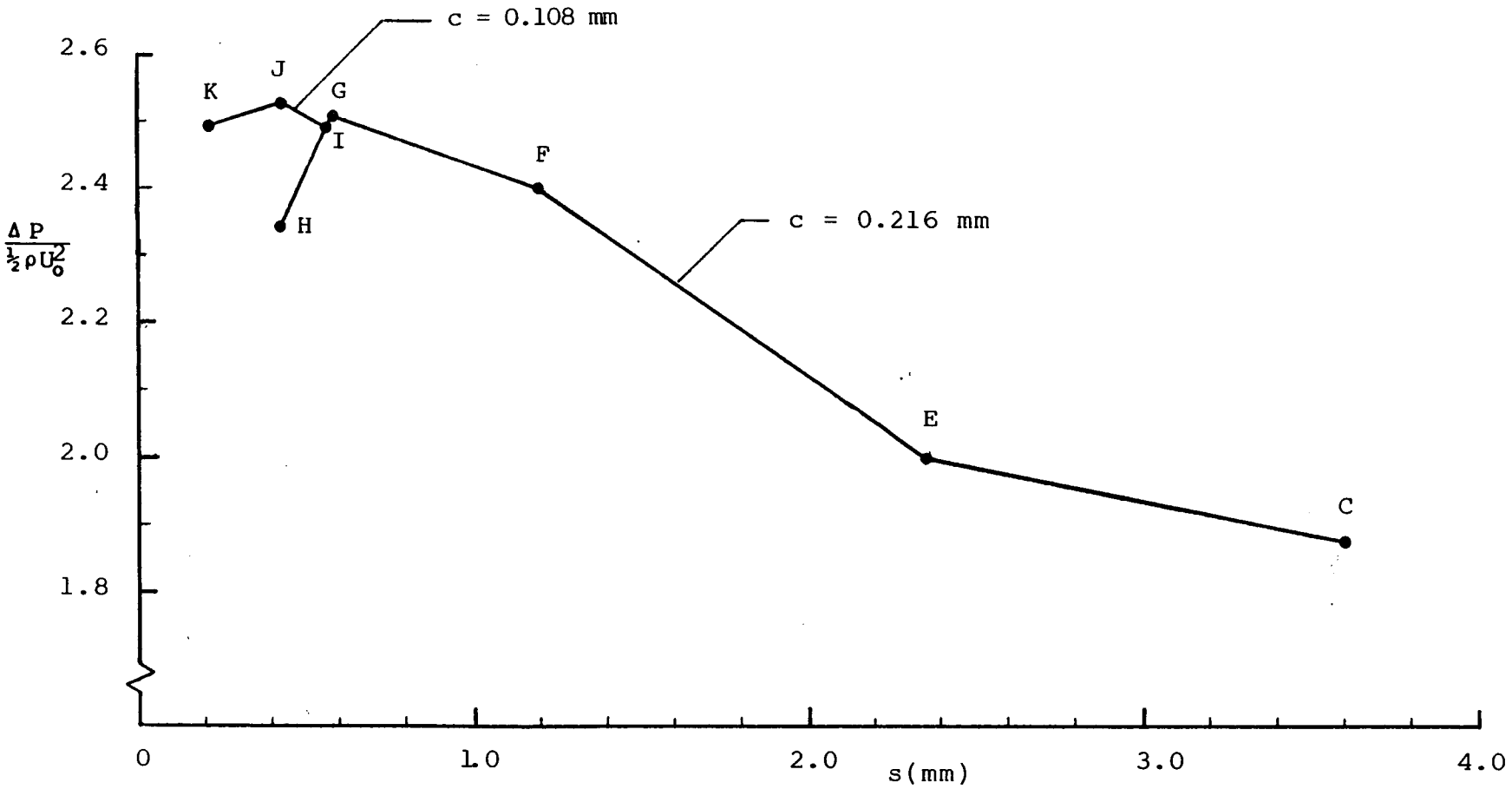

Fig. 15 Predicted effect of cavity step height on bulk cavity inlet-to-outlet pressure drop for cavity Types C and E through K

step height, noting the small difference in step height between Type J and Type G.

The effect of tooth height was investigated next while holding pitch and step height at the optimum values just shown. The values plotted for h/c in Fig. 16 are the height of the tooth at the flow exit from the cavity. The predicted cases shown indicate only a slight dependence of pressure drop on tooth height. Observe that the optimum choice here is Type G, which happens to have the same tooth height as that chosen for Types E through H in predicitng the best step height.

Maintaining the optimum values for pitch, step height and tooth height, the effect of tooth thickness was investigated next. Figure 17 shows a substantial decrease in pressure drop for t/c less than approximately 1.2. This is attributed to the more gradual curvature of the leakage flow streamlines shown in Fig. 13. As stated previously, the tightly curved streamlines are expected to give more turbulence energy generation.

The final effect investigated in Phase I was that of adding a cavity to the stator wall of the Type 0 cavity shown in Fig. 13. The stator cavity extended axially from $x/L = 0.12$ to $x/L = 0.6$, and radially it extended a distance of 0.648 mm (0.0255 in) above the stator wall. The predicted pressure drop was identical to that of Type 0 and thus this alternative was abandoned.

The Type 0 cavity was selected for experimental verification and was denoted seal #2 for that portion of the investigation. The seal currently employed in the turbopump was tested earlier for comparison purposes and was denoted seal #1.

Effect of QUICK on the k and ε Equations for a Seal

The implementation of QUICK into the k and ε difference equations was conducted and evaluated while the Phase I study was in progress. This refinement to the finite difference code was discussed in the previous chapter where quantitative comparisons were shown. The Phase II study employed this new

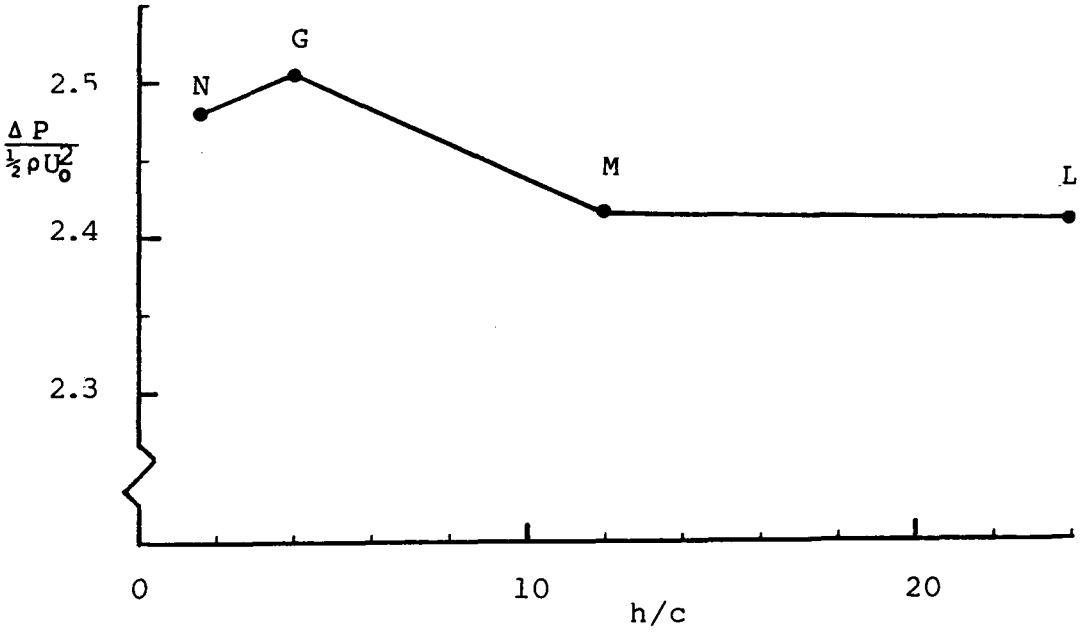

Fig. 16 Predicted effect of cavity exit tooth height on bulk cavity inlet-to-outlet pressure drop for cavity Types G and L through N

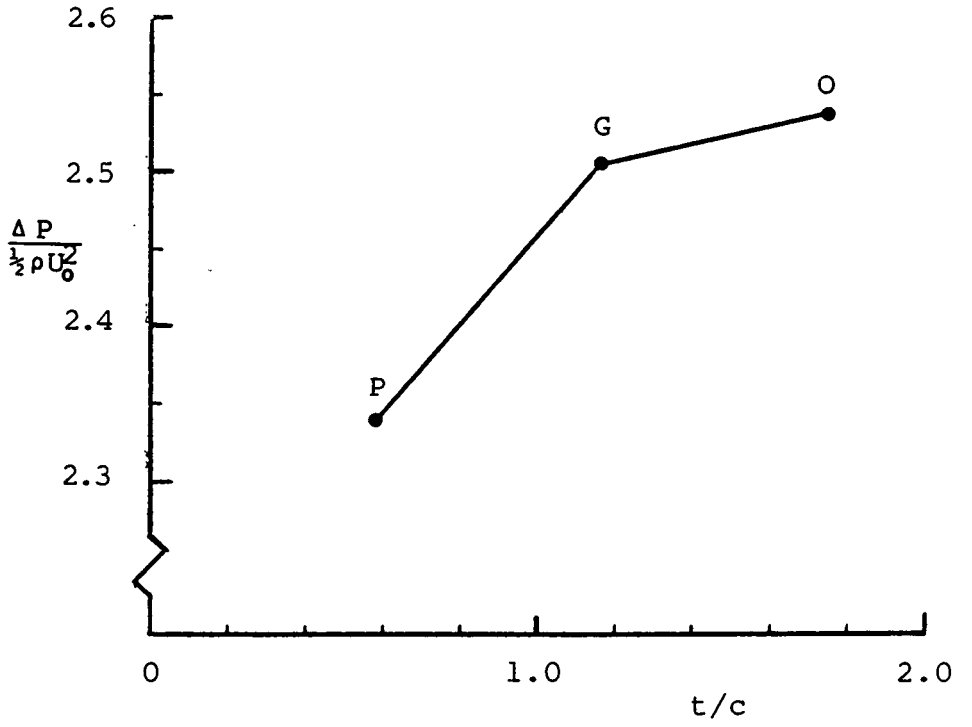

Fig. 17 Predicted effect of tooth thickness on bulk cavity inlet-to-outlet pressure drop for cavity Types O,G and P

version of the code. To determine the effect of QUICK on the k and ε equations applied to an actual seal, further computations were conducted for the Type 0 seal which had been optimized by previous MQ computations (only momentum equations using QUICK).

The axial velocity distributions from the AQ and MQ solutions shown in Fig.18 indicate that most deviations occur near x/L = 0.5 and 0.65, where false diffusion was expected. Based on the wall cavity test case results shown earlier, along with the fact that QUICK (barring the presence of wiggles in the solution) generally involves reduced false diffusion, the AQ solution is considered to be the more realistic. Figure 19 gives the radial velocity distributions which reveal that the values for solution AQ are smaller than those of the solution MQ at every location except at r/R=0.99 and x/L=0.7, where false diffusion effects are expected. The distribution of pressure relative to the inlet value P_o is shown in Fig. 20. The solution AQ predicts a larger pressure drop than the solution MQ by eight percent.

Far greater discrepancies were found, however, for turbulence kinetic energy which is shown in Fig. 21. The differences between these solutions are up to 50 percent of the values for the MQ solution. The location of maximum k is x/L=0.865 and r/R=0.992. The sharp streamline curvature shown in Fig.13 helps produce these high turbulence levels. Figure 22 shows the distribution of μ_{eff} which has deviations up to 100 percent of the solution values for MQ. These discrepancies are higher than those for k since μ_{eff} involves both k and ε values.

Phase II Computations

For this phase of the parametric study, a design is sought which could be used in the current turbopump without changing the axial movement of the stator housing relative to the rotor. This means that the axial location of the radial step should be fixed at about x/L = 0.8. It was decided that an important feature should be assessed before optimizing the step height s for this longer

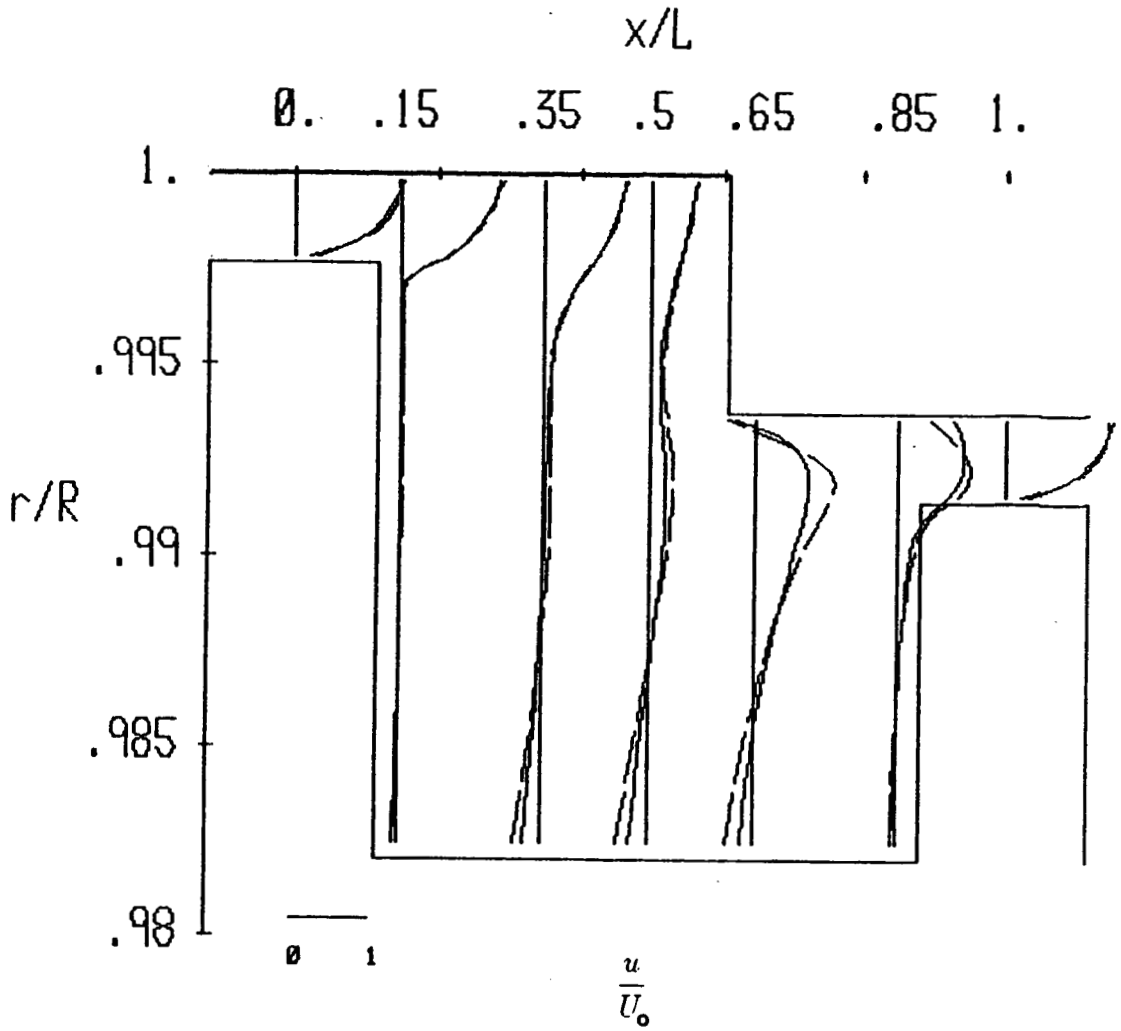

Fig. 18 Axial velocity distribution for the Type 0 cavity showing predictions using (a) QUICK for all equations (———) and (b) QUICK only for the momentum equations (-----)

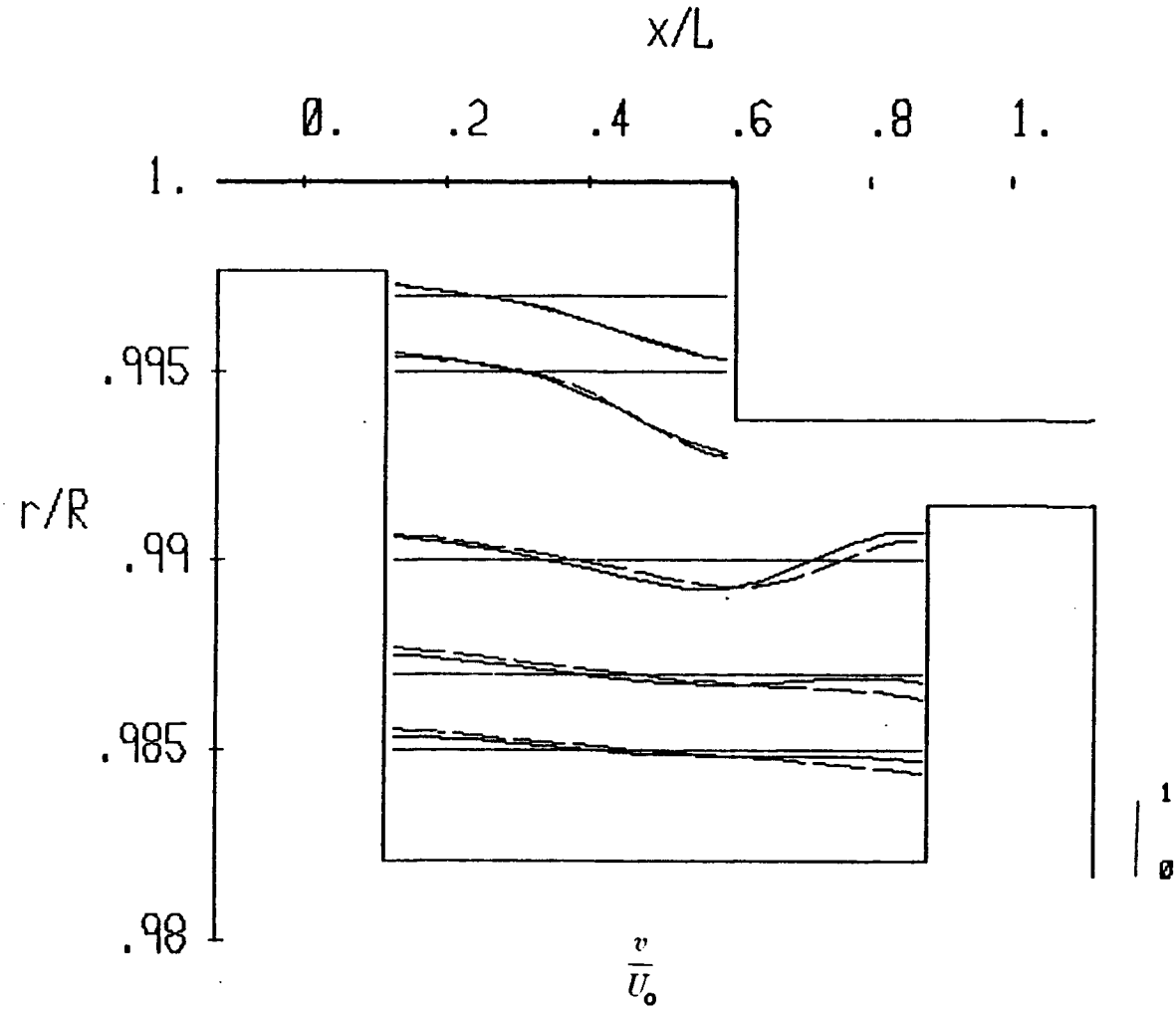

Fig. 19 Radial velocity distribution for the Type 0 cavity showing predictions using (a) QUICK for all equations (———) and (b) QUICK only for the momentum equations (----)

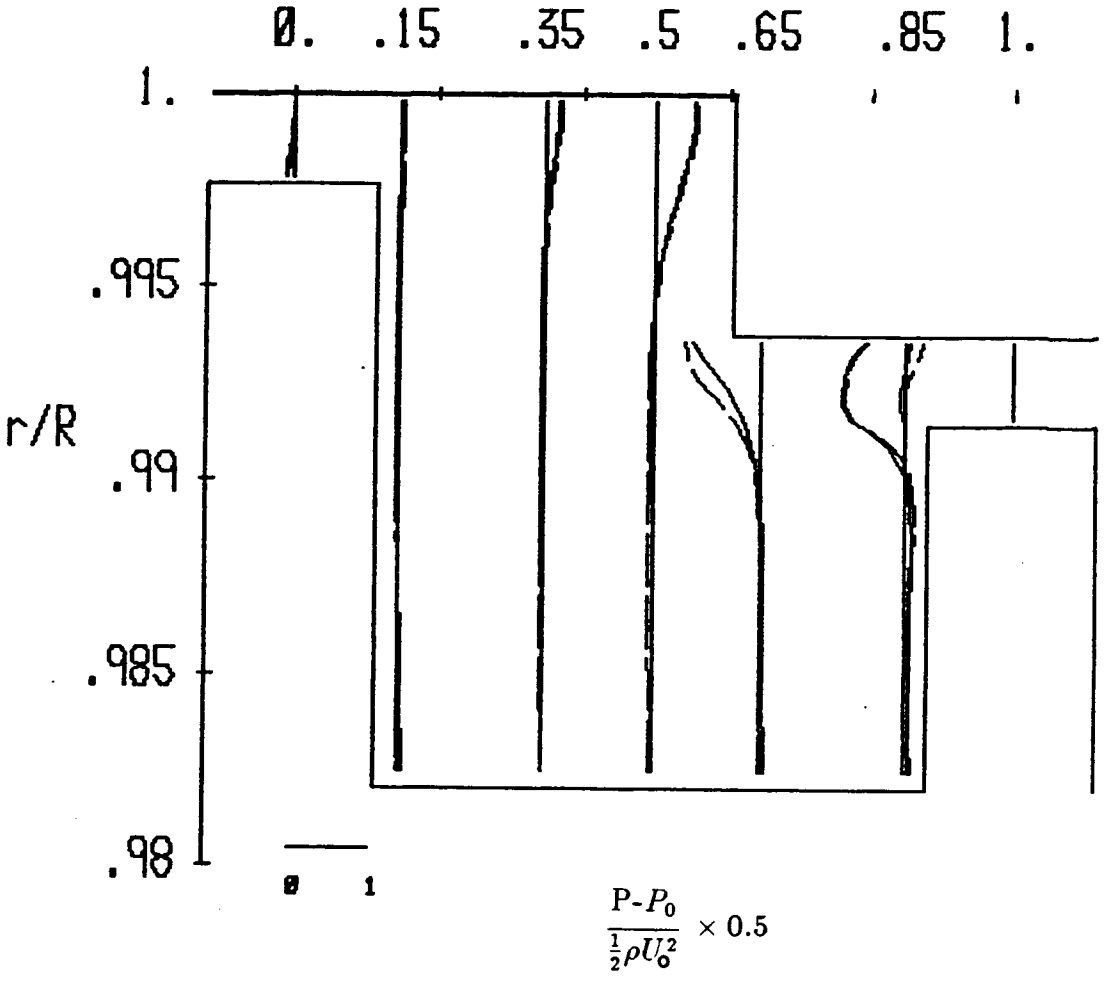

Fig. 20 Relative pressure distribution for the Type 0 cavity showing predictions using (a) QUICK for all equations (——) and (b) QUICK only for the momentum equations (----)

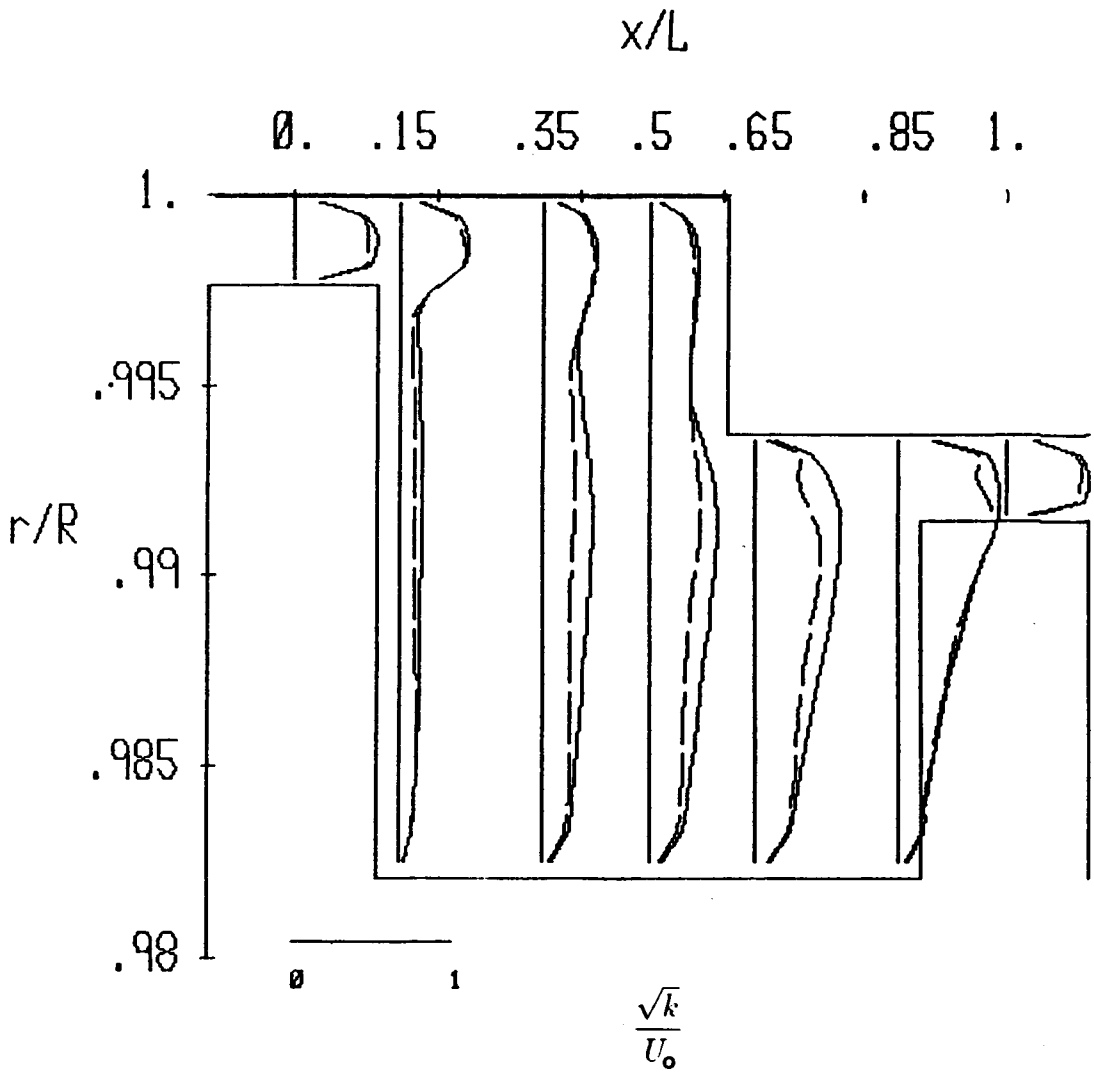

Fig. 21 Turbulence kinetic energy distribution for the Type 0 cavity showing predictions using (a) QUICK for all equations (——) and (b) QUICK only for the momentum equations (----)

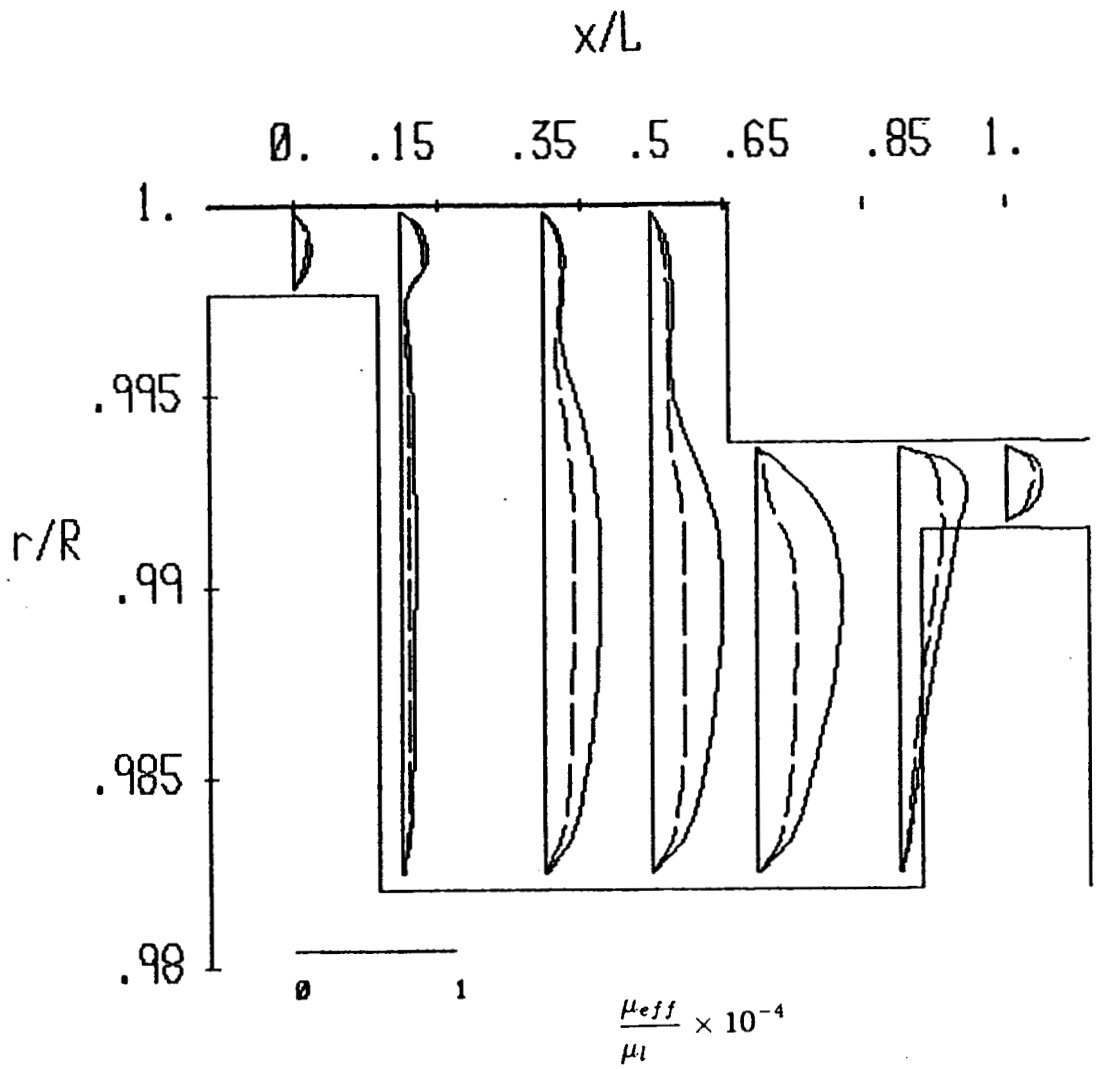

Fig. 22 Effective viscosity distribution for the Type 0 cavity showing predictions using (a) QUICK for all equations (——) and (b) QUICK only for the momentum equations (----)

cavity. This feature is a groove in the stator wall downstream of the step, which should further promote turbulence generation. Also involved is a downstream tooth of greater thickness in order to guide the flow into the groove.

Effect of the Stator Groove

Solutions were obtained using the MQ code for Type Q and Type R cavity designs in order to evaluate the stator groove, which is the only difference between these designs. As shown in the streamline pattern of Fig.23, the flow pattern of Type Q is very similar to that of Type O. Upon comparing the streamline pattern for Type R in Fig.24 to that of Type Q, one finds they are almost identical except for the presence of the recirculating zone inside the stator groove. From these MQ solutions, the cavity inlet-to-outlet bulk dimensionless pressure drop for Type Q equals 2.0, whereas that for Type R is equal to 2.25. Since the stator groove yields a twelve percent increase in pressure drop, it was decided to proceed by optimizing the step height while keeping the stator groove design feature.

Optimization of Step Height

An AQ solution was obtained for the Type R, S, and T cavities which have the stator groove and an s/c ratio of 2.67, 5.0,and 6.5 respectively. The MQ streamline pattern in Fig.24 for Type R is almost identical to that shown in Fig.25 for the AQ case. The solution MQ in Fig.24 gives the recirculating flow rate inside the secondary cavity of 21 percent of the leakage flow rate, whereas the solution AQ in Fig.25 gives a value of 15 percent.

The AQ solution values of important flowfield variables for Type R are shown in Figs. 26 through 29. The axial velocity distribution is shown in Fig.26. Observe that the exit velocity profile at x/L=1.0 is much different from that for Type O shown in Fig.18 . Figures 26 and 27 reveal that there is a single recirculation zone in the stator groove. The relative pressure distribution in Fig.28 indicates that the pressure within the groove at x/L=0.9

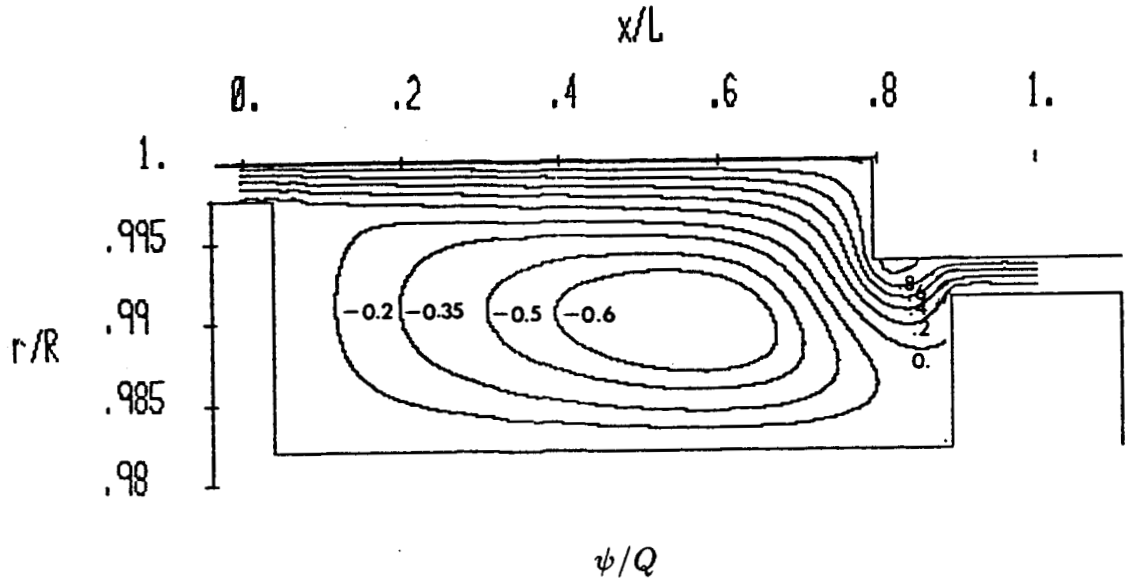

Fig. 23 Streamline pattern for the Type Q cavity using QUICK only for the momentum equations

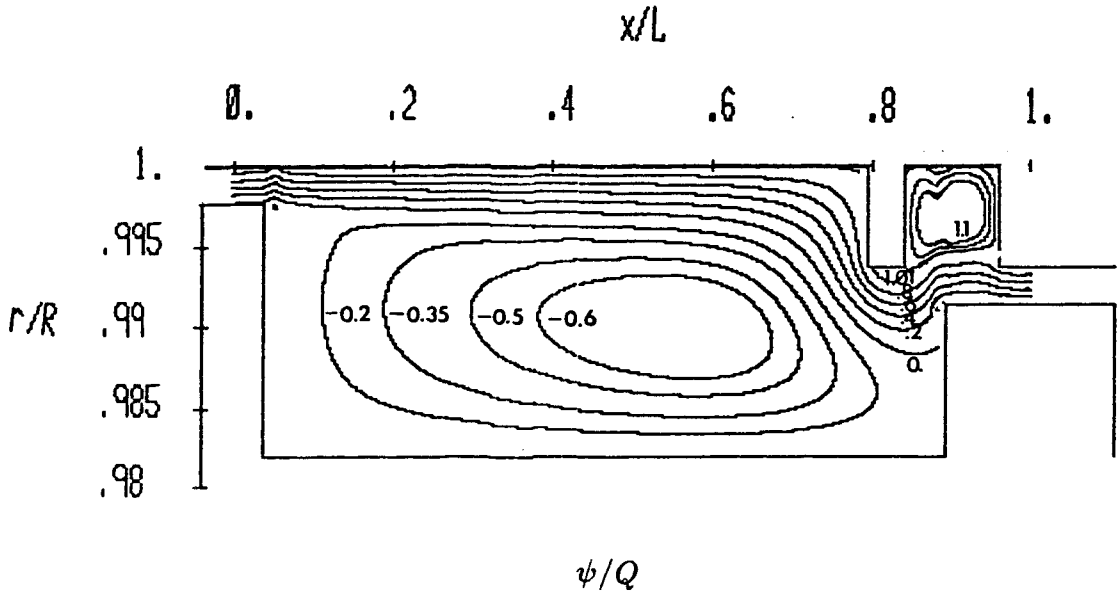

Fig. 24 Streamline pattern for the Type R cavity using QUICK only for the momentum equations

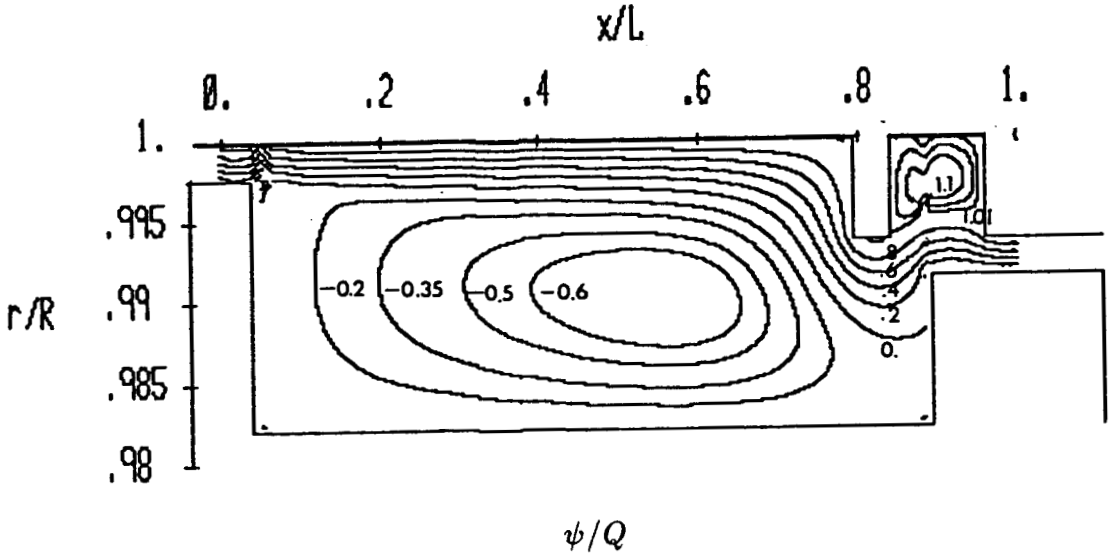

Fig. 25 Streamline pattern for the Type R cavity using QUICK for all equations

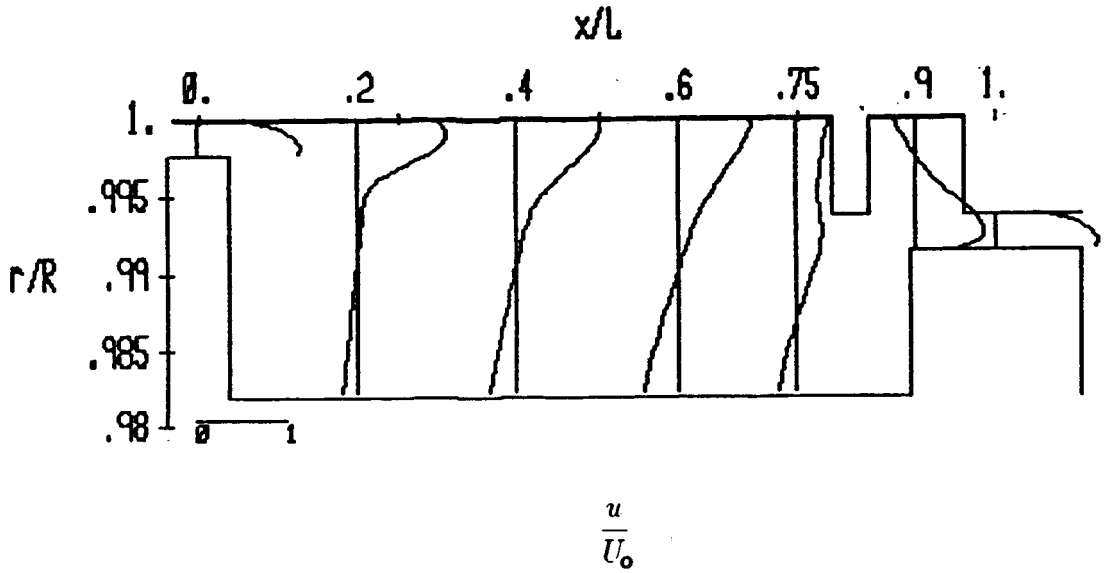

Fig. 26 Axial velocity distribution for the Type R cavity using QUICK for all equations

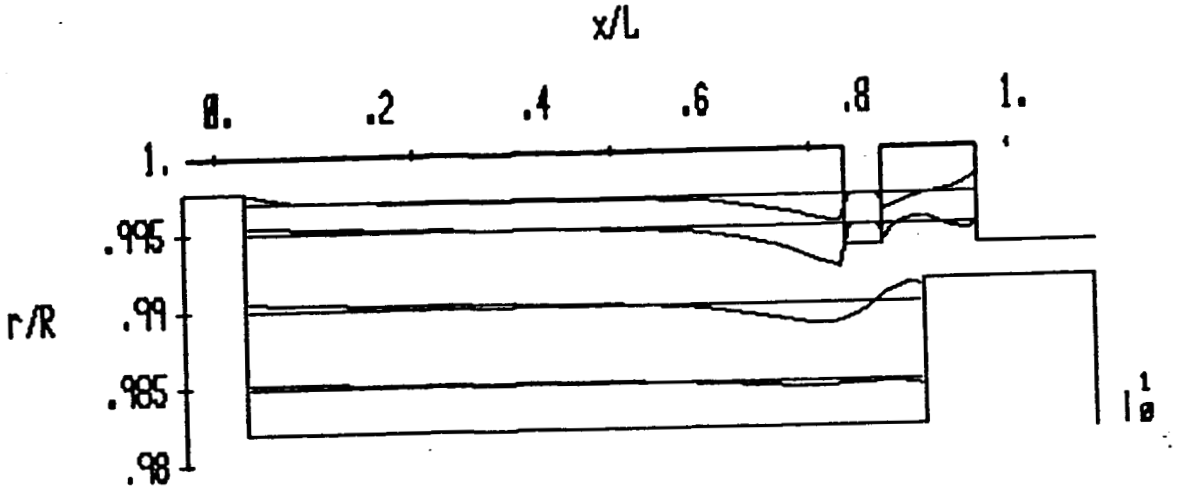

$$\frac{v}{U_o} \times 0.5$$

Fig. 27 Radial velocity distribution for the type R cavity using QUICK for all equations

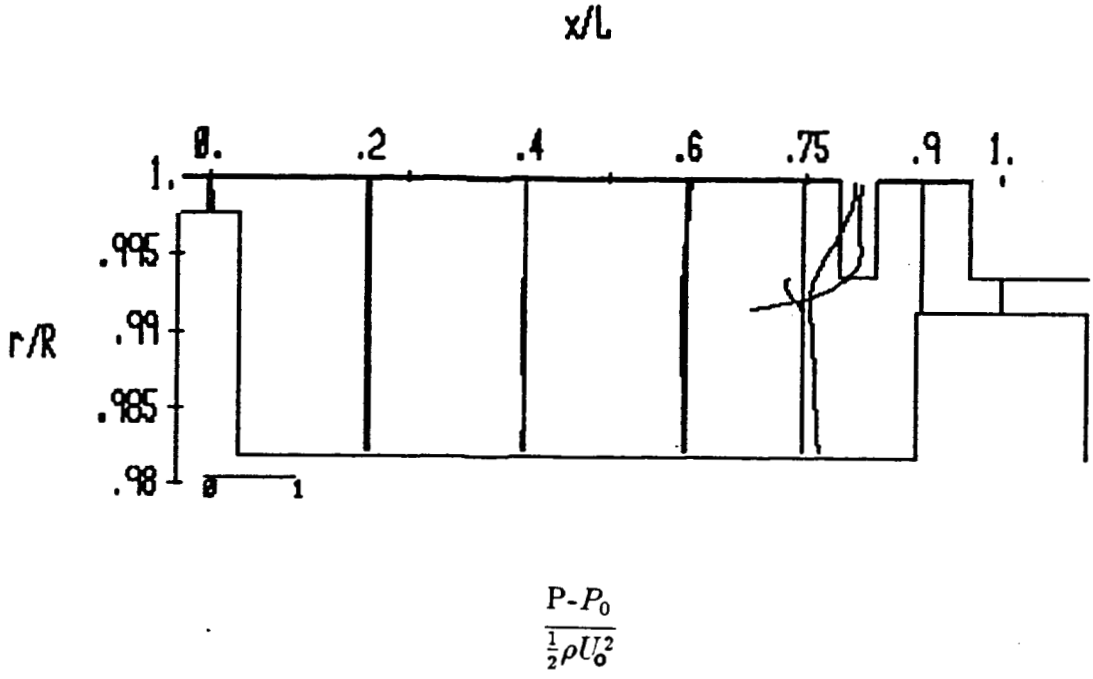

Fig. 28 Relative pressure distribution for the Type R cavity using QUICK for all equations

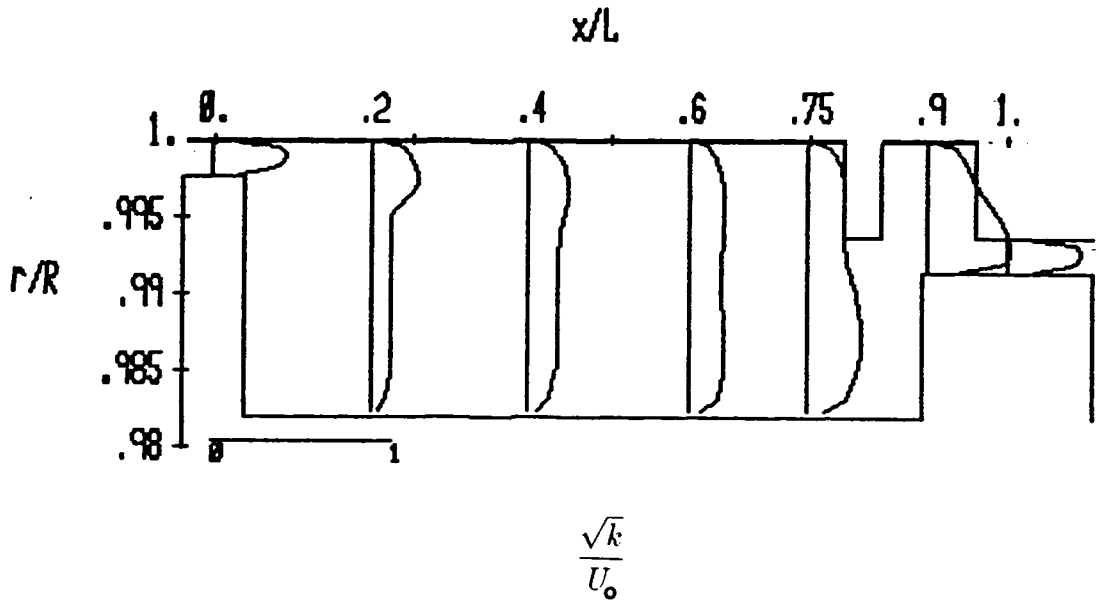

Fig. 29 Turbulence kinetic energy distribution for the Type R cavity using QUICK for all equations

is much higher than in the tooth clearance area at the same axial location. Observe that all of the pressure drop occurs in the region for x/L>0.7. The cavity inlet-to-outlet bulk dimensionless pressure drop for Type R is 2.39. The turbulence energy distribution is shown in Fig. 29 and the maximum value of $\sqrt{k}/U_o$ = 0.6 occurs at x/L=0.954 and r/R=0.9935. This location was expected to have a high turbulence energy value as it is very near the reattachment stagnation point of the groove recirculation zone.

The solution AQ for the Type S seal is shown in Figs.30 through 35. The streamline pattern is given in Fig.30, which reveals that the reattachment stagnation point is on the bottom wall in this case. The recirculating flow inside the groove is 12 percent of the leakage rate. Figure 31 shows an axial velocity distribution which is similar to that of Type R. One difference is that the deeper groove of Type S gives less axial velocity on the stator wall. The radial velocity distribution shown in Fig.32 is also similar to that for Type R except that it exhibits larger values along the step. Figure 33 shows that once again the major pressure drop occurs in the region for x/L>0.7. The cavity bulk dimensionless pressure drop for Type S is 2.77. Figure 34 reveals that the turbulence energy distribution is very similar to that for Type R. The location for maximum turbulence energy is x/L=0.954 and r/R=0.988.

For Type T which has an s/c value of 6.5, Figs. 35 through 39 show the same distribution as before.The flow pattern is very similar to that for Type S except that naturally the shape of the recirculation zone in the groove depends on the step height. The cavity bulk dimensionless pressure drop for Type T is 2.78. As before, the peak value of turbulence energy is at x/L=0.954 and r/R=0.985 which is near the reattachment point in the groove. The value of $\sqrt{k}/U_o$ there is 0.65.

In Fig.40, the cavity bulk dimensionless pressure drop is plotted versus s/c. This quantity for Type S gives a 16 percent improvement over Type R and a

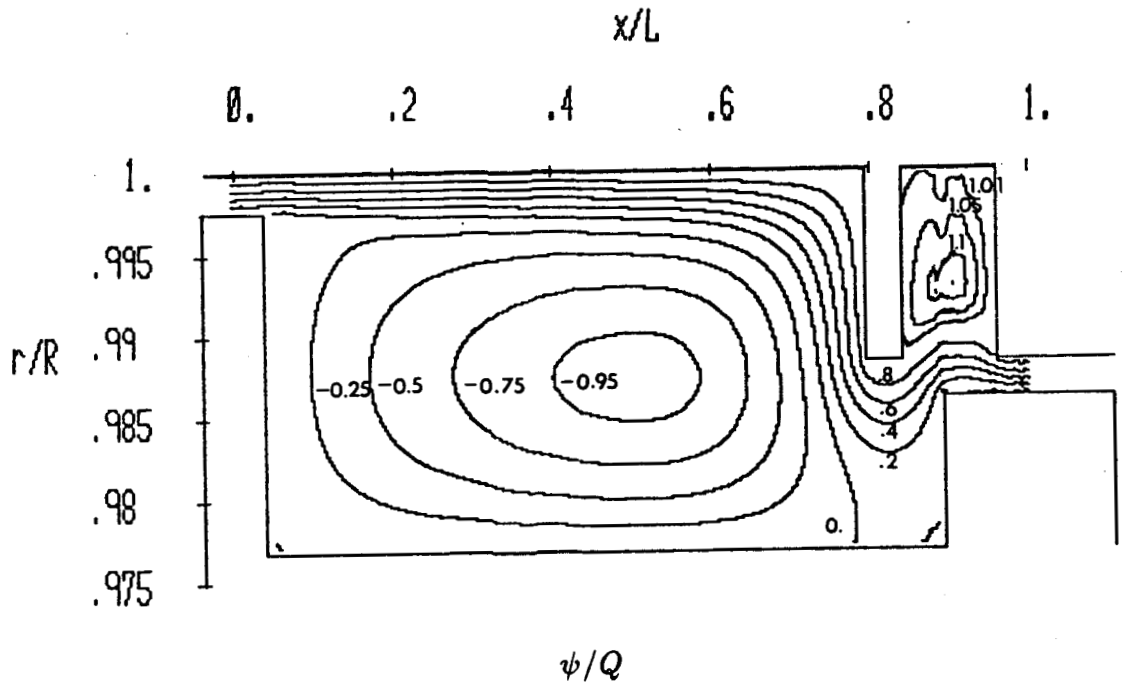

Fig. 30 Streamline pattern for the Type S cavity using QUICK for all equations

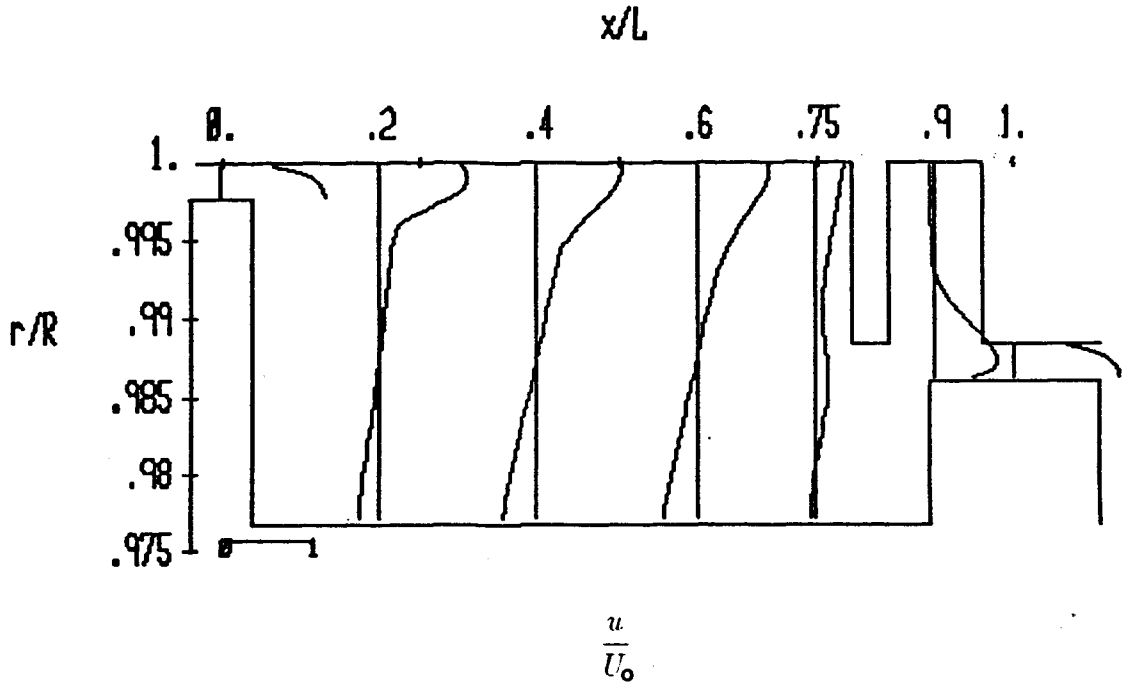

Fig. 31 Axial velocity distribution for the Type S cavity using QUICK for all equations

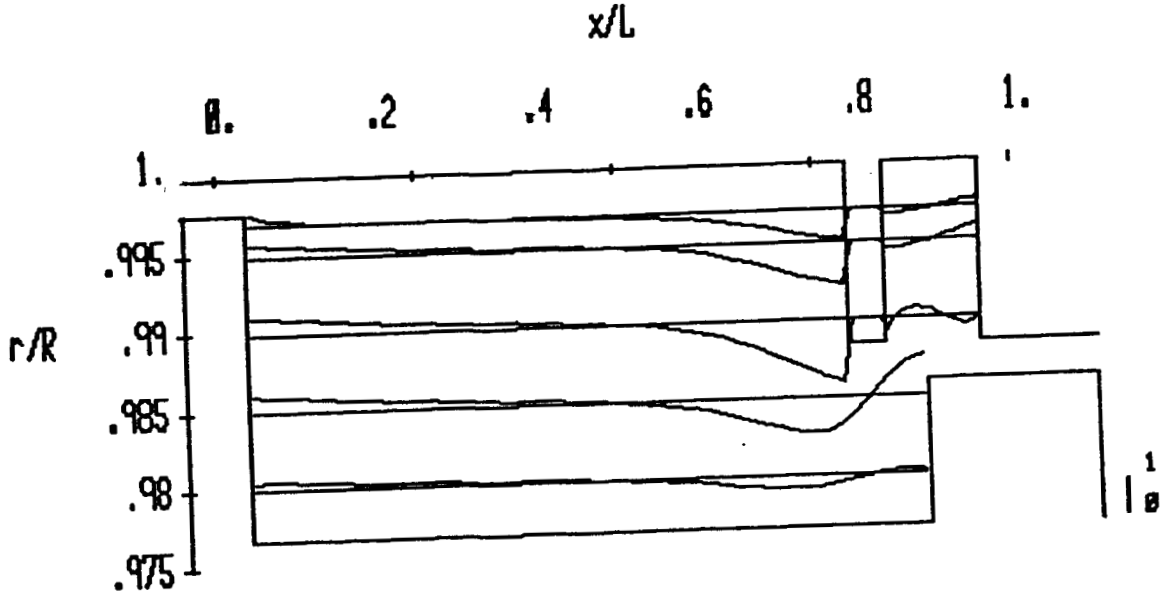

$$\frac{v}{U_o} \times 0.5$$

Fig. 32 Radial velocity distribution for the Type S cavity using QUICK for all equations

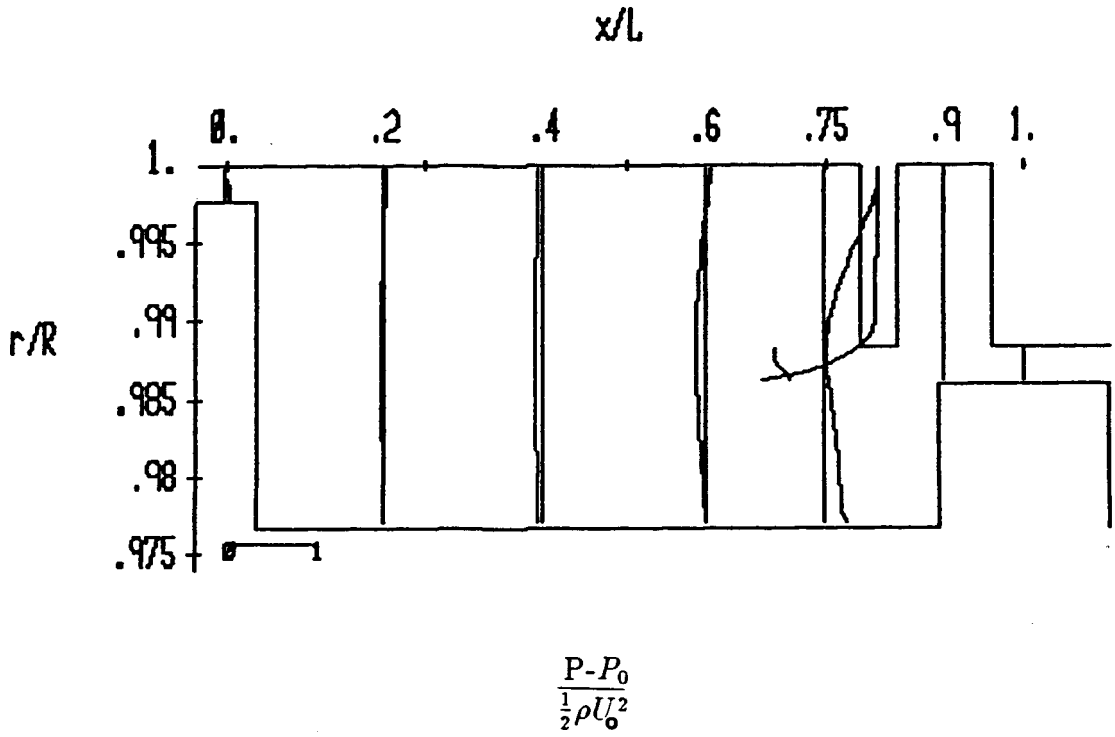

Fig. 33 Relative pressure distribution for the Type S cavity using QUICK for all equations

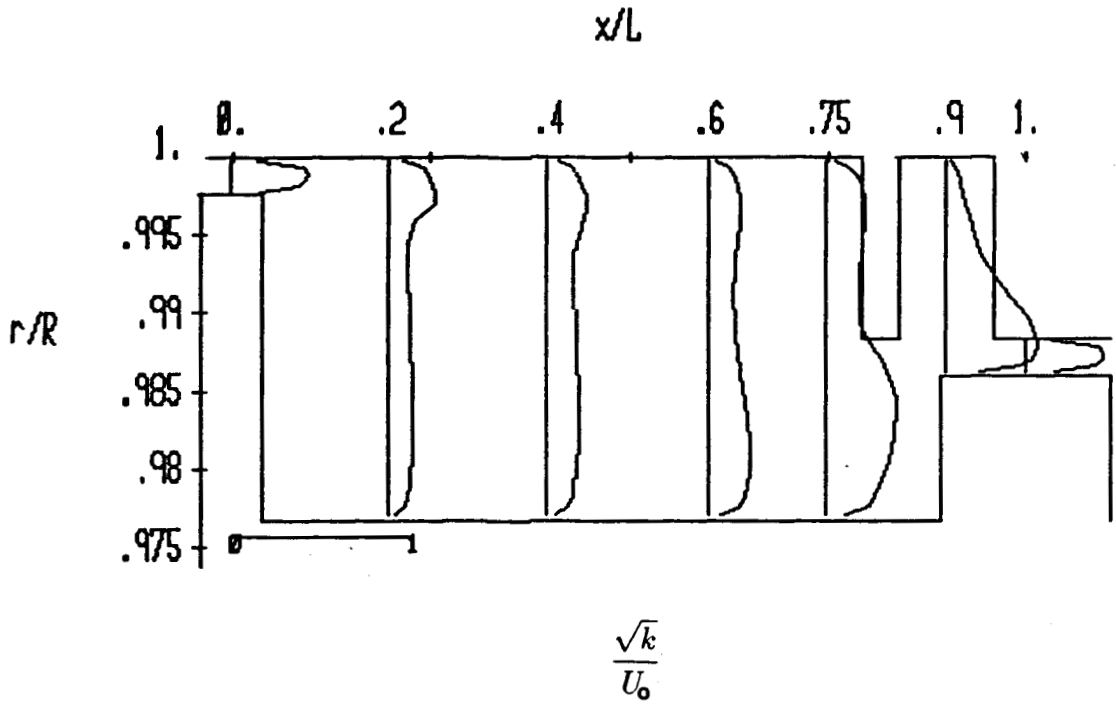

Fig. 34 Turbulence kinetic energy distribution for the Type S cavity using QUICK for all equaitons

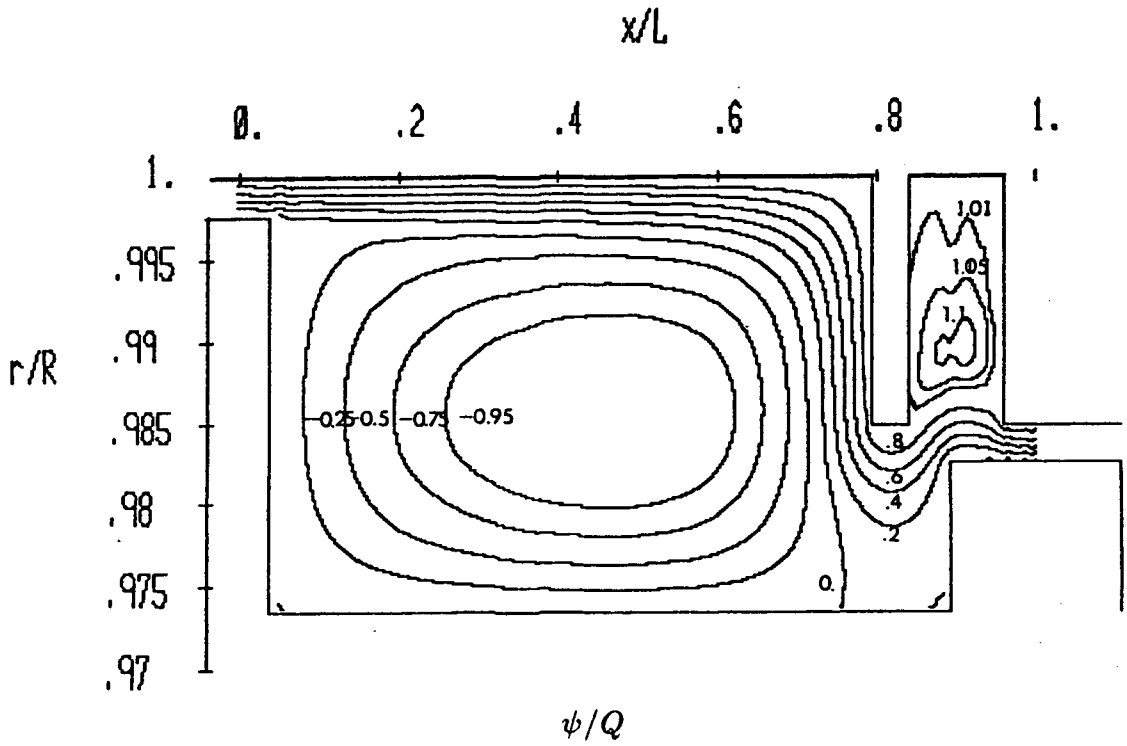

Fig. 35 Streamline pattern for the Type T cavity usign QUICK for all equations

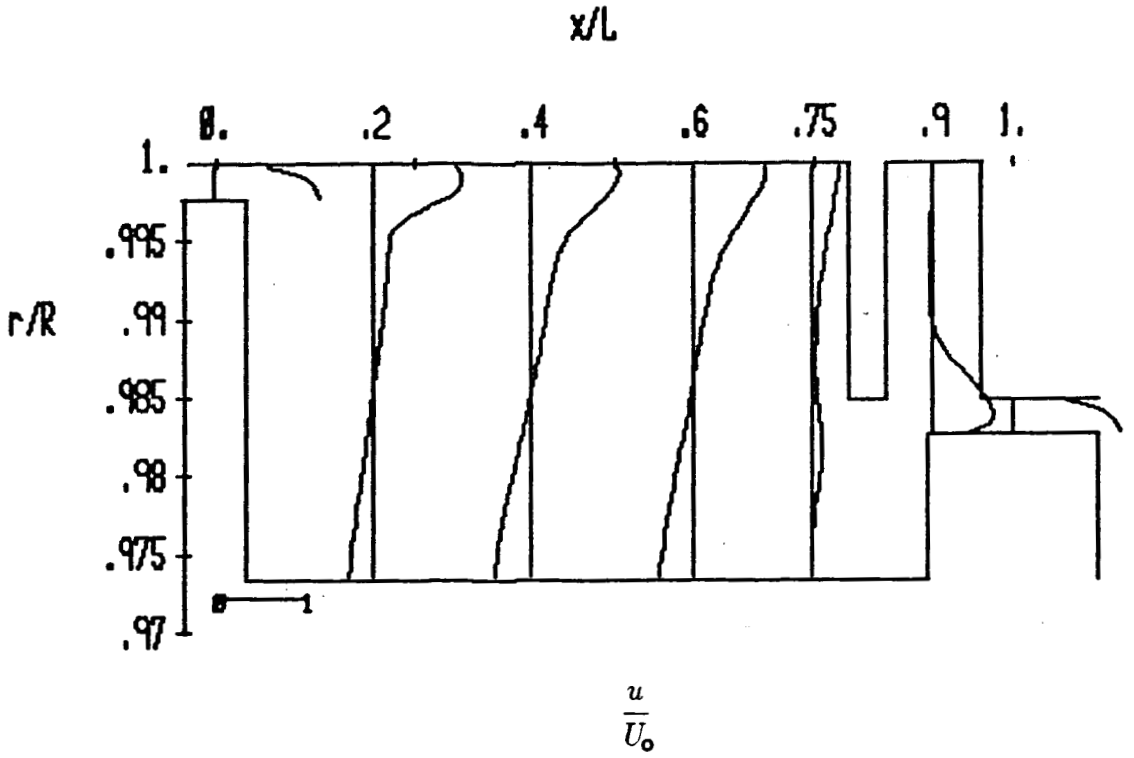

Fig. 36 Axial velocity distribution for the Type T cavity using QUICK for all equations

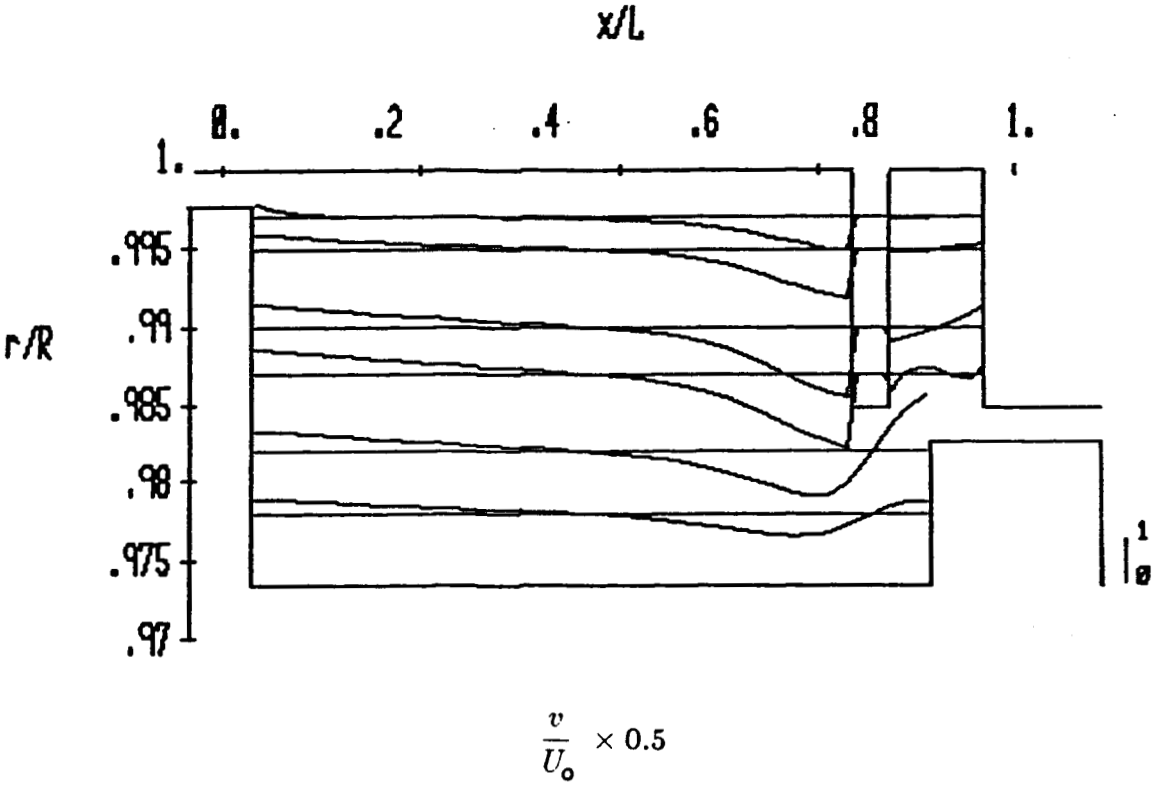

Fig. 37 Radial velocity distribution for the type T cavity using QUICK for all equations

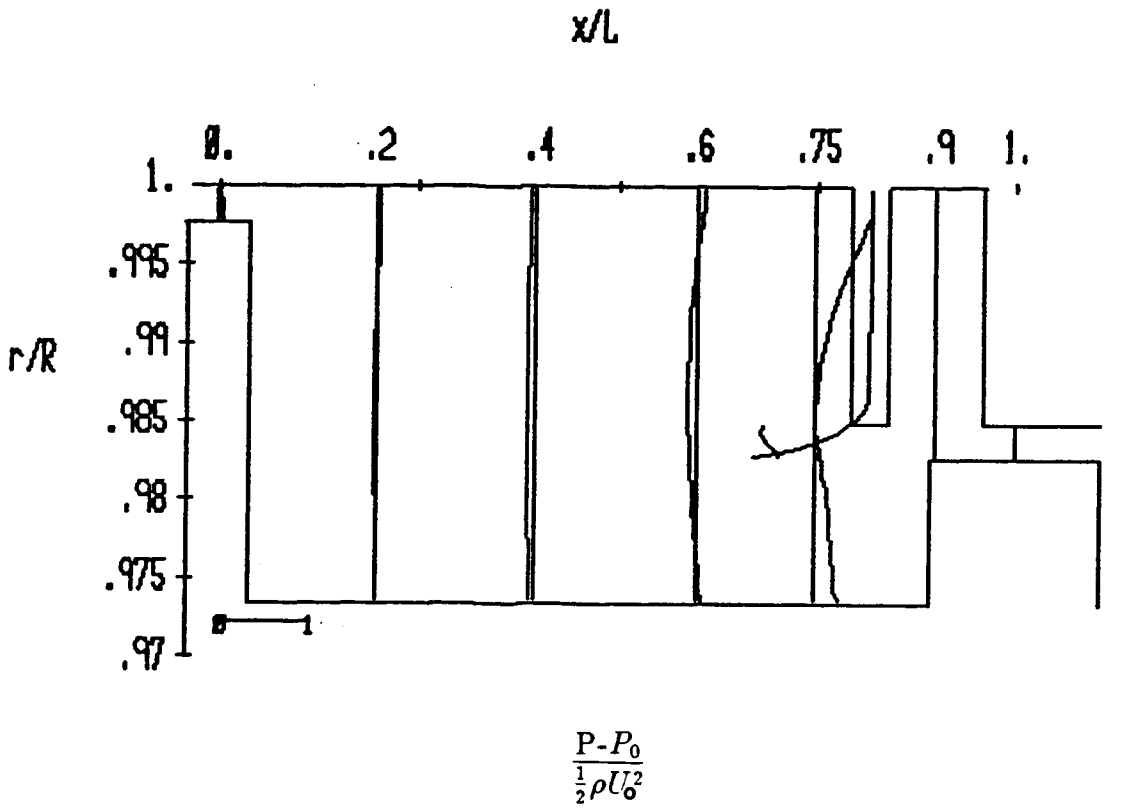

Fig. 38 Relative pressure distribution for the Type T cavity using QUICK for all equations

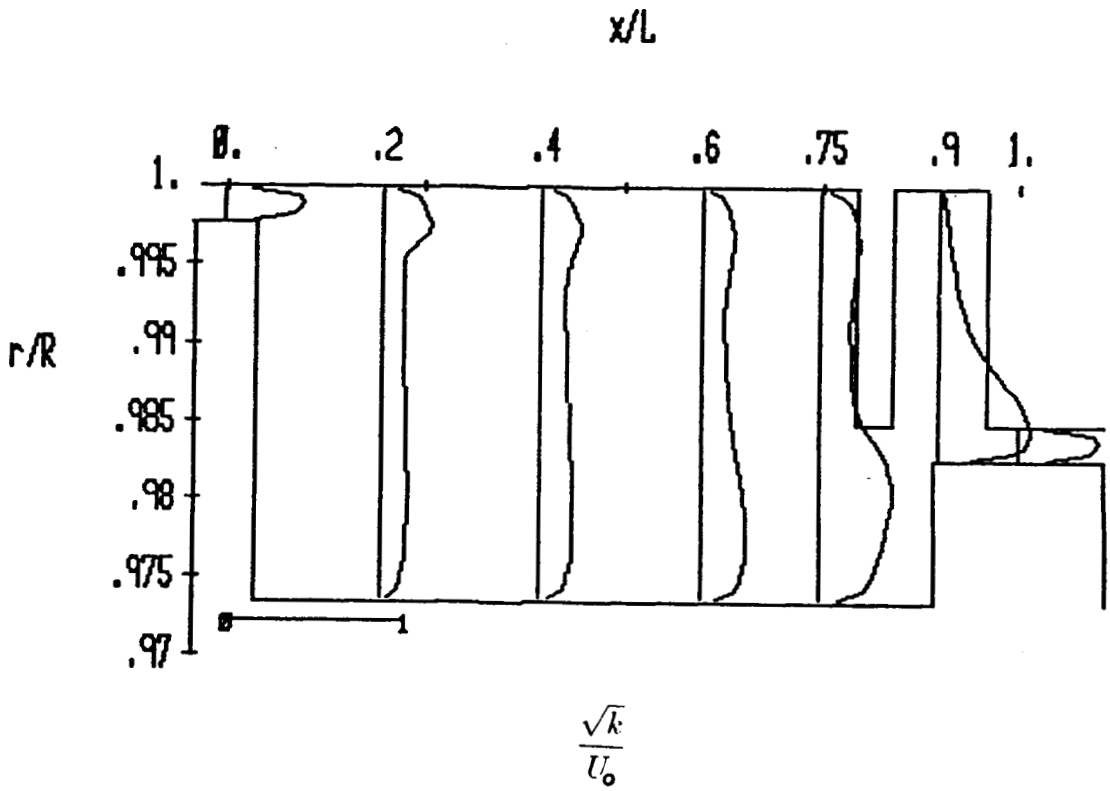

Fig. 39 Turbulence kinetic energy distribution for the Type T cavity using QUICK for all equations

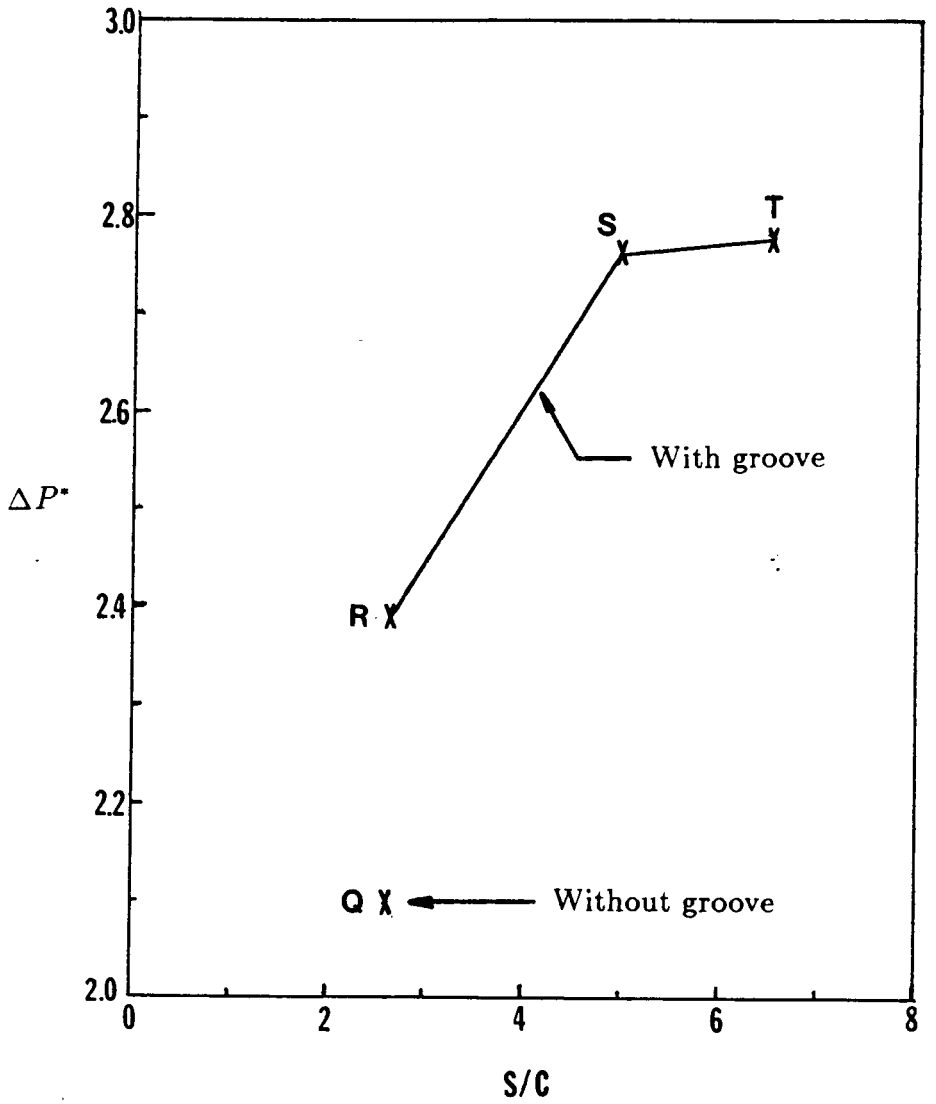

Fig. 40 Effect of step height on cavity inlet-to-outlet bulk pressure drop

31 percent improvement over Type Q. Since Type S and Type T give essentially the same performance, Type S was selected for testing because the new tooth on the stator wall would be slightly less likely to break off.

VI. EMPIRICAL LEAKAGE PREDICTION PROGRAM

During our previous study[25], an empirical leakage prediction program was developed using data available in the open literature and data obtained in our laboratory on the front wear ring seal of the oxygen turbopump. In this chapter, the original program will be reviewed followed by a section on how the program was modified.

Original Empirical Leakage Prediction Program

There is only a small data base available in the open literature from which to determine the value of the flow coefficient for stepped labyrinth seals. There were no data available which relates leakage of incompressible fluids in stepped labyrinth seals to tooth width, tooth height, step height, tooth to step distance, or pitch. Therefore, some data for straight-through labyrinth seals was used for the leakage estimation in stepped labyrinth seals. Yamada[26] investigated the effects of ratios of clearance to pitch, tooth width to pitch; and tooth height to clearance with various parameters for incompressible fluids in straight-through labyrinth seals. This data along with data specifying the effects of axial location, number of throttles, rpm, and pressure ratio, determined in the present test rig for the front wear ring seal of the oxygen turbo pump seal (See Figure 41) were used to develop the leakage estimation model.

The leakage data has been normalized according to the following equation:

$$\alpha = \frac{\dot{m}}{\varepsilon c A_t} \sqrt{\frac{(n+\ln(Po/Pn))}{\rho_o Po(1-(Pn/Po)^2)}} \qquad (14)$$

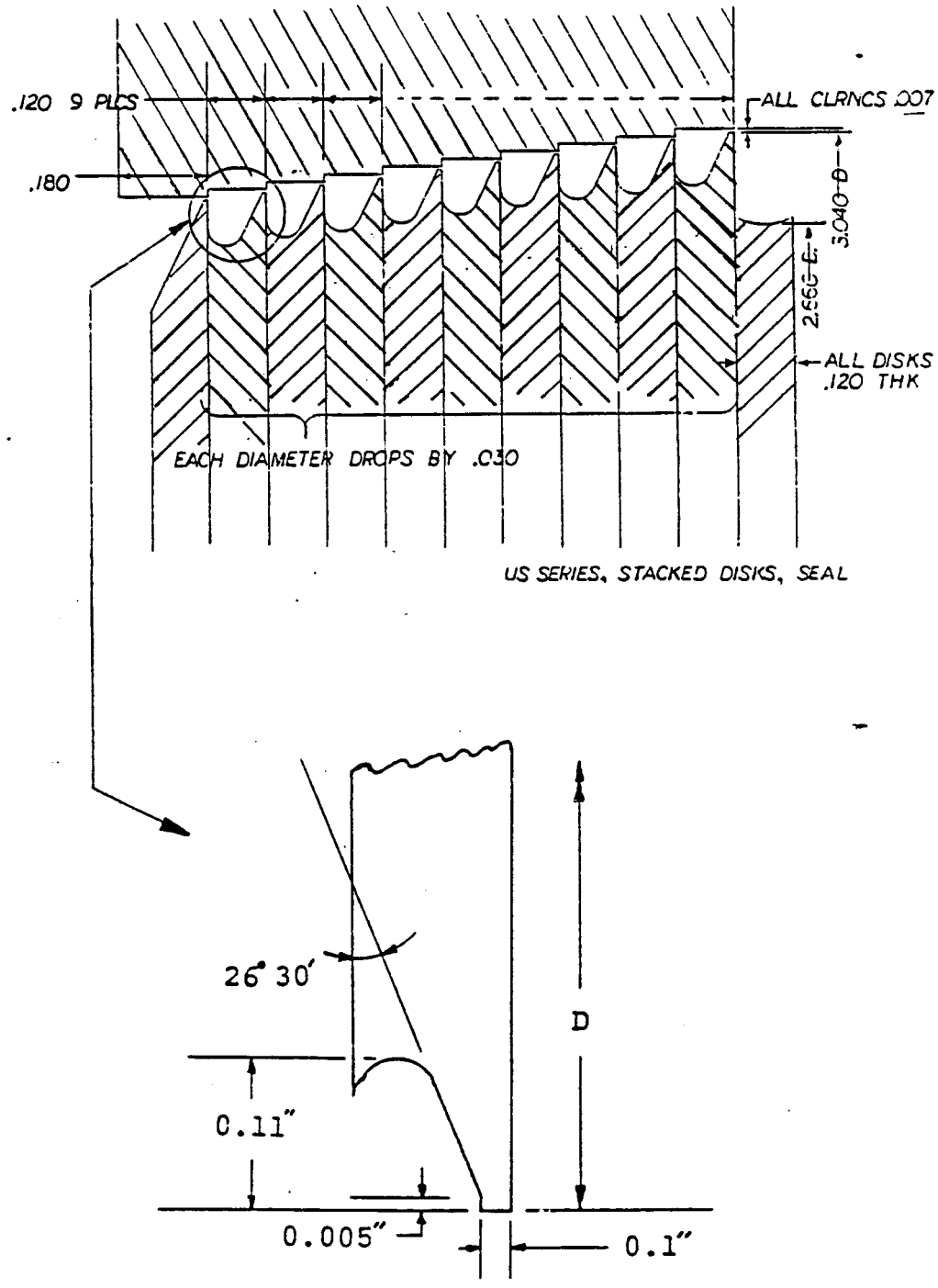

Figure 41. Configuration of the Oxygen Front Wear Ring Stepped Labyrinth Seal.

Table 1. Specifications of Stepped Labyrinth Seals Used in Experiment.

Clearance = 0.007 inches

Pitch = 0.12 inches

Tooth Width = 0.01 inches

Tooth Height= 0.11 inches

Step Distance = 0.12 inches

Step Height = 0.015

Seal Diameter = 2.8 inches

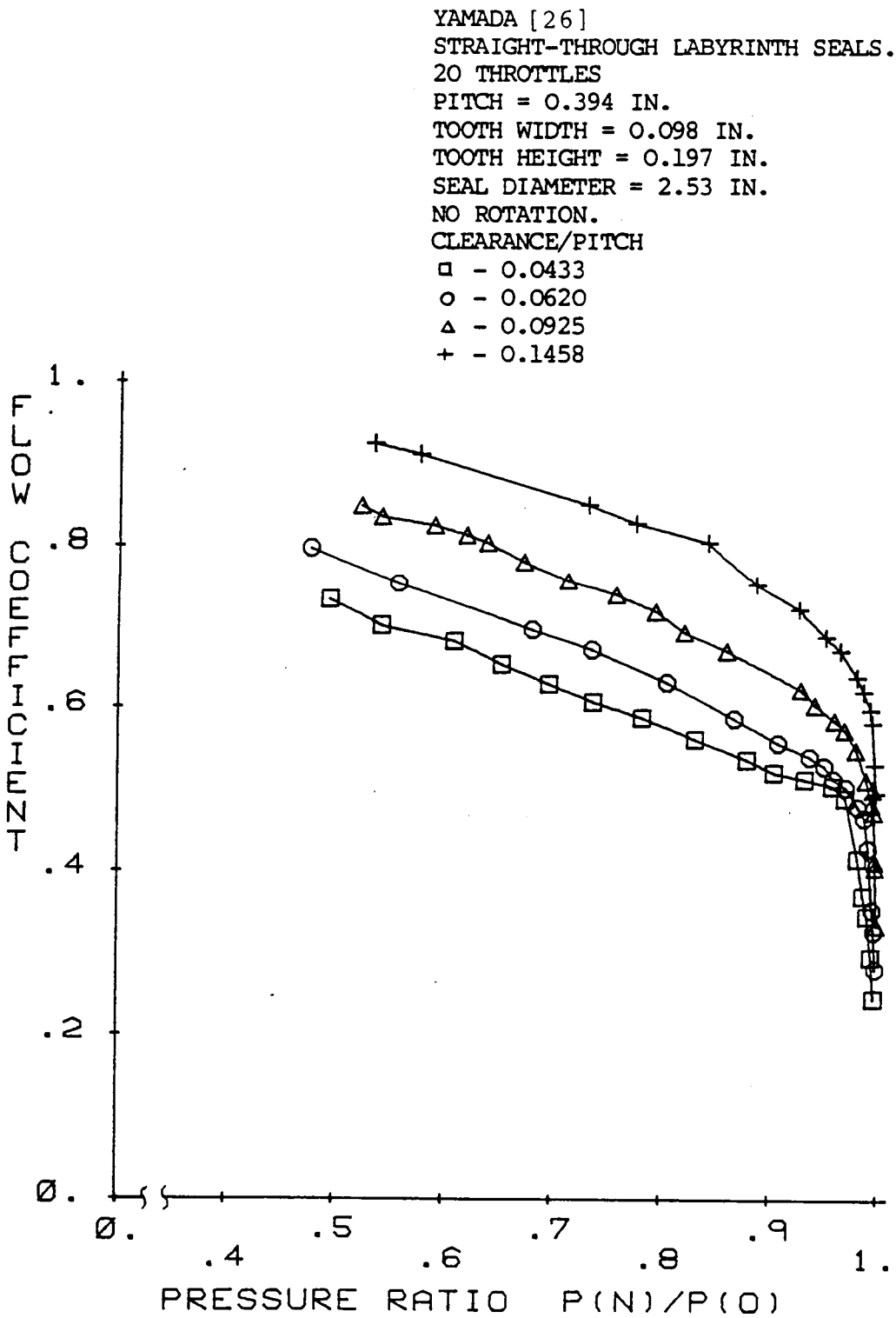

Figure 42. Flow Coefficient vs. Pressure Ratio for Straight-through Labyrinth Seals.

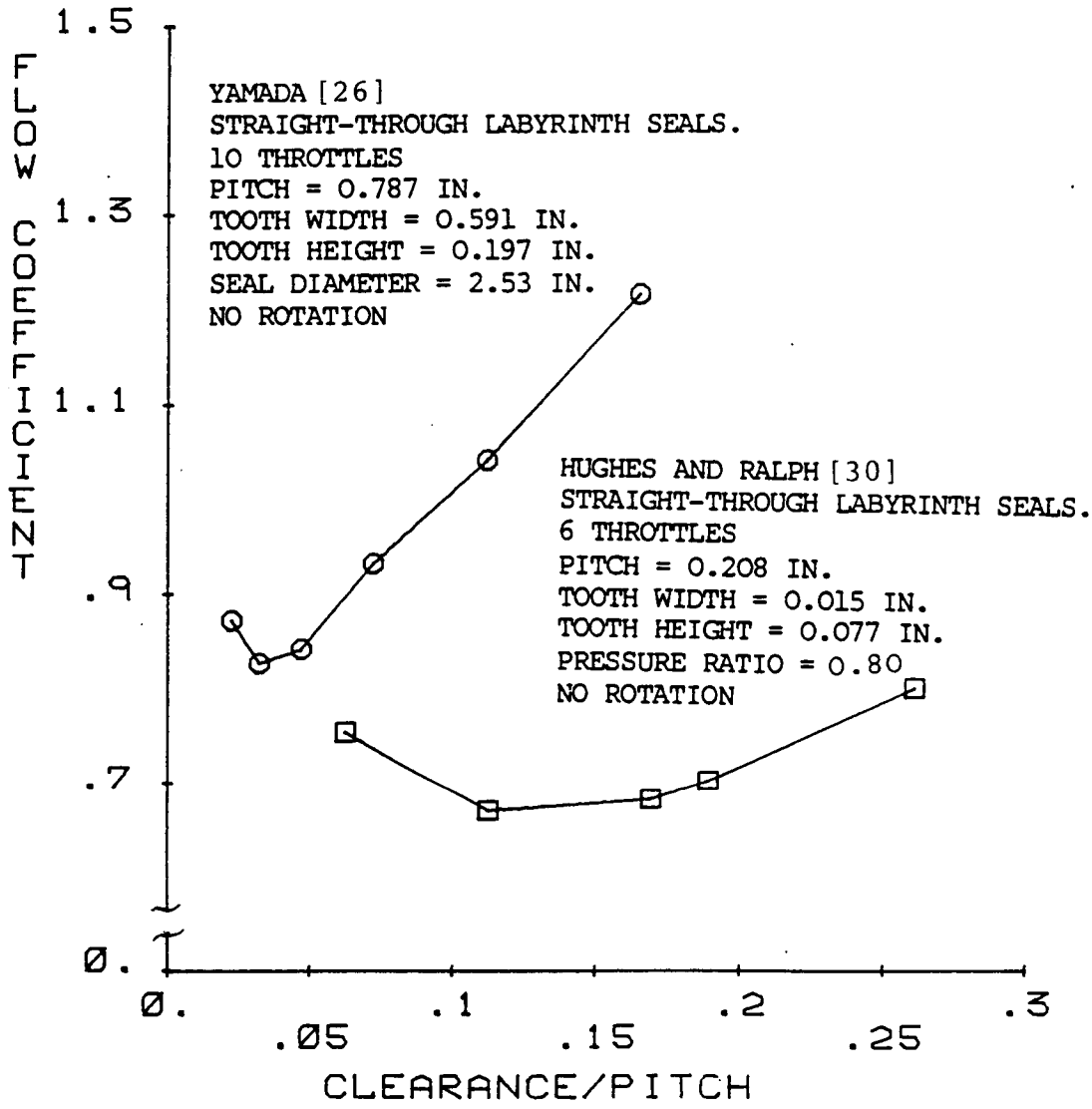

Figure 43. Flow Coefficient vs. Clearance/Pitch for Two Different Straight-through Labyrinth Seals.

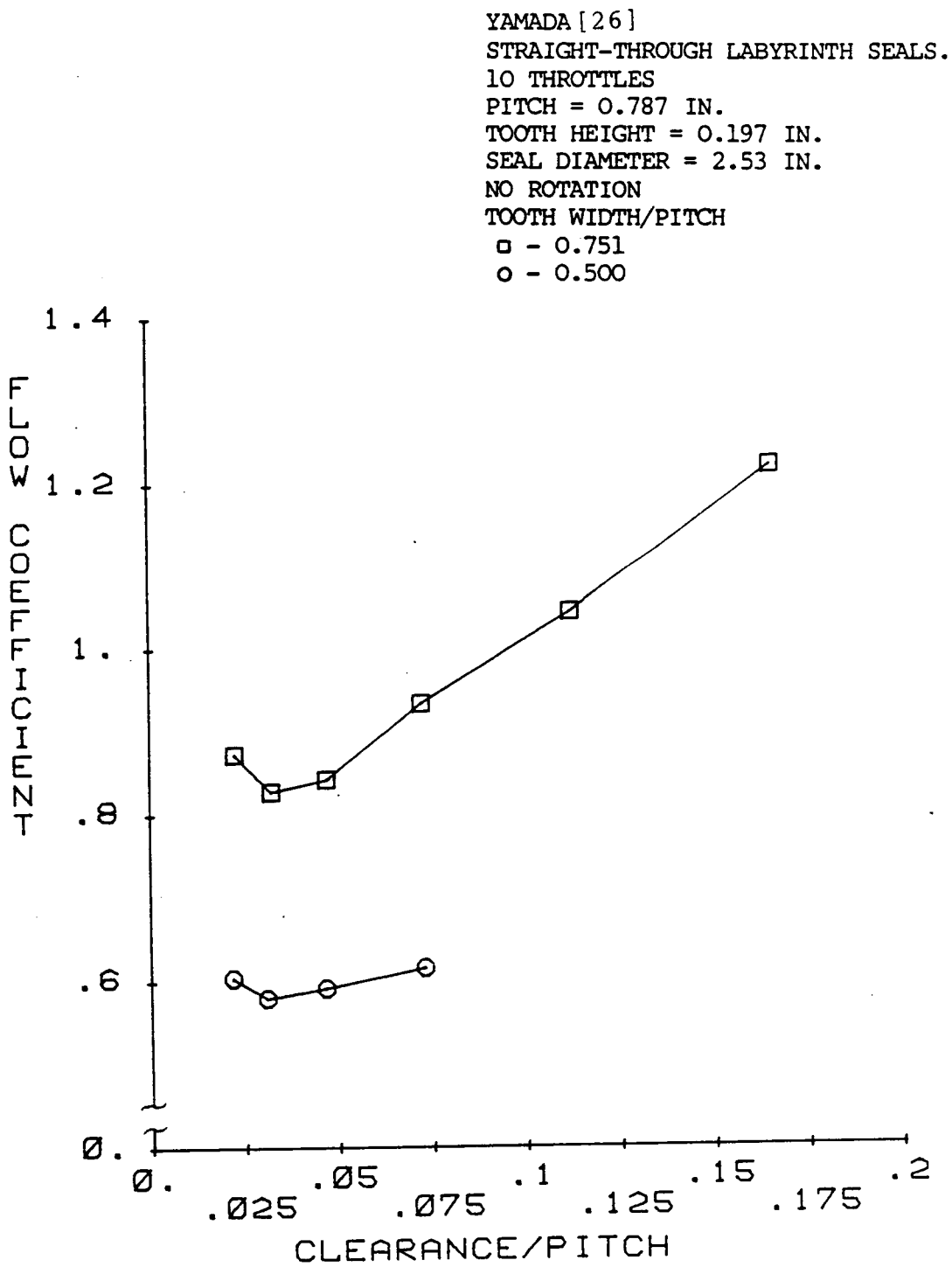

Figure 44. Flow Coefficient vs. Clearance/Pitch for Two Different Tooth Widths in Straight-through Labyrinth Seals.

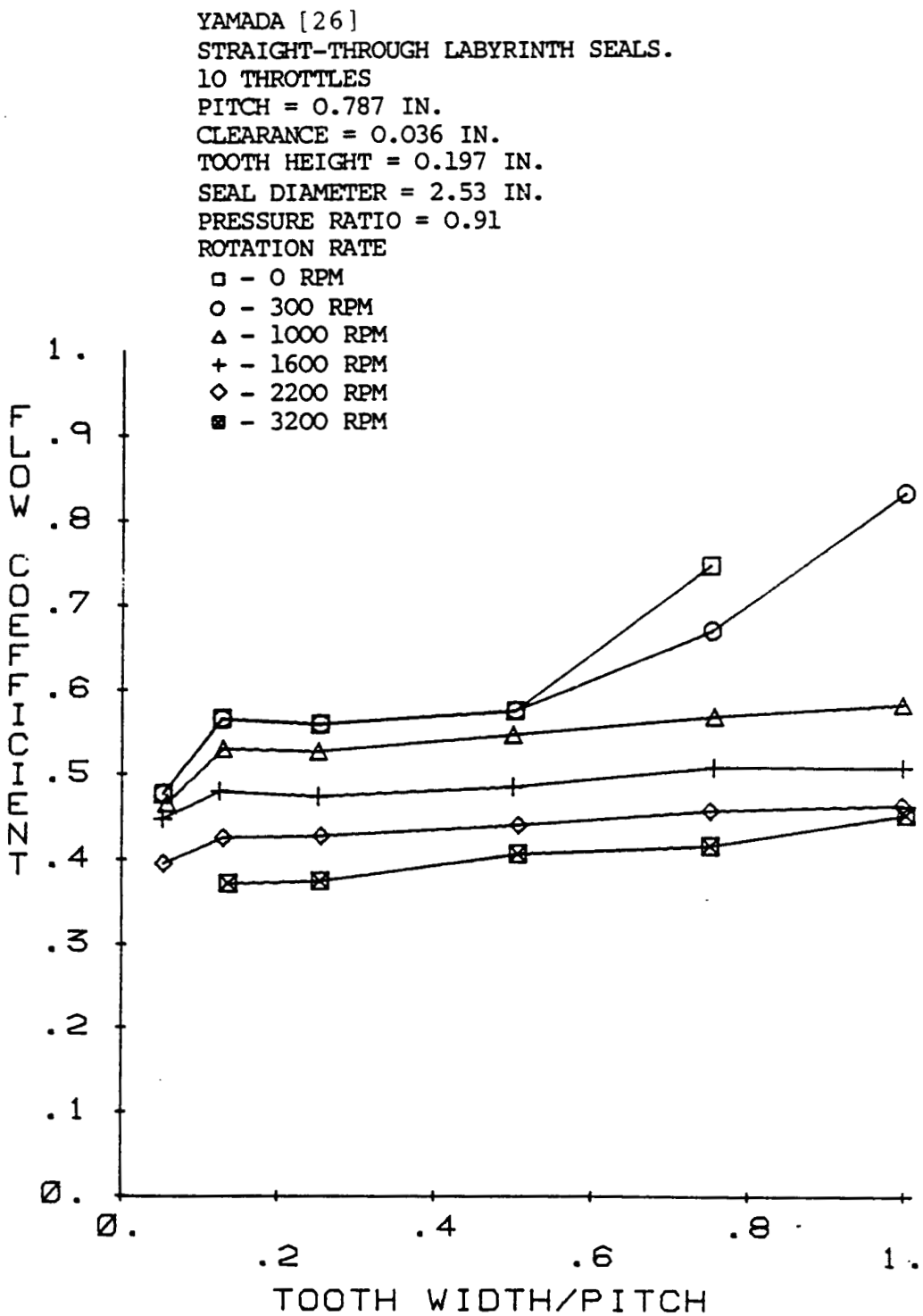

Figure 45. Flow Coefficient vs. Tooth Width/Pitch for a Ten Throttle Straight-through Labyrinth Seal.

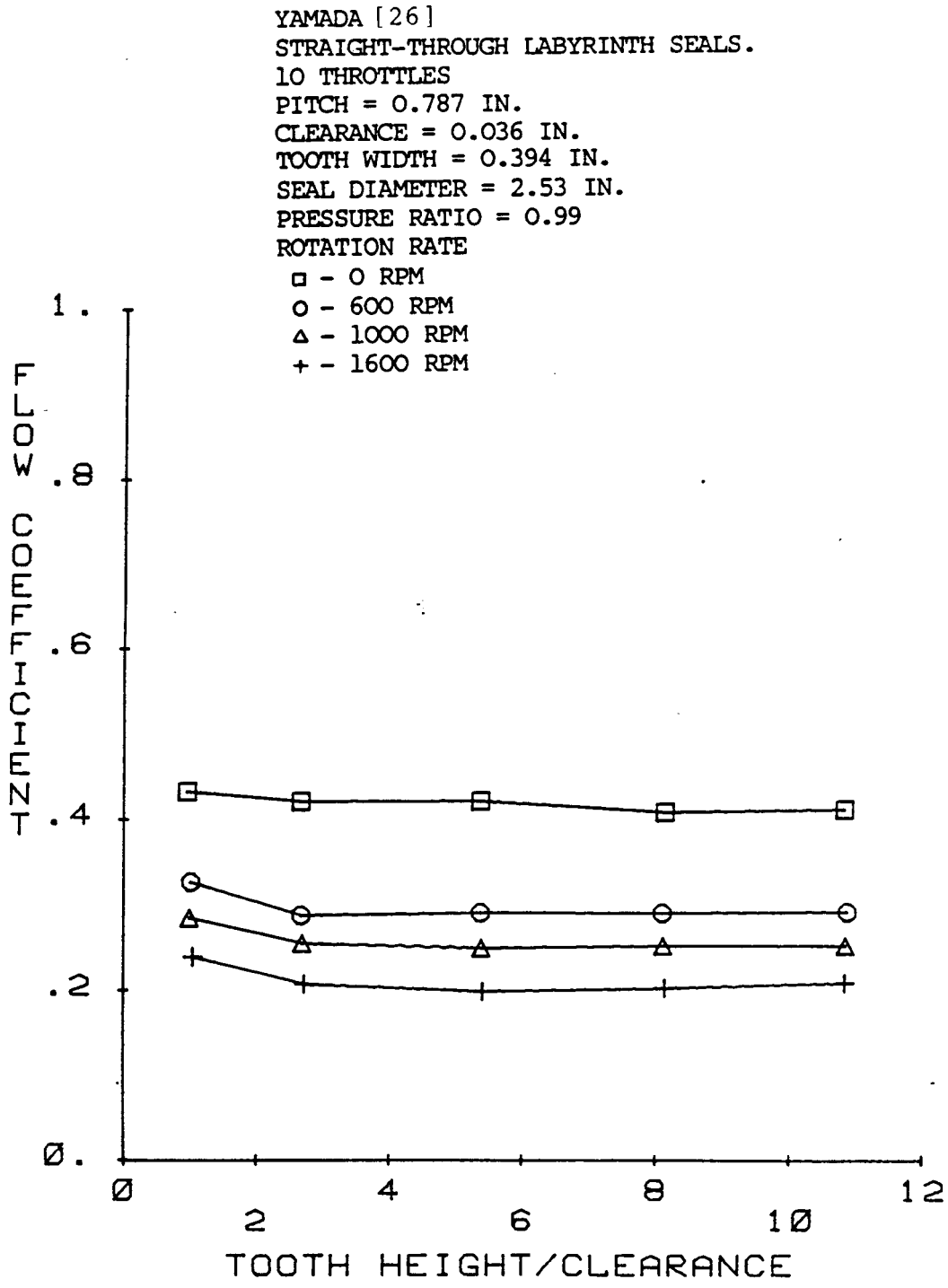

Figure 46. Flow Coefficient vs. Tooth Height/Clearance for Straight-through Labyrinth Seals.

In order to calculate the mass leakage rate in a stepped labyrinth seal, a value for the flow coefficent was determined for a straight-through labyrinth seal with a clearance to pitch ratio of 0.0433, seven throttles, a tooth width to pitch ratio of 0.25, and a tooth height to clearance ratio of 2.7 using Dodge's[27] method. Then the data of Figures 42-46 were used to modify the flow coefficient for the effects of ratios of clearance to pitch, tooth width to pitch, and tooth height to clearance for straight-through labyrinth seals. Then experimental data, which include the effects of rotation rate, pressure ratio, and axial location for a stepped labyrinth seal was used to modify the flow coefficient and to obtain the final value. This flow coefficient was then applied in the following equation:

$$\dot{m} = \alpha \epsilon_c A_t \sqrt{\frac{Po(1-(Pn/Po)^2)\rho_o}{(n+\ln(Po/Pn))}} \qquad (15)$$

The value of the carry-over coefficient, , shown in Figure 47 is given by:

$$\epsilon_c = \sqrt{\frac{1}{1 - \frac{(n-1)\ (c/m)}{n\ (c/m+0.02)}}} \qquad (16)$$

In the application of this method, it is assumed that the following dimensions of the seal are known: radial clearance, tooth width, tooth height, pitch, and seal diameter. In addition to this information, the number of throttles, inlet pressure, outlet pressure, axial location of the tooth, fluid density, kinematic viscosity, and the rotation rate are required.

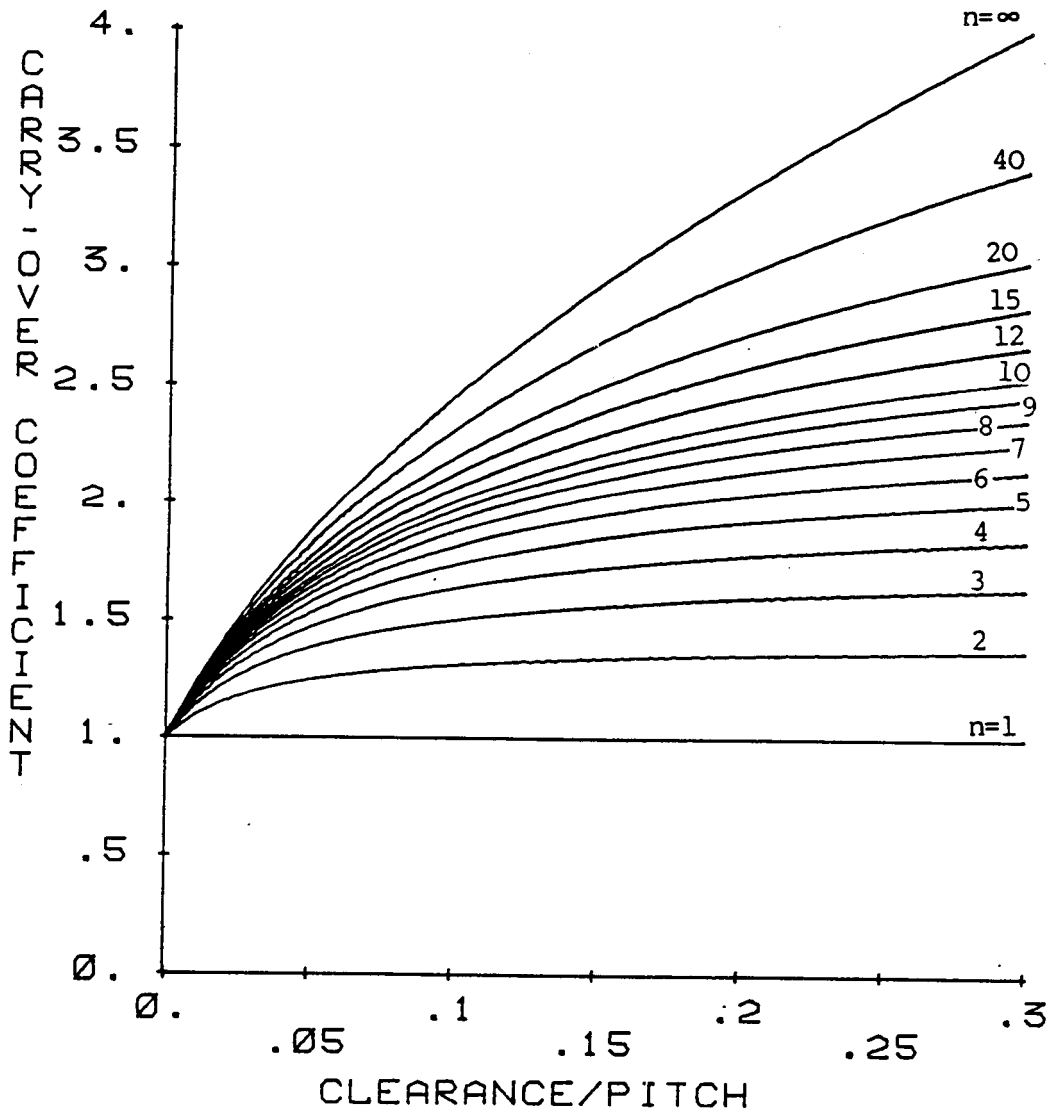

Figure 47. Carry-over Coefficient vs. Clearance/Pitch for Straight-through Labyrinth Seals.

To calculate the mass flow rate from equation (15), the area, A_t, is calculated by:

$$A_t = \pi cD \tag{17}$$

The carry-over coefficient is calculated from equation (16). These two quantities, along with the other fluid and geometric parameters are substituted into the right hand side of equation (15) to solve for the mass flow rate.

The following gives a detailed description of how the flow coefficient was determined. First, the value of the flow coefficient is calculated using Dodge's method[27] for seven throttles and a clearance to pitch ratio of 0.0433. These values were used since Dodge's technique[27] seems to work best at these values. The following procedures were used to calculate the flow coefficient by Dodge's method:

1. Initially assumed axial velocity, U, of 1 ft/sec.
2. Calculate the Reynolds number. $Re=2cU/\nu$.
3. Calculate the friction factor. $f=64/Re$ ($Re<2320$), or $f=0.316/\ Re$ ($Re>2320$).
4. Calculate a new axial velocity.

$$U = \sqrt{\frac{2(Po-Pn)}{[1.5+7f/(c/m)+6]}}$$

5. Compare the assumed and calculated velocities. If the difference is less than 0.005 ft/sec, go to step 7.
6. Repeat the calculation using the new calculated axial velocity.
7. Calculate the leakage rate and flow coefficient (ALFA) using the following equations:

$$\dot{m} = \rho UA_t$$

$$ALFA = \left[\frac{\dot{m}}{A_t} \frac{(7+\ln(Po/Pn))}{\rho Po(1-(Pn/Po)^2)} \times (1-0.0433(7-1)/(7(0.0433+0.02))) \right]^{0.5}$$

Once the initial value of the flow coefficient was determined using Dodge's method, corrections for clearance to pitch ratios were performed. The value of the flow coefficient was modified using data from Figure 42 for the given pressure ratio and the clearance to pitch ratio. For ease of reference, this value of the corrected flow coefficient was designated as Cl. Note that the data in Figure 42 was based upon a seal with a tooth width to clearance ratio of 0.25.

If when determining the value of Cl from Figure 42, the value of the clearance to pitch ratio was greater than 0.15, Cl was calculated by the following equation which is extrapolated from the data of Figure 44.

$$Cl = ALFA + 3.16522(CTOP-0.0433)$$

where ALFA is the flow coefficient calculated from Dodge's method and CTOP is the clearance to pitch ratio.

If the value of the clearance to pitch ratio was less than 0.15, the value of the flow coefficient, ClB, at a clearance to pitch ratio of 0.0433, was found from Figure 42, at the designated pressure ratio. The value of the corresponding flow coefficinet at the required clearance to pitch ratio, ClA, was interpolated from the data in Figure 42 at the designated clearance to pitch ratio. Then Cl was calculated from Cl=ALFA(ClA)/ClB.

To correct Cl for tooth width effects, Figure 45 was used to obtain C2. The value of the flow coefficient, C2B, for a tooth width to pitch ratio of 0.25 was found from Figure 45. The value of the flow coefficient at the required tooth width to pitch

ratio, C2A, was interpolated from Figure 45 as well. Then C2 was calculated by C2=(C1)(C2A)/C2B. Since data was not available when the rotation rate is greater than 3200 rpm, the following equation, which was an average curve fit of the higher rpm speeds, was determined. This equation was then used to calculate C2:

$$C2 = C1 + 0.059205(WTOP - 0.25)$$

where WTOP is the tooth width to pitch ratio.

To correct C2 for tooth height effects and obtain C3, Figure 46 was used. If the tooth height to clearance ratio was greater than 2.7, the value of the flow coefficient was constant. Therefore, there was no need to correct C2 and C3 = C2. On the other hand, if the tooth height to clearance ratio was less than 2.7, C2 must be corrected using the following equation which was a curve fit obtained from Figure 46:

$$C3 = C2 + 0.0199(2.7 - HTOC)$$

where HTOC is the tooth height to clearance ratio.

Leakage data for straight-through labyrinth seals have been used so far to estimate the value of the flow coefficient. However, experimental data for stepped labyrinth seals were used for the remainder of the empirical leakage model to estimate the value of the flow coefficient.

To correct C3 for rotation effects and obtain C4, the following equation was used: C4 = (C3)(C4A)/C4B. C4A is the value of the flow coefficient at the required rotation rate and C4B is the value of the flow coefficient at 0 rpm. The data used for this correction was obtained by Chi[29] in a previous project at this laboratory. A recap of this data is presented in Ref[25] and this specific data is presented in Figures 51 and 52 for two

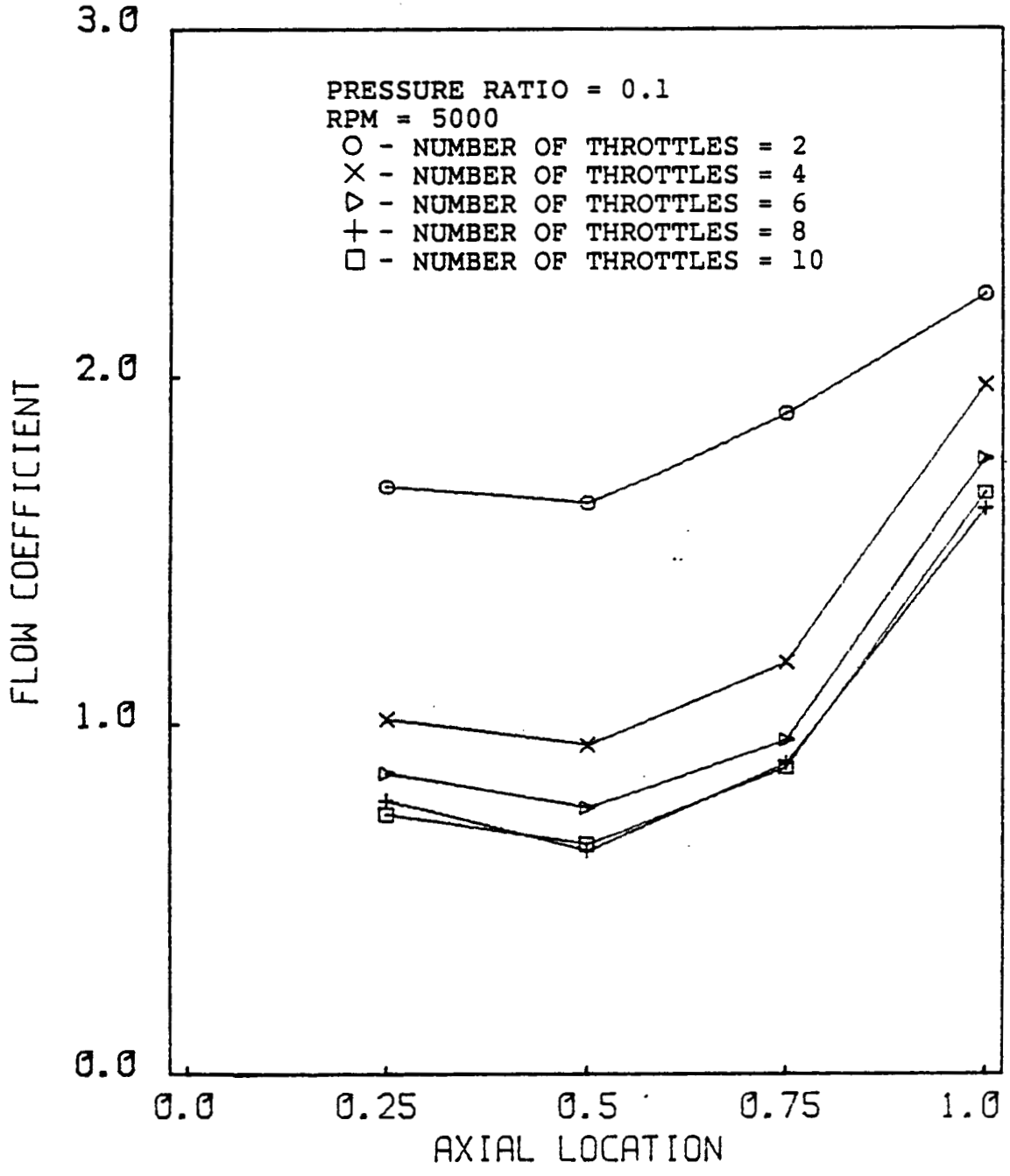

Figure 48. The Effects of Number of Throttles at Different Axial Locations.

different axial locations.

Figure 48 illustrates how the axial location of the tooth with respect to the step in the stator wall (AXLO) and the number of throttles effect the flow coefficient for a pressure ratio of 0.1 and a shaft speed of 5000 rpm. As is evident, the axial location of the throttle greatly effects the leakage rate and, as was the case for straight-through labyrinth seals, as the number of throttles increases above 7, the flow coefficient becomes relatively independent of the number of throttles.

Therefore, to correct C4 for number of throttles and axial location effects, four seperate cases of number of throttles and axial locations were used:

1. Number of throttles $\geq$ 8 and the axial location $\geq$ 0.8.
2. Number of throttles $\geq$ 8 and the axial location < 0.8.
3. Number of throttles < 8 and the axial location $\geq$ 0.8.
4. Number of throttles < 8 and the axial location < 0.8.

The reason that 0.8 was chosen as a reference value was that axial location 0.8 might be a transition point in the increase of flow coefficient. That is, the increasing rate of the flow coefficient at axial location 1.0 with increasing number of throttles was less than those at axial location of 0.75, 0.5, and 0.25 as shown in Figure 48. Therefore, it was observed that the transition point would be around 0.8.

If condition 1 existed, there was no need to correct for the number of throttles effects, and C4 should be corrected only for axial location effects with the following equation: C5 = (C4)(C5A)/C5B. C5A was the value of the flow coefficient from Figure 48 at the required axial location and C5B was the value at

an axial location of 0.8. If condition 2 existed, the same procedure as case 1 was used.

For condition 3, C4 had to be corrected for both number of throttles and axial location effects. The following equations were used: C8 = (C4)(C7A)/C7B and C9 = (C8)(C5A)/C5B. C7A was the value of the flow coefficient at the required number of throttles and C7B was the value for eight throttles at an axial location of 1.0. Thus, C8 was the flow coefficient corrected for the number of throttles effect. The C5A and C5B were the same values as for conditions 1 and 2 which were used to correct for the axial location effects.

For condition 4, C4 was corrected for both number of throttles and axial location effects with the following equations: C10 = (C4)(C8A)/C8B and C11 = (C10)(C5A)/C5B. C8A was the value of the flow coefficient at the required number of throttles and C8B was the value of the flow coefficient at eight throttles and axial location of 0.75. Thus C10 was the flow coefficient corrected for the number of throttles effect. The C5A and C5B were the same values as before which are used to correct for the axial location effects.

With the appropriate value of the flow coefficient now determined, the mass leakage rate was then calculated according to equation (15).

Modifications to Original Empirical Leakage Estimation Model

Experimental data was used to evaluate and modify the empirical leakage estimation model which had previously been developed. Modifications to the program were the following: (a) empirical data, which was previously read into the program from a

separate file, was curve fitted; (b) the effect of swirl on the flow coefficient was incorporated into the program; and (c) a correction factor for clearances greater than 0.007 inches was added.

Empirical data was curve fitted using on a Hewlett-Packard 41-CX. The curve fit program used the least squares method to select the best fit out of nineteen possible equations. Figures 49-54 show the curve fit lines and their corresponding empirical data points. The empirical data points are darkened. The figures show that the data was fit quite effectively by the curve fit program. The data used for the curve fits can be found in Appendix A. Equations for the curve fits can be found in Tables 2-11 corresponding to Figures 49-53 (i.e. Figure 49 corresponds to Table 2). In order to obtain the desired correction factor, each subroutine linearly interpolates between calculated data points.

The effect of swirl on the flow coefficient was incorporated into the program. In order to obtain the flow coefficient for swirled flow, the unswirled flow coefficient was multiplied by a flow ratio. The flow ratio is an empirical ratio of the flow coefficient with swirl divided by the flow coefficient without swirl. These ratios were expeimentally determined using the oxygen turbopump front wear ring seal. Tables 8 and 9 show some of the empirical flow ratios for a clearance of 0.007 inches as measured in the present study for the oxygen pump front wear ring seal. Table 10 shows the corresponding flow ratios used by the leakage estimation program. Flow ratios for a clearance of 0.014 inches are found in Table 11. Table 12 shows the computational

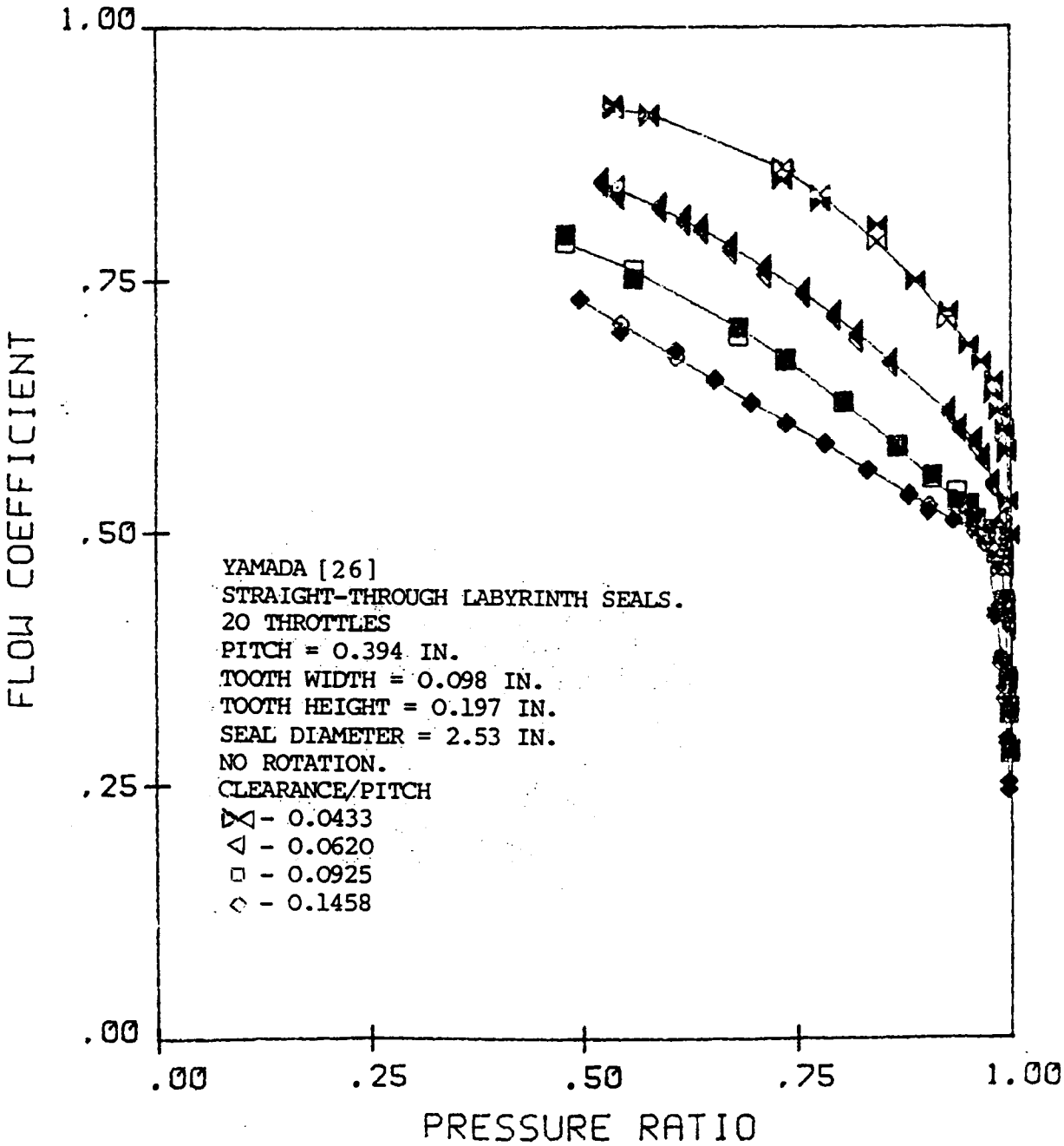

Figure 49. Comparison of Curve Fit and Experimental Data of Flow Coefficient vs. Pressure Ratio for Straight-through Labyrinth Seals.

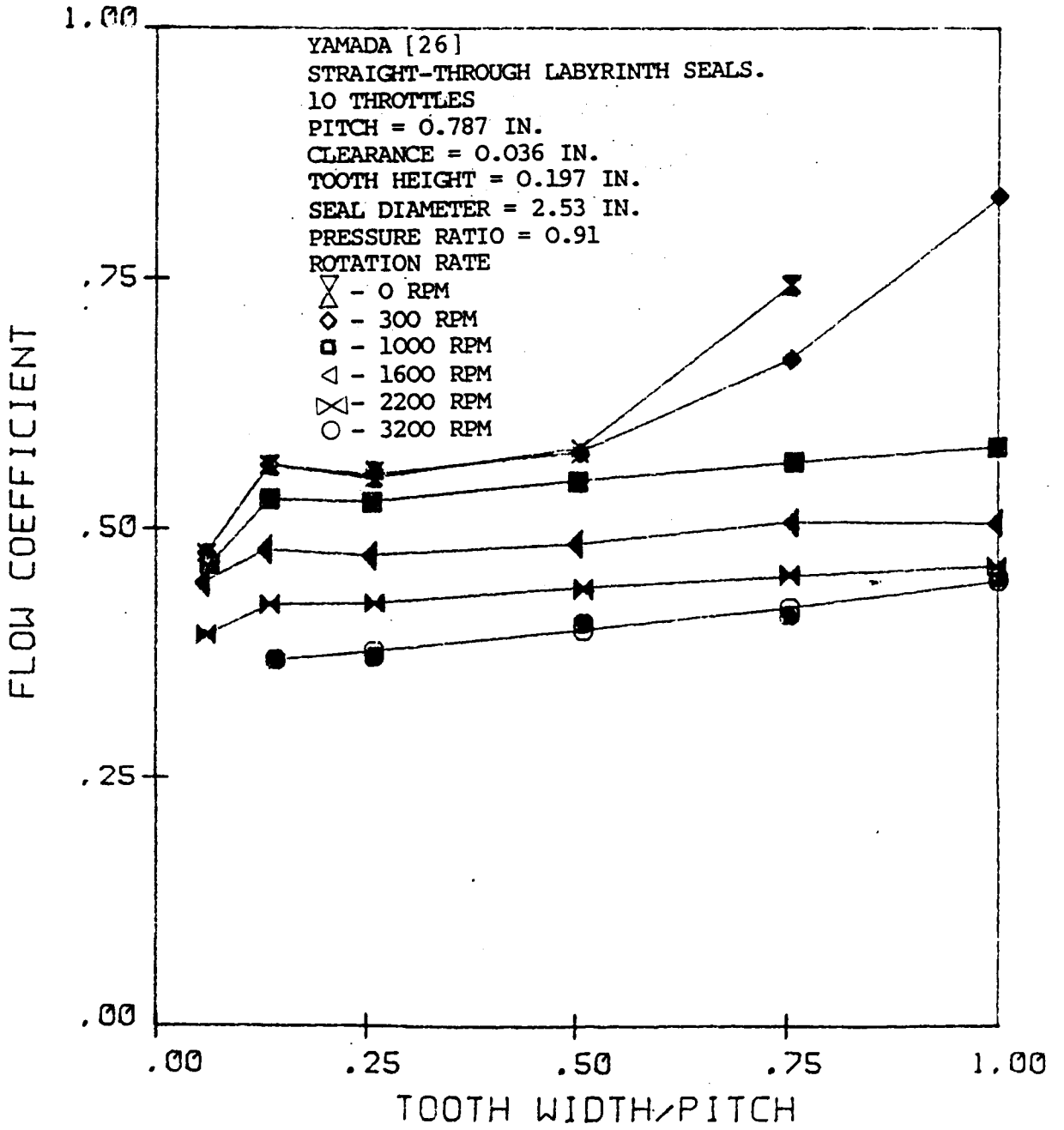

Figure 50. Comparison of Curve Fit and Experimental Data of Flow Coefficient vs. Tooth Width/Pitch for a Ten Throttle Straight-through Labyrinth Seal.

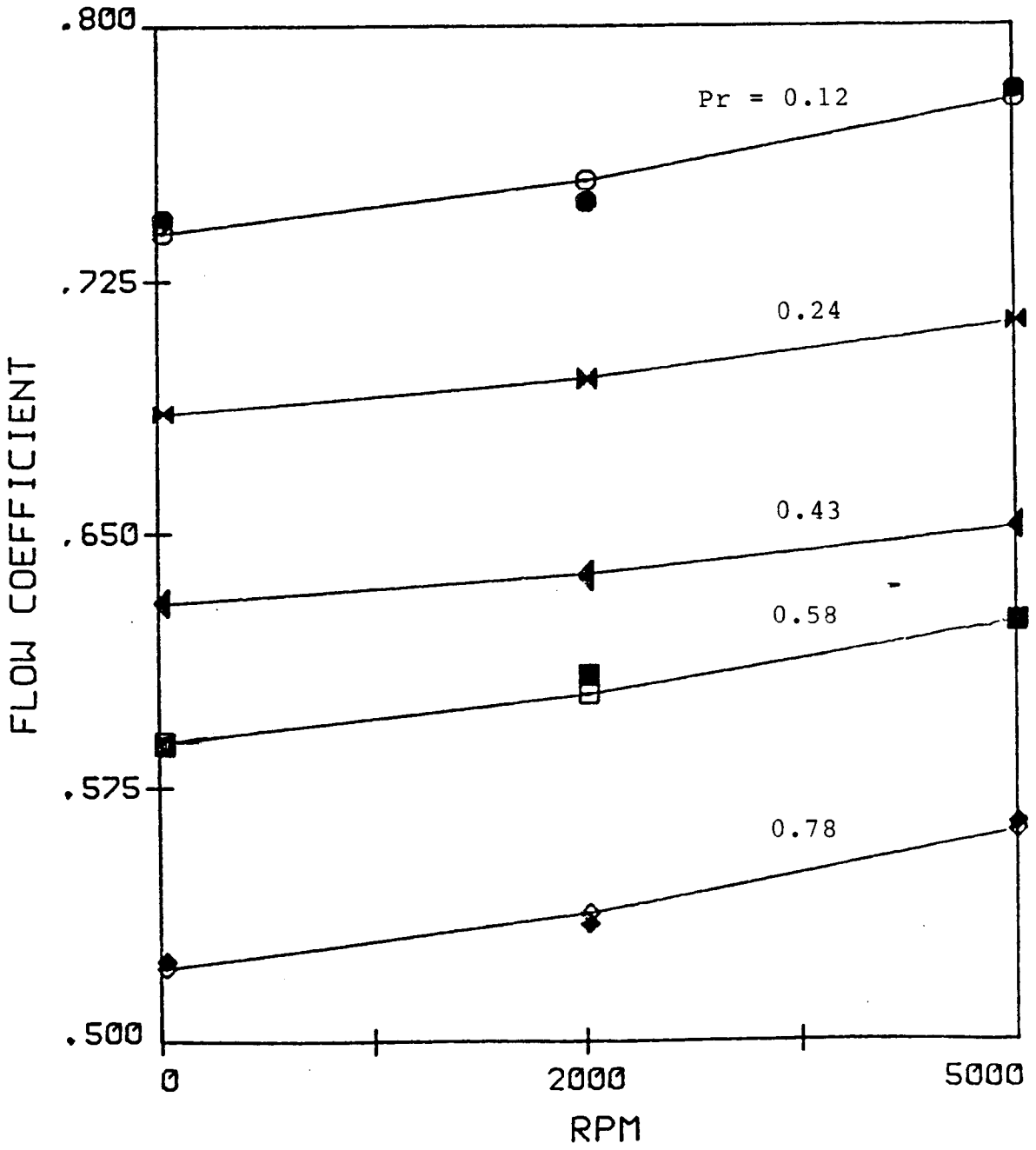

Figure 51. Comparison of Curve Fit and Experimental Data of Flow Coefficient vs. Shaft Speed for Various Pressure Ratios, AXLO=0.50, Ten Teeth.

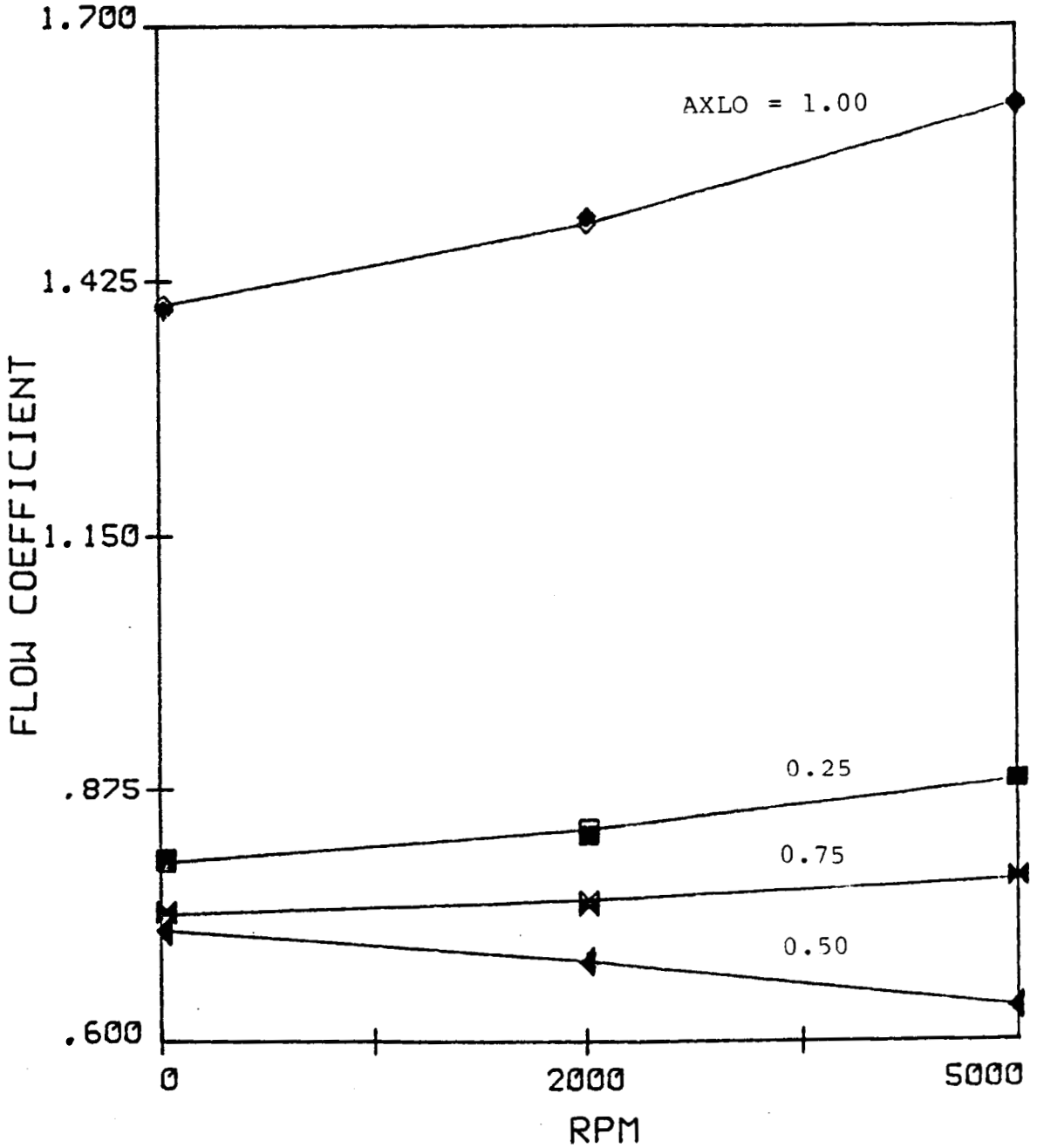

Figure 52. Comparison of Curve Fit and Experimental Data of Flow Coefficient vs. shaft speed, Pr = 0.12, Ten Teeth.

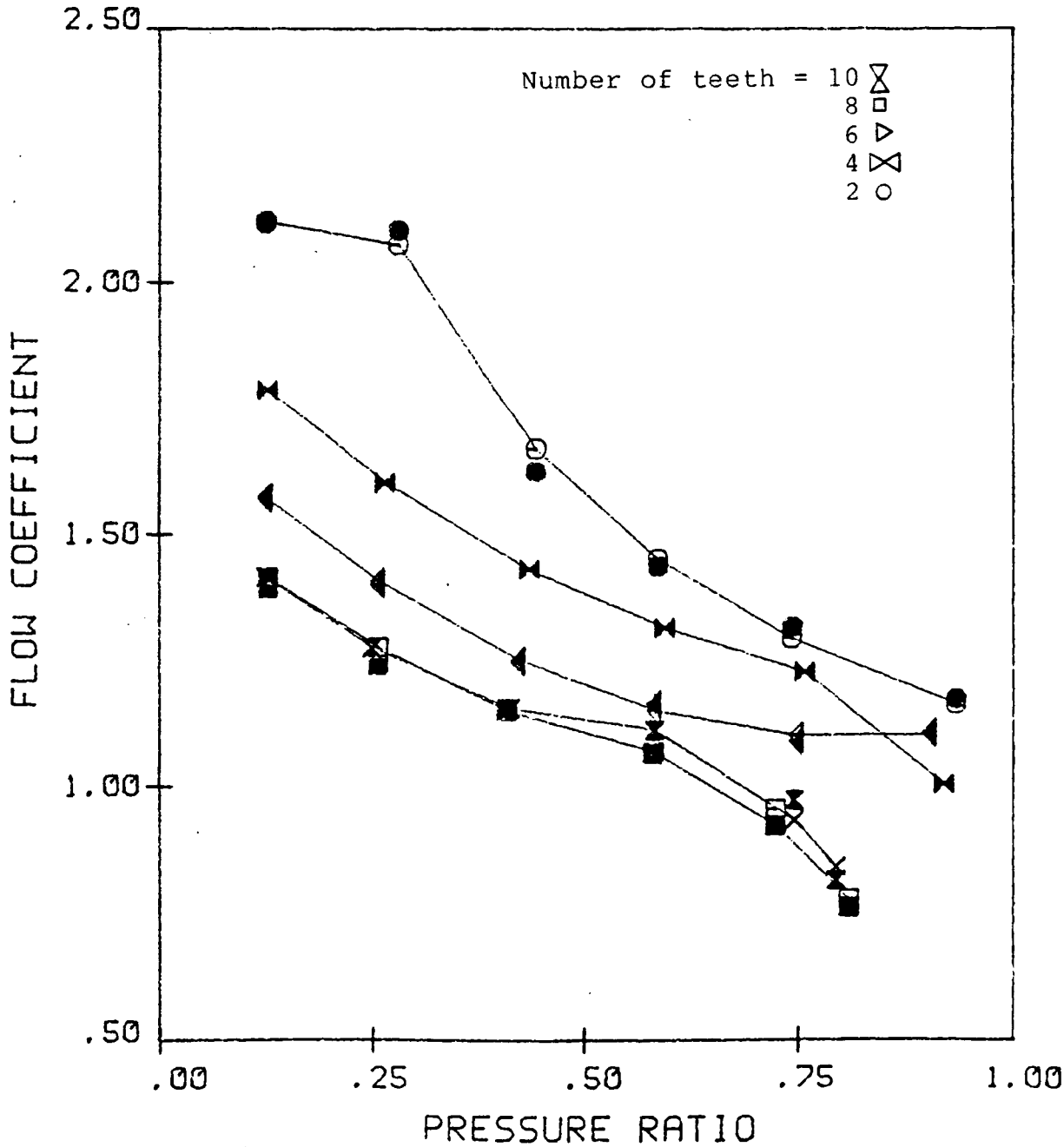

Figure 53. Comparison of Curve Fit and Experimental Data of Flow Coefficient vs. Pressure Ratio, AXLO=1.00.

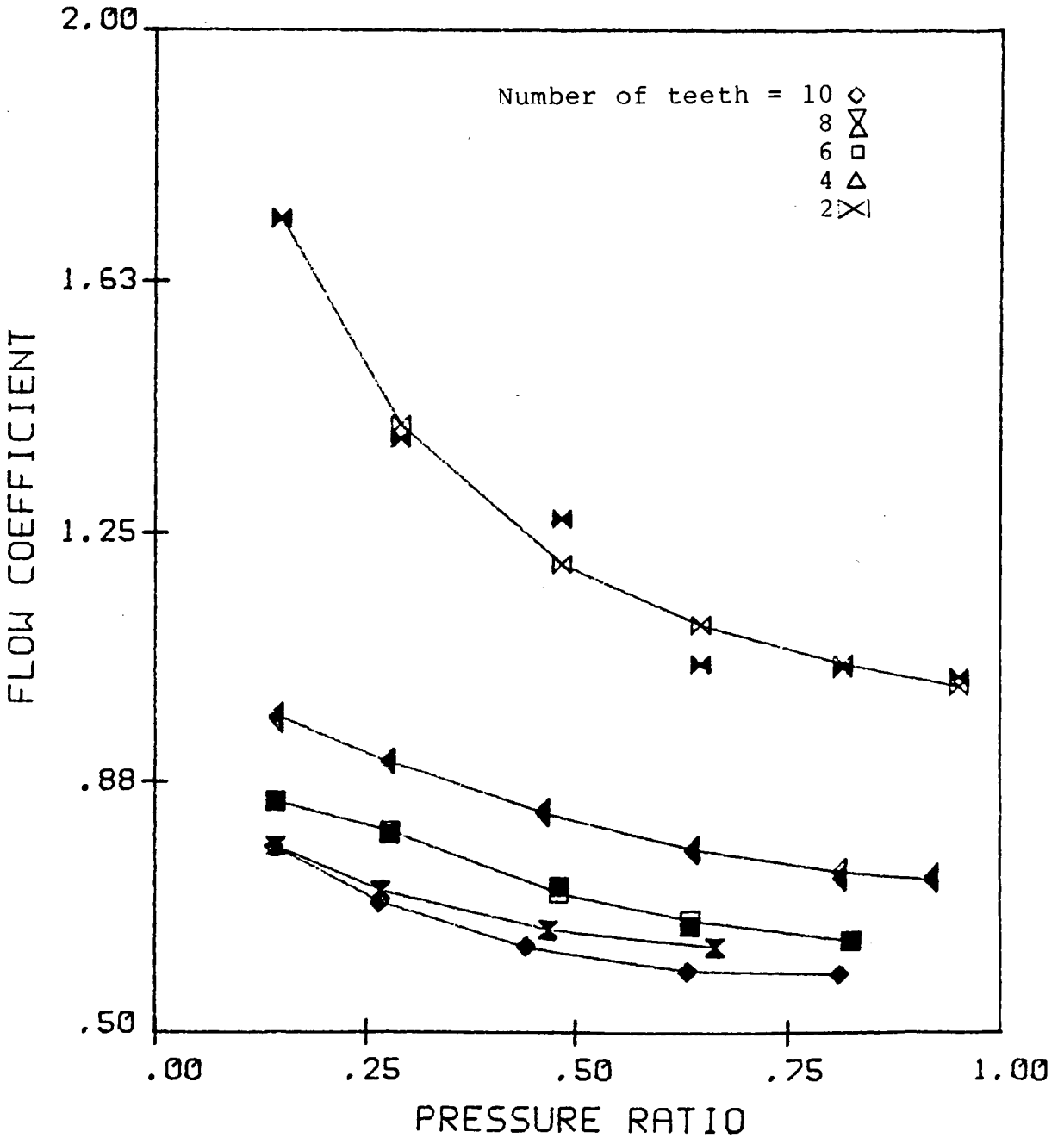

Figure 54. Comparison of Curve Fit and Experimental Data of Flow Coefficient vs. Pressure Ratio, AXLO=0.75

Table 2. Curve Fit Equations Corresponding to Figure 49.

CTOP	PR	FLOW COEFFICIENT
0.0433	>0.96	=367.049-190.772*PR-.07/PR
	≤0.96	=0.98-0.5031*PR
0.0620	≥0.98	=0.465*EXP(((-0.014-LOG(PR))**2)/(-.000289))
	<0.98	=0.828+.164*PR-.514*PR**2
0.0925	>0.9936	=0.493*EXP(((-.006-LOG(PR))**2)/(.00004953))
	0.9403< PR ≤0.9936	=81.728*PR-43.385*PR**2-37.887
	≤0.9403	=0.866+.259*PR-.568*PR**2
0.15	>0.9789	=0.626*EXP(((-.013*LOG(PR))**2)/(-.0004663))
	≤0.9789)	=0.587+1.287*PR-1.246*PR**2

Table 3. Curve Fit Equations Corresponding to Figure 50.

RPM	WTOP	FLOW COEFFICIENT
3200	≤1.00	=1/(2.786-.546*WTOP)
2200	≥0.13	=.457*(1.017**(1./WTOP))*WTOP**.097
	<0.13	=.399*WTOP+.373
1600	≥0.125	=.501*(1.02**(1/WTOP))*WTOP**(.097)
	<0.125	=.448*WTOP+.424
1000	≥0.130	=.569*(1.024**(1/WTOP))*WTOP**.124
	<0.130	=.895*WTOP+.413
300	≥0.128	=.601-.330*WTOP+.560*WTOP**2
	<0.128	=1.181*WTOP+.413
0	≥0.128	=1./(1.819-2.267*(WTOP-.295)**2)
	<0.128	=1.181*WTOP+.413

Table 4. Curve Fit Equations Corresponding to Figure 51.

PR	RPM	FLOW COEFFICIENT
0.75	$\leq$5000	=RPM*8.063E-6+.52245
0.58	$\leq$5000	=RPM*7.0105E-6+.58873
0.43	$\leq$5000	=RPM*4.4079E-6+.62939
0.24	$\leq$5000	=RPM*5.365E-6+.68572
0.12	$\leq$5000	=RPM*7.8505E-6+.73897

Table 5. Curve Fit Equations Corresponding to Figure 52.

AXLO	RPM	FLOW COEFFICIENT
1.00	$\leq$5000	=RPM*4.3723E-5+1.39917
0.75	$\leq$5000	=RPM*1.8151E-5+.795412
0.50	$\leq$5000	=RPM*(-1.6817E-5)+.721041
0.25	$\leq$5000	=RPM*7.8505E-6+.738972

Table 6. Curve Fit Equations Corresponding to Figure 53.

TNUM	PR	FLOW COEFFICIENT
10	≥0.578	=.495+2.985*PR-3.155*PR**2
	<0.578	=1.589-1.626*PR+1.368*PR**2
8	≥0.577	=.714+2.082*PR-2.48*PR**2
	<0.577	=1.25-.380*PR+.023/PR
6	≤1.00	=1.747-1.596*PR+.98*PR**2
4	≥0.755	=2.258-1.363*PR
	<0.755	=1.139*EXP((PR-1.193)**2/2.55)
2	≤1.00	=.603+.573/PR-.047/PR**2

Table 7. Curve Fit Equations Corresponding to Figure 54.

TNUM	PR	FLOW COEFFICIENT
10	$\leq$1.00	=.555+.053/PR-.003/PR**2
8	$\leq$1.00	=1/((-1.049)*(PR-.766)**2+1.702)
6	$\leq$1.00	=.513+.113/PR-.009/PR**2
4	$\leq$1.00	=1.063-.648*PR+.310*PR**2
2	$\leq$1.00	=.809+.215/PR-.012/PR**2

Table 8. Empirical Flow Ratio at a Rotation Rate of 0 rpm and a Clearance of 0.007 inches for Various Seal Configurations.

AXIAL LOCATION	NUMBER OF THROTTLES	PRESSURE RATIO	FLOW RATIO CCW SWIRL	FLOW RATIO CW SWIRL
		0.13	1.00	1.01
	2	0.45	1.00	1.05
		0.60	0.99	1.08
		0.13	0.99	1.00
1.00	4	0.45	1.01	1.01
		0.60	1.02	0.99
		0.13	0.97	0.97
	6	0.45	0.96	0.95
		0.60	0.96	0.97
		0.13	0.91	0.83
	2	0.45	0.95	0.79
		0.60	0.94	0.80
		0.13	0.90	0.85
0.75	4	0.45	0.91	0.88
		0.60	0.85	0.81
		0.13	0.93	1.01
	6	0.45	0.88	0.94
		0.60	0.83	0.91
		0.13	0.96	0.98
	2	0.45	0.95	0.98
		0.60	0.96	0.98
		0.13	0.98	0.94
0.50	4	0.45	0.99	0.96
		0.60	0.99	0.93
		0.13	0.99	1.02
	6	0.45	0.98	0.99
		0.60	0.97	0.98
		0.13	1.25	1.06
0.25	4	0.45	1.20	1.05
		0.60	1.18	1.05
		0.13	1.09	1.15
	6	0.45	1.12	1.18
		0.60	1.11	1.16

Table 9. Empirical Flow Ratio at a Rotation Rate of 5000 rpm and a Clearance of 0.007 inches for Various Seal Configurations.

AXIAL LOCATION	NUMBER OF THROTTLES	PRESSURE RATIO	FLOW RATIO CCW SWIRL	FLOW RATIO CW SWIRL
		0.13	0.99	1.05
	2	0.45	1.00	1.06
		0.60	1.00	1.07
		0.13	0.99	0.99
1.00	4	0.45	0.99	0.99
		0.60	1.01	1.00
		0.13	0.96	0.95
	6	0.45	0.96	0.94
		0.60	0.97	0.96
		0.13	0.95	0.85
	2	0.45	0.93	0.80
		0.60	0.92	0.80
		0.13	0.92	0.85
0.75	4	0.45	0.88	0.85
		0.60	0.85	0.80
		0.13	0.87	0.96
	6	0.45	0.08	0.95
		0.60	0.84	0.92
		0.13	0.97	0.98
	2	0.45	0.96	0.99
		0.60	0.96	1.00
		0.13	0.99	0.98
0.50	4	0.45	0.99	0.96
		0.60	0.98	0.95
		0.13	0.98	1.01
	6	0.45	0.98	0.99
		0.60	0.96	0.98
		0.13	1.19	1.01
0.25	4	0.45	1.18	1.04
		0.60	1.17	1.02
		0.13	1.08	1.14
	6	0.45	1.10	1.16
		0.60	1.11	1.16

Table 10. Computational Flow Ratio at a Clearance of 0.007 inches for Various Seal Configurations.

AXIAL LOCATION	NUMBER OF THROTTLES	PRESSURE RATIO	FLOW RATIO
>0.87	<3	<0.45	1.03
		≥0.45	1.03
		≥0.75	1.03
	≥3 and <5	<0.45	1.00
		≥0.45	1.00
		≥0.75	1.00
	≥5	<0.45	0.96
		≥0.45	0.96
		≥0.75	0.96
≤0.87 and >0.63	2	<0.45	0.89
		≥0.45	0.87
		≥0.75	0.87
	4	<0.45	0.88
		≥0.45	0.88
		≥0.75	0.83
	6	<0.45	0.92
		≥0.45	0.90
		≥0.75	0.88
≤0.63 and >0.37	2	<0.45	0.98
		≥0.45	0.98
		≥0.75	0.98
	4	<0.45	0.98
		≥0.45	0.98
		≥0.75	0.98
	6	<0.45	0.99
		≥0.45	0.99
		≥0.60	0.99
≤0.37	2	<0.45	1.10
		≥0.45	1.10
		≥0.75	1.10
	4	<0.45	1.10
		≥0.45	1.10
		≥0.75	1.10
	6	<0.45	1.13
		≥0.45	1.13
		≥0.60	1.13

Table 11. Empirical Flow Ratio at a Clearance of 0.014 inches for Various Seal Conditions.

AXIAL LOCATION	NUMBER OF THROTTLES	PRESSURE RATIO	FLOW RATIO CCW SWIRL	FLOW RATIO CW SWIRL
		0.25	1.02	1.00
	2	0.45	1.04	1.01
		0.75	1.02	1.02
		0.25	1.00	1.00
0.75	4	0.45	1.00	1.00
		0.75	1.01	1.00
		0.25	0.91	0.91
	6	0.45	0.91	0.96
		0.75	0.91	0.96
		0.25	1.00	1.02
	2	0.45	1.04	1.01
		0.75	1.02	1.01
		0.25	1.03	
0.50	4	0.45	1.02	
		0.75	1.00	
		0.25	0.85	
	6	0.45	0.83	
		0.75	0.85	

Table 12. Computational Flow Ratio at a Clearance of 0.014 inches for Various Seal Configurations.

AXIAL LOCATION	NUMBER OF THROTTLES	FLOW RATIO
> 0.625	<3	1.02
		1.02
		1.02
	3≥ and <5	1.00
		1.00
		1.00
	≥5	0.93
		0.93
		0.93
≤ 0.625	<3	1.02
		1.02
		1.02
	3≥ and <5	1.02
		1.02
		1.02
	≥5	0.86
		0.86
		0.86

flow ratios corresponding to this clearance. The flow ratios for clearances of 0.007 and 0.014 inches are found by checking the axial location, number of throttles, pressure ratio and swirl direction as shown in Tables 10 and 12. If the clearance is less than 0.007 inches, the program used the flow ratio for the clearance of 0.007 inches. Linear interpolation, using the flow ratios for both clearances, was used to calculate flow ratios for clearances between and greater than 0.007 and 0.014 inches.

Figures 55-58 show the comparison of the leakage estimation program with experimental data obtained for the oxygen turbopump front wear ring seal. Except for the axial location of 1.00, the flow coefficients are predicted accurately by this program for the oxygen pump front wear ring seal. The seal design was shown previously in Figure 41. The poor predictions by the leakage estimation program for the axial location of 1.00 are caused by a disagreement between experimental data used in the original leakage estimation program and the experimental data used in this effort. The original leakage estimation data predicted a much higher flow coefficient at an axial location of 1.00.

The origianl leakage estimation program poorly predicted the flow coefficient for clearances greater than 0.007 inches. A correction factor was added to accurately predict flow coefficients for larger clearances. Table 13 shows the ratio of the experimental flow coefficient divided by the analytical flow coefficient for seal rotation rates of 0 and 5000 rpm.

The ratios in Table 13 were curve fitted and used in the leakage estimation program as the correction factor. Equations for the curve fits can be found in Table 14. Empirical ratios

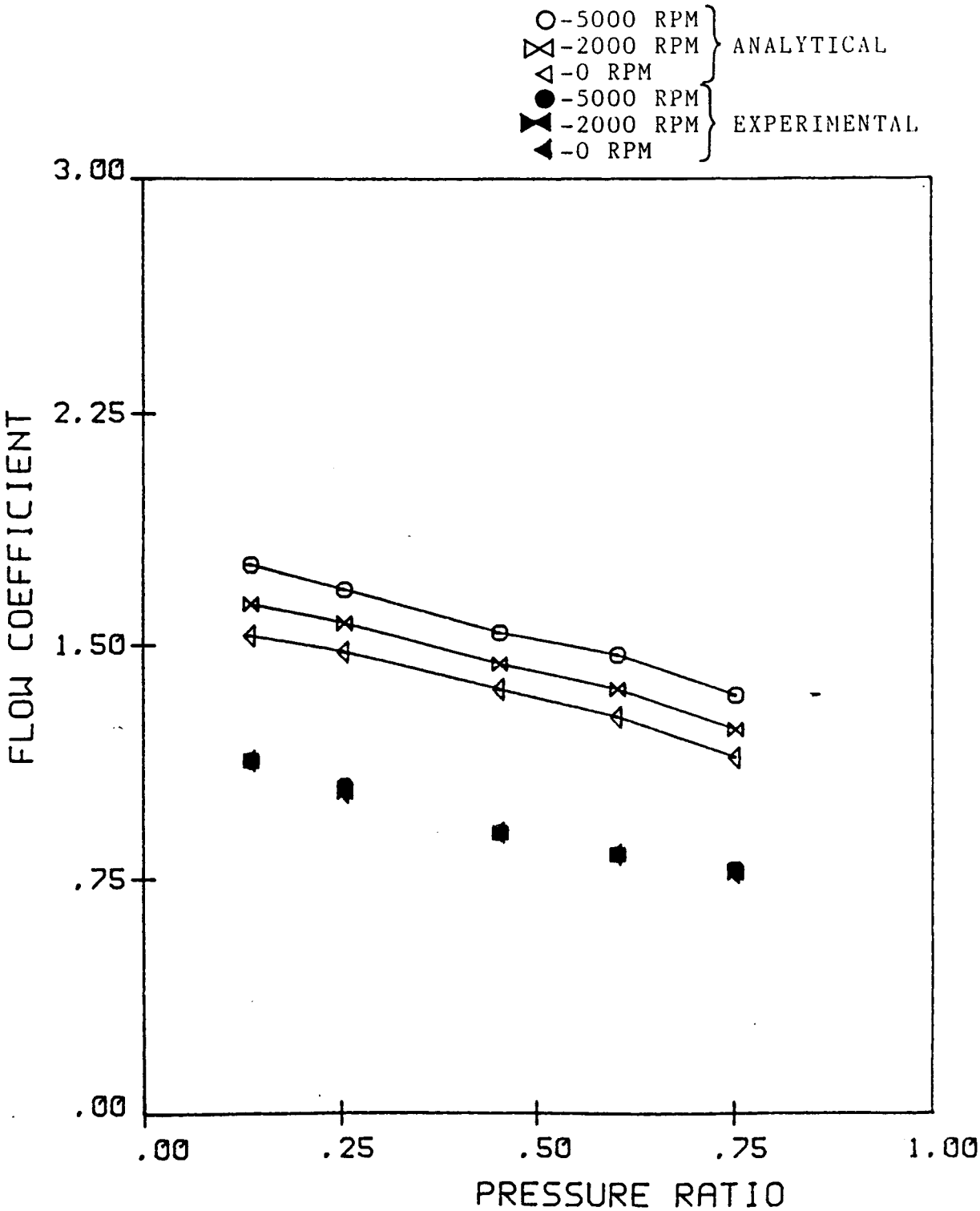

Figure 55. Comparison of Analytic Flow Coefficients with Experimental Data for Various Rotation Rates, Four Throttles, a Clearance of 0.007 in., Counter-clockwise Swirl, and an Axial Location of 1.00.

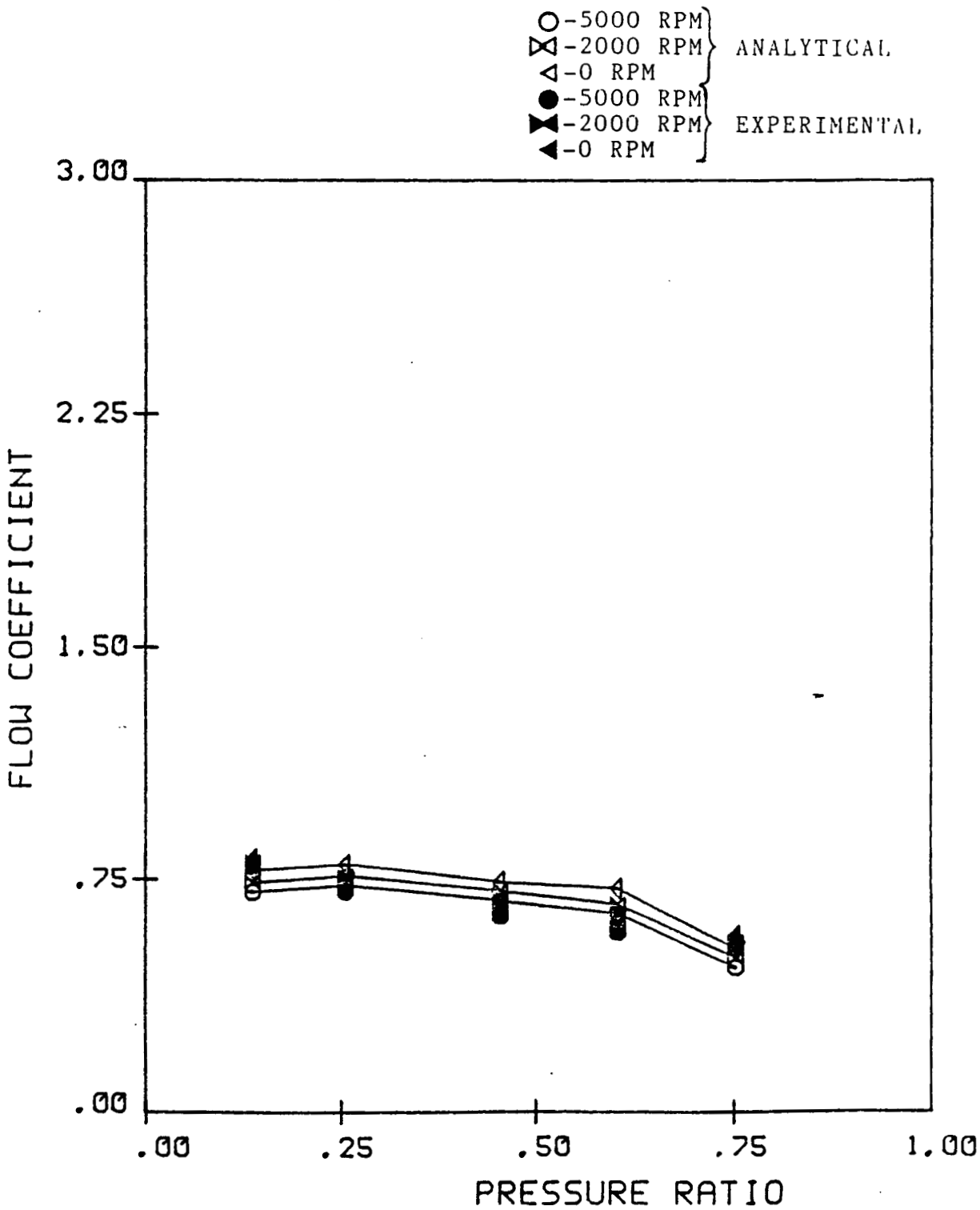

Figure 56. Comparison of Analytic Flow Coefficients with Experimental Data for Various Rotation Rates, Four Throttles, a Clearance of 0.007 inc., Clockwise Swirl, and an Axial Location of 0.75.

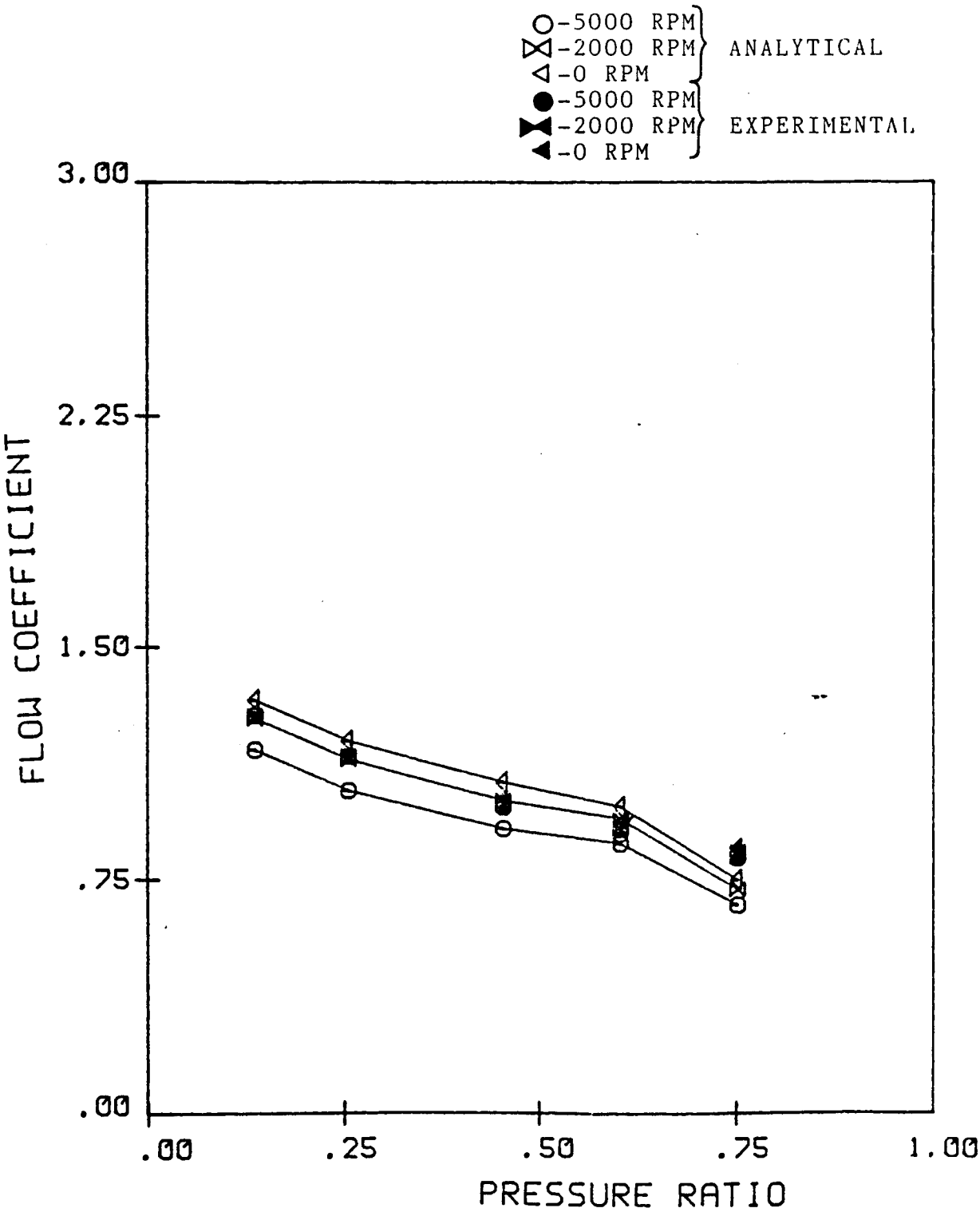

Figure 57. Comparison of Analytic Flow Coefficients with Experimental Data For Various Rotation Rates, Four Throttles, a Clearance of 0.007 in., Counter-clockwise Swirl, and an Axial Location of 0.50.

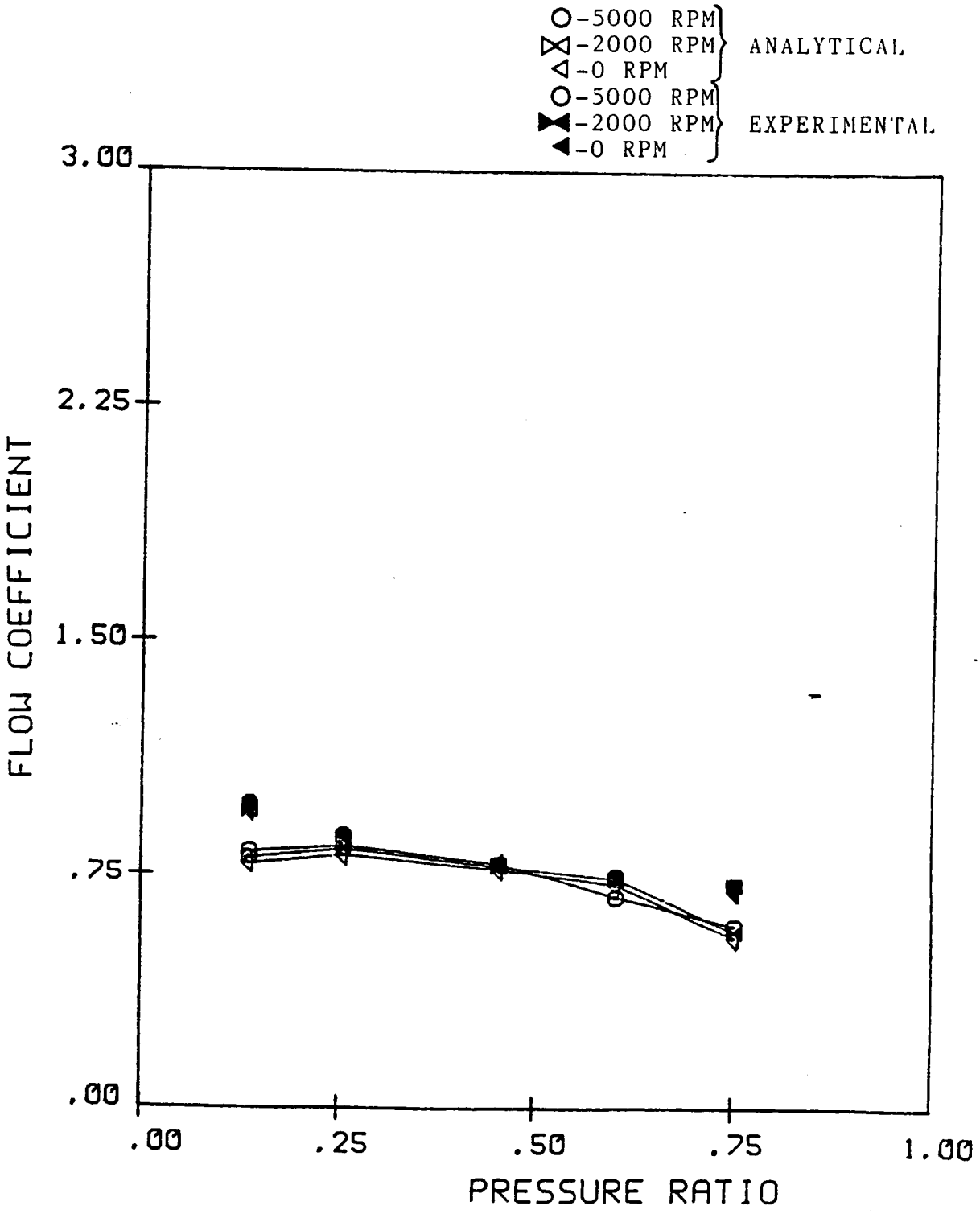

Figure 58. Comparison of Analytic Flow Coefficients with Experimental Data for Various Rotation Rates, Four Throttles, a Clearance of 0.007 in., Clockwise Swirl, and an Axial Location of 0.25.

Table 13. Ratio of Experimental/Analytical Data for a Clearance of 0.014 inches for Various Seal Configurations.

AXIAL LOCATION	NUMBER OF THROTTLES	PRESSURE RATIO	EXPERIMENTAL/ ANALYTICAL RPM 0	5000
		0.25	3.01	2.63
	2	0.45	2.55	2.28
		0.60	2.41	2.10
		0.75	2.36	2.02
		0.25	4.32	3.71
0.75	4	0.45	3.55	3.14
		0.60	3.38	2.91
		0.75	2.96	2.82
		0.25	4.45	3.80
	6	0.45	3.81	3.33
		0.60	3.66	3.10
		0.75	3.76	3.03
		0.25	2.77	3.16
	2	0.45	2.43	2.85
		0.60	2.31	2.61
		0.75	2.27	2.52
		0.25	3.97	4.47
0.50	4	0.45	3.34	3.81
		0.60	3.14	3.53
		0.75	3.23	3.46
		0.25	3.99	4.65
	6	0.45	3.56	4.08
		0.60	3.42	3.78
		0.75	3.54	3.74

Table 14. Curve Fit Equations Corresponding to Table 13.

AXLO	TNUM	RPM	FLOW RATIO
≤0.625	2	0	=1./(.44-.305*(PR-.758)**2.)
		5000	=3.74-2.622*PR+1.309*PR**2.
	4	0	=5.412-7.205*PR+5.726*PR**2.
		5000	=5.771-6.276*PR+4.248*PR**2.
	6	0	=5.07-5.431*PR+4.513*PR**2.
		5000	=5.839-5.698*PR+3.85*PR**2.
>0.625	2	0	=1.369*1.724**PR*PR**(-.47)
		5000	=3.282-3.047*PR+1.811*PR**2.
	4	0	=1./(.183+.203*PR)
		5000	=4.821-5.328*PR+3.556*PR**2.
	6	0	=5.913-7.354*PR+5.981*PR**2.
		5000	=4.717-4.357*PR+2.803*PR**2.

for axial location 0.75 were used to correct flow coefficients for axial locations greater than 0.625, and ratios for axial location 0.50 were used to correct flow coefficients for axial locations less than or equal to an axial location of 0.625. The correct correction factor was found by linearly interpolating the existing data.

The data was grouped by number of throttles and rotation rate. Each group was then curve fitted as previously described. The subroutine calculates correction factors for 0 to 5000 rpm. If the rotation rate was greater than 5000 rpm, the rotation rate was set at 5000 rpm for the calculation. Linear interpolation was then used to obtain a correction factor for the required rotation rate. Linear interpolation was used again to obtain the correction factor for the required number of throttles. Linear interpolation was used a third and final time to claculate the final correction factor which corresponds to the desired clearance and seal configuration. This subroutine was only used if the clearance was greater than 0.007 inches. The program and subroutine can be found in Appendix B.

Figure 59 displays the comparison of the corrected leakage estimation program with the experimental data for the oxygen pump front wear ring seal shown in Figure 41 operating with a clearance of 0.014 inches. The program predicts the flow coefficient very accurately for all cases tested.

Summary

The accuracy and versatility of the leakage estimation model were increased by this experimental program. The model was modified to incorporate the effects of swirl, and the accuracy of

ORIGINAL PAGE IS
OF POOR QUALITY

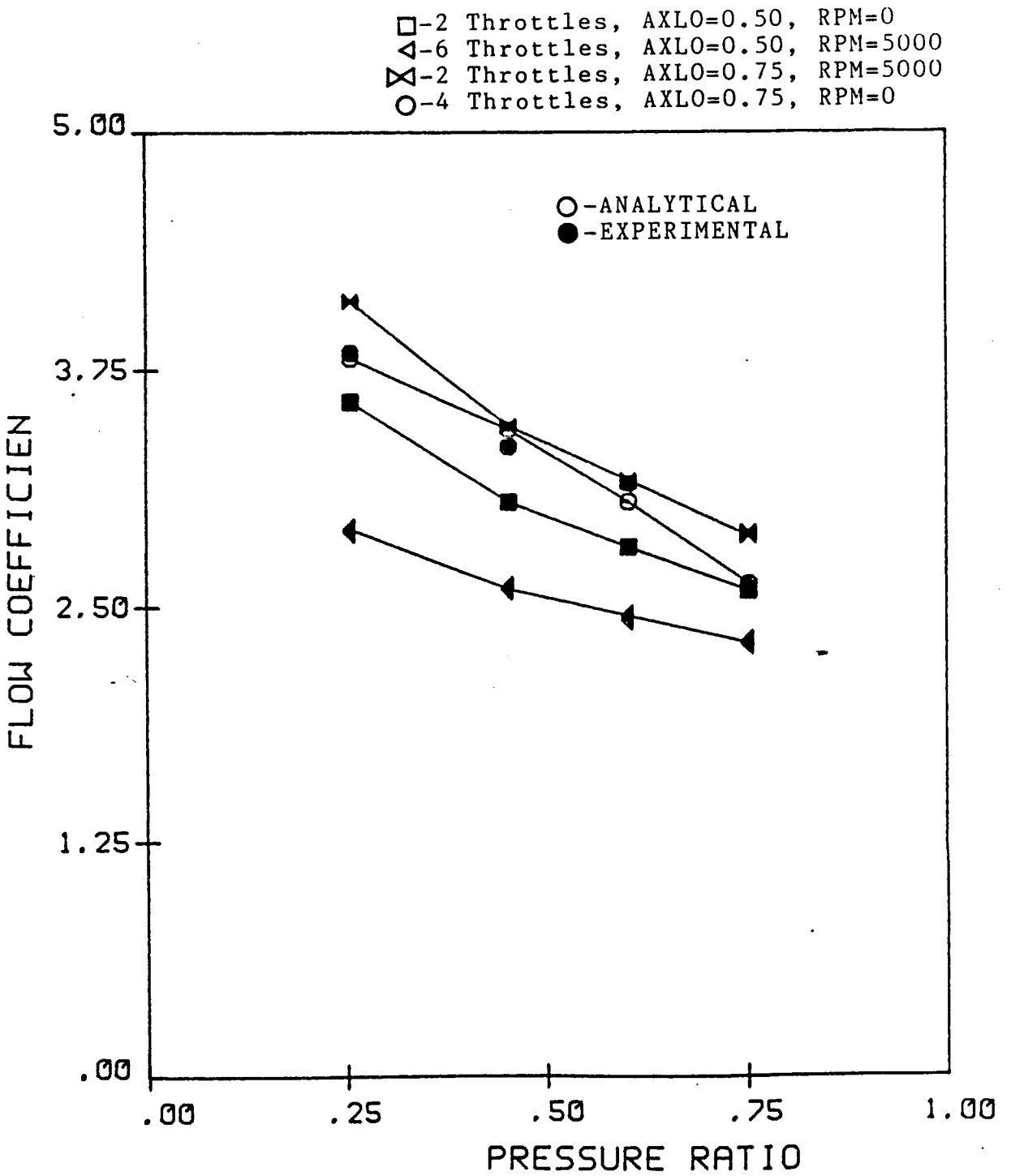

Figure 59. Comparison of Analytic Flow Coefficients with Experimental Data for Various Seal Configurations for a Clearance of 0.014 in. and No Swirl.

the model was greatly improved for seals with a clearance greater than 0.007 inches. The modified leakage estimation model gave good predictions for most cases tested.

Further data is needed to verify and modify the leakage estimation model. More data is also needed to understand the turbulent flow inside the tooth cavity and how the flow is affected by different variables. Such data would help greatly in the understanding of stepped labyrinth seals and in the development of an analytical method for leakage estimation.

VII. EXPERIMENTAL FACILITY

The overall layout of the experimental facility is shown in Figure 60. Water at approximately 80°F was used for the working fluid. The water was pumped from a 10,000 gallon storage tank by a 75 hp, 400 gpm, 400 ft head centrifugal pump. The water was strained, filtered (10 micron) and metered before being introduced into the test section. Between the pump and the strainers were shutoff valves and a bypass valve for returning excess water to the storage tank. The strainer, filter, and metering section was divided into two parallel lines equiped with valves so that either of the two legs could be operated alone or together. In one leg, a 4 to 26 gpm turbine meter was installed. The other leg had a 25 to 225 gpm turbine meter. This arrangement allowed switching between turbine meters so that the flow was maintained well within the operating range of the flow meters.

The water pressure at the inlet of the test section was maintained at about 145 psia and the valve at the exit of the test section was used to select the back pressure such that ratios of the outlet to inlet pressure were varied from 0.1 to 0.9. After exiting the test section, the water was returned to the reservoir. The large water reservoir was effective in maintaining a constant water supply temperature. During the operation of the facility, the water flowing through the test section would increase a maximum of 2 °F as measured by thermocouples located in the entrance and exit plenums of the test section.

Figure 61 is a schematic of the test section. The test section was mounted with a vertical axis of rotation. The water

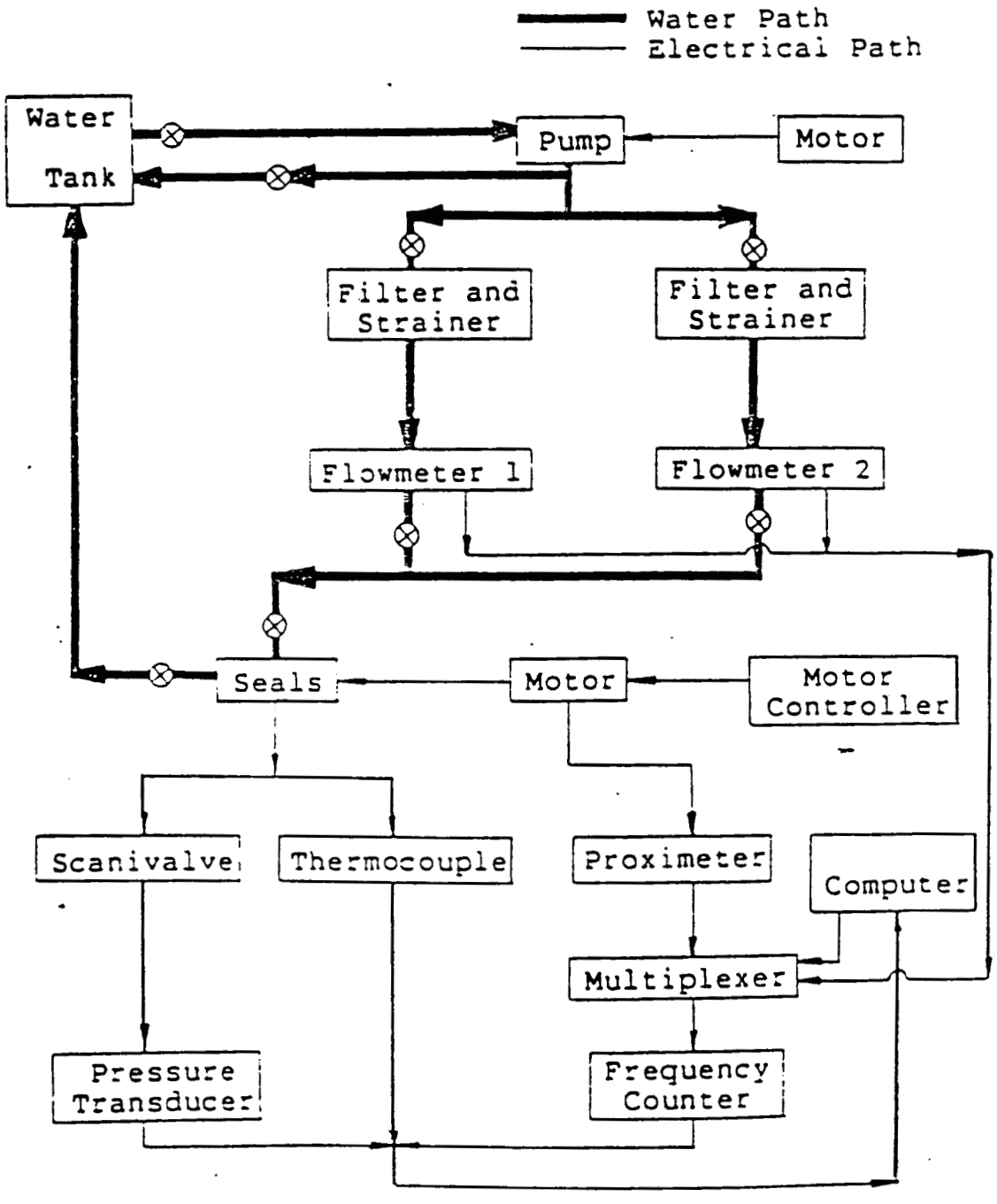

Figure 60. Schematic Diagram of the Experimental Facility.

ORIGINAL PAGE IS
OF POOR QUALITY

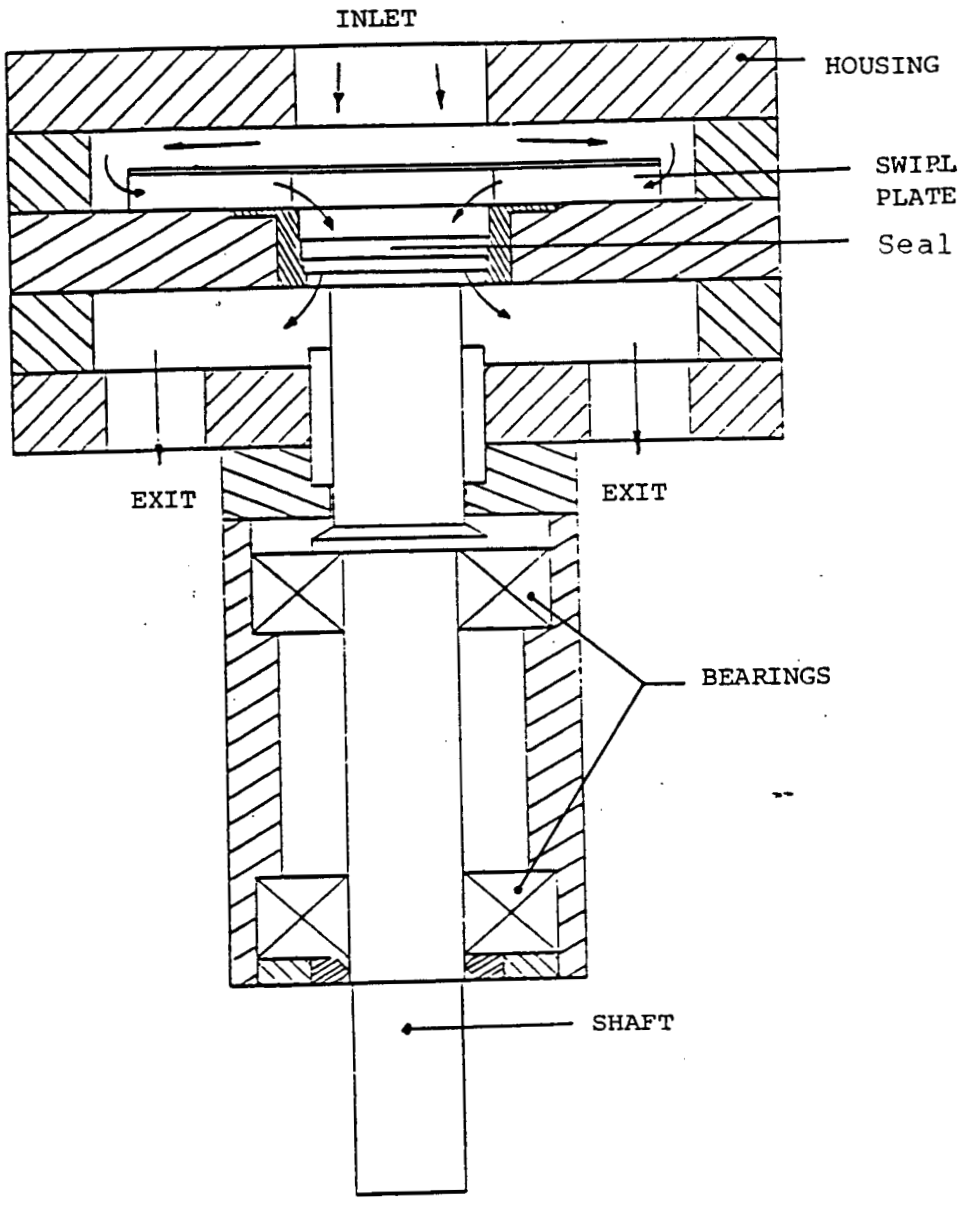

Figure 61. Configuration of the Test Section.

entered through a 3 inch flange fitting in the top, was deflected in the radial direction by a flat plate, turned 180° at the outside edge of the plenum and was directed inward by swirl vanes to the center of the test section. These swirl vanes, shown in Figures 62 and 63, can be set for various amounts of swirl. However, for the current series of tests, the vanes were set for zero swirl. The seal housing is mounted in the center of the support disk and the seal rotor is mounted on the shaft. After passing through the seal, the water exits the test section through two pipes.

The shaft of the test section is overhung and is supported by two tapered roller bearings immersed in an oil bath. The oil was pumped through the bearings by an oil pump and cooled by a six pass tube and shell heat exchanger using tap water as the cooling fluid. The shaft was rotated by a 50 hp electric motor which was driven by a variable frequency drive. In this manner, shaft speeds from 0 to 5000 rpm were obtained. The shaft speed was monitored by a proximiter probe which sensed the passing of the connecting bolts on the motor coupling. This signal was then input into a frequency counter which displayed the shaft speed.

A MINC computer system was used to monitor and record all data. The frequency counter which determined the shaft speed, was fitted with an analog multiplexor controlled by the computer such that the outputs from the two turbine meters could be input into the frequency counter as well as the shaft's speed. The frequency counter possessed a BCD parallel output which was input into the computer system. The thermocouple in the inlet plenum of the test section was connected to a digital thermometer which was also

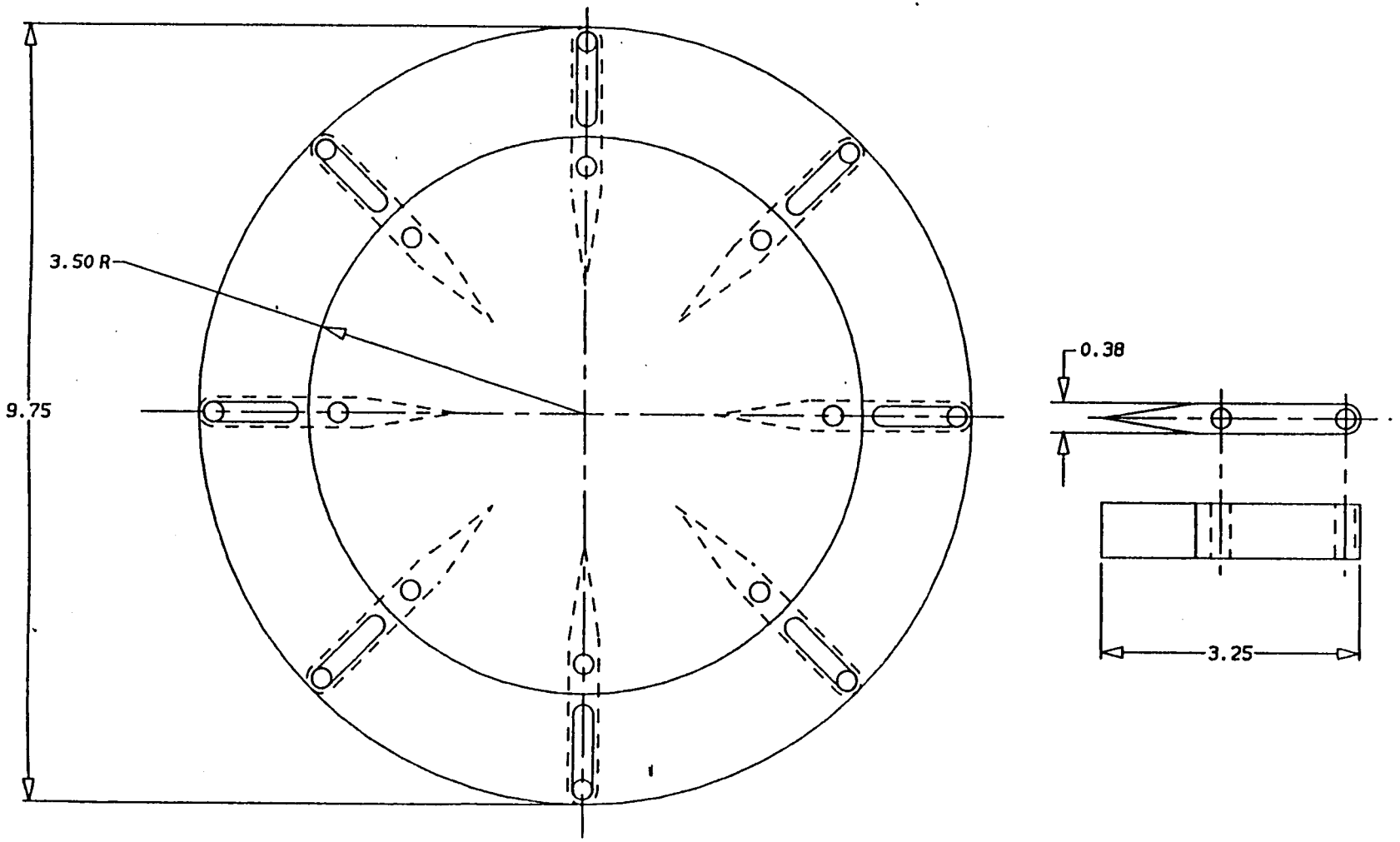

Figure 62. Swirl Plate Detail. Set for No Swirl.

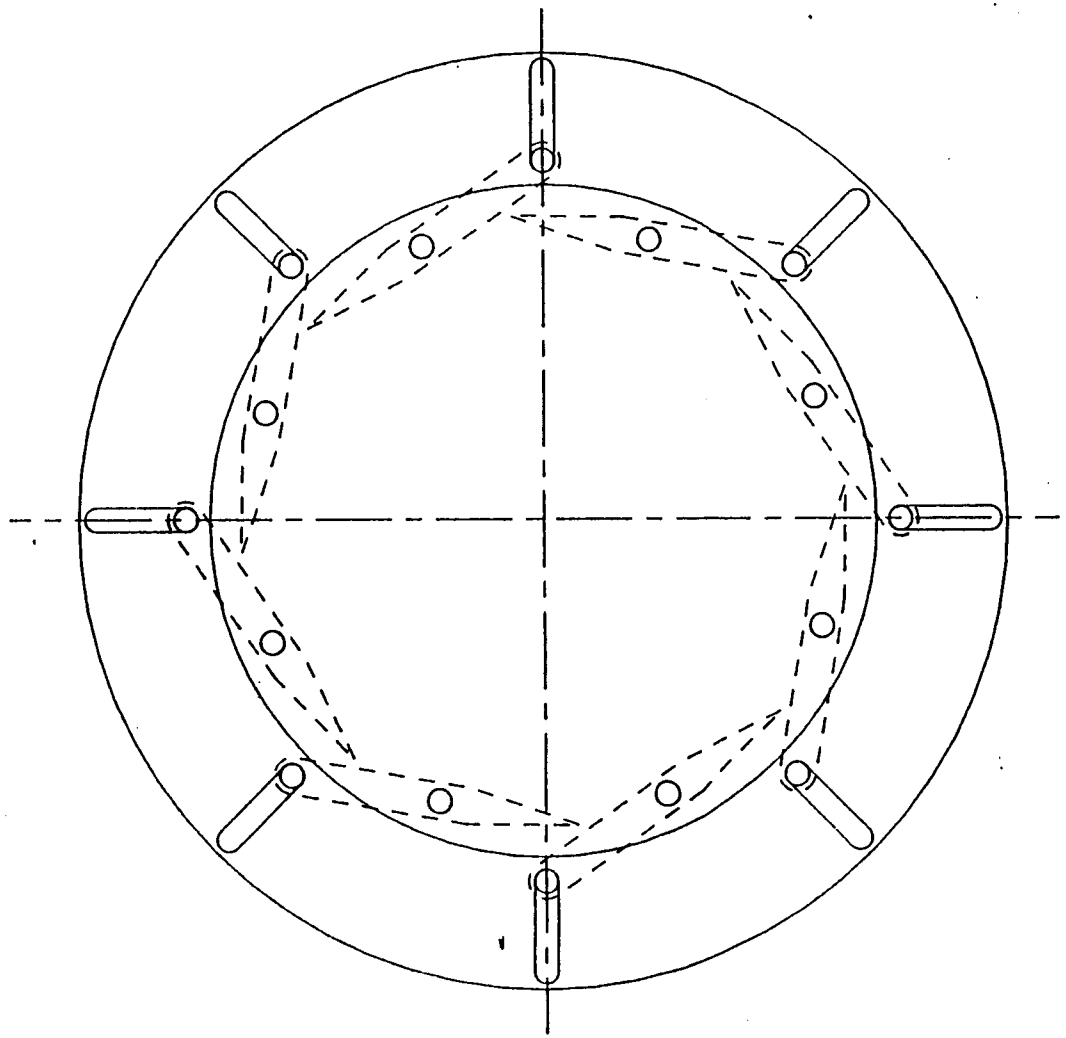

Figure 63. Swirl Plate Detail. Set for Counter-clockwise Swirl.

interfaced to the MINC computer. In this manner, the shaft speed, water flow rate and temperature were recorded.

The pressure in the inlet and exit plenums were measured as well as selected pressures in the interior of the seals. These pressures were measured using a Scanivalve system. The Scanivalve system was interfaced to the computer such that the computer could select any pressure port required, confirm the port number from the Scanivalve port number indicator, and measure the output of the pressure transducer attached to the Scanivalve. A list of the equipment used and their associated specifications are presented in Appendix C.

VIII. EXPERIMENTAL RESULTS

Seal Design #1

The first seal design to be tested was the current front wear ring seal of the hydrogen turbopump. Figures 64-66 show the design used. This seal was tested so that a basis for comparison with improved seal designs supplied by Dr. Rhode from his computational work would be available.

Figure 67 presents the flow coefficient (leakage rate) as a function of the pressure ratio across the seal (Pout/Pin) and the rotation rate of the seal. Three different axial locations (AXLO) were tested, 1.0, 0.75, and 0.50. The axial location of 1.0 corresponds to the tooth of the seal aligning with the step on the stator. Axial location 0.5 corresponds to the tooth being in the center of the step.

As we have seen before[25,28], the seal leaks less when the tooth of the rotor is near the center of the step, i.e. axial locations 0.75 and 0.50. As the pressure ratio decreased (the pressure drop across the seal increasing) the leakage rate increased from a minimum of about 0.3 for Pr=0.6 to 0.93 for Pr=0.15. For this particular seal there were no significant shaft rotation rate effects.

In order to further investigate the performance of this seal, axial pressure distribution measurements were performed. Figures 68-74 present this data for the three different axial locations for the various pressure ratios and shaft speeds. For the axial location of 1.0, there was no dependence of the pressure distribution upon either the pressure ratio or the shaft speed since all of the graphs are identical in Figures 68 and 69.

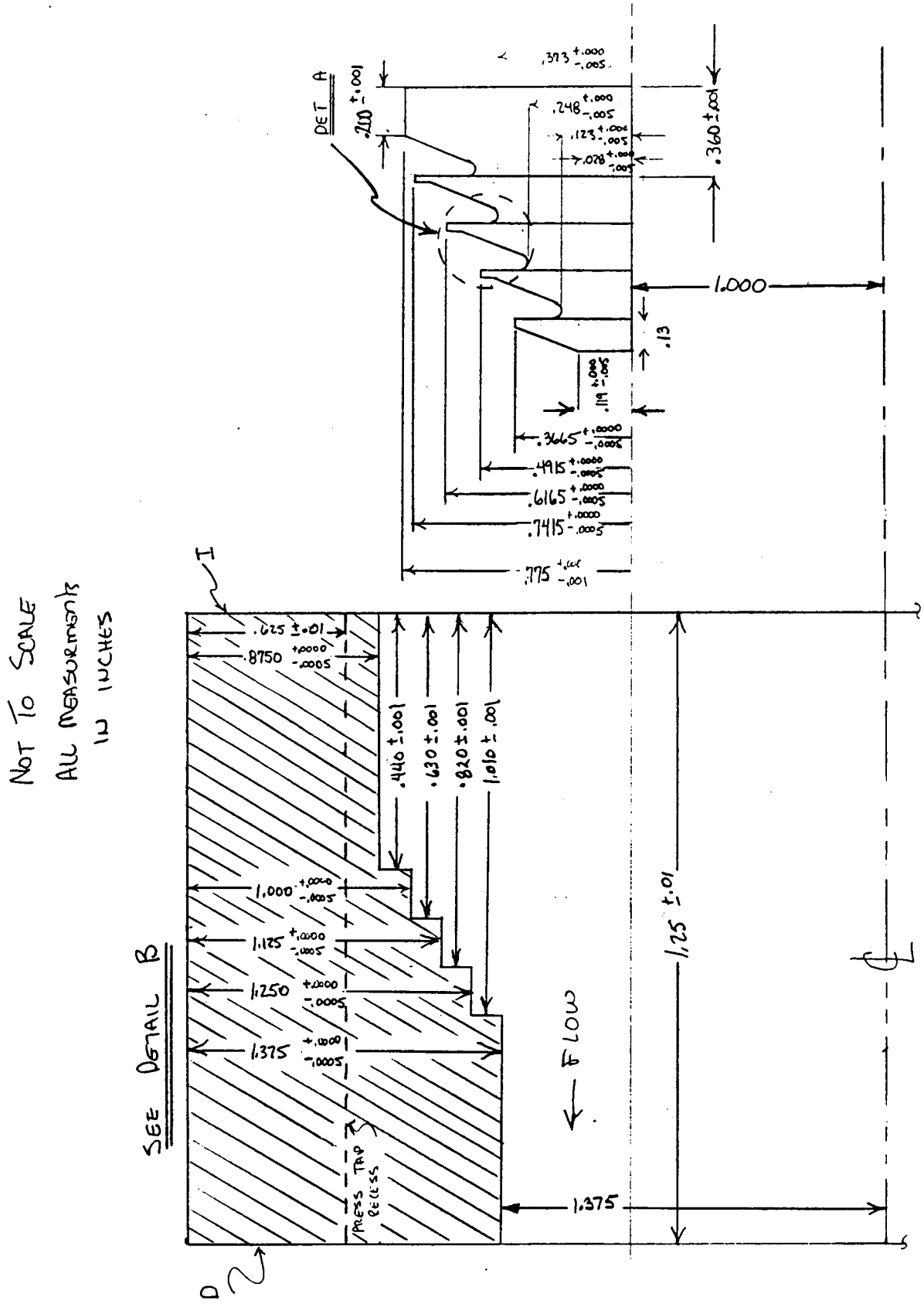

Figure 64. Seal #1. Hydrogen Turbopump Front Wear Ring Seal.

ORIGINAL PAGE IS
OF POOR QUALITY

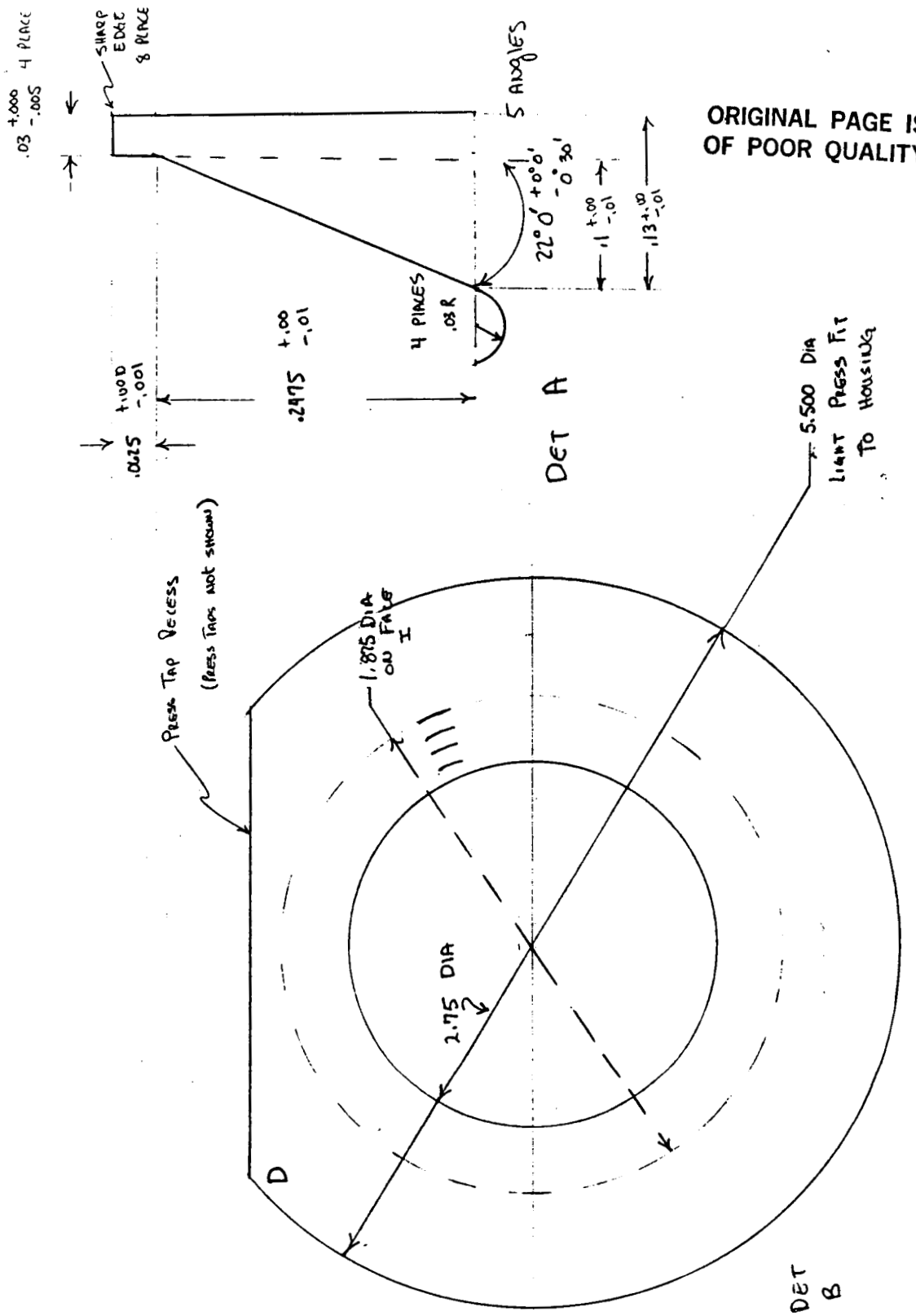

ORIGINAL PAGE IS
OF POOR QUALITY

Figure 65. Seal #1 Details.

ORIGINAL PAGE IS
OF POOR QUALITY

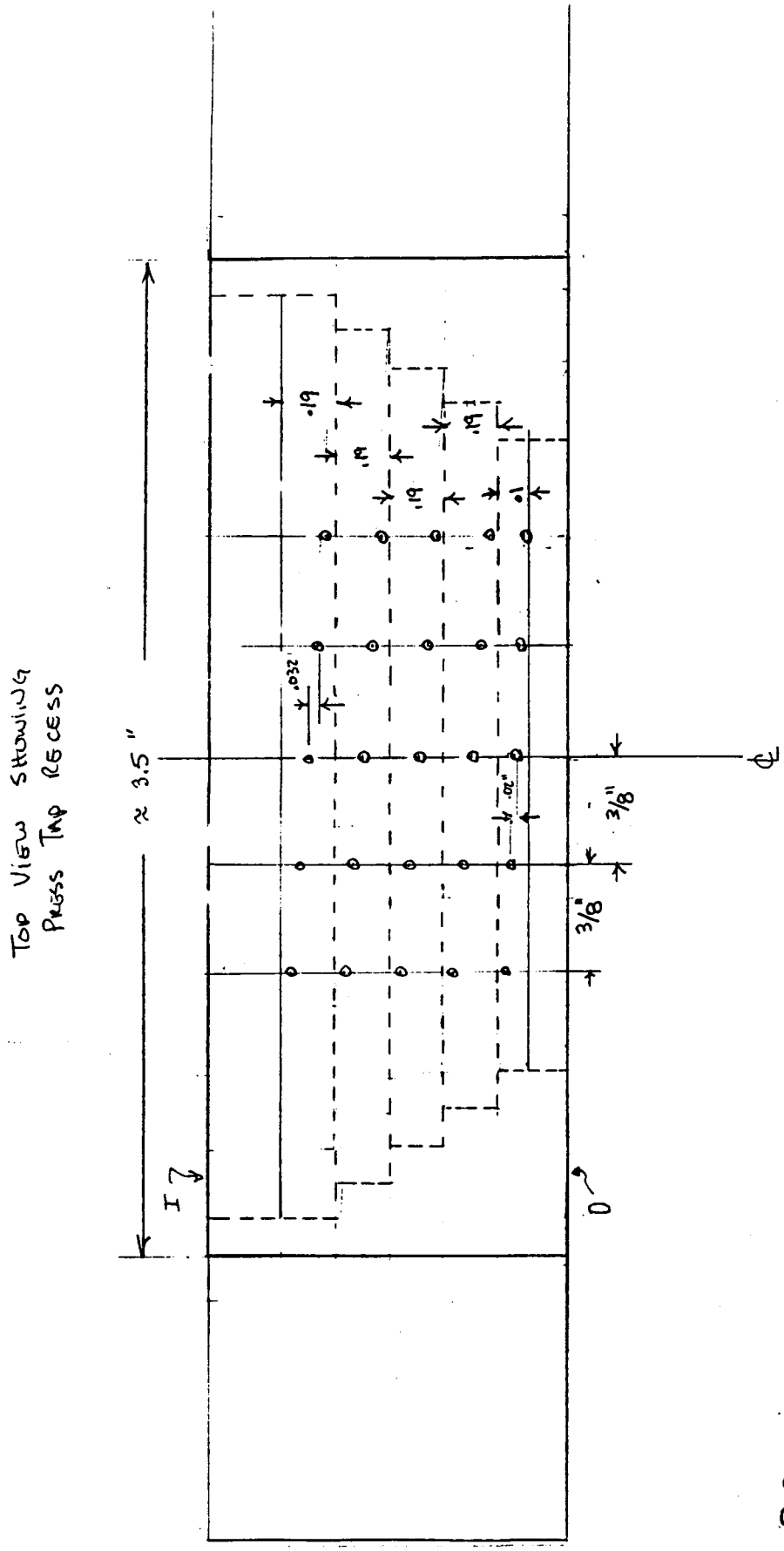

ORIGINAL PAGE IS
OF POOR QUALITY

Figure 66. Seal #1 Details.

ORIGINAL PAGE IS
OF POOR QUALITY

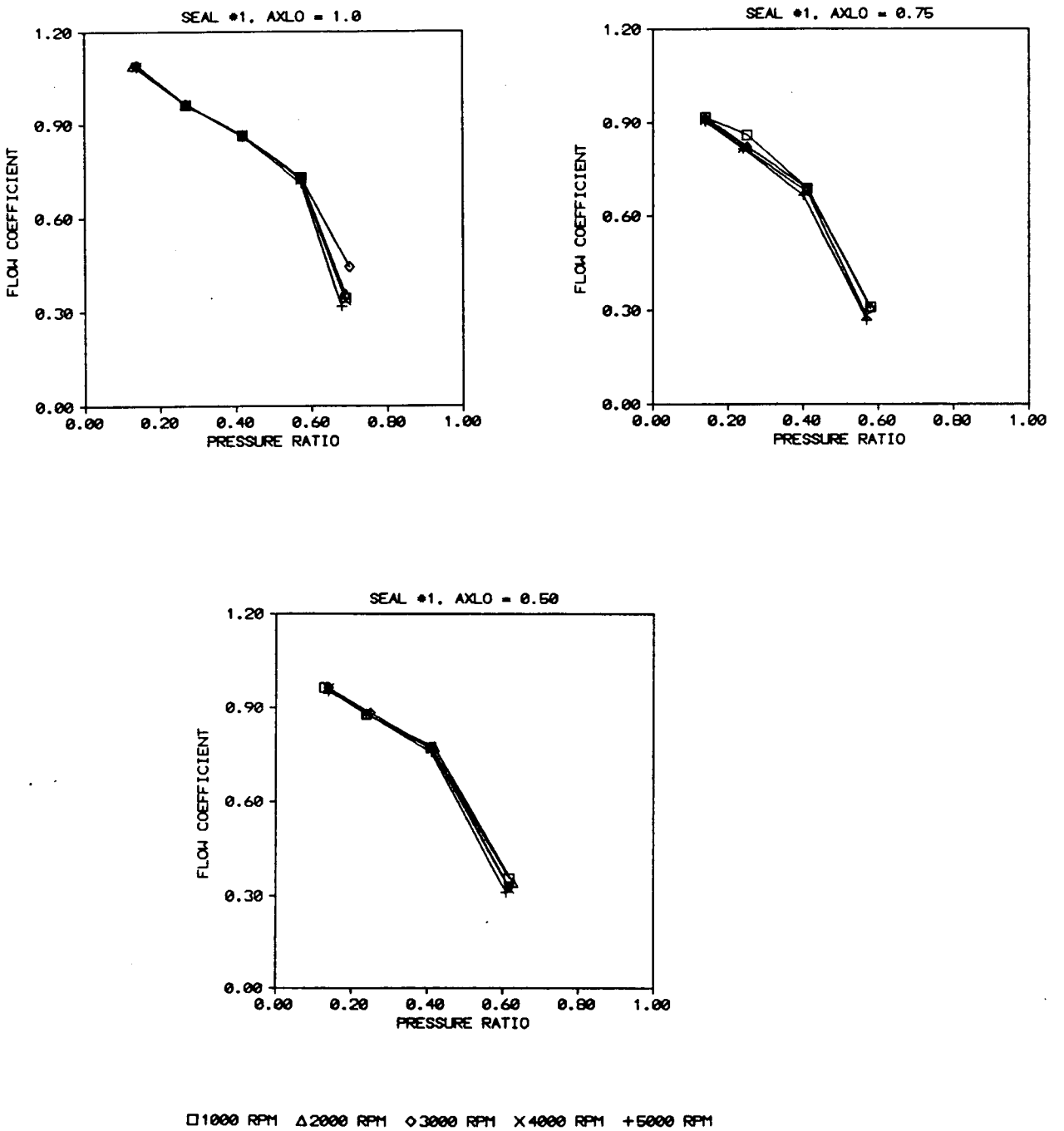

Figure 67. Seal #1 Flow Coefficient vs. Pressure Ratio for Various Shaft Speeds.

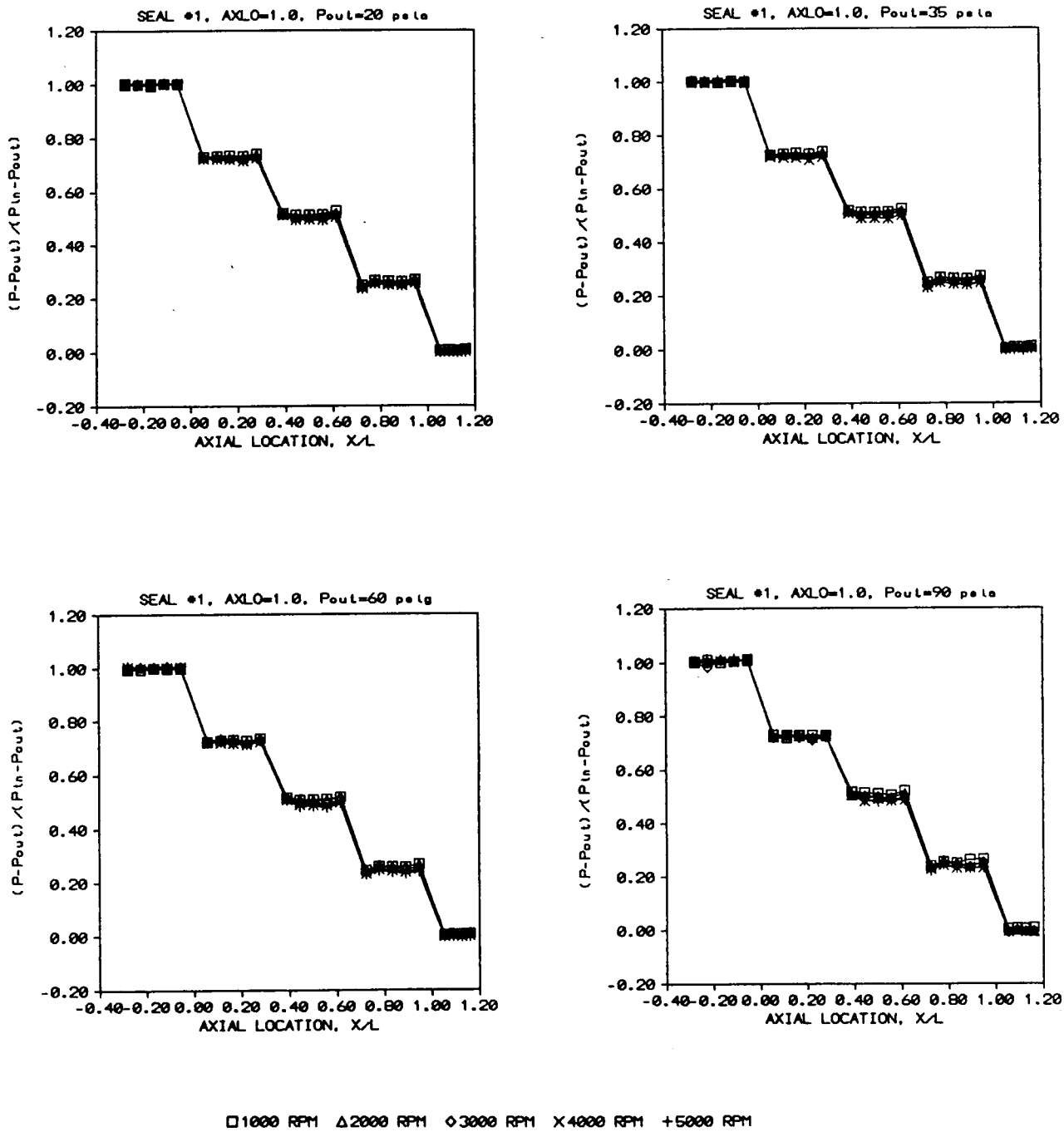

Figure 68. Seal #1 Axial Pressure Distribution For a Given Exit Pressure for Various Shaft Speeds. AXLO=1.0

ORIGINAL PAGE IS
OF POOR QUALITY

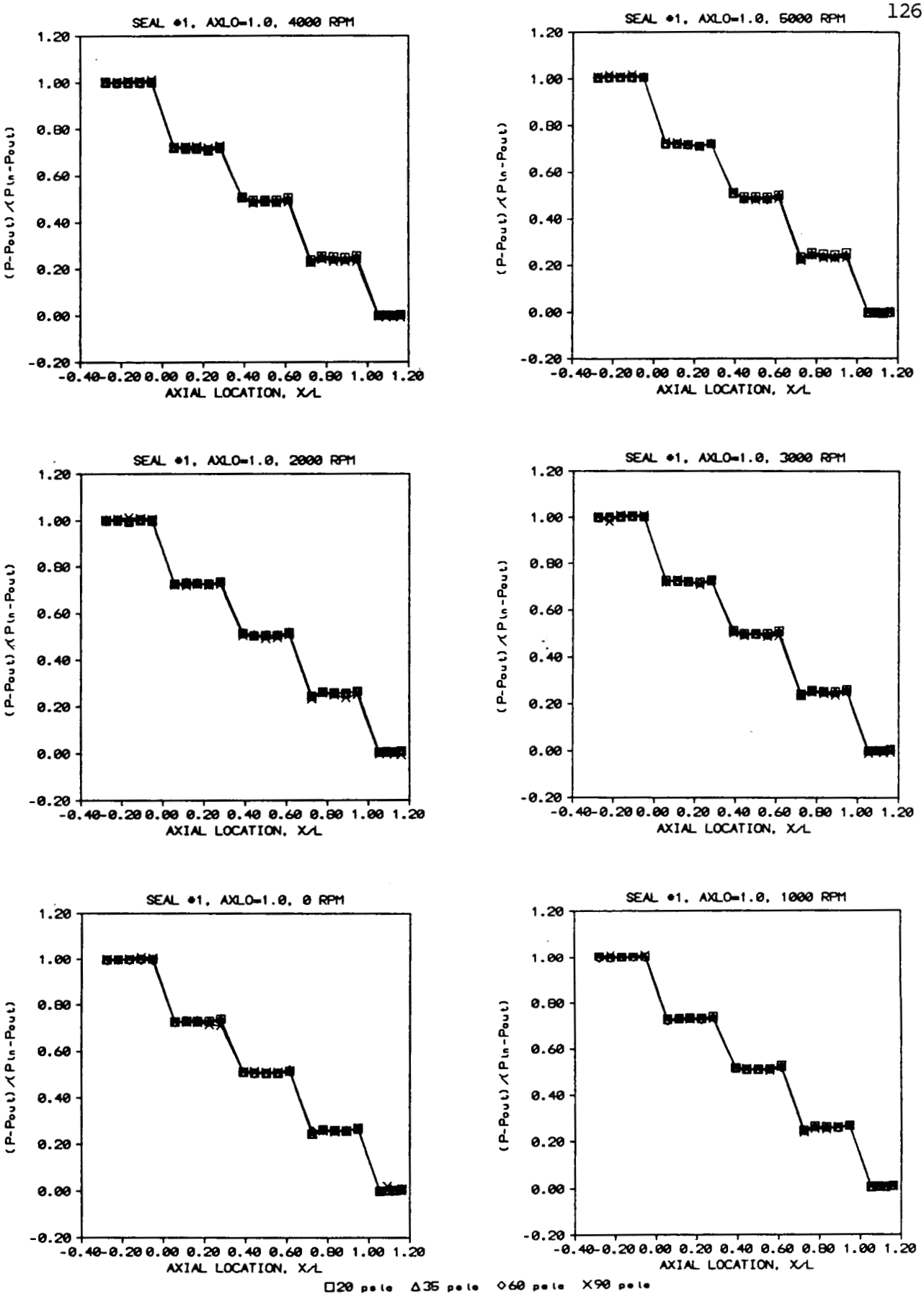

Figure 69. Seal #1 Axial Pressure Distribution For a Given Shaft Speed for Various Pressure Ratios. AXLO=1.0.

ORIGINAL PAGE IS
OF POOR QUALITY

When the tooth is relocated to AXLO=0.75, the same holds true again as shown in Figures 70 and 71. For both of these cases, the static wall pressure along the stator wall was essentially constant for each step with the pressure changing only as the flow progressed from one step to another. The amount of pressure drop across each step was also essentially constant.

For the axial location of 0.50, the pressure distributions and their dependence upon pressure ratio and shaft speed changed. Figure 72 illustrates that for Pout=20, 35, and 60 psia (Pin was approximately 145 psia in all cases) there were no shaft speed effects. However, for the lowest pressure drop (highest pressure ratio) there were shaft speed effects at the highest shaft speed tested. For all of the other cases, the static wall pressure along the stator wall would show a more gradual decrease occuring over one half of the step's length until the tooth was encountered. At that point, the minimum pressure on the step was attained and there was a slight pressure recovery behind the tooth. The total pressure drop attained for each step was approximately the same. When the pressure ratio was large (small pressure drop) and the shaft speed was large, the pressure distribution reverted to the one present for the other axial locations with the pressure remaining constant along each step and dropping as the flow progressed from step to step. However, the pressure drop across each step was the same for both pressure distributions observed. Figure 73 presents a cross plot of the data presented in Figure 72 showing pressure ratio effects for various shaft speeds.

Figure 74 presents a summary of the pressure distribution

ORIGINAL PAGE IS
OF POOR QUALITY

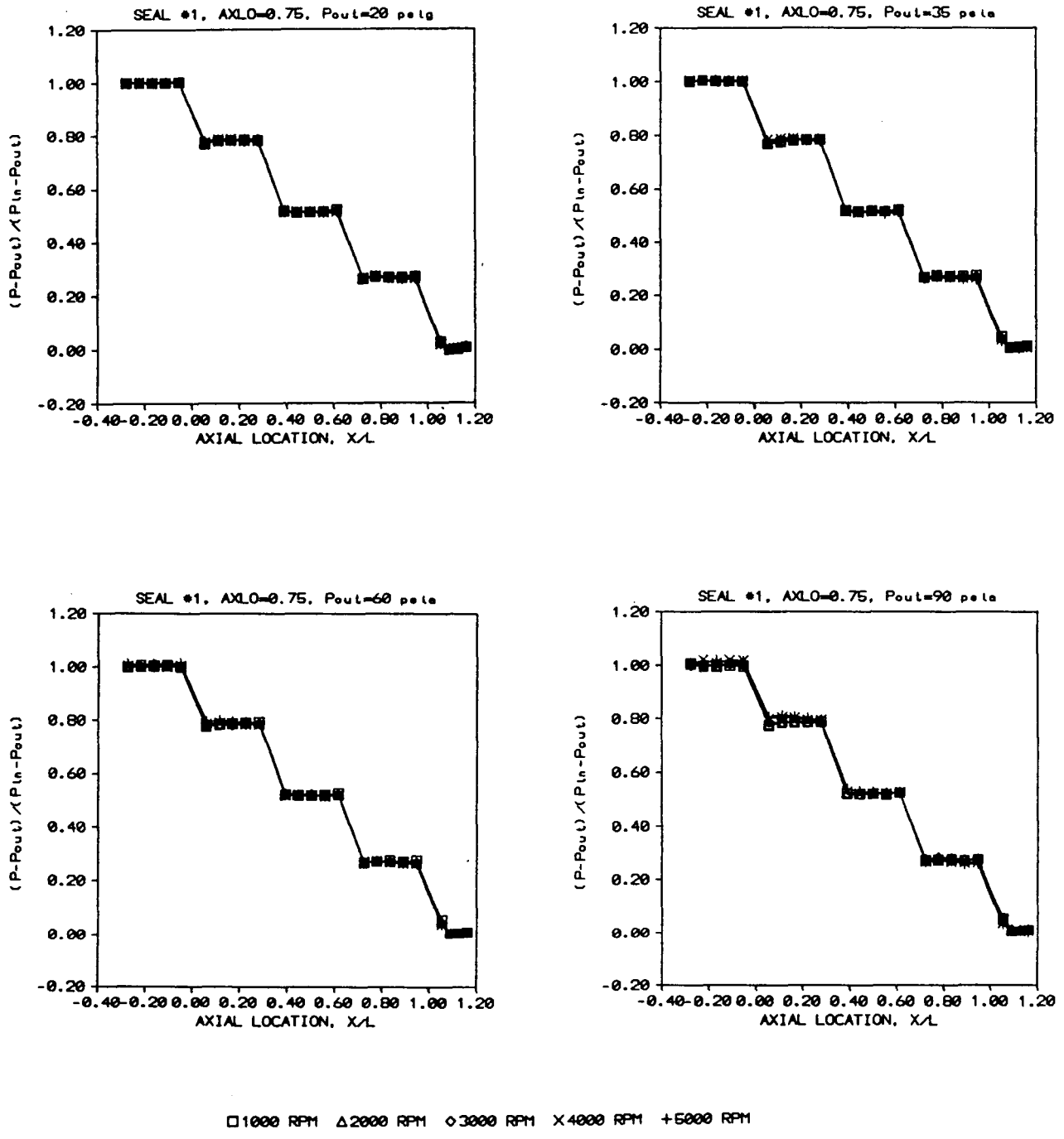

Figure 70. Seal #1 Axial Pressure Distribution For a Given Exit Pressure for Various Shaft Speeds. AXLO=0.75.

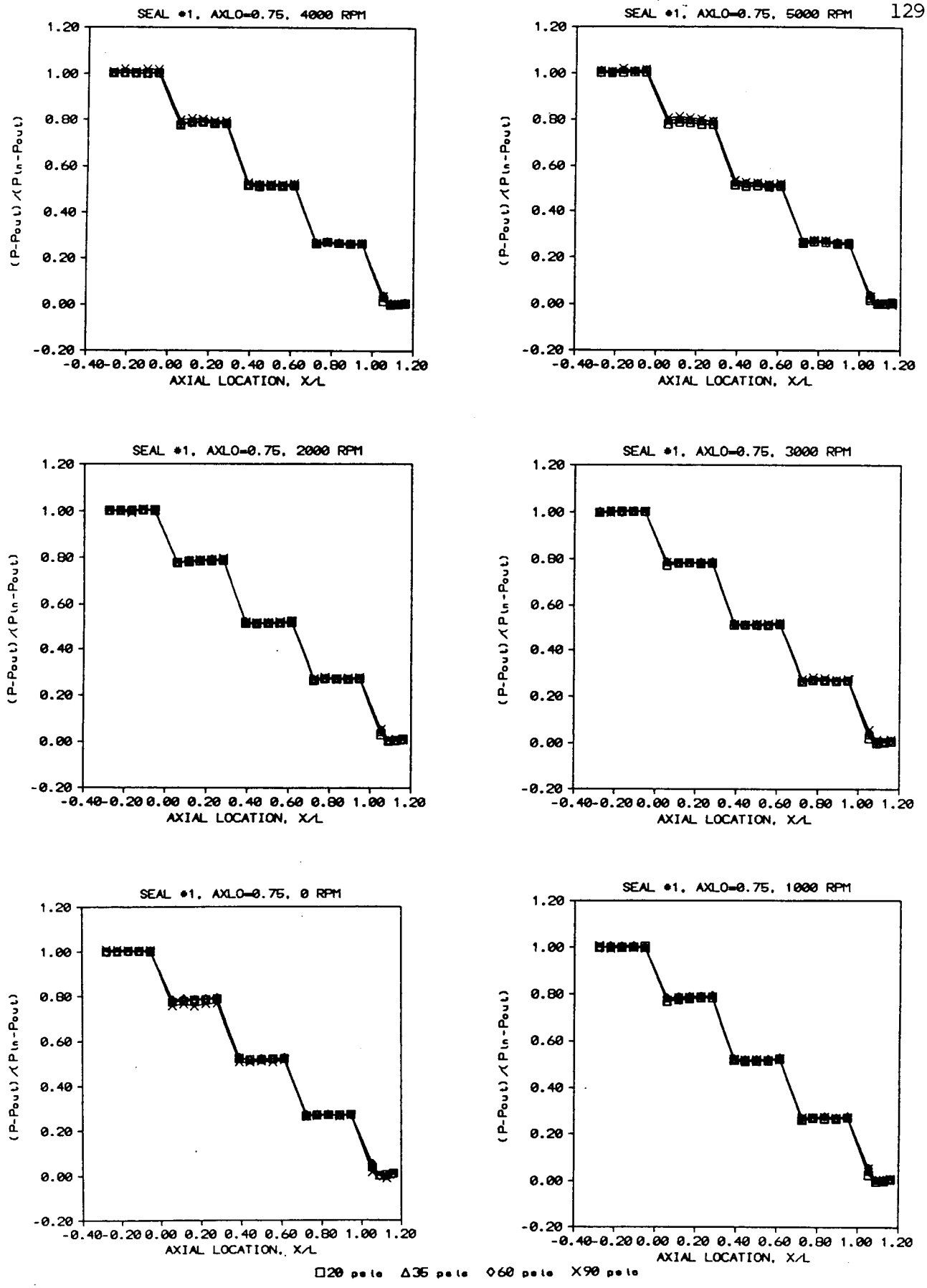

Figure 71. Seal #1 Axial Pressure Distribution For a Given Shaft Speed for Various Pressure Ratios. AXLO=0.75.

ORIGINAL PAGE IS
OF POOR QUALITY

ORIGINAL PAGE IS
OF POOR QUALITY

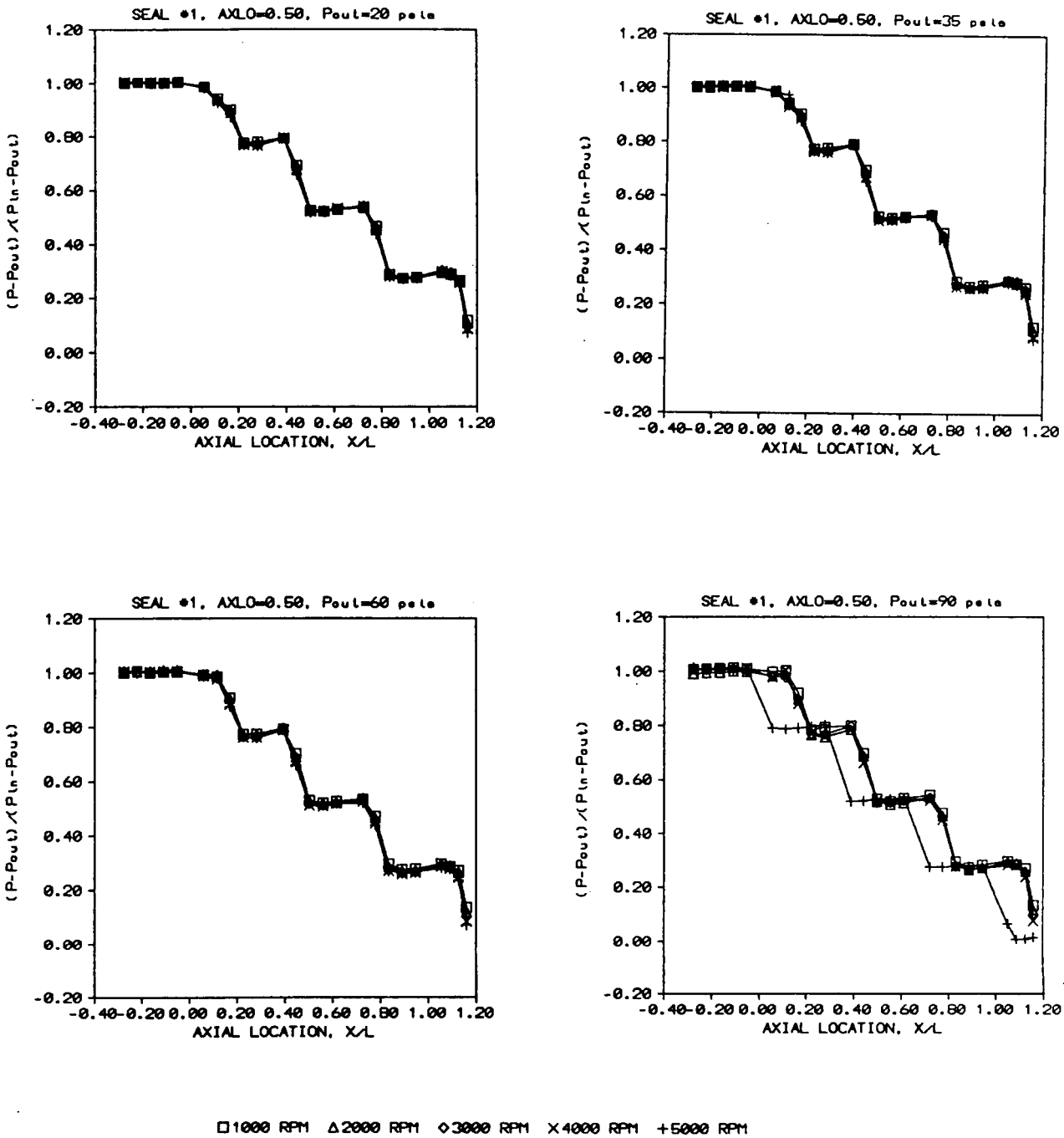

Figure 72. Seal #1 Axial Pressure Distribution For a Given Exit Pressure for Various Shaft Speeds. AXLO=0.50.

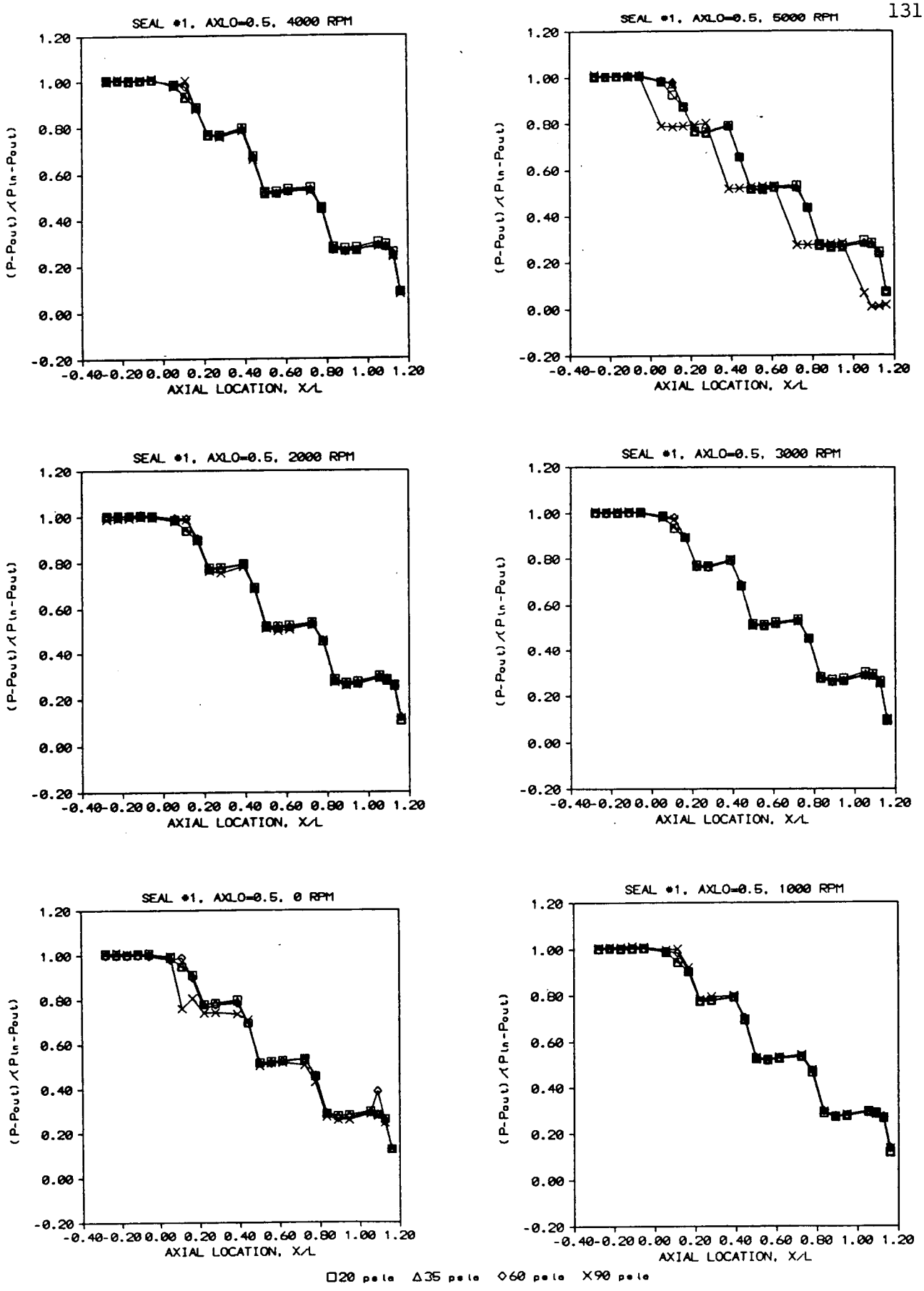

Figure 73. Seal #1 Axial Pressure Distribution For a Given Shaft Speed for Various Pressure Ratios. AXLO=0.50.

ORIGINAL PAGE IS
OF POOR QUALITY

ORIGINAL PAGE IS
OF POOR QUALITY

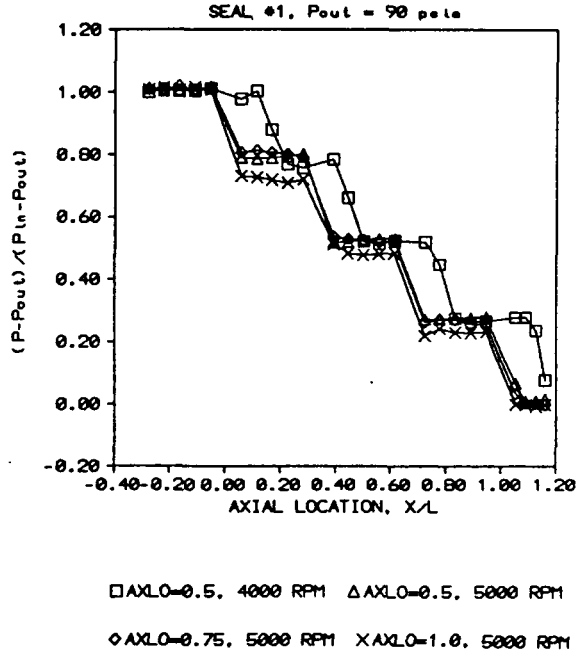

Figure 74. Seal #1 Axial Pressure Distribution For Pout=90 psia for Various Axial Locations and Shaft Speeds.

measurements obtained in seal #1. Only one pressure distribution was presented for the axial locations of 1.0 and 0.75 since they did not posses any pressure ratio or shaft speed dependence. For the axial location of 0.5, two conditions are presented, 4000 rpm, Pout=90 psia which represents the majority of the pressure distributions obtained at this axial location, and the one different distribution obtained at 5000 rpm and 90 psia. This figure shows that for the axial locations of 0.75 and 0.50, the pressure drop across each step was the same and except for the low pressure drop, high shaft speed case, the pressure distribution remained the same. For the axial location of 1.0, the pressure distribution remained very similar, but the pressure drop across each step was slightly different from that which occurred for the other two axial locations.

Seal Design #2

The second seal to be tested was designed by Dr. Rhode. It is shown in Figures 75 and 76. The flow into and out of this seal was preconditioned using the first and last "teeth" from seal #1. The purpose of this was to try and maintain the same inlet and exit conditions for the different seals tested. For this particular design, the pitch of the seal was reduced significantly and more teeth were added. Due to these conditions, the number of pressure taps placed in each step were reduced to two. In addition, the number of axial locations investigated were also reduced to two.

Figure 77 presents the flow coefficients measured as a function of pressure ratio and shaft speed for axial locations of 1.0 and 0.50. At the axial location of 1.0, there is a slight

ORIGINAL PAGE IS
OF POOR QUALITY

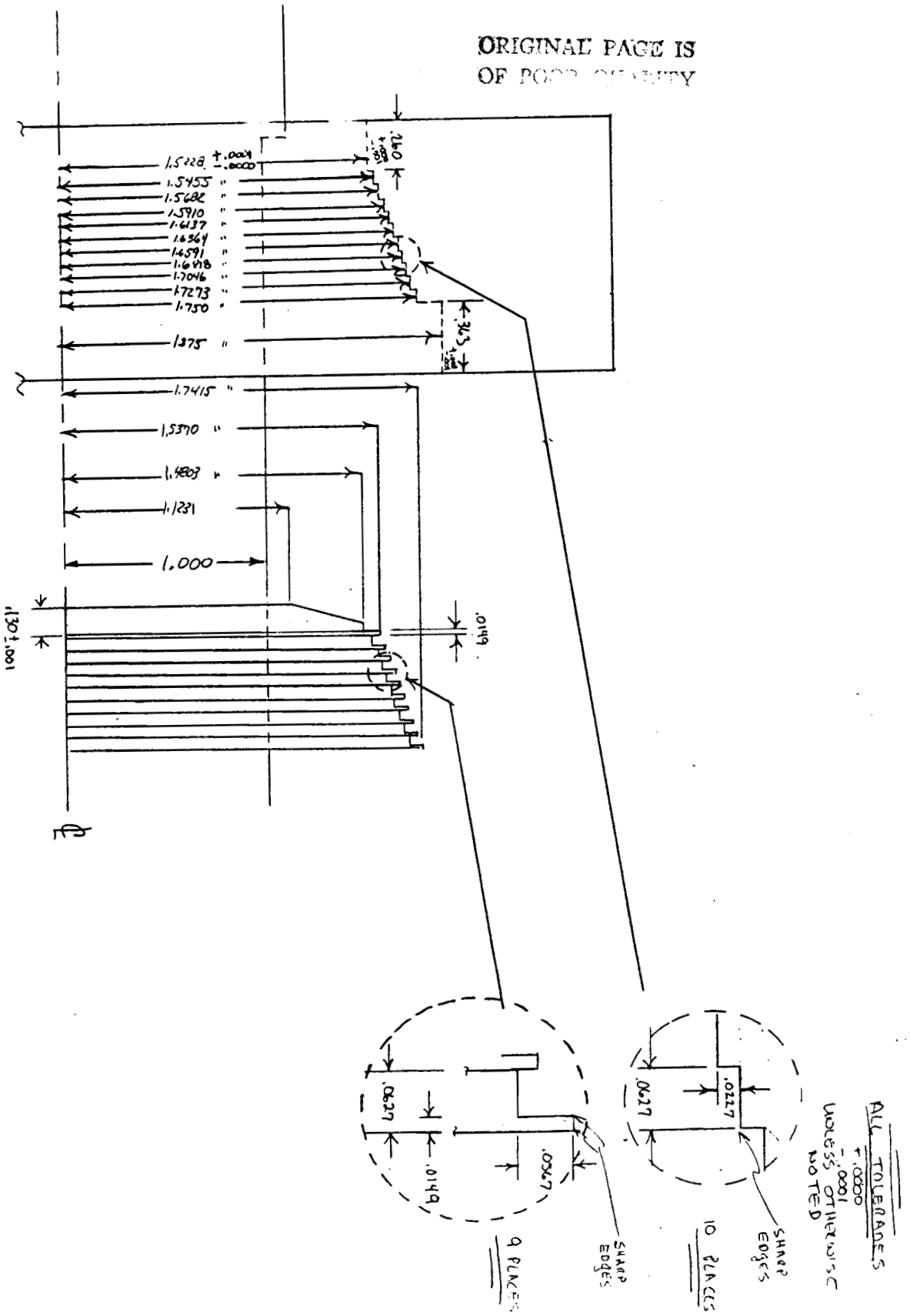

Figure 75. Seal #2.

ORIGINAL PAGE IS
OF POOR QUALITY

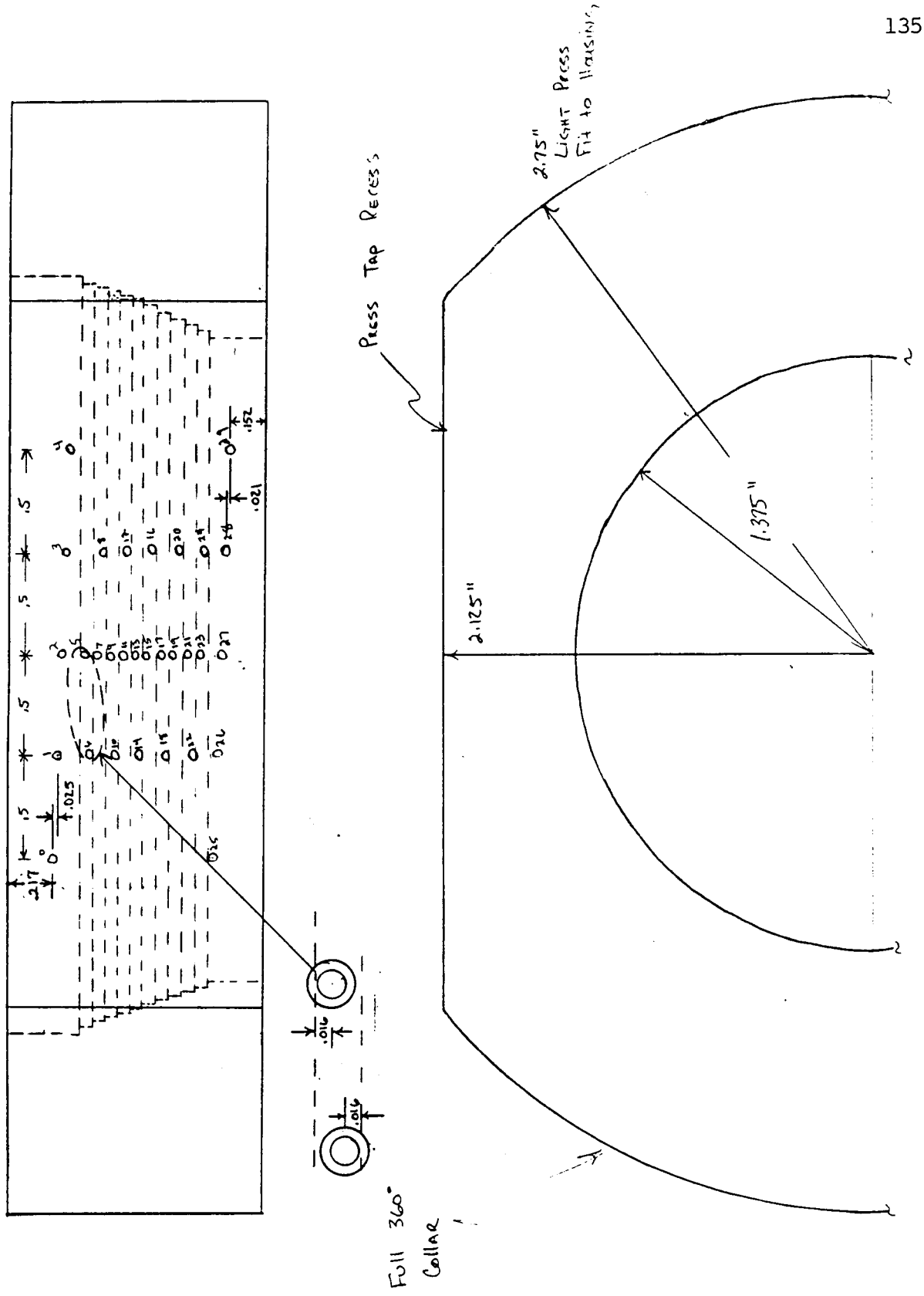

Figure 76. Seal #2 Details.

ORIGINAL PAGE IS
OF POOR QUALITY

ORIGINAL PAGE IS
OF POOR QUALITY

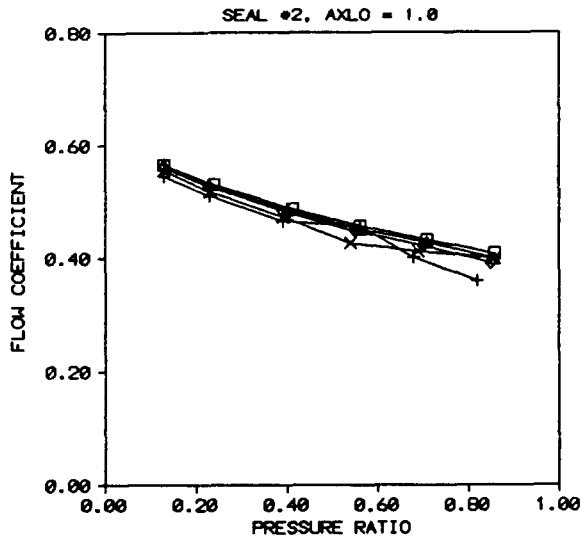

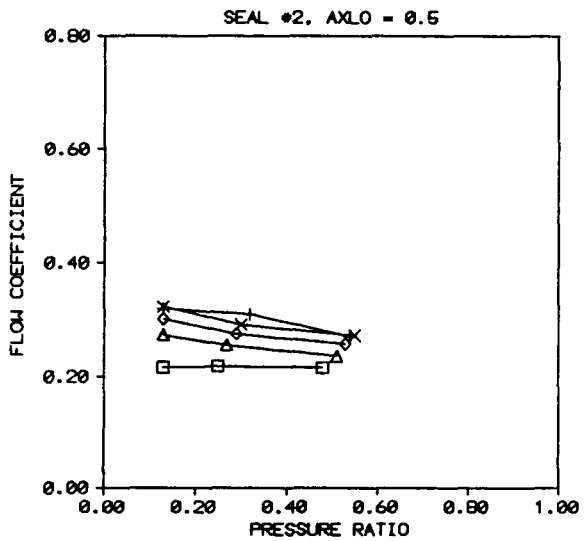

□1000 RPM △2000 RPM ◇3000 RPM ×4000 RPM +5000 RPM

Figure 77. Seal #2 Flow Coefficient vs. Pressure Ratio for Various Shaft Speeds.

dependence upon shaft speed with higher speeds reducing the leakage rate. As before, as the pressure ratio increases, the flow coefficient decreases. For the axial location 0.50, there is a significant effect of shaft speed upon the flow coefficient. In this case, increases in shaft speed cause the flow coefficient to increase. For both of these operating conditions, the flow coefficients measured for seal #2 which ranged from 0.6 to 0.2 are significantly less than those present in seal #1 which ranged from 1.1 to 0.3. Specifically, at the experimental condition closest to actual flight conditions (large pressure drops, low pressure ratios), seal #2 showed a 67% reduction in leakage over seal #1 for AXLO=0.50.

Figures 78 and 79 present the axial pressure distributions present for the various pressure ratios and shaft speeds for AXLO = 1.0. Under most operating conditions, there was no dependence of this pressure distribution upon pressure ratio or shaft speed. For these conditions, the pressure distribution through the seal is essentially linear with the same pressure drop occurring across each step.

The only operating condition which produce a shaft speed dependence was for an exit pressure of 130 psia (a pressure drop of only 15 psia across the seal). As was illustrated in seal #1 as well, when the axial flow rate becomes very small (for very low pressure drops), the pressure distribution becomes dependent upon the shaft speed. This was much more evident in seal #2 at the axial location of 0.50 where the leakage rate was substantially lower.

Figures 80 and 81 present the pressure distribution for

ORIGINAL PAGE IS
OF POOR QUALITY

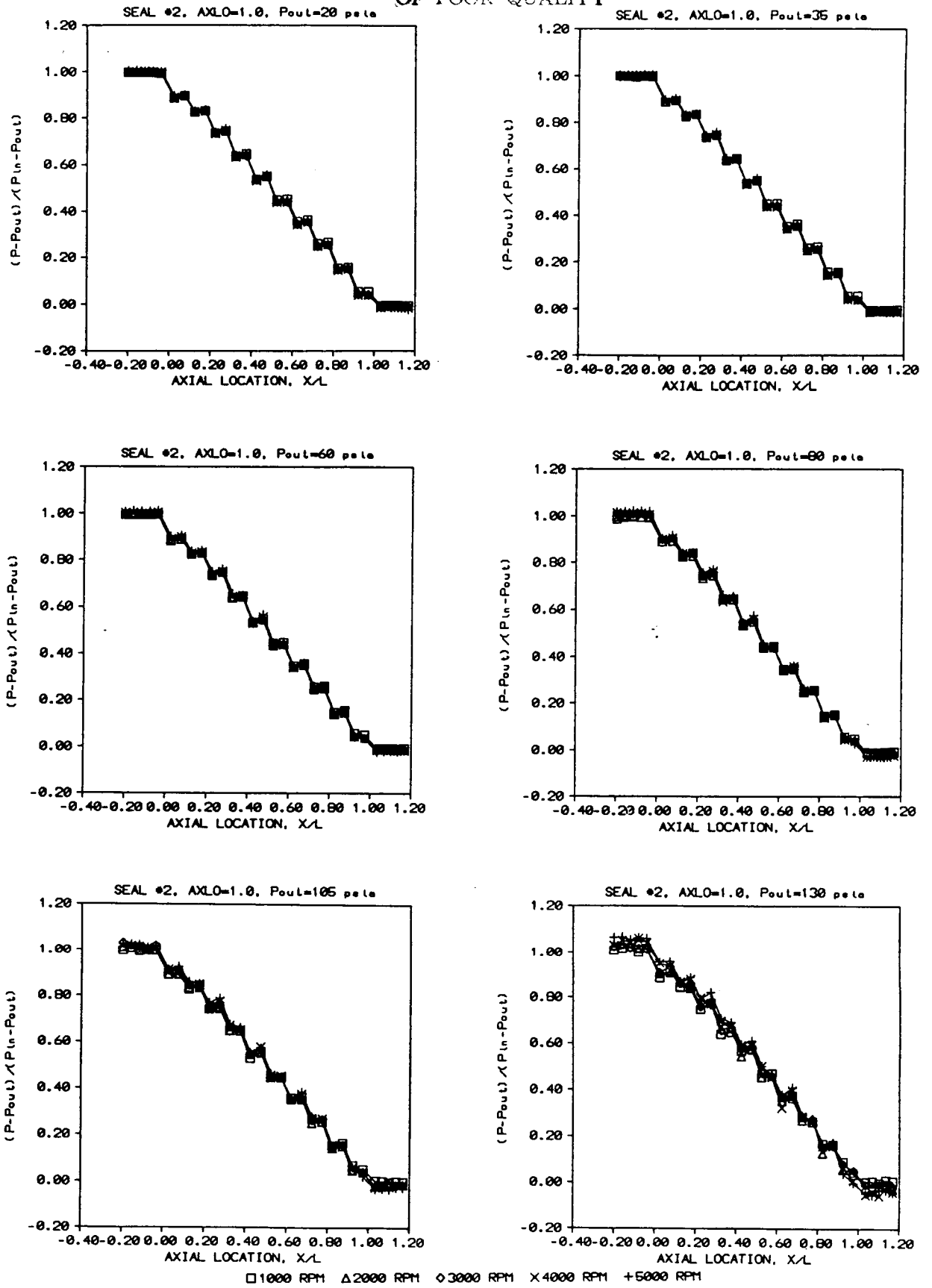

Figure 78. Seal #2 Axial Pressure Distribution For a Given Exit Pressure for Various Shaft Speeds. AXLO=1.00.

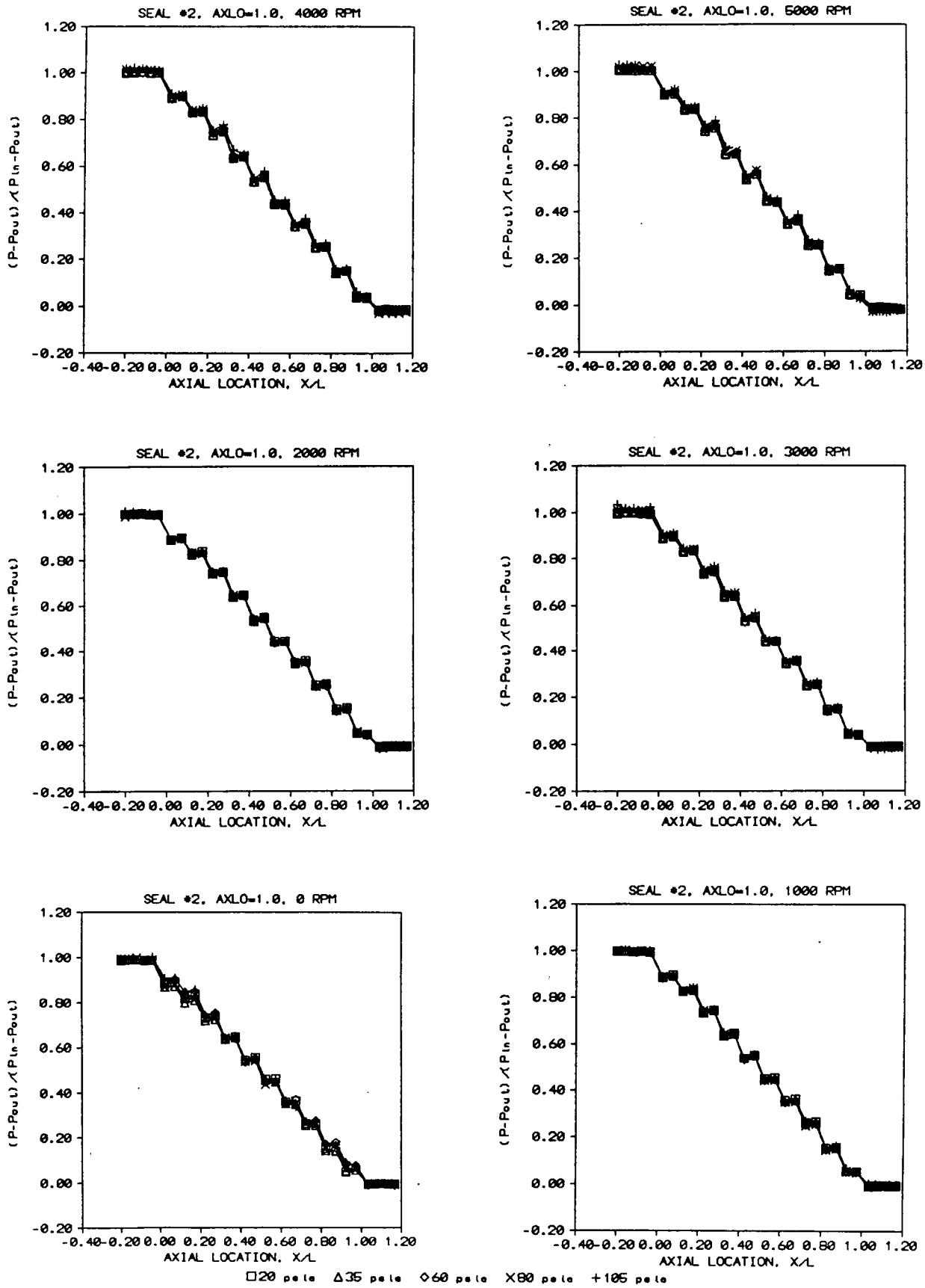

Figure 79. Seal #2 Axial Pressure Distribution For a Given Shaft Speed for Various Pressure Ratios. AXLO=1.00.

ORIGINAL PAGE IS
OF POOR QUALITY

ORIGINAL PAGE IS
OF POOR QUALITY

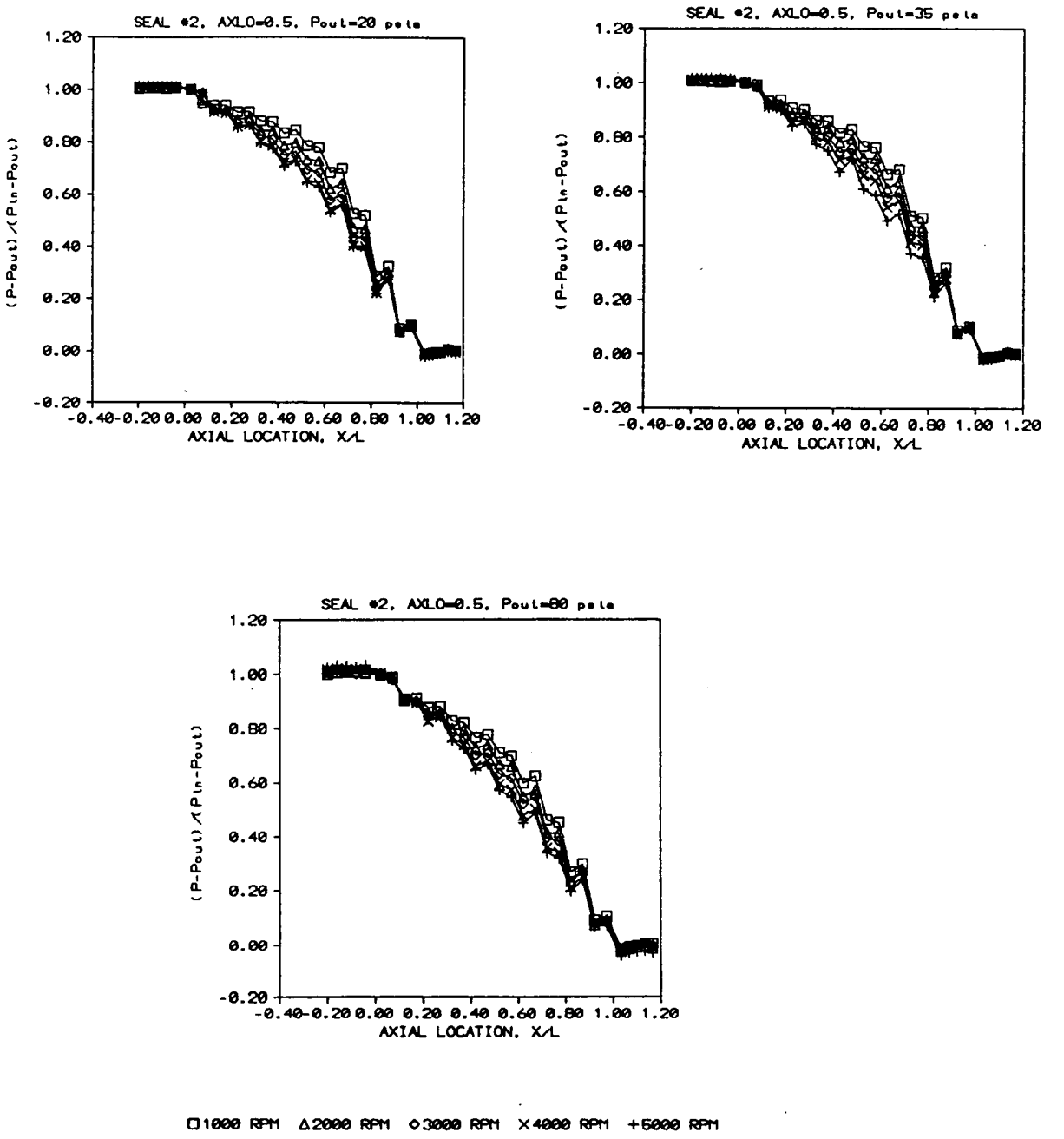

Figure 80. Seal #2 Axial Pressure Distribution For a Given Exit Pressure for Various Shaft Speeds. AXLO=0.50.

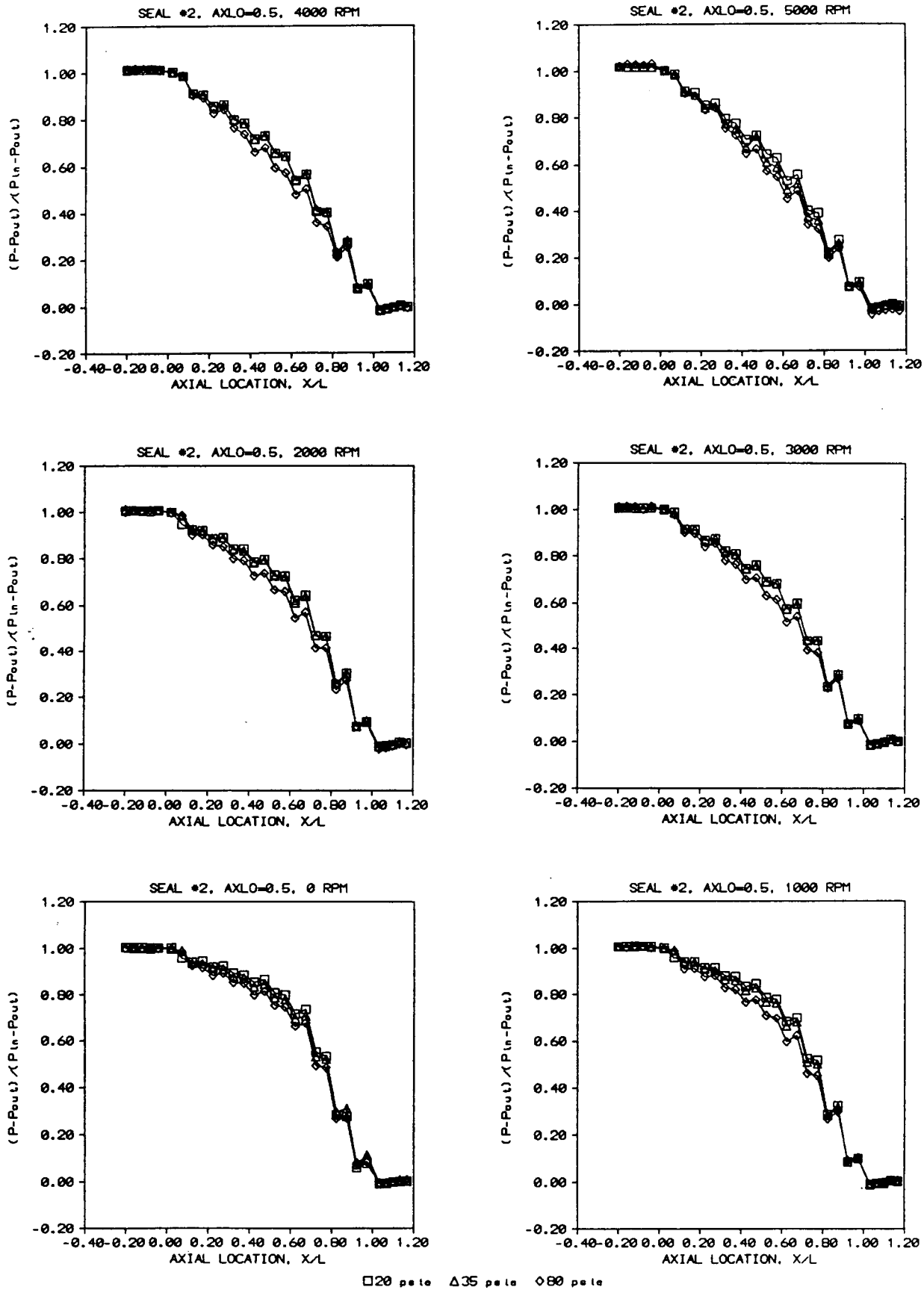

Figure 81. Seal #2 Axial Pressure Distribution For a Given Shaft Speed for Various Pressure Ratios. AXLO=0.50.

ORIGINAL PAGE IS
OF POOR QUALITY

seal #2 at an axial location of 0.50. For this axial location, the leakage through the seal has been substatially reduced and the shearing effects and induced tangential velocity caused by the shaft rotation begin to greatly influence the flow field inside the seal. This was observed in the flow coefficient data which included a significant dependence upon shaft speed. For this axial location, the pressure distributions through the seal are no longer linear. The pressure gradient increases as the flow progresses through the seal with the largest pressure drop occurring through the last step. For the non-rotating condition, this non-linear pressure distribution is at its maximum with 50% of the pressure drop occurring over the last 30% of the seal. As the shaft speed in increased, the pressure distribution tends to become more linear as was the case for the axial location of 1.0 data. This could be due to the increased velocity magnitude present due to the rotating shaft imparting tangential velocity into the fluid. As the magnitude of the fluid velocity increases towards the value present for the higher leakage rate AXLO=1.0 position, the pressure distributions and leakage rates approach those present at the AXLO = 1.0 position. Figure 82 compares the pressure distributions for the two different axial locations under two different operating conditions. Here it is clear that as the shaft speed increases, the pressure distribution for the AXLO = 0.5 condition approaches the AXLO = 1.0 condition.

Seal Design 3

The third seal which was designed by Dr. Rhode is shown in Figures 83-86. As was the case for seal #2, the inlet and outlet of the seal were conditioned by the addition of the first and

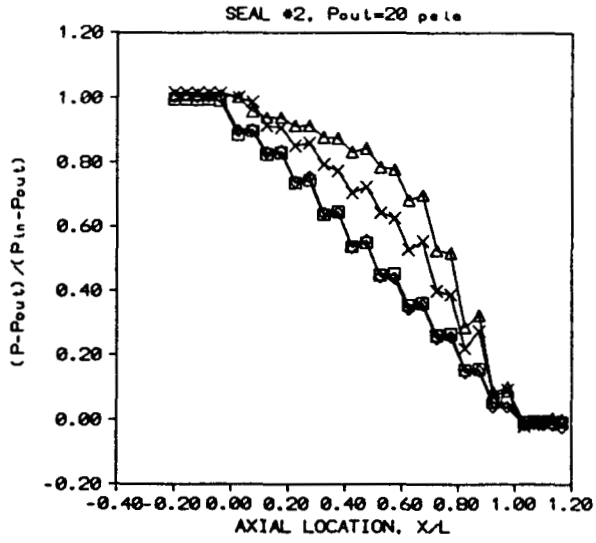

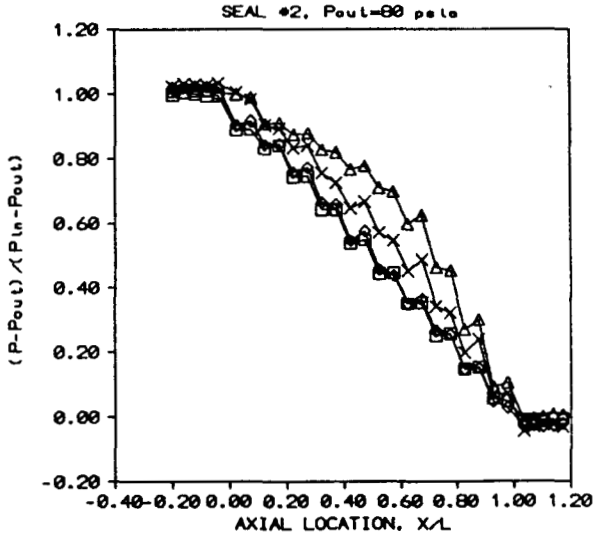

□AXLO=1.0, 1000 RPM ΔAXLO=0.5, 1000 RPM
◇AXLO=1.0, 5000 RPM XAXLO=0.5, 5000 RPM

Figure 82. Seal #2 Axial Pressure Distribution for Various Axial Locations, Pressure Ratios, and Shaft Speeds.

ORIGINAL PAGE IS
OF POOR QUALITY

ORIGINAL PAGE IS
OF POOR QUALITY

ORIGINAL PAGE IS
OF POOR QUALITY

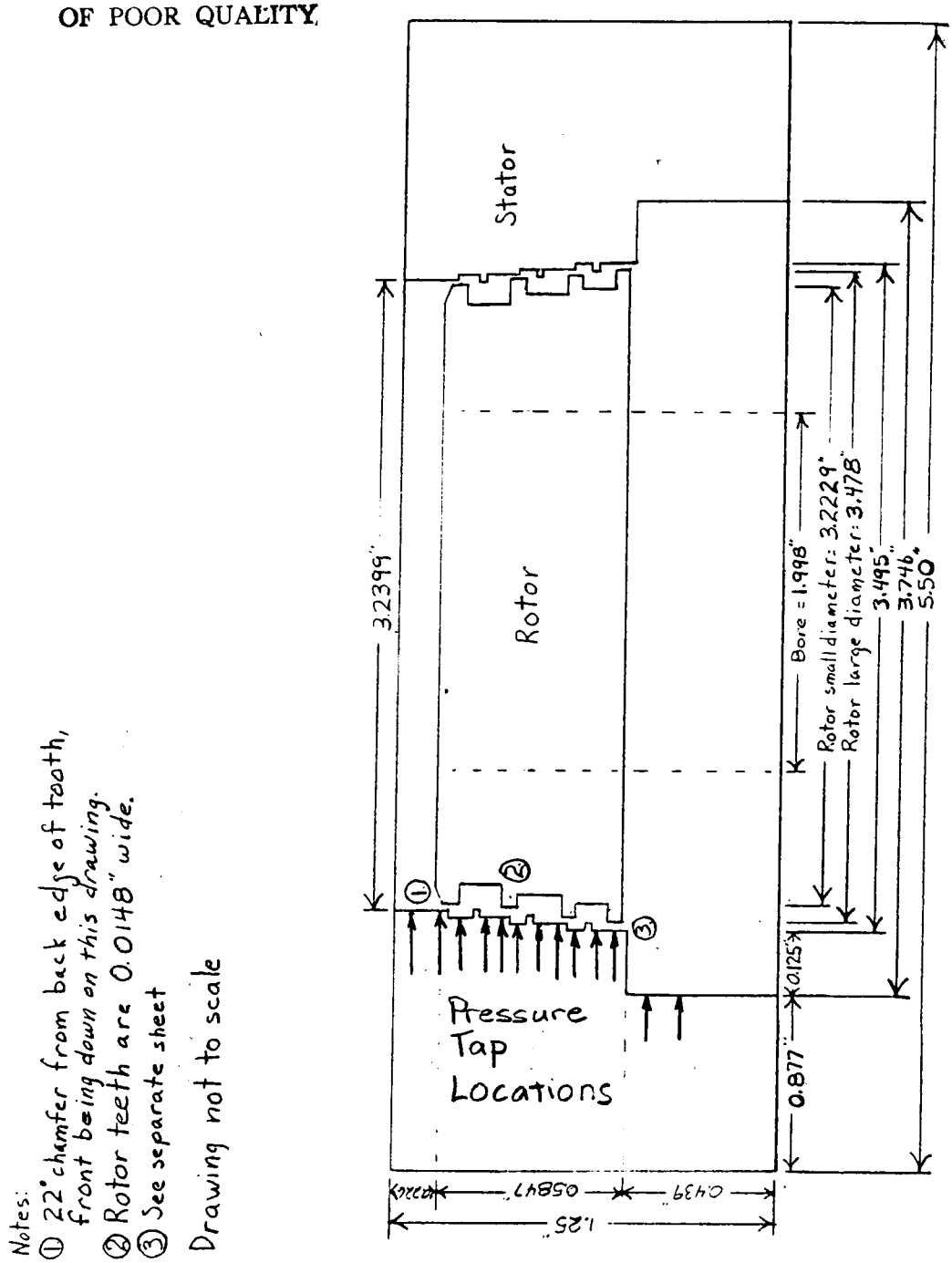

Figure 83. Seal #3.

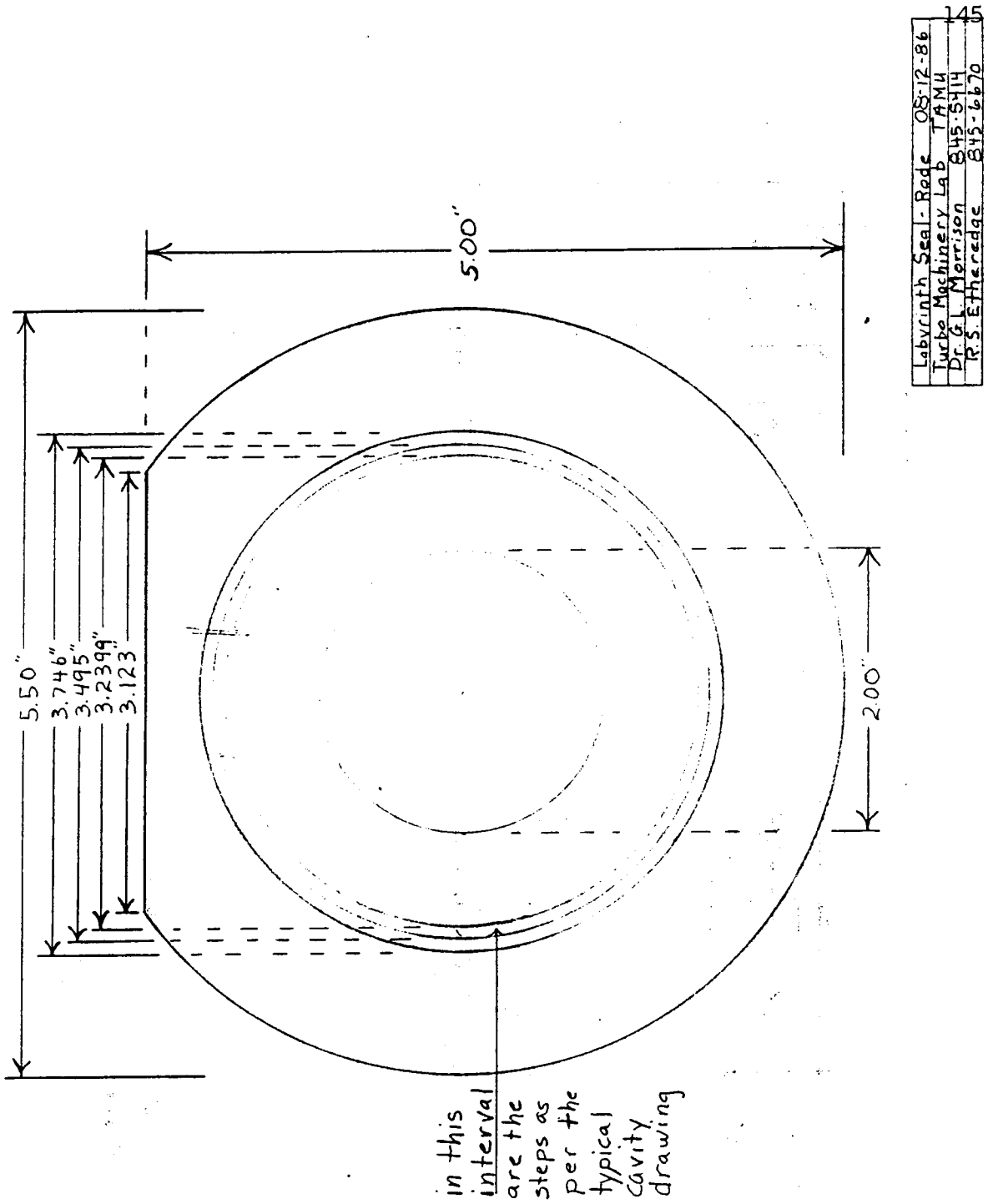

Figure 84. Seal #3 Detail.

ORIGINAL PAGE IS
OF POOR QUALITY

ORIGINAL PAGE IS
OF POOR QUALITY

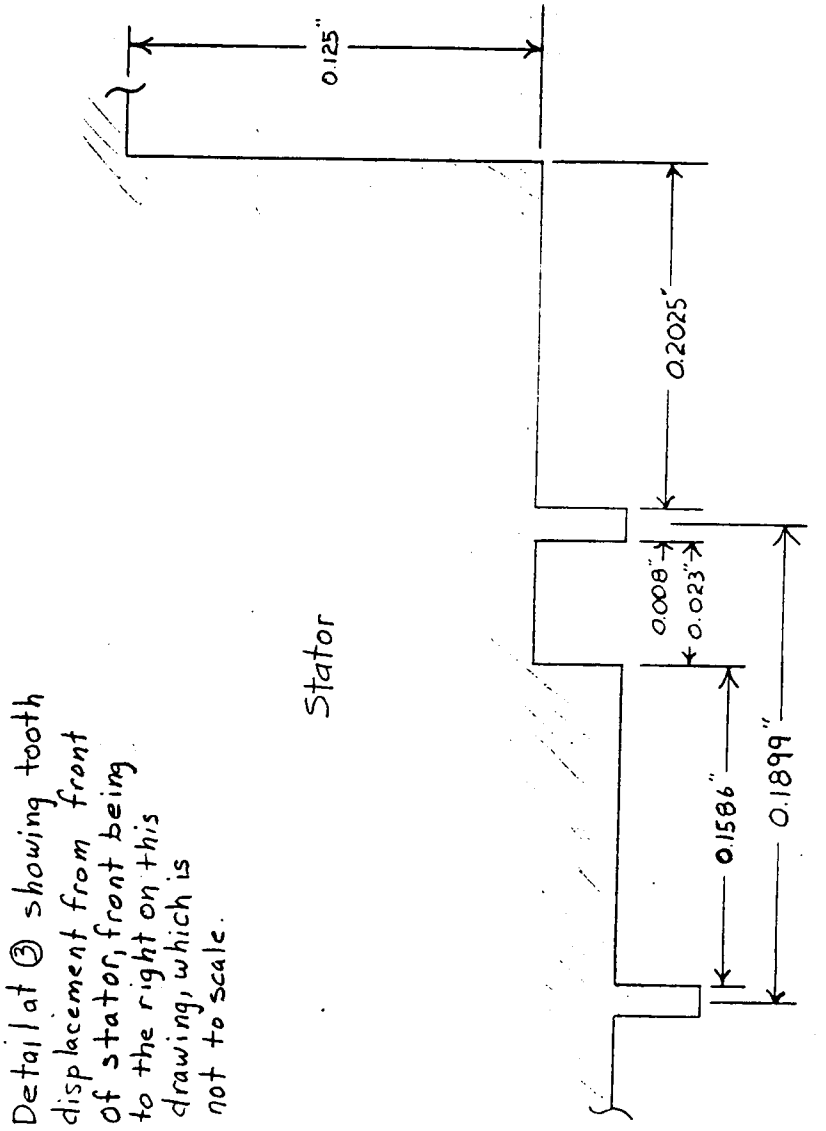

Figure 85. Seal #3 Detail.

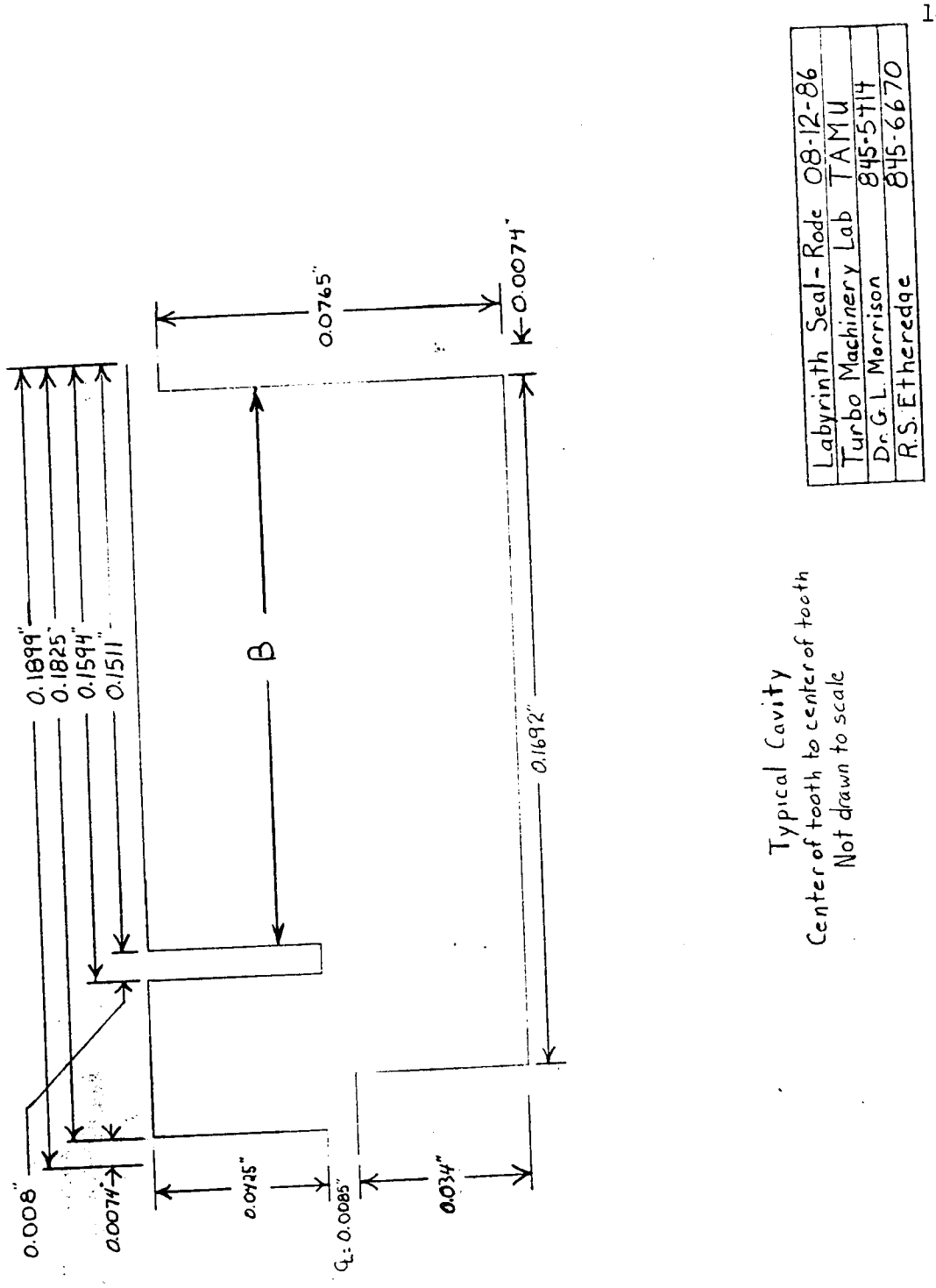

Figure 86. Seal #3 Detail.

ORIGINAL PAGE IS
OF POOR QUALITY

last "teeth" from seal #1. For this design Dr. Rhode has maintained the same clearance and pitch as is present on the current front wear ring seal. He has modified the step height and added a tooth on the stator. Pressure taps were installed just before and after each step, in the cavity between the step and the tooth and just upsteam of the tooth.

Figure 87 presents the flow coefficients for seal #3 for various pressure ratios, axial locations, and shaft speeds. For axial location X1, the distance B shown in Figure 86 was 0.0098", for X2, 0.0172" and for X3, 0.0049". The first two axial locations result in the least leakage with flow coefficients varying from a maximum of 0.75 to a minimum of 0.45. This compares to the current front wear ring seal (seal #1) leakage rates from 1.1 to 0.3. When compared with at the lowest pressure ratio (largest pressure drop), seal #3 leaks only 68% as much as seal #1. As with the other seals tested, the flow coefficient decreased with increasing pressure ratio. For this seal there was negligible dependence of the flow coefficient upon the shaft speed.

Figures 88 and 89 present the axial pressure distributions for seal #3 for axial location X1. As was previously observed for seal #1, there is essentially no dependence upon pressure ratio or shaft speed except for the condition of very little pressure drop (large pressure ratio) across the seal with the accompianied low leakage rate. As before, increasing shaft speed caused the pressure distributions to approach the values obtained for the smaller pressure ratios. At this axial location, the pressure distribution through the seal is not linear. There is a large

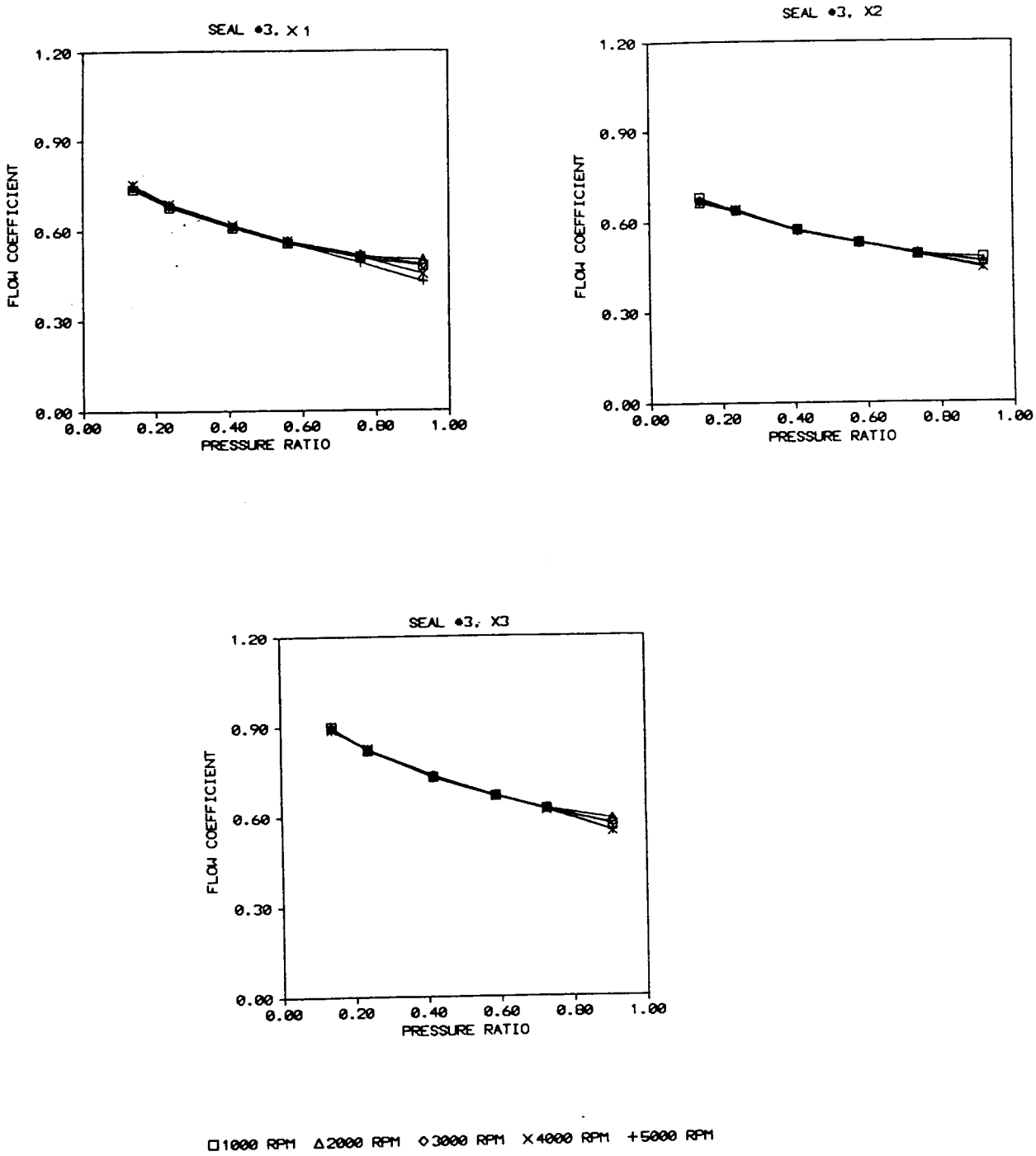

Figure 87. Flow Coefficient vs. Pressure Ratio for Various Axial Locations and Shaft Speeds.

ORIGINAL PAGE IS
OF POOR QUALITY

ORIGINAL PAGE IS
OF POOR QUALITY

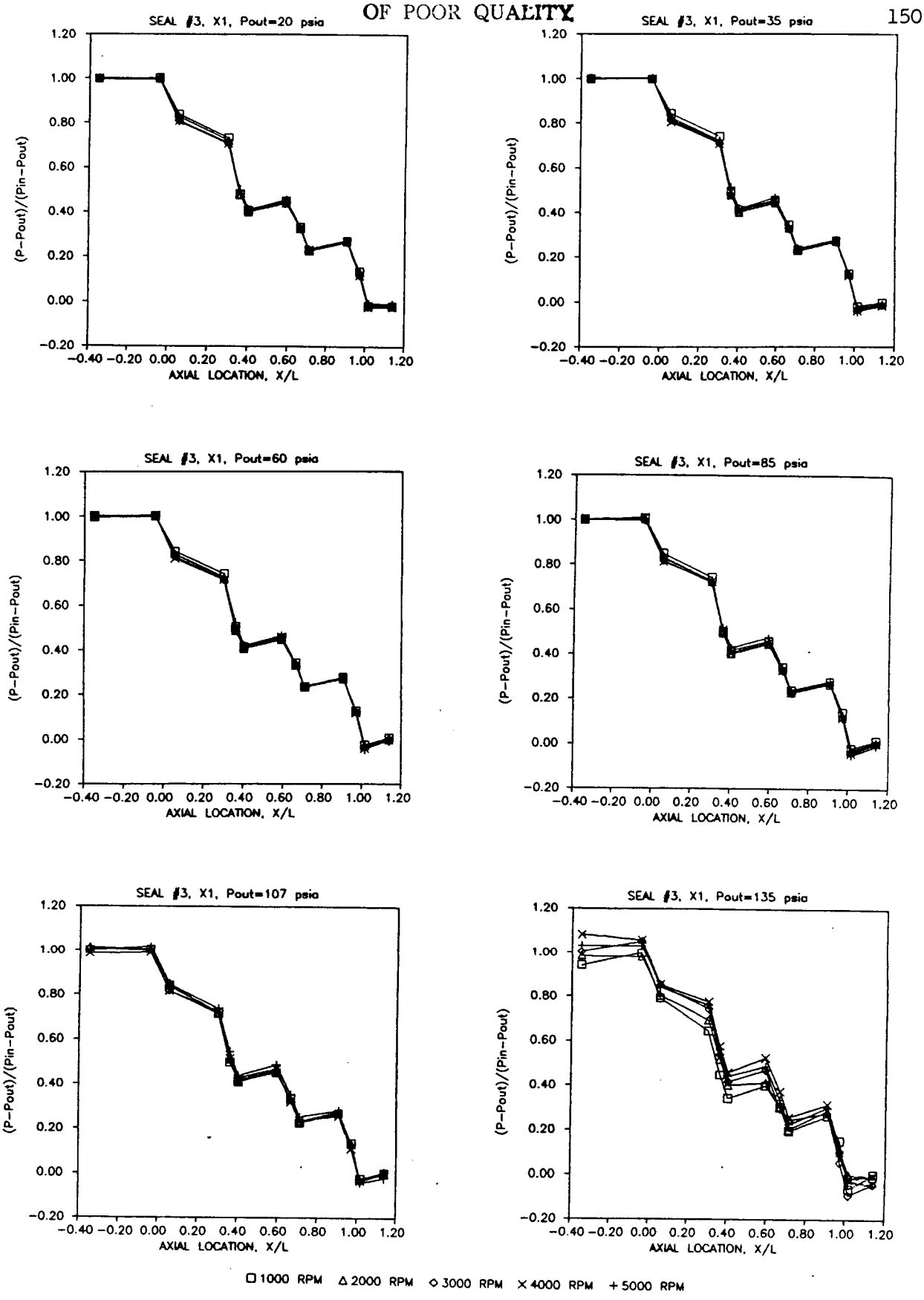

Figure 88. Seal #3 Axial Pressure Distribution For a Given Exit Pressure for Various Shaft Speeds, X1.

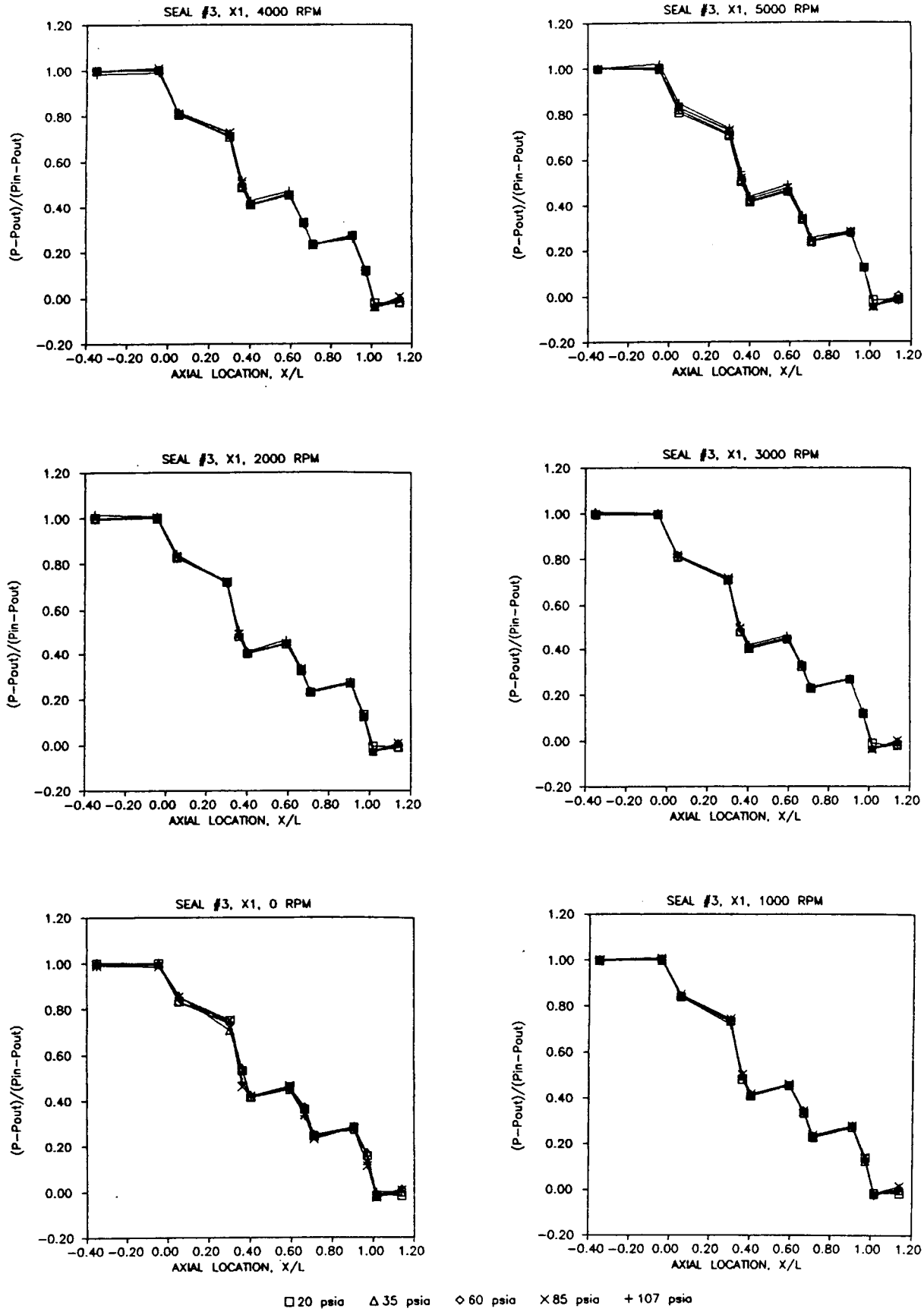

Figure 89. Seal #3 Axial Pressure Distribution For a Given Shaft Speed for Various Pressure Ratios, X1.

ORIGINAL PAGE IS
OF POOR QUALITY

pressure drop across the first seal with no pressure recovery after the tooth is encountered. In the second and thrid cavities, there is a pressure recovery after the tooth.

For axial location X2, the pressure distributions are presented in Figures 90 and 91. Again, the pressure distribution is not linear with a substantial loss occurring over the first cavity followed by two cavities with pressure recovery after the teeth. At this axial location, there is some dependence upon shaft speed and pressure ratio with low shaft speeds at low pressure ratios tending to alter the pressure distribution in the first cavity.

Figures 92 and 93 show the pressure distributions for axial location X3. At this location (minimum value of B) the tooth on the rotor is almost aligned with the step. This results in a modified pressure distribution which is now almost linear and showing a pressure recovery in each cavity. Under these conditions, there is no dependence upon the shaft speed or pressure ratio except for the largest pressure ratio (smallest pressure drop) across the seal. It is interesting to note, that this is the axial location with the most leakage. Evidently, the non-linear pressure distribution decreases the leakage substantially. This was also observed in seal #2.

Summary

Table 15 summarizes the measured values of the flow coefficients and the seal geometries measured. The two seals designed by Dr. Rhode (Seals #2 and #3) were successful in producing less leakage, both by about 30% at the smallest pressure ratio (largest pressure drop). It was interesting to

Seal #1 AXLO=1

P_r \ RPM	0	1000	2000	3000	4000	5000
0.14	1.0834		1.0901	1.0924	1.0875	1.0835
0.27	.9606	.9634	.9652	.9669	.9655	.9662
0.42	.8631	.8666	.8688	.8681	.8690	.8645
0.57	.7312	.7326	.7294	.7321	.7266	.7134
0.69	.7176	.3457	.3572	.4447	.3380	.3188
			AXLO=0.75			
0.14	.9146	.9194	.9184	.9153	.9124	.9040
0.25	.8267	.8264	.8256	.8246	.8208	.8117
0.41	.6910	.6916	.6907	.6914	.6798	.6687
0.58	.3054	.3107	.3115	.3053	.2842	.2689
			AXLO=0.50			
0.14	.9587	.9638	.9615	.9634	.9601	.9538
0.24	.8779	.8786	.8800	.8845	.8818	.8737
0.41	.7678	.7724	.7753	.7736	.7704	.7592
0.62	.3242	.3567	.3435	.3310	.3255	.3122

Seal #2 AXLO=1.0

P_r \ RPM	0	1000	2000	3000	4000	5000
0.85	.4153	.4087	.4000	.3916	.3770	.3609
0.70	.4348	.4316	.4274	.4218	.4119	.4011
0.56	.4551	.4574	.4514	.4473	.4266	.4342
0.40	.4862	.4872	.4854	.4809	.4734	.4661
0.23	.5292	.5309	.5304	.5263	.5178	.5107
0.13	.5659	.5663	.5669	.5627	.5564	.5458
			AXLO=0.5			
0.51	.2443	.2165	.2374	.2587	.2733	.2715
0.29	.1633	.2189	.2570	.2767	.2921	.3101
0.13	.1267	.2167	.2745	.3021	.3240	.3207

SEAL #3

X1

P_r \ RPM	0	1000	2000	3000	4000	5000
0.14	.7377	.7387	.7394	.7466	.7546	.7534
0.24	.6729	.6790	.6787	.6842	.6908	.6882
0.41	.6072	.6104	.6096	.6137	.6194	.6105
0.56	.5533	.5564	.5592	.5641	.5650	.5584
0.76	.5079	.5089	.5125	.5181	.5131	.4937
0.93	.4734	.4828	.5030	.4862	.4648	.4303
			X2			
0.14	.6875	.6823	.6652	.6724	.6678	.6643
0.24	.6426	.6385	.6423	.6387	.6429	.6356
0.41	.5806	.5760	.5736	.5749	.5737	.5695
0.58	.5355	.5309	.5332	.5342	.5325	.5296
0.74	.4981	.4924	.4969	.4956	.4899	.4930
0.92	.4648	.4808	.4685	.4638	.4467	.4522
			X3			
0.14	.9132	.9010	.8995	.8969	.8919	.8890
0.24	.8310	.8266	.8263	.8271	.8280	.8255
0.42	.7252	.7326	.7339	.7347	.7330	.7289
0.59	.6773	.6692	.6697	.6702	.6687	.6664
0.73	.6330	.6243	.6253	.6240	.6179	.6233
0.91	.5584	.5672	.5889	.5717	.5458	.5473

	Seal 1	Seal 2	Seal 3
Clearance	.0085	.0085	.0085
Pitch	0.190	.0627	.190
Tooth Height	0.340	.0567	.0425
Diameter Ave	3.108	3.2728	3.367
Tooth Width	0.030	.0149	.0207
Step Height	0.125	.0227	.0425
Trottles	4	10	4

Table 15. Tabular Summary of Measured Flow Coefficients and Seal Geometries, Distances are in inches.

ORIGINAL PAGE IS OF POOR QUALITY

note that the more nonlinear the pressure distribution through the seal was, the better it sealed. Strangely enough, for one seal the largest pressure drop was at the inlet and the other was at the outlet. The exact reason for this behavior is not known.

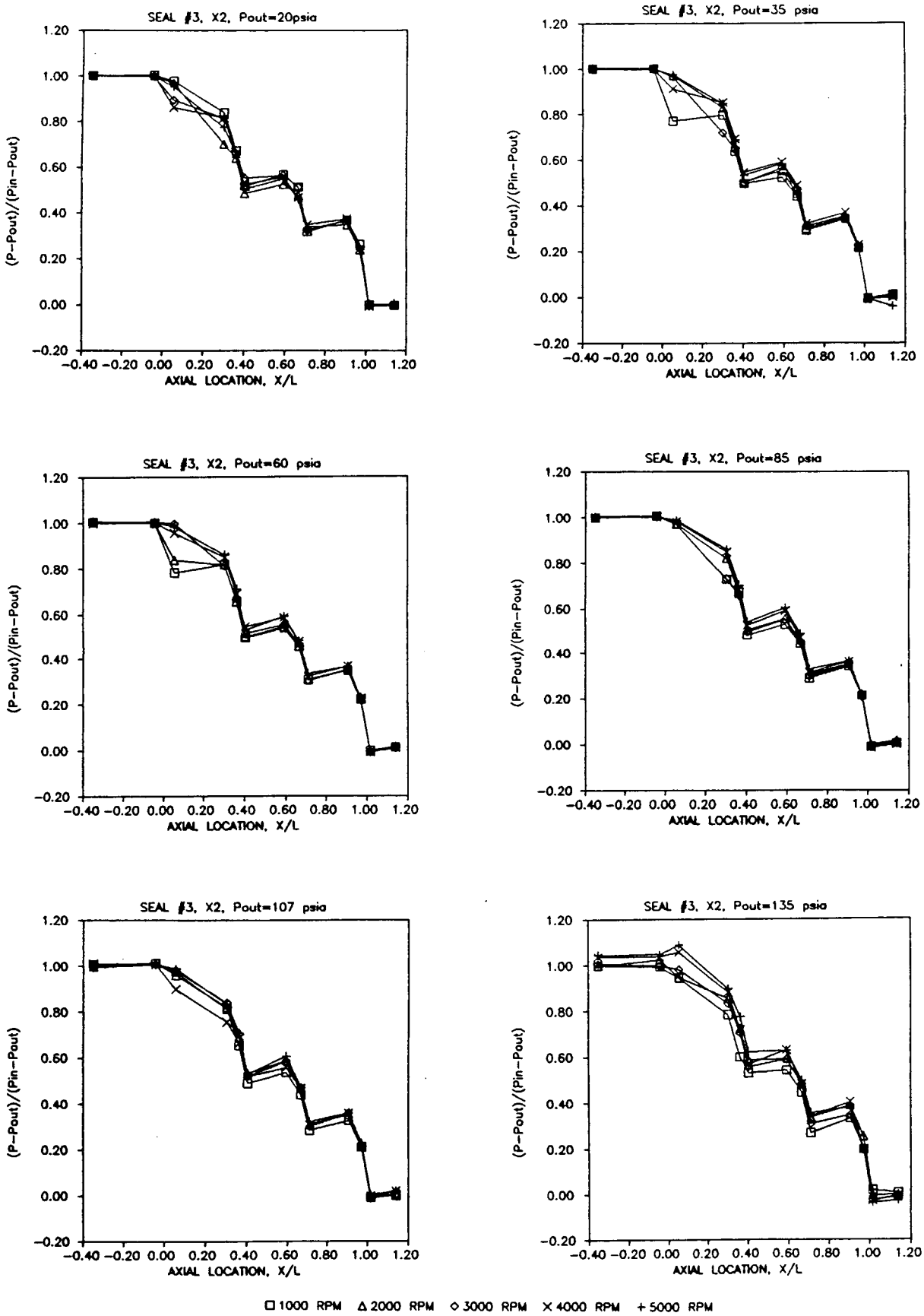

Figure 90. Seal #3 Axial Pressure Distribution For a Given Exit Pressure for Various Shaft Speeds, X2.

ORIGINAL PAGE IS
OF POOR QUALITY

ORIGINAL PAGE IS
OF POOR QUALITY

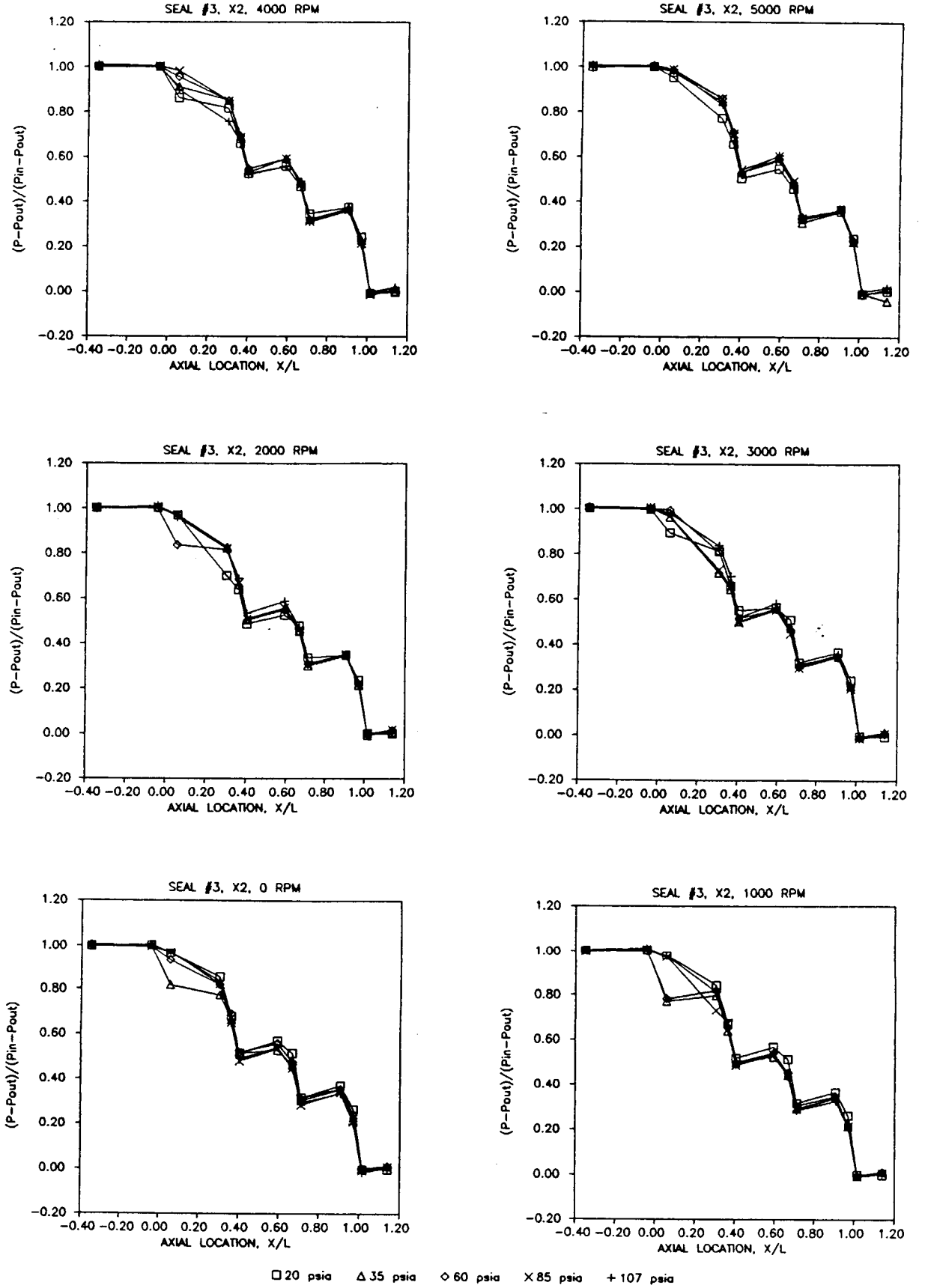

Figure 91. Seal #3 Axial Pressure Distribution For a Given Shaft Speed for Various Pressure Ratios, X2.

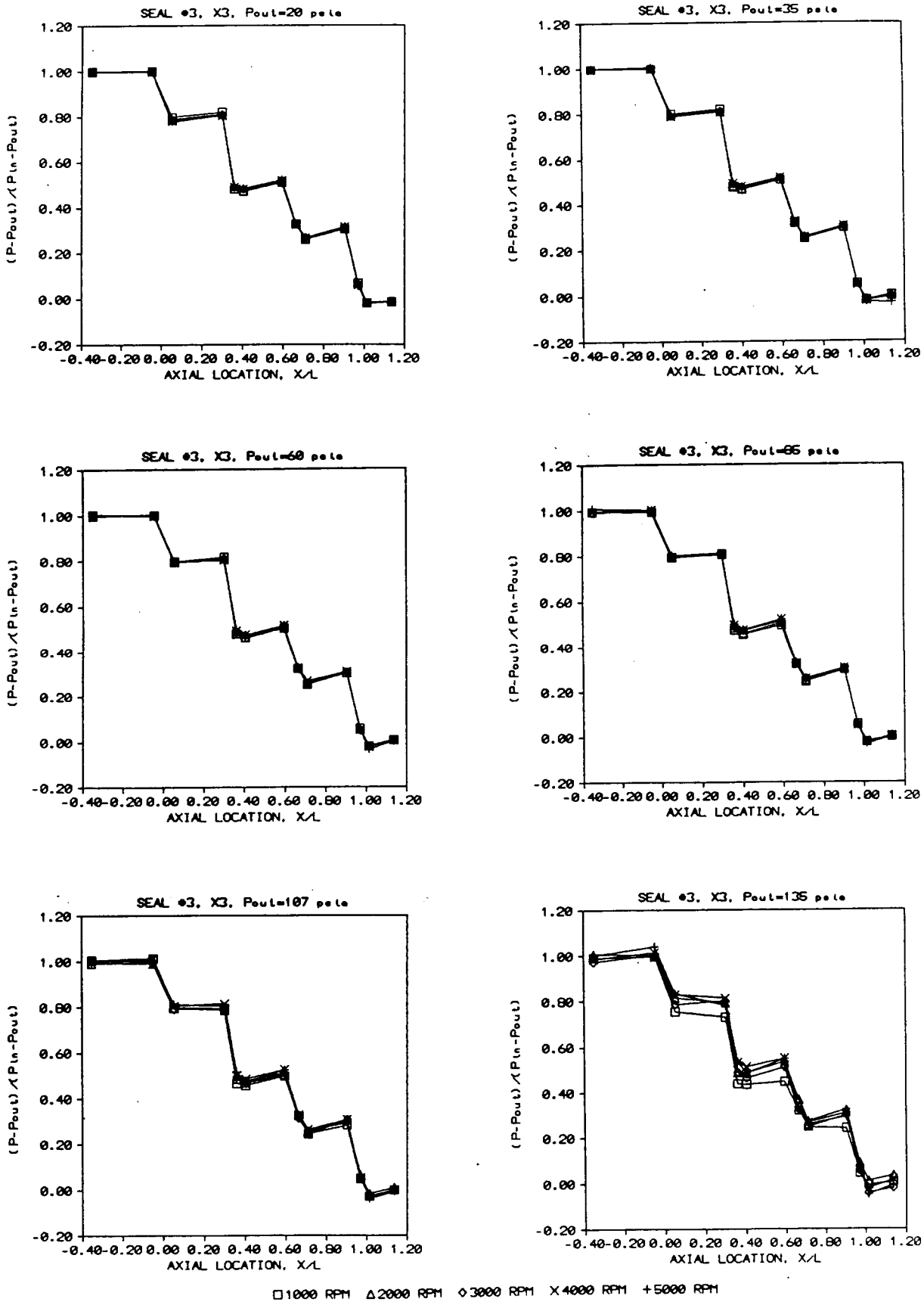

Figure 92. Seal #3 Axial Pressure Distribution For a Given Exit Pressure for Various Shaft Speeds, X3.

ORIGINAL PAGE IS
OF POOR QUALITY

ORIGINAL PAGE IS
OF POOR QUALITY

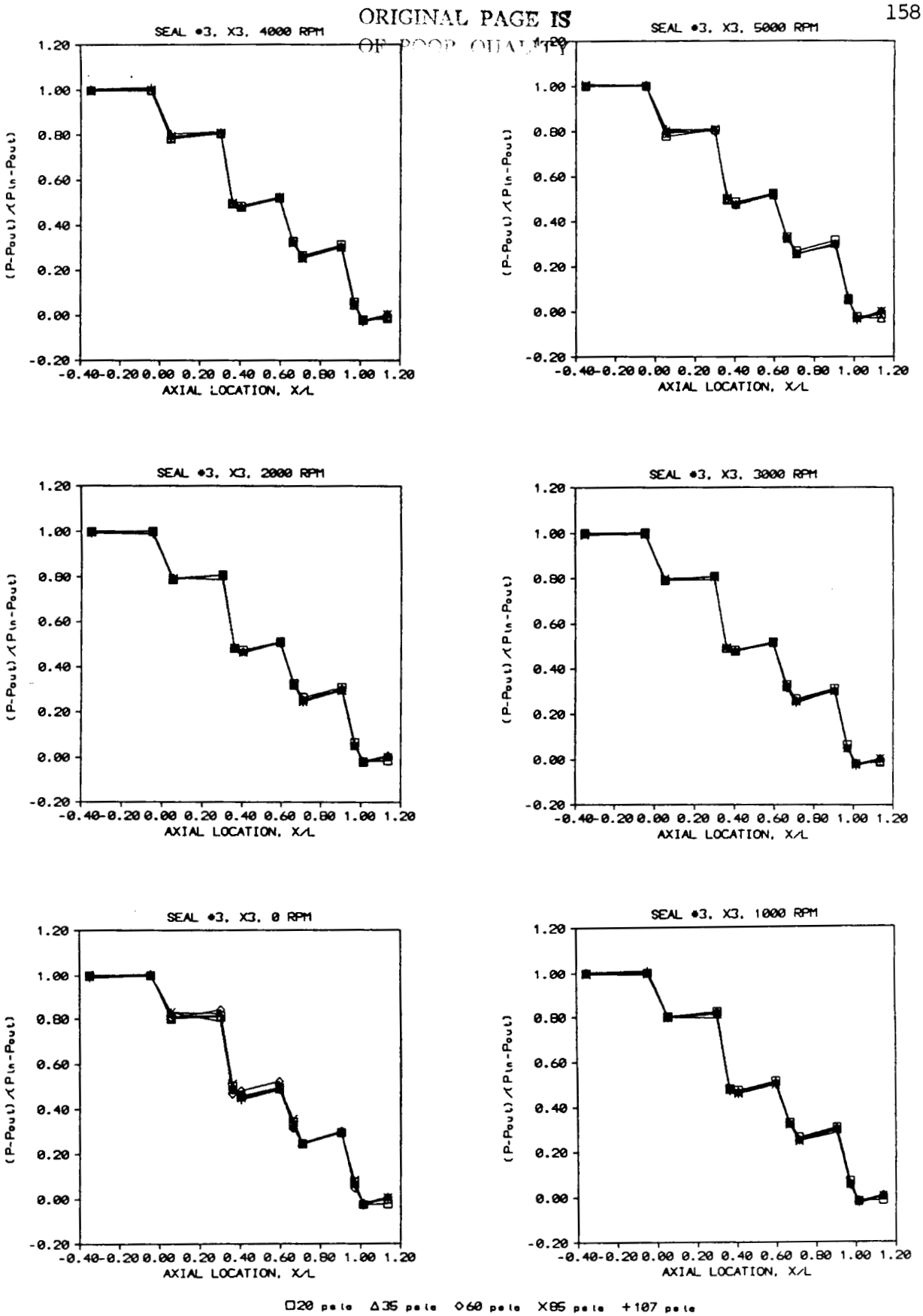

Figure 93. Seal #3 Axial Pressure Distribution For a Given Shaft Speed for Various Pressure Ratios, X3.

ORIGINAL PAGE IS
OF POOR QUALITY

IX. EMPIRICAL PREDICTION COMPARISON WITH CURRENT DATA

The empirical prediction program was produced using data available from the open literature and data previously obtained (Chi[28]) for the oxygen pump front wear ring seal. This program will now be used to predict the flow coefficients for the hydrogen pump front wear ring seal and the two seals designed by Dr. Rhode.

Figure 94 presents the predicted and the measured flow coefficients for the three seals tested for various pressure ratios at shaft speeds of 0 and 5000 rpm. For seal #1, the predictions for AXLO=1.0 are high by a factor of three. This same type of discrepancy was observed previously with this program. However, this was not corrected since all seals are designed to operated in the middle of the step (AXLO=0.50) and the previous comparisons were good at that location. When seal #1 is operated at axial locations of 0.75 and 0.50 the agreement is better but the predictions are still high by a factor of up to two. Similar performace of the empirical prediction are present for seal #2 and #3.

The exact reason for the discrepancies is not known. However, this clearly illustrates the problems of generating empirical leakage prediction schemes. The predictions can be fine tuned for a particular seal upon which the program is based. However, once a significant change in the type of seal being used is made, the predictions become inaccurate. One promising aspect of the leakage estimation program is its ability to predict overall improvements in the seal based upon changes in the seal design even though the absolute value of the flow coefficient was

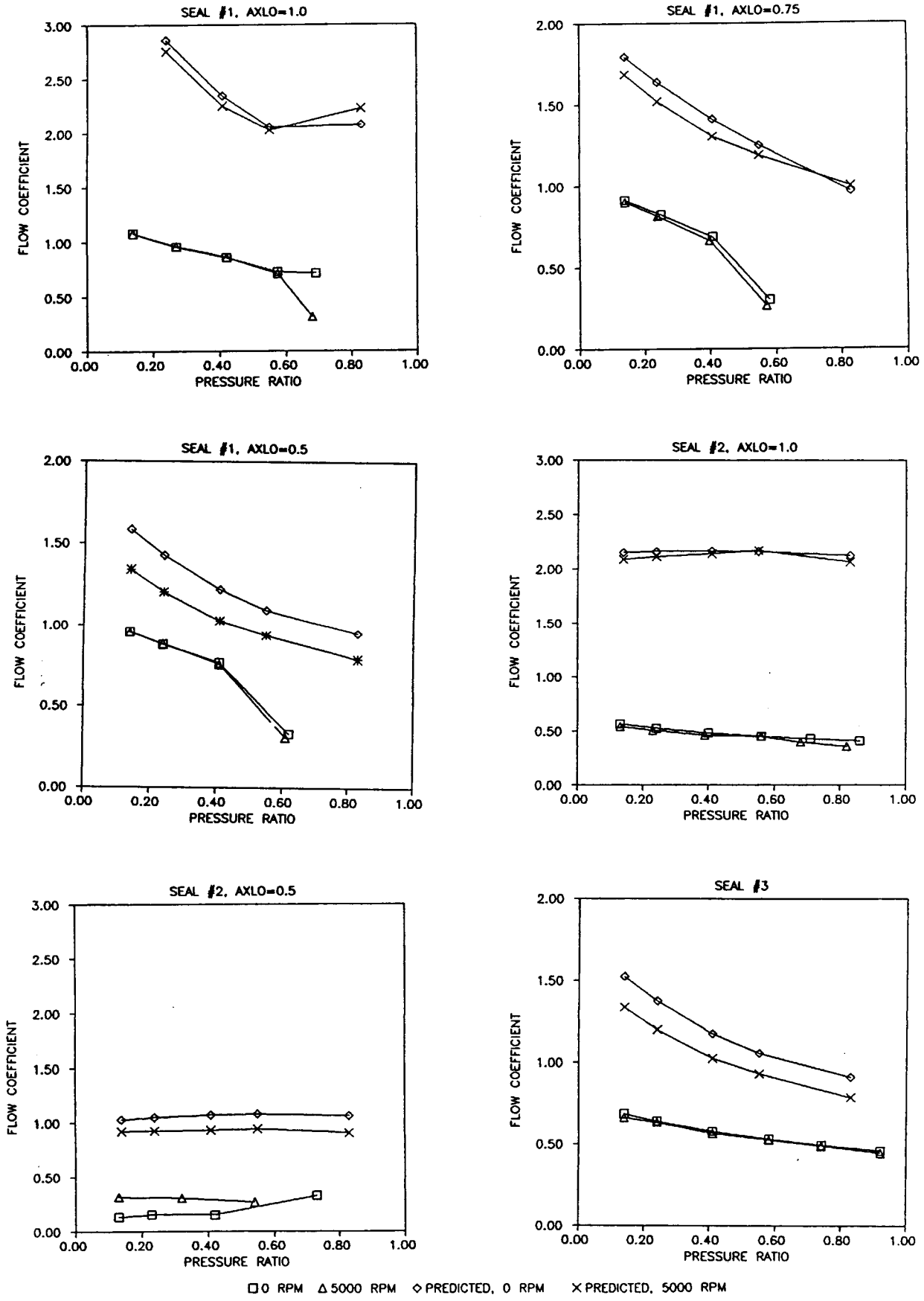

Figure 94. Comparison of Analytic Flow Coefficients with Experimental Data for Various Seal Configurations.

ORIGINAL PAGE IS
OF POOR QUALITY

in error.

X. CLOSURE

Conclusion

A parametric design study was conducted in order to obtain two more effective seal designs for the impeller wear ring of the high pressure fuel pump for the space shuttle. A two-dimensional finite difference computer code was employed using an inverse design approach for computational convenience. It was found that the number of cavities, the step height, and the presence of a novel small stator groove are important design elements. Adding more cavities brings diminishing returns as shown by Egli's [9] leakage equation. It was estimated from analyzing various computations that approximately nine cavities is near the optimum for this case.

Two opposing mechanisms governing the optimum step height were indicated. A short step does not produce the sharp streamline curvature near the cavity discharge which yields the desired high turbulence energy level there. A long step produces broader streamtubes of lower velocity fluid entering this sharply curved streamline region, again resulting in lower turbulence energy levels. The addition of the small stator groove provides additional streamline curvature and an additional reattachment stagnation point, which produce ever higher turbulence levels.

The accuracy and versatility of the empirical leakage estimation model were enhanced by the experimental program by comparisons with the oxygen turbopump front wear ring seal. The model was modified to incorporate the effects of swirl, and the accuracy of the model was greatly improved for seals with a clearance greater than 0.007 inches. The modified leakage estimation model gave good predictions when compared to the oxygen turbopump front wear ring seal. However, when compared to the hydrogen turbopump front wear ring seal, the program consistently over-predicted the leakage rate. This points out the problem of using empirical prediction schemes based upon one seal design and applying them to other designs. However, this model did realistically predict

the trends of the new seal designs.

Accomplishment

Two new designs, as well as the current one, were fabricated and tested. The new designs were denoted Type O (Seal #2 of the test program) and Type S (Seal #3 of the test program). The test data showed that Type O and Type S give 67 and 30 percent reduction in leakage over the current design, respectively. The potential performance enhancement available from using Type O is considerable. However, the axial shift of the stator housing upon start-up and shut-down must be reduced from about 3.0 mm(0.118 in) to about 0.74 mm (0.029 in).

The length-to-width ratio of the teeth of Type O is essentially the same as that of the currently used design. Therefore, there should be no additional problems due to the breakage of teeth. When the reduction in axial shift is achieved, this design should be tested in the actual turbopump using, of course, the smallest clearance which is permissible. This will actually be closer to Type J than Type O.

If the axial shift reduction is not immediately feasible, it is recommended that Type S be seriously considered. Recall that no reduction in axial shift is required in order to use this design. It would probably be preferable to use a stator groove of lesser radial extent than that of Type S, as the additional long tooth from the stator could break off. Since the flow near the top of the stator groove of Types R,S, and T showed little meaningful effect, this groove can be specified with a depth of 0.54 mm(0.0213 in), for example, rather than 1.08 mm(0.0425 in) with negligible effect on the leakage rate. Further, a stress analysis could be conducted to determine a groove depth giving a reliable length-to-width ratio for this new tooth.

REFERENCES

[1] Leschziner, M.A., and Rodi, W., "Calculation of Annular and Twin Parallel Jets Using Various Discretization Schemes and Turbulence-Model Variations," Trans. ASME, Journal of Fluids Engineering, vol. 13, pp. 352-360, 1981.

[2] Leonard, B.P., Leschziner, M.A., and McGurik, J., "Third-Order Finite-Difference Method for Steady Two-Dimensional Convection," Sonderforschungsbereich 1980, University of Karlsruhe, Germany

[3] Leonard, B.P., "A Stable and Accurate Convective Modeling Procedure Based on Quadratic Upstream Interpolation," Comp. Meths. in appl. Mech. Eng., vol. 19, pp. 59-98, 1979.

[4] Rhode, D.L., Demko, J.A., Morrison, G.L., Traegner, U.K., and Sobolik, S.R., "On the Prediction of Incompressible Flow in Labyrinth Seals," Trans. ASME, Journal of Fluids Engineering, vol. 108, pp. 19-25, 1984.

[5] Martin, H.M., "Labyrinth Packings," Engineer, pp. 35-36, Jan. 10, 1908.

[6] Becker, E., "Stromungsvergange in Ringformiggen Spalten," V.D.I., vol. 51, pp. 1133-1141, 1907.

[7] Stodola, A., Steam and Gas Turbines, sixth ed., McGraw-Hill, Vol. 1, pp. 189-194, 1927

[8] Gercke, M.J., "Berechnung der Ausflussmengen von Labyrinth ichtungen," Die Warme, vol. 57, pp. 678-680, 1934.

[9] Egli, A., "The Leakage of Steam Through Labyrinth Seals," Trans. ASME, vol. 57, pp. 115-122, 1935.

[10] Hodkinson, B. "Estimation of the Leakage Through a Labyrinth Gland," Proc.

Inst. Mech. Engrs., vol. 141, pp. 283-288, 1939.

[11] Jeri, J., "Flow Through Straight-Through Labyrinth Seals," Proc. Seventh Int. Cong. Appl. Mech., vol. 2, pp. 70-82, 1948.

[12] Kearton, W.J., and Keh, T.H, "Leakage of Air Through Radial Labyrinth Glands of the Staggered Type," Proc. Inst. Mech. Engrs., vol. 166, pp. 180-195, 1952.

[13] Zabriskie. W., and Sternlicht, B., "Labyrinth Seal Analysis," Journal of Basic Engineering, Trans. ASME, Series D, Vol. 81, No. 3, pp. 332-340, Sept. 1959.

[14] Vermes, G., "A Fluid Mechanics Approach to the Labyrinth Seal leakage Problem," Journal of Basic Engineering, Trans. ASME, Series D, Vol. 83, No. 1, pp. 161-169, April 1961.

[15] Bell, K.J., and Bergelin, O.P., "Flow Through Annular Orifices," Trans. ASME, vol. 79, pp. 593-601, 1957.

[16] Han, J.T., "A Fluid Mechanics Model to Estimate the Leakage of Incompressible Fluids through Labyrinth Seals," ASME Paper 79-FE-4, presented at the Joint ASME/CSME Applied mechanics, Fluids Engineering and Bioengineering Conference, Niagara Falls, June 18-20, 1979.

[17] Stoff, H., "Incompressible Flow in a Labyrinth Seal," Journal of Fluid Mechanics, vol. 100, pp. 817-829, 1980.

[18] Gosman, A.D. and Pun, W.M., "Calculations of Recirculating Flows," Research Report, Rept. No. HTS/74/2, Department of Mechanical Engineering, Imperial college, London, England, 1974.

[19] Jones,W.P., and Launder, B.E. "The Prediction of Laminarization With a Two-

Equation Model of Turbulence," Int. Journal of Heat and Mass Transfer, vol. 5, pp. 301-314, 1973.

[20] Patankar, S.V., Numerical Heat Transfer and Fluid Flow. United States: Hemisphere Publishing company, McGraw-Hill, 1980.

[21] Leschziner, M.A., and Rodi, W., "Calculation of Annular and Twin Parallel Jets Using Various Discretization Schemes and Turbulence-model Variations," Trans. ASME, Journal of Fluids Engineering, vol. 103, pp. 352-360, 1981.

[22] Ko, Sung-Ho, "Numerical Simulation of Geometry Effects for Concentric-Rotor Labyrinth Seals" thesis submitted to the Department of Mechanical Engineering, Texas A&M University, 1986.

[23] Van Den Berg, B., "A Three-Dimensional law of the Wall for Turbulent Shear Flows," Journal of Fluid Mechanics, Vol. 70, part 1, pp. 149-160, 1975.

[24] Sinha, Satya Narain, "Two Dimensional Laminar and Turbulent Separating Flows Over Backward Facing Steps and Rectangular Cavities," University Microfilms International, 1984.

[25] Morrison, G.L., Rhode, D.L., Cogan, K.C., Chi, D. and Demko, J., "Labyrinth Seals for Incompressible Flow", Final Report for contract NAS8-34536, November 1983.

[26] Yamada, Y., "On the Pressure Loss of Flow Between Rotating Co-Axial Cylinders with Rectangular Grooves, " Bulletin of the ASME, Vol. 5, No. 20, 1962, pp. 642-651.

[27] Dodge, L., "Labyrinth Shaft Seals, " Product Engineering, Vol. 34, No. 17, Aug. 19, 1963, pp. 75-79

[28] Chi, D., "Leakage Estimation of Incompressible Fluids in Stepped

Labyrinth Seals," Thesis submitted to the Department of Mechanical Engineering, Texas A&M University, December, 1983.

[29] Hughes, A.F., and Ralph, N., "The Leakage of Air Through Stepped Labyrinth Seals," Thesis submitted to the Department of Mechanical Engineering, University of Bristol, Bristol, England, June, 1970.

APPENDIX A

CURVE FIT EXPERIMENTAL DATA

GRAPH 1: 4 CURVES. ORIGINALLY FIG_04

CURVE NUMBER 1 0.04330000 18 DATA POINTS

1	0.996705	0.245360
2	0.993738	0.296017
3	0.990079	0.346053
4	0.986191	0.370836
5	0.980739	0.416287
6	0.968867	0.489983
7	0.956772	0.504933
8	0.931329	0.512591
9	0.902942	0.521029
10	0.878103	0.536659
11	0.830112	0.561622
12	0.781342	0.588261
13	0.736434	0.607358
14	0.695972	0.629389
15	0.652231	0.653184
16	0.607920	0.681468
17	0.541270	0.700701
18	0.493793	0.732913

CURVE NUMBER 2 0.06200000 17 DATA POINTS

1	0.997755	0.281537
2	0.996266	0.327376
3	0.994687	0.353819
4	0.990554	0.429054
5	0.986464	0.466161
6	0.980719	0.479495
7	0.969388	0.502999
8	0.957517	0.513565
9	0.949066	0.528922
10	0.935773	0.540413
11	0.906591	0.557016
12	0.865880	0.586872
13	0.803639	0.631165
14	0.735034	0.671484
15	0.680379	0.695799
16	0.556238	0.752716
17	0.476005	0.796826

CURVE NUMBER 3 0.09250000 23 DATA POINTS

1	0.998707	0.334729
2	0.997321	0.405426
3	0.997053	0.412878
4	0.995903	0.473712
5	0.994652	0.500406
6	0.993571	0.482213
7	0.988160	0.511827
8	0.978280	0.548964
9	0.967700	0.573217
10	0.958316	0.584974
11	0.940289	0.603786
12	0.927411	0.622610
13	0.859315	0.669789

```
 14   0.819983        0.692982
 15   0.793271        0.717913
 16   0.757016        0.739180
 17   0.712986        0.756179
 18   0.672689        0.780151
 19   0.638402        0.803604
 20   0.618556        0.812679
 21   0.589232        0.824620
 22   0.540821        0.834909
 23   0.521905        0.848400
CURVE NUMBER  4  0.14580000  15 DATA POINTS
  1   0.997471        0.495652
  2   0.995898        0.530585
  3   0.993279        0.581350
  4   0.991414        0.597521
  5   0.984959        0.620055
  6   0.978980        0.637866
  7   0.963495        0.669739
  8   0.949889        0.687323
  9   0.925228        0.720575
 10   0.886169        0.751665
 11   0.841792        0.804024
 12   0.775261        0.827209
 13   0.731458        0.849909
 14   0.575564        0.911080
 15   0.533772        0.924664
GRAPH 2: 1 CURVE.  ORIGINALLY FIG_05
CURVE NUMBER  1  0.07211500  05 DATA POINTS
  1   0.626936E-01    0.754156
  2   0.112659        0.668815
  3   0.169559        0.681585
  4   0.189736        0.702601
  5   0.261697        0.800080
GRAPH 3: 6 CURVES. ORIGINALLY FIG_09
CURVE NUMBER  1  0.00000000  05 DATA POINTS
  1   0.752245        0.746574
  2   0.502812        0.575194
  3   0.253457        0.558987
  4   0.128217        0.564958
  5   0.533339E-01    0.476493
CURVE NUMBER  2  320.000000  06 DATA POINTS
  1    1.00102        0.832862
  2   0.753772        0.669678
  3   0.502812        0.575194
  4   0.253457        0.558987
  5   0.128217        0.564958
  6   0.533339E-01    0.476493
CURVE NUMBER  3  1000.00000  06 DATA POINTS
  1   0.998752        0.582310
  2   0.756863        0.568254
  3   0.500188        0.546790
  4   0.251124        0.526985
```

```
  5   0.129780        0.529699
  6   0.579213E-01    0.465320
CURVE NUMBER  4  1600.00000  06 DATA POINTS
  1   0.998382        0.507041
  2   0.755912        0.507937
  3   0.499709        0.485263
  4   0.250500        0.473617
  5   0.125078        0.479793
  6   0.518008E-01    0.446984
CURVE NUMBER  5  2200.00000  06 DATA POINTS
  1   0.997467        0.463078
  2   0.751791        0.456205
  3   0.506951        0.439935
  4   0.254391        0.426876
  5   0.129586        0.424925
  6   0.534675E-01    0.394582
CURVE NUMBER  6  3200.00000  05 DATA POINTS
  1    1.00216        0.451528
  2   0.751785        0.415308
  3   0.506582        0.406307
  4   0.253325        0.373848
  5   0.136386        0.370720
GRAPH 4: 4 CURVES. ORIGINALLY FIG_10
CURVE NUMBER  1  0.00000000  05 DATA POINTS
  1   0.962703        0.432000
  2    2.67416        0.420717
  3    5.36680        0.421555
  4    8.13848        0.408757
  5    10.8315        0.411398
CURVE NUMBER  2  600.000000  05 DATA POINTS
  1    1.01711        0.325875
  2    2.67146        0.287106
  3    5.36592        0.290618
  4    8.09899        0.290226
  5    10.8736        0.291149
CURVE NUMBER  3  1000.00000  05 DATA POINTS
  1   0.997177        0.284199
  2    2.68979        0.254302
  3    5.37808        0.249343
  4    8.11369        0.252047
  5    10.8468        0.251792
CURVE NUMBER  4  1600.00000  05 DATA POINTS
  1    1.04325        0.238091
  2    2.71738        0.206627
  3    5.39661        0.198552
  4    8.13584        0.202052
  5    10.8375        0.207866
GRAPH 5: 5 CURVES. ORIGINALLY FIG_??
CURVE NUMBER  1  0.75000000  03 DATA POINTS
  1    0.00000        0.52447
  2    2000.00        0.53520
  3    5000.00        0.56411
```

```
CURVE NUMBER  2  0.58000000  03 DATA POINTS
  1     0.00000        0.58745
  2     2000.00        0.60489
  3     5000.00        0.62293
CURVE NUMBER  3  0.43000000  03 DATA POINTS
  1     0.00000        0.62990
  2     2000.00        0.63736
  3     5000.00        0.65177
CURVE NUMBER  4  0.24000000  03 DATA POINTS
  1     0.00000        0.68597
  2     2000.00        0.69602
  3     5000.00        0.71271
CURVE NUMBER  5  0.12000000  03 DATA POINTS
  1     0.00000        0.74282
  2     2000.00        0.74826
  3     5000.00        0.78079
GRAPH 6: 4 CURVES. ORIGINALLY FIG_??
CURVE NUMBER  1  1.00000000  03 DATA POINTS
  1     0.00000        1.39463
  2     2000.00        1.49419
  3     5000.00        1.61476
CURVE NUMBER  2  0.75000000  03 DATA POINTS
  1     0.00000        0.79905
  2     2000.00        0.82565
  3     5000.00        0.88859
CURVE NUMBER  3  0.50000000  03 DATA POINTS
  1     0.00000        0.72108
  2     2000.00        0.68734
  3     5000.00        0.63698
CURVE NUMBER  4  0.25000000  03 DATA POINTS
  1     0.00000        0.74282
  2     2000.00        0.74826
  3     5000.00        0.78079
GRAPH 7: 5 CURVEA. ORIGINALLY FIG_??
CURVE NUMBER  1  10.0000000  06 DATA POINTS
  1     0.79230        0.81717
  2     0.74307        0.97416
  3     0.57863        1.11221
  4     0.40890        1.15713
  5     0.24331        1.27449
  6     0.11832        1.41669
CURVE NUMBER  2  08.0000000  06 DATA POINTS
  1     0.80722        0.76333
  2     0.72151        0.95683
  3     0.57718        1.06828
  4     0.40446        1.15629
  5     0.25141        1.24214
  6     0.12007        1.39463
CURVE NUMBER  3  06.0000000  06 DATA POINTS
  1     0.90376        1.10929
  2     0.74811        1.09006
  3     0.58087        1.16408
```

```
  4     0.42016        1.24805
  5     0.25245        1.40160
  6     0.11909        1.57409
CURVE NUMBER  4  04.0000000  06 DATA POINTS
  1     0.91853        1.00637
  2     0.75579        1.22805
  3     0.59032        1.31296
  4     0.43167        1.43162
  5     0.25987        1.60119
  6     0.11979        1.79033
CURVE NUMBER  5  02.0000000  06 DATA POINTS
  1     0.93213        1.17479
  2     0.74009        1.31556
  3     0.58213        1.43663
  4     0.43832        1.62460
  5     0.27396        2.10394
  6     0.11808        2.11858
GRAPH 8: 5 CURVES. ORIGINALLY FIG_??
CURVE NUMBER  1  10.0000000  04
  1     0.66108       0.62827
  2     0.46360       0.65642
  3     0.26221       0.71327
  4     0.13776       0.77945
CURVE NUMBER  2  08.0000000  05
  1     0.80800       0.58880
  2     0.62985       0.59214
  3     0.43795       0.63282
  4     0.26054       0.69414
  5     0.13579       0.77924
CURVE NUMBER  3  06.0000000  05
  1     0.82239       0.63808
  2     0.63236       0.66171
  3     0.47629       0.72139
  4     0.27327       0.80049
  5     0.13720       0.84751
CURVE NUMBER  4  04.0000000  06
  1     0.91938       0.73578
  2     0.81112       0.73311
  3     0.63647       0.77429
  4     0.45948       0.83422
  5     0.27362       0.91282
  6     0.13983       0.97461
CURVE NUMBER  5  02.0000000  06
  1     0.95006        1.03653
  2     0.81203        1.05008
  3     0.64416        1.05693
  4     0.47940        1.27200
  5     0.28524        1.39237
  6     0.14145        1.72076
```

APPENDIX B

EMPIRICAL LEAKAGE ESTIMATION PROGRAM

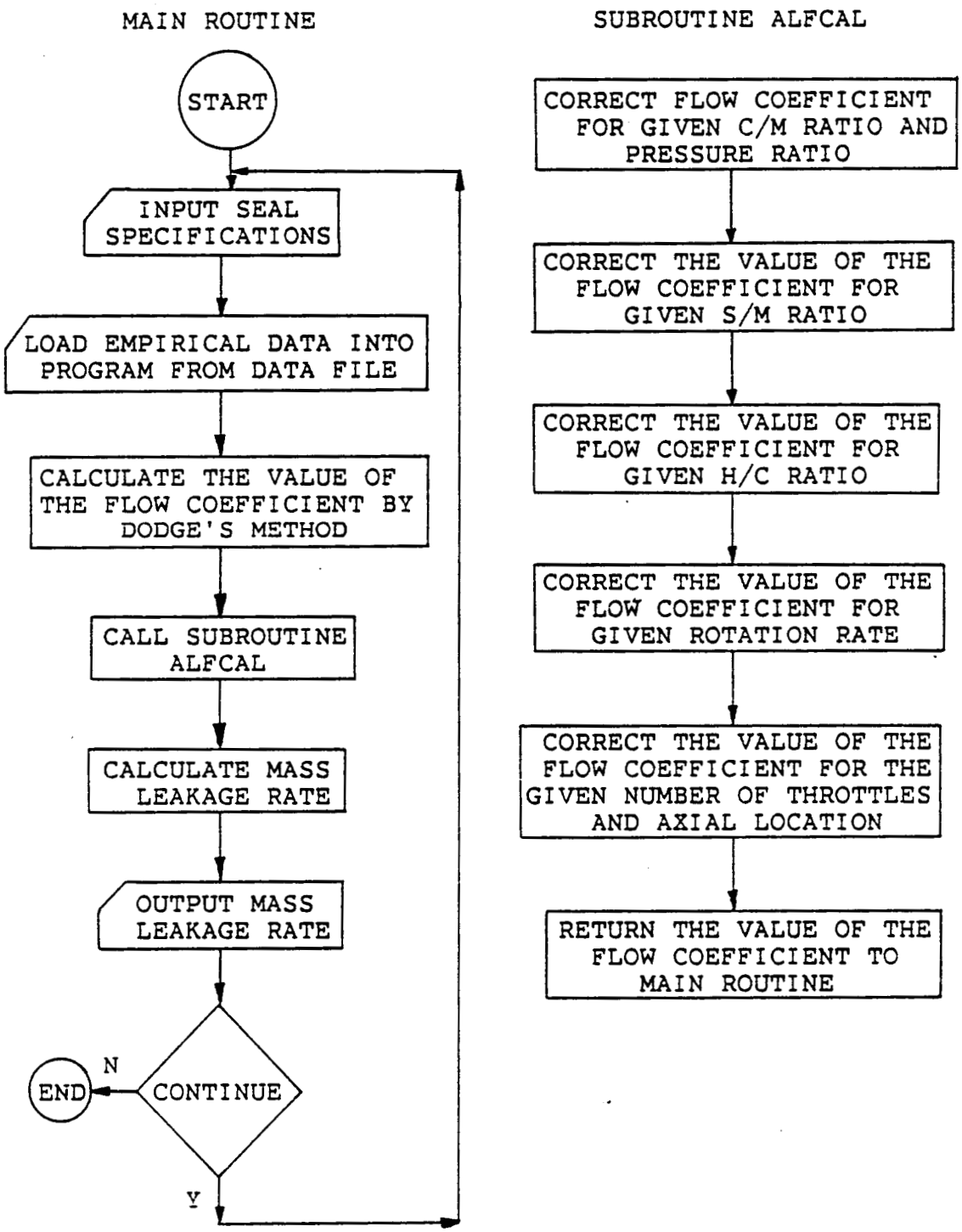

FLOWCHART FOR LEAKAGE PREDICTION PROGRAM FOR STEPPED LABYRINTH SEALS

```
C*****************************************************
C  PROGRAM MODIFIED TO RUN ON THE IBM-PC USING MS
C  FORTRAN AND THE VAX USING VAX FORTRAN C
C  MODIFIED BY SCOTT WAUGHTAL
C
C*****************************************************
C
C       PROGRAM BY KEVIN COGAN.  FALL, 1982.
C       LABYRINTH SEALS PROJECT, UNDER THE DIRECTION OF
C       DR. G.L. MORRISON.  MECHANICAL ENGINEERING DEPT.
C       TEXAS A&M UNIVERSITY.
C
C       MODIFIED BY DAESUNG CHI, SUMMER, 1983
C       PROGRAM NOW CALCULATES LEAKAGE RATES FOR
C       STEPPED LABYRINTH SEALS
C
C
C       CALCULATION OF THE LEAKAGE RATE IS ACHIEVED BY
C       FIRST USING DODGE'S TECHNIQUE TO DETERMINE THE
C       FLOWRATE IN A SEVEN TOOTHED STRAIGHT-THROUGH
C       LABYRINTH SEAL. THEN THE RESULT IS MODIFIED BY
C       USING INTERPOLATION OF EXPERIMENTAL DATA
C       SUBROUTINE ALFCAL
C
C*****************************************************
C
C       A LIST OF VARIABLES USED IN THIS ROUTINE IS AS
C       FOLLOWS:
C
C        DEN    - FLUID DENSITY
C        XNU    - FLUID KINEMATIC VISCOSITY
C        PIN    - INLET PRESSURE
C        PEX    - EXHAUST PRESSURE
C        CLR    - SEAL CLEARANCE
C        PCH    - PITCH
C        WTH    - TOOTH WIDTH
C        HIT    - TOOTH HEIGHT
C        TNUM   - NUMBER OF THROTLES
C        DIA    - SEAL DIAMETER
C        RPM    - SEAL ROTATION RATE
C        AXLO   - AXIAL LOCATION
C        IFLAG  - INPUT FLAG
C        ICODE  - VALUE SPECIFIES VARIABLES TO BE
C        CHANGED
C        ALFA   - FLOW COEFFICIENT
C        CCOEF  -CARRY-OVER COEFFICIENT
C        FLOW   - MASS LEAKAGE RATE
C        ICRT   - LOGICAL UNIT NUMBER FOR CRT CONSOLE
C        IPRINT - LOCIGAL UNIT NUMBER FOR PRINTER
C  SWIRL  - MULTIPLICATION FACTOR DUE TO SWIRL
C  II     - SWIRL DIRECTION( 0-NO SWIRL,1-SWIRL
C
```

```
C*****************************************************
C
C       THIS MAIN ROUTINE IS ESTABLISHED TO HANDLE THE
C       REQUIRED INPUT AND OUTPUT.  INITIALLY, IFLAG IS
C       SET TO '0', WHICH WILL CAUSE THE PROGRAM TO
C       PROMPT THE USER FOR ALL NECESSARY INFORMATION.
C       AFTER THIS INITIAL PASS, THE USER MAY CHANGE ANY
C       OR ALL OF THE SEAL DATA BY SPECIFYING THE
C       APPROPRIATE CODE WHEN PROMPTED.
C
C*****************************************************
C
      DIMENSION NAME(6)
      IPRINT=6
      IDISK=0
      OPEN(UNIT=6,STATUS='NEW',FILE='PRN')
  101 IFLAG=0
      GOTO 1
  102 IFLAG=1
C
      WRITE (*,105) DEN,PIN,PEX,CLR
  105 FORMAT (' INPUT CODE IF CHANGE IS DESIRED:' ,/,' 1
     & = DENSITY = ' ,
     + G12.5,/,' 2 = INITIAL P = ' ,G12.5,/,
     + ' 3 = FINAL P = ' ,G12.5,/,' 4 = CLEARANCE = '
     & ,G12.5)
      WRITE (*,106) PCH,WTH,HIT,TNUM,DIA,RPM,XNU,AXLO,II
  106 FORMAT (' 5 = PITCH = ' ,G12.5,/,' 6 = TOOTH WIDTH
     & = ' ,
     + G12.5,/,' 7 = TOOTH HEIGHT = ' ,G12.5,/,' 8 =
     & THROTTLES = ' ,
     + G12.5,/,' 9 = DIAMETER = ' ,G12.5,/,' 10 = RPM =
     & ',G12.5,
     +/,' 11 = KINEMATIC VISCOSITY = ',G12.5,/,
     +' 12 = AXIAL LOCATION = ',G12.5,/,' 13 = SWIRL
     & =',I3)
      WRITE (*,107)
  107 FORMAT (' 14 = CHANGE ALL' ,/,' 15 = RUN' ,/,' 16
     & = QUIT' )
C*****************************************************
C
C       USER IS PROMPTED FOR REQUIRED SEAL INFORMATION C
C*****************************************************
  199 WRITE(*,200)
  200 FORMAT(' CHANGE CODE: ')
      READ(*,201)ICODE
 IF(ICODE.EQ.0) GOTO 199
  201 FORMAT(I2)
      GO TO (1,2,3,4,5,6,7,8,9,10,11,13,15,101,12),ICODE
      STOP
    1 WRITE(*,202)
  202 FORMAT(' FLUID DENSITY (LBM/FT**3) : ')
```

```
      READ(*,203)DEN
  203 FORMAT(F10.4)
      IF (IFLAG .EQ. 1) GO TO 102
    2 WRITE(*,204)
  204 FORMAT(' INITIAL PRESSURE (PSIA) : ')
      READ(*,203)PIN
      IF (IFLAG .EQ. 1) GO TO 102
    3 WRITE(*,215)
  215 FORMAT(' EXIT PRESSURE (PSIA) :')
      READ(*,203)PEX
      IF(IFLAG.EQ.1)GO TO 102
    4 WRITE(*,205)
  205 FORMAT(' CLEARANCE (IN.) : ')
      READ(*,203)CLR
CLRA=CLR
      IF (IFLAG .EQ. 1) GO TO 102
    5 WRITE(*,206)
  206 FORMAT(' PITCH (IN.) : ')
      READ(*,203)PCH
      IF (IFLAG .EQ. 1) GO TO 102
    6 WRITE(*,207)
  207 FORMAT(' TOOTH WIDTH (IN.) : ')
      READ(*,203)WTH
      IF(IFLAG.EQ.1)GO TO 102
    7 WRITE(*,208)
  208 FORMAT(' TOOTH HEIGHT (IN.) : ')
      READ(*,203)HIT
      IF(IFLAG.EQ.1)GO TO 102
    8 WRITE(*,209)
  209 FORMAT(' NUMBER OF THROTTLES : ')
      READ(*,203)TNUM
      IF (IFLAG .EQ. 1) GO TO 102
    9 WRITE(*,210)
  210 FORMAT(' SEAL DIAMETER (IN.) : ')
      READ(*,203)DIA
      IF (IFLAG .EQ. 1) GO TO 102
   10 WRITE(*,211)
  211 FORMAT(' SEAL RPM : ')
      READ(*,203)RPM
      IF(IFLAG.EQ.1)GO TO 102
   11 WRITE(*,212)
  212 FORMAT(' KINEMATIC VISCOSITY (FT**2/SEC) : ')
      READ(*,203)XNU
      IF(IFLAG.EQ.1)GO TO 102
   13 WRITE(*,230)
  230 FORMAT(' AXIAL LOCATION : ')
      READ(*,203)AXLO
      IF(IFLAG.EQ.1) GOTO 102
   15 WRITE(*,225)
  225 FORMAT(' 0. -NO SWIRL,1. -SWIRL ')
      READ(*,203)FII
      II=INT(FII)
```

```
      GO TO 102
C*****************************************************
C
C       FIRST THE FLOW COEFFICIENT FOR THE GIVEN
C       PRESSURE CONDITIONS AND A CLEARANCE TO PITCH
C       RATIO OF 0.0433 AND SEVEN TEETH IS CALCULATED
C       USING DODGE'S TECHNIQUE, THEN
C       SUBROUTINE ALFCAL IS CALLED.  THIS SUBROUTINE
C       CALCULATES AND RETURNS THE VALUE OF THE FLOW
C       COEFFICIENT.
C*****************************************************
   12 CONTINUE
      WRITE(IPRINT,105)DEN,PIN,PEX,CLR
      WRITE(IPRINT,106)PCH,WTH,HIT,TNUM,DIA,RPM,XNU,
     & AXLO,II
C INITIALLY GUESS AN AXIAL VELOCITY OF 1 FT/SEC
      U=1.
      ICOUNT=0
  213 RE=2.*CLR*U/(12.*XNU)
      ICOUNT=ICOUNT+1
      F=64./RE
      IF(RE.GT.2320.)F=0.316/(RE**0.50)
      PART1=2.*(PIN-PEX)*32.2*144.
      PART2=DEN*(1.5+(F*7./(.0433))+1.0*(7.-1.))
      UNEW=SQRT(PART1/PART2)
      ERR=ABS(U-UNEW)
      IF(ERR.LT.0.005)GO TO 214
      U=UNEW
      IF(ICOUNT.GT.1000)GO TO 214
      GO TO 213
  214 CONTINUE
      IF(ICOUNT.GT.1000)U=0.
      WRITE(*,217)U,RE,F
      WRITE(IPRINT,217)U,RE,F
  217 FORMAT(' U = ',G12.5,' FT/SEC',/,' RE = ',G12.5,
     &/,' FRICTION FACTOR = ',G12.5)
C*****************************************************
C
C     CALCULATE THE CARRY OVER COEFFICIENT FOR TNUM = 7
C     AND A CLEARANCE TO PITCH RATIO OF 0.0433
C     FOR USE IN DETERMINING THE FLOW COEFFICIENT FROM
C     THE DODGE CALCULATION WHERE TNUM=7
C
C*****************************************************
       CCOEF=1./SQRT(1.-(7.-1.)*(0.0433)/(7.*
     & (0.0433+0.02)))
      FLOW=DEN*U*3.1416*DIA*CLR/144.
      PART1=(7.+ALOG(PIN/PEX))/(DEN*PIN*144.*32.2)
      PART1=PART1/(1.-(PEX/PIN)**2.)
      ALFA=FLOW*SQRT(PART1)/(CCOEF*3.1416*DIA*CLR/144.)
      WRITE(*,216)ALFA
      WRITE(IPRINT,216)ALFA
```

```
  216 FORMAT(' VALUE OF THE FLOW COEFFICIENT FROM DODGE
     &CALCULATION IS: ',G12.5)
      CALL
      ALFCAL(PEX/PIN,CLR/PCH,WTH/PCH,HIT/CLR,CLR,
     &TNUM,RPM,ALFA,IDISK,ICRT,IPRINT,AXLO,AAXLO)
      PRAT=PEX/PIN
C*****************************************************
C
C       THE CARRY-OVER COEFFICIENT AND LEAKAGE RATE ARE
C       CALCULATED.
C*****************************************************
      CCOEF=1./SQRT(1.-(TNUM-1.)
     &*(CLR/PCH)/(TNUM*(CLR/PCH+.02)))
      FLOW=ALFA*CCOEF*3.1416*CLR*DIA*SQRT(PIN*DEN*(1.-
     &(PEX/PIN)**2))/
     +  SQRT(TNUM+ALOG(PIN/PEX))*SQRT(32.174/144.)
C*****************************************************
C
C SUBROUTINE TO MODIFY THE FLOW COEFFICIENT DUE TO THE
C EFFECTS OF SWIRL.  THE SUBROUTINE CALCULATES THE
C EFFECT OF SWIRL FOR CLEARANCES OF 0.007 AND 0.014 IN.
C AND INTERPOLATES TO FIND THE EFFECT OF SWIRL ON THE
C FLOW COEFFICIENT AT THE SPECIFIED CLEARANCE.
C
C*****************************************************
      CALL SWIRLER(AXLO,TNUM,PRAT,II,SWIRL,CLRA)
      ALFA=ALFA*SWIRL
C*****************************************************
C
C       RESULTS ARE OUTPUT.
C
C*****************************************************
      WRITE(*,231)ALFA
      WRITE(IPRINT,231)ALFA
  231 FORMAT(' THE FLOW COEFFICIENT WITH SWIRL=',G12.5)
  241 WRITE(IPRINT,222)ALFA,CCOEF,FLOW
      WRITE(*,222)ALFA,CCOEF,FLOW
  222 FORMAT(//,' THE FLOW COEFFICIENT IS ',G12.5,/,
     &' THE CARRY-OVER COEFFICIENT IS ',G12.5,/,
     &' THE LEAKAGE RATE IS ',G12.5,' LBM/SEC',//)
      WRITE(IPRINT,108)
  108 FORMAT(1H1)
      GOTO 102
      END
C
C
C
C*****************************************************
C
C    SUBROUTINE ALFCAL CALCULATES THE VALUE OF THE FLOW
C    COEFFICIENT.  THE VALUE OF THE FLOW COEFFICIENT IS
C    DETERMINED BY INTERPOLATION AND EXTRAPOLATION OF
```

```
C THE DATA READ IN FROM THE DATA FILE.
C
C*****************************************************
C
C       THE LIST OF VARIABLES FOR THIS ROUTINE IS AS
C       FOLLOWS:
C        PR     - PRESSURE RATIO
C        CTOP   - CLEARANCE/PITCH
C        WTOP   - TOOTH WIDTH/PITCH
C        HTOC   - TOOTH HEIGHT/CLEARANCE
C        CLR    - CLEARANCE
C        TNUM   - NUMBER OF THROTTLES
C        RPM    - SEAL ROTATION RATE
C        AXLO   - AXIAL LOCATION
C        AAXLO  - AXIAL LOCATION FOR CALCULATION
C        ALFA   - FLOW COEFFICIENT
C        DATA   - DATA FROM DATA FILE
C        NDATA  - NUMBER OF DATA POINTS
C        CURV   - CURVE VALUES
C        NCURV  - NUMBER OF CURVES
C        IDISK  - TELLS SUBROUTINE TO READ DISK DATA
C                 WHEN = 0
C        ICRT   - LOGICAL UNIT NUMBER FOR CRT CONSOLE
C        IPRINT - LOGICAL UNIT NUMBER FOR PRINTER
C
C*****************************************************

      SUBROUTINE ALFCAL(PR,CTOP,WTOP,HTOC,CLR,TNUM,
     &IDISK,ALFA,RPM,ICRT,IPRINT,AXLO,AAXLO)
C*****************************************************
C
C DATA PREVIOUSLY READ IN FROM A SEPERATE FILE WERE
C CURVE FIT.  ALL CURVE FIT SUBROUTINES, GRAPH1-GRAPH8,
C CORRESPOND TO DATA READ UNDER THOSE TITLES.
C*****************************************************
C
C IF THE SHAFT SPEED IS ABOVE 5000 RPM, ASSUME THERE
C IS NO ADDITIONAL EFFECTS OF THE SHAFT SPEED UPON THE
C FLOW COEFFICIENT FOR SHAFT SPEEDS EXCEEDING 5000 RPM
C
C*****************************************************
      IF(RPM.GT.5000.)RPM=5000.
      IF(AXLO.LT.0.25)GO TO 37
      AAXLO=AXLO
      GO TO 38
   37 AAXLO=1.0-AXLO
   38 CONTINUE
      IF (CTOP .LE. 0.15) GOTO 30
      C1=ALFA+3.16522*(CTOP-0.0433)
      WRITE (*,500) C1
      WRITE(IPRINT,500)C1
  500 FORMAT (' FLOW COEFFICIENT FOR C/M > 0.15:
```

```
     & ',G12.5)
      GOTO 35
   30 CALL GRAPH1(C1A,CTOP,PR)
      CALL GRAPH1(C1B,.0433,PR)
      C1=ALFA*C1A/C1B
      WRITE (*,505) C1
      WRITE(IPRINT,505)C1
  505 FORMAT (' FLOW COEFFICIENT FOR C/M <= 0.15:
     & ',G12.5)
   35 CALL GRAPH3 (WTOP,RPM,C2A)
      CALL GRAPH3 (0.25,RPM,C2B)
      C2=C1*C2A/C2B
      IF(RPM.LE.3200.)GO TO 36
      C2=C1+0.059205*(WTOP-0.25)
   36 CONTINUE
      WRITE (*,510) C2
      WRITE(IPRINT,510)C2
  510 FORMAT (' FLOW COEFFICIENT  WITH W/M EFFECTS:
     & ',G12.5)
      C3=C2
      IF(HTOC.LT.2.7)C3= (2.7-HTOC)*0.0199+C2
      WRITE (*,515) C3
      WRITE(IPRINT,515)C3
  515 FORMAT (' VALUE WITH H/C EFFECTS: ',G12.5)
      CALL GRAF5(PR,RPM,C4A)
      CALL GRAF5(PR,0.0,C4B)
      C4=C3*C4A/C4B
      WRITE (*,520) C4
      WRITE(IPRINT,520)C4
  520 FORMAT (' VALUE WITH ROTATION EFFECTS: ',G12.5)
      CALL GRAF6(AAXLO,RPM,C5A)
      CALL GRAF6(0.8,RPM,C5B)
      IF(TNUM.GE.8.0.AND.AAXLO.GE.0.8)GO TO 45
      IF(TNUM.GE.8.0.AND.AAXLO.LT.0.8)GO TO 46
      IF(TNUM.LT.8.0.AND.AAXLO.GE.0.8)GO TO 47
      IF(TNUM.LT.8.0.AND.AAXLO.LT.0.8)GO TO 48
   45 C5=C4*C5A/C5B
      ALFA=C5
      GO TO 50
   46 C6=C4*C5A/C5B
      ALFA=C6
      GO TO 50
   47 CALL GRAF7(TNUM,PR,C7A)
      CALL GRAF7(8.0,PR,C7B)
      C8=C4*C7A/C7B
      C9=C8*C5A/C5B
      ALFA=C9
      GO TO 50
   48 CALL GRAF8(TNUM,PR,C8A)
      CALL GRAF8(8.0,PR,C8B)
      C10=C4*C8A/C8B
      C11=C10*C5A/C5B
```

```
      ALFA=C11
   50 CONTINUE
C*****************************************************
C
C        AFTER THE FLOW COEFFICIENT IS DETERMINED, ITS
C        VALUE IS RETURNED TO THE MAIN ROUTINE.
C
C*****************************************************
      WRITE(*,524)ALFA
      WRITE(IPRINT,524)ALFA
  524 FORMAT(' VALUE WITH NUMBER OF TEETH AND AXIAL ',
     &'LOCATION EFFECTS: ',G12.5)
C*****************************************************
C
C GRAPH9 MODIFIES THE FLOW COEFFICIENT TO TAKE INTO
C ACCOUNT THE EFFECTS OF CLEARANCES GREATER THE 0.007
INCHES.
C
C*****************************************************
      IF(CLR.LE.0.007)GOTO 241
      CALL GRAPH9(AXLO,TNUM,PR,RPM,CLR,GO)
      ALFA=ALFA*GO
      WRITE(*,242)ALFA
      WRITE(IPRINT,242)ALFA
  242 FORMAT(' THE FLOW COEFFICIENT WITH CLR > 0.007
     *IN.=',G12.5)
  241 RETURN
      END
C
C
C
C*****************************************************
C
C ALL PREVIOUSLY INTERPOLATED DATA WAS CURVE FIT USING
C THE LEAST SQUARES METHOD.  THE CURVE FIT PROGRAM FOUND
C THE BEST FIT EQUATION OUT OF 19 POSSIBLE EQUATIONS.
C THE PROGRAM RAN ON A HEWETT-PACKARD 41-CX.
C*****************************************************
C
C SUBROUTINE GRAPH1
C
C*****************************************************
      SUBROUTINE GRAPH1(C1A,CTOP,PR)
      IF (CTOP.LE.0.0433.AND.PR.GT.0.96) C1A=367.049-
     &190.772*PR-176.07/PR
      IF(CTOP.LE.0.0433.AND.PR.LE.0.96) C1A=0.98-
     &0.5031*PR
      IF (CTOP.GT.0.0433.AND.CTOP.LE.0.062) THEN
      IF(PR.GT.0.96) Y1=367.049-190.772*PR-.07/PR
      IF(PR.LE.0.96) Y1=0.98-0.5031*PR
      IF(PR.GE.0.98) Y2=.465*EXP(((-0.014-
     &LOG(PR))**2)/(-.000289))
```

```
      IF(PR.LT.0.98) Y2=.828+.164*PR-.514*PR**2
      CALL LINN(0.0433,0.062,Y1,Y2,CTOP,C1A)
      ENDIF
      IF (CTOP.GT.0.062.AND.CTOP.LE.0.0925) THEN
      IF(PR.GE.0.98) Y1=.465*EXP(((-0.014-
     &LOG(PR))**2)/(-.000289))
      IF(PR.LT.0.98) Y1=.828+.164*PR-.514*PR**2
      IF(PR.GT.0.9936) Y2=.493*EXP(((-.006-
     &LOG(PR))**2)/(.00004953))
      IF(PR.LE.0.9936.AND.PR.GT.0.9403) Y2=81.728*PR-
     &43.385*PR**2-37.887
      IF(PR.LE.0.9403) Y2=.866+.259*PR-.568*PR**2
      CALL LINN(0.062,0.0925,Y1,Y2,CTOP,C1A)
      ENDIF
      IF (CTOP.GT.0.0925.AND.CTOP.LE.0.15) THEN
      IF(PR.GT.0.9936) Y1=.493*EXP(((-.006-
     &LOG(PR))**2)/(.00004953))
      IF(PR.LE.0.9936.AND.PR.GT.0.9403) Y1=81.728*PR-
     &43.385*PR**2-37.887
      IF(PR.LE.0.9403) Y1=.866+.259*PR-.568*PR**2
      IF(PR.GT.0.9789) Y2=.626*EXP(((-
     &.013*LOG(PR))**2)/(-.0004663))
      IF(PR.LE.0.9789) Y2=.587+1.287*PR-1.246*PR**2
      CALL LINN(0.0925,0.1458,Y1,Y2,CTOP,C1A)
      ENDIF
      IF(CTOP.GT.0.15)THEN
      IF(PR.GT.0.9789) C1A=.626*EXP(((-
     &.013*LOG(PR))**2)/(-.0004663))
      IF(PR.LE.0.9789) C1A=.587+1.287*PR-1.246*PR**2
      ENDIF
      RETURN
      END
C*********************************************************
C
C     LINN IS A LINEAR CURVE FIT PROGRAM
C
C*********************************************************
      SUBROUTINE LINN(X1,X2,Y1,Y2,X,OUT)
      OUT=((Y2-Y1)/(X2-X1))*(X-X1)+Y1
      RETURN
      END
      SUBROUTINE GRAPH3(WTOP,RPM,OUT)
      RPA=RPM
      IF(RPM.GT.3200.) RPM=3200.
      IF (RPM.LE.3200.0.AND.RPM.GT.2200.0)THEN
      Y1=1/(2.786-.546*WTOP)
      IF(WTOP.GE.0.13)
     &Y2=.457*(1.017**(1./WTOP))*WTOP**.097
      IF(WTOP.LT.0.13) Y2=.399*WTOP+.373
      CALL LINN(3200.0,2200.0,Y1,Y2,RPM,OUT)
      ENDIF
      IF (RPM.LE.2200.0.AND.RPM.GT.1600.0)THEN
```

```
      IF(WTOP.GE.0.13)
     &Y1=.457*(1.017**(1./WTOP))*WTOP**.097
      IF(WTOP.LT.0.13) Y1=.399*WTOP+.373
      IF(WTOP.GE.0.125)
     &Y2=.501*(1.02**(1/WTOP))*WTOP**(.097)
      IF(WTOP.LT.0.125) Y2=.448*WTOP+.424
      CALL LINN(2200.0,1600.0,Y1,Y2,RPM,OUT)
      ENDIF
      IF (RPM.LE.1600.0.AND.RPM.GT.1000.0)THEN
      IF(WTOP.GE.0.125)
     &Y1=.501*(1.02**(1/WTOP))*WTOP**(.097)
      IF(WTOP.LT.0.125) Y1=.448*WTOP+.424
      IF(WTOP.GE.0.130)
     &Y2=.569*(1.024**(1/WTOP))*WTOP**.124
      IF(WTOP.LT.0.130) Y2=.895*WTOP+.413
      CALL LINN(1600.0,1000.0,Y1,Y2,RPM,OUT)
      ENDIF
      IF (RPM.LE.1000.0.AND.RPM.GT.300.0)THEN
      IF(WTOP.GE.0.130)
     &Y1=.569*(1.024**(1/WTOP))*WTOP**.124
      IF(WTOP.LT.0.130) Y1=.895*WTOP+.413
      IF(WTOP.GE.0.128) Y2=.601-.330*WTOP+.560*WTOP**2
      IF(WTOP.LT.0.128) Y2=1.181*WTOP+.413
      CALL LINN(1000.0,300.0,Y1,Y2,RPM,OUT)
      ENDIF
      IF (RPM.LE.300.0.AND.RPM.GE.0.0)THEN
      IF(WTOP.GE.0.128) Y1=.601-.330*WTOP+.560*WTOP**2
      IF(WTOP.LT.0.128) Y1=1.181*WTOP+.413
      IF(WTOP.GE.0.128) Y2=1./(1.819-2.267*(WTOP-
     &.295)**2)
      IF(WTOP.LT.0.128) Y2=1.181*WTOP+.413
      CALL LINN(300.0,0.0,Y1,Y2,RPM,OUT)
      ENDIF
      RPM=RPA
      RETURN
      END
C*****************************************************
C
C  SUBROUTINE FOR GRAPH 5
C
C*****************************************************
      SUBROUTINE GRAF5(PR,RPM,OUT)
      IF(PR.GT.0.75) OUT=RPM*8.063E-6+.52245
      IF(PR.LE.0.75.AND.PR.GT.0.58) THEN
      Y1=RPM*8.063E-6+.52245
      Y2=RPM*7.0105E-6+.58873
      CALL LINN(0.75,0.58,Y1,Y2,PR,OUT)
      ENDIF
      IF(PR.LE.0.58.AND.PR.GT.0.43) THEN
      Y1=RPM*7.0105E-6+.58873
      Y2=RPM*4.4079E-6+.62939
      CALL LINN(.58,.43,Y1,Y2,PR,OUT)
```

```
      ENDIF
      IF(PR.LE.0.43.AND.PR.GT.0.24) THEN
      Y1=RPM*4.4079E-6+.62939
      Y2=RPM*5.365E-6+.68572
      CALL LINN(.43,.24,Y1,Y2,PR,OUT)
      ENDIF
      IF(PR.LE.0.24.AND.PR.GT.0.12) THEN
      Y1=RPM*5.365E-6+.68572
      Y2=RPM*7.8505E-6+.73897
      CALL LINN(.24,.12,Y1,Y2,PR,OUT)
      ENDIF
      IF(PR.LE.0.12) OUT=RPM*7.8505E-6+.73897
      RETURN
      END
C*****************************************************
C
C   SUBROUTINE FOR CURVE FIT 6
C
C*****************************************************
      SUBROUTINE GRAF6(AAXLO,RPM,OUT)
      IF(AAXLO.LE.1.0.AND.AAXLO.GT.0.75) THEN
      Y1=RPM*4.3723E-5+1.39917
      Y2=RPM*1.8151E-5+.795412
      CALL LINN(1.0,.75,Y1,Y2,AAXLO,OUT)
      ENDIF
      IF(AAXLO.LE.0.75.AND.AAXLO.GT.0.5) THEN
      Y1=RPM*1.8151E-5+.795412
      Y2=RPM*(-1.6817E-5)+.721041
      CALL LINN(.75,.5,Y1,Y2,AAXLO,OUT)
      ENDIF
      IF(AAXLO.LE.0.5.AND.AAXLO.GT.0.25) THEN
      Y1=RPM*(-1.6817E-5)+.721041
      Y2=RPM*7.8505E-6+.738972
      CALL LINN(.5,.25,Y1,Y2,AAXLO,OUT)
      ENDIF
      IF(AAXLO.LE.0.25) OUT=RPM*7.8505E-6+.738972
      RETURN
      END
C*****************************************************
C
C   SUBROUTINE FOR CURVE FIT 7
C
C*****************************************************
      SUBROUTINE GRAF7(TNUM,PR,OUT)
      IF(TNUM.GT.10.) TNUM=10.
      IF(TNUM.LE.10.0.AND.TNUM.GT.8.0) THEN
      IF(PR.GE.0.578) Y1=.495+2.985*PR-3.155*PR**2
      IF(PR.LT.0.578) Y1=1.589-1.626*PR+1.368*PR**2
      IF(PR.GE.0.577) Y2=.714+2.082*PR-2.48*PR**2
      IF(PR.LT.0.577) Y2=1.25-.380*PR+.023/PR
      CALL LINN(10.0,8.0,Y1,Y2,TNUM,OUT)
      ENDIF
```

```
      IF(TNUM.LE.8.0.AND.TNUM.GT.6.0) THEN
      IF(PR.GE.0.577) Y1=.714+2.082*PR-2.48*PR**2
      IF(PR.LT.0.577) Y1=1.25-.380*PR+.023/PR
      Y2=1.747-1.596*PR+.98*PR**2
      CALL LINN(8.0,6.0,Y1,Y2,TNUM,OUT)
      ENDIF
      IF(TNUM.LE.6.0.AND.TNUM.GT.4.0) THEN
      Y1=1.747-1.596*PR+.98*PR**2
      IF(PR.GT.0.755) Y2=2.258-1.363*PR
      IF(PR.LT.0.755) Y2=1.139*EXP((PR-1.193)**2/2.55)
      CALL LINN(6.0,4.0,Y1,Y2,TNUM,OUT)
      ENDIF

      IF(TNUM.LE.4.0.AND.TNUM.GT.2.0) THEN
      IF(PR.GT.0.755) Y1=2.258-1.363*PR
      IF(PR.LT.0.755) Y1=1.139*EXP((PR-1.193)**2/2.55)
      Y2=.603+.573/PR-.047/PR**2
      CALL LINN(4.0,2.0,Y1,Y2,TNUM,OUT)
      ENDIF
      IF(TNUM.LE.2.0) OUT=.603+.573/PR-.047/PR**2
      RETURN
      END
C*****************************************************
C  SUBROUTINE FOR CURVE FIT 8
C*****************************************************
      SUBROUTINE GRAF8(TNUM,PR,OUT)
      IF(TNUM.GT.10.0) TNUM=10.0
      IF(TNUM.LE.10.0.AND.TNUM.GT.8.0) THEN
      Y1=.555+.053/PR-.003/PR**2
      Y2=1/((-1.049)*(PR-.766)**2+1.702)
      CALL LINN(10.0,8.0,Y1,Y2,TNUM,OUT)
      ENDIF
      IF(TNUM.LE.8.0.AND.TNUM.GT.6.0) THEN
      Y1=1/((-1.049)*(PR-.766)**2+1.702)
      Y2=.513+.113/PR-.009/PR**2
      CALL LINN(8.0,6.0,Y1,Y2,TNUM,OUT)
      ENDIF
      IF(TNUM.LE.6.0.AND.TNUM.GT.4.0) THEN
      Y1=.513+.113/PR-.009/PR**2
      Y2=1.063-.648*PR+.310*PR**2
      CALL LINN(6.0,4.0,Y1,Y2,TNUM,OUT)
      ENDIF
      IF(TNUM.LE.4.0.AND.TNUM.GT.2.0) THEN
      Y1=1.063-.648*PR+.310*PR**2
      Y2=.809+.215/PR-.012/PR**2
      CALL LINN(4.0,2.0,Y1,Y2,TNUM,OUT)
      ENDIF
      IF(TNUM.LE.2.0) THEN
      OUT=.809+.215/PR-.012/PR**2
      ENDIF
      RETURN
      END
```

```
 SUBROUTINE SWIRLER(AXLO,TN,PRAT,JJJ,SWIRL,CLR)
C*****************************************************
C
C THIS SUBROUTINE INCORPORATES THE EFFECTS OF SWIRL AND
C TAKES INTO ACCOUNT THE CLEARANCE IN DOING SO
C
C*****************************************************
C
C    VARIABLE LIST
C SWIRL = FLOW COEF. WITH SWIRL/FLOW COEFFICIENT WITHOUT
C SWIRL AT A CLEARANCE OF 0.007 INCHES.  VARIABLE ALSO
C USED TO PASS BACK FINAL FLOW RATIO.
C SWIRL2= FLOW RATIO FOR A CLEARANCE OF 0.014 INCHES.
C CLRA  = CLEARANCE
C
C*****************************************************
      N=INT(TN)
      JA=JJJ
      SWIRL=1.0
      IF(JJJ.EQ.0) RETURN
      IF(JJJ.NE.0) JJJ=3
      IF(JJJ.GE.2) GOTO 500
C
C COUNTER-CLOCKWISE SWIRL
C
   10 IF(AXLO.LE.0.87.AND.AXLO.GT.0.63) GOTO 100
      IF(AXLO.LE.0.63.AND.AXLO.GT.0.37) GOTO 200
      IF(AXLO.LE.0.37) GOTO 300
C
C* AXLO=1.0
C
      SWIRL2=1.02
      IF(N.GT.5) SWIRL2=.84
      IF(N.GT.5) SWIRL=.96
      GOTO 1000
C
C* AXLO=0.75
C
  100 SWIRL2=1.02
      IF(N.GT.5) SWIRL2=.84
      SWIRL=.93
      IF(N.GT.3) SWIRL=.90
      IF(N.GT.3.AND.PRAT.GE.0.75) SWIRL=0.85
      IF(N.GT.5) SWIRL=.89
      IF(N.GT.5.AND.PRAT.GE.0.75) SWIRL=.84
      GOTO 1000
C
C* AXLO=0.50
C
  200 SWIRL2=1.03
      IF(N.GT.3)SWIRL2=1.00
      IF(N.GT.5)SWIRL2=0.91
```

C-3

```
      SWIRL=.97
      IF(N.GT.3) SWIRL=1.0
      IF(N.GT.5) SWIRL=.98
      GOTO 1000
C
C* AXLO=0.25
C
300   SWIRL2=1.03
      IF(N.GT.3)SWIRL2=1.00
      IF(N.GT.5)SWIRL2=0.91
      SWIRL=1.18
      IF(N.GT.5) SWIRL=1.10
      GOTO 1000
C
C* CLOCKWISE SWIRL
C
  500 IF(AXLO.LE.0.87.AND.AXLO.GT.0.63) GOTO 600
      IF(AXLO.LE.0.63.AND.AXLO.GT.0.37) GOTO 700
      IF(AXLO.LE.0.37) GOTO 800
C
C* AXLO=1.0
C
      SWIRL2=1.01
      IF(N.GT.3)SWIRL2=1.02
      IF(N.GT.5)SWIRL2=0.88
      SWIRL=1.06
      IF(N.GT.3) SWIRL=1.
      IF(N.GT.5) SWIRL=.95
      GOTO 1000
C
C* AXLO=0.75
C
  600 SWIRL2=1.01
      IF(N.GT.3)SWIRL2=1.02
      IF(N.GT.5)SWIRL2=0.88
      SWIRL=.85
      IF(N.GT.0.AND.PRAT.GE.0.45) SWIRL=.80
      IF(N.GT.3) SWIRL=.86
      IF(N.GT.3.AND.PRAT.GE.0.75) SWIRL=.80
      IF(N.GT.5) SWIRL=.96
      IF(N.GT.5.AND.PRAT.GE.0.75) SWIRL=.92
      GOTO 1000
C
C* AXLO=0.5
C
  700 SWIRL2=1.01
      IF(N.GT.3)SWIRL2=1.00
      IF(N.GT.5)SWIRL2=0.94
      SWIRL=.99
      IF(N.GT.3) SWIRL=.96
      IF(N.GT.5) SWIRL=1.0
      GOTO 1000
```

```
C
C* AXLO=.25
C
  800 SWIRL2=1.01
      IF(N.GT.3)SWIRL2=1.00
      IF(N.GT.5)SWIRL2=0.94
      SWIRL=1.02
      IF(N.GT.4) SWIRL=1.16
      IF(JJJ.GT.2) SWIRL1=SWIRL
      IF(JJJ.GT.2) SWIRL22=SWIRL
      IF(JJJ.GT.2) GOTO 10
 1000 CONTINUE
      IF(JJJ.EQ.3) SWIRL=(SWIRL1+SWIRL)/2.0
      IF(JJJ.EQ.3) SWIRL2=(SWIRL22+SWIRL2)/2.0
      CLRA=CLR
C
C* EFFECTS OF CLEARANCE
C
      IF(CLRA.LT.0.007) CLRA=0.007
      CALL LINN(0.007,0.014,SWIRL,SWIRL2,CLRA,GO)
      SWIRL=GO
      JJJ=JA
      RETURN
      END
C*****************************************************
C
C SUBROUTINE GRAPH9 TO CALCULATE THE INCREASE IN FLOW
C COEFFICIENT DUE TO A CLEARANCE > 0.007 INCHES.
C
C*****************************************************
      SUBROUTINE GRAPH9(AXLO,N,PR,RPM,CLR,GO)
      REAL N
      RPA=RPM
      IF(RPA.GT.5000.)RPA=5000.
C* AXIAL LOCATION LESS THAN 0.625
      IF(AXLO.LE.0.625)THEN
      Y1=1./(.44-.305*(PR-.758)**2.)
      Y2=3.74-2.622*PR+1.309*PR**2.
      Y3=5.412-7.205*PR+5.726*PR**2.
      Y4=5.771-6.276*PR+4.248*PR**2.
      Y5=5.07-5.431*PR+4.513*PR**2.
      Y6=5.839-5.698*PR+3.85*PR**2.
      ENDIF
      IF(AXLO.GT.0.625)THEN
      Y1=1.369*1.724**PR*PR**(-.47)
      Y2=3.282-3.047*PR+1.811*PR**2.
      Y3=1./(.183+.203*PR)
      Y4=4.821-5.328*PR+3.556*PR**2.
      Y5=5.913-7.354*PR+5.981*PR**2.
      Y6=4.717-4.357*PR+2.803*PR**2.
      ENDIF
      IF(N.LE.2) CALL LINN(0.,5000.,Y1,Y2,RPA,OUT)
```

```
IF(N.GT.2.AND.N.LE.4)THEN
CALL LINN(0.,5000.,Y1,Y2,RPA,OUT1)
CALL LINN(0.,5000.,Y3,Y4,RPA,OUT2)
CALL LINN(2.,4.,OUT1,OUT2,N,OUT)
ENDIF
IF(N.GT.4.AND.N.LE.6)THEN
CALL LINN(0.,5000.,Y3,Y4,RPA,OUT1)
CALL LINN(0.,5000.,Y5,Y6,RPA,OUT2)
CALL LINN(4.,6.,OUT1,OUT2,N,OUT)
ENDIF
IF(N.GT.6)CALL LINN(0.,5000.,Y5,Y6,RPA,OUT)
CALL LINN(0.007,0.014,1.0,OUT,CLR,GO)
RETURN
END
```

APPENDIX C

EQUIPMENT SPECIFICATIONS

EQUIPMENT SPECIFICATIONS

The following list states the instrument used and it's response and accuracy. Following the list is a brief description of how the equipment was used to record the data.

3000 series Bently Nevada proximiter probe system.

Hewlett Packard 5301A counter with a 5300A mainframe display and a 10533A recorder interface. Response, 10 Hz to 10 Mhz. Accuracy, ± 1 count, ± 1 time base accuracy.

Omega 199 themocouple indicator with copper-constantin thermocouples. Response, $-245^{o}F$ to $750^{o}F$. Accuracy $\pm 2.5^{o}F$.

Daniel 2" model 1503-1D 'CR' turbine meter. Response, 25 GPM to 225 GPM. Accuracy, $\pm 0.5\%$ linearity, $\pm 0.05\%$ repeatability.

Daniel 1" model 3/4 5000 'CR' turbine meter. Response, 4 GPM to 25 GPM. Accuracy, $\pm 0.5\%$ linearity, $\pm 0.05\%$ repeatability.

Scanivalve 48 port pressure measuring system with PDCR22-200 psid pressure transducer. Response, 0 to 200 psid. Accuracy $\pm 0.06\%$ of full scale.

Digital Equipment Corporation MINC-PDP 11/23 computer system. Analog to digital converter, range ± 5 volts. Resolution, 12 bits (2.5 mv).

The rotation rate of the test section was measured using a 3000 series Bently Nevada proximiter probe system. This system was used to sense the passing of the six bolts on the perimenter of the coupling between the variable speed electric motor and the test section. The output from the proximiter probe system was input into a Hewlett Packard 5301A frequency counter which determined the frequency of the signal. This frequency was then transferred digitally to the MINC computer.

The same frequency counter was used to measure the output of the turbine flow meters by using a computer controlled multiplexer which would input either of the flow meters or the proximiter probe outputs into the frequency counter. The frequency was then recorded by the computer.

The temperature of the water exiting the labyrinth seal was recorded by the computer by digitally interfacing to Omega 199 thermocouple indicator to the computer. The water temperature at the inlet of the seal was manually monitored to determine if there were significant temperature changes occurring within the seal.

All of the pressure measurements were made using the Scanivalve system. Pressures at the inlet and exit of the labyrinth seal were recorded along with the axial pressure distributions on the outer seal wall. The computer system was interfaced to the Scanivalve system such that the computer controlled the selection of which port of the valve was connected to the pressure transducer while the analog to digital converter of the computer recorded the pressure. Before and after data were recorded, the pressure transducer was calibrated using a dead weight tester.